

Attention Microfiche User,

The original document from which this microfiche was made was found to contain some imperfection or imperfections that reduce full comprehension of some of the text despite the good technical quality of the microfiche itself. The imperfections may be:

- missing or illegible pages/figures
- wrong pagination
- poor overall printing quality, etc.

We normally refuse to microfiche such a document and request a replacement document (or pages) from the National INIS Centre concerned. However, our experience shows that many months pass before such documents are replaced. Sometimes the Centre is not able to supply a better copy or, in some cases, the pages that were supposed to be missing correspond to a wrong pagination only. We feel that it is better to proceed with distributing the microfiche made of these documents than to withhold them till the imperfections are removed. If the removals are subsequently made then replacement microfiche can be issued. In line with this approach then, our specific practice for microficheing documents with imperfections is as follows:

1. A microfiche of an imperfect document will be marked with a special symbol (black circle) on the left of the title. This symbol will appear on all masters and copies of the document (1st fiche and trailer fiches) even if the imperfection is on one fiche of the report only.
2. If imperfection is not too general the reason will be specified on a sheet such as this, in the space below.
3. The microfiche will be considered as temporary, but sold at the normal price. Replacements, if they can be issued, will be available for purchase at the regular price.
4. A new document will be requested from the supplying Centre.
5. If the Centre can supply the necessary pages/document a new master fiche will be made to permit production of any replacement microfiche that may be requested.

The original document from which this microfiche has been prepared has these imperfections:

- ☒ missing pages/~~figures~~ numbered: 77 - 78.
- ☐ wrong pagination
- ☐ poor overall printing quality
- ☐ combinations of the above
- ☐ other

INIS Clearinghouse
IAEA
P. O. Box 100
A-1400, Vienna, Austria

1



2

Report Rapport

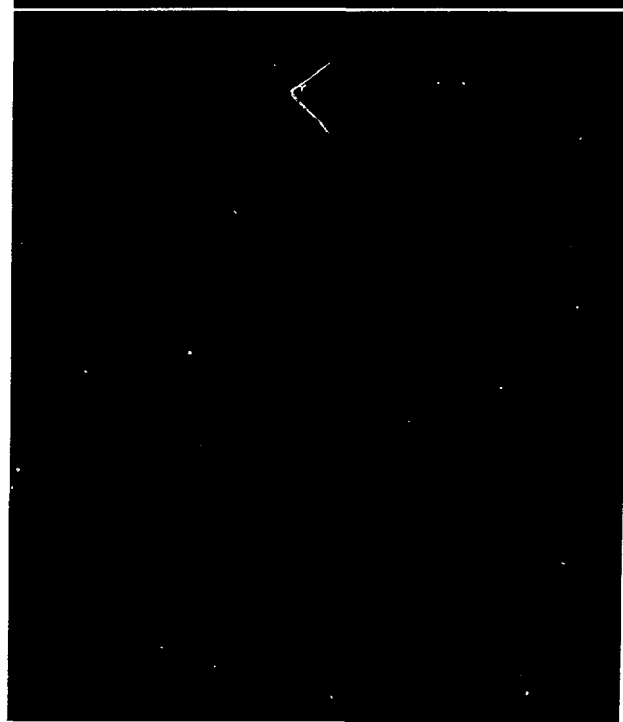


Atomic Energy
Control Board

Commission de contrôle
de l'énergie atomique

CA8507858

INFO-0105





Atomic Energy
Control Board

Commission de contrôle
de l'énergie atomique

P.O. Box 1046
Ottawa, Canada
K1P 5S9

C.P. 1046
Ottawa, Canada
K1P 5S9

INFO-0105

ORIGIN AND SUBSURFACE MIGRATION OF
RADIONUCLIDES FROM WASTE ROCK AT AN
ABANDONED URANIUM MINE NEAR
BANCROFT, ONTARIO

A research report prepared for the
Atomic Energy Control Board by

E. Veska, J.A. Cherry,
H.D. Sharma
Departments of Earth Sciences
and Chemistry
University of Waterloo
Waterloo, Ontario

RESEARCH REPORT

October 1983

ORIGIN AND SUBSURFACE MIGRATION OF
RADIONUCLIDES FROM WASTE ROCK AT AN
ABANDONED URANIUM MINE NEAR BANCROFT,
ONTARIO

ABSTRACT

Uranium-mine waste rock dump sites may require long-term surveillance because of the potential contamination of radionuclides from waste rock to the subsurface environment. In order to assess the conditions and controls on the migration in groundwater of waste-rock-derived contaminants, an area of old waste rock on a sand aquifer at the abandoned Greyhawk uranium mine near Bancroft, Ontario, was monitored. The waste rock has been abandoned for more than two decades. The results of a four-year hydrological and radiological investigation at the Greyhawk site indicated the presence of contaminant plumes of ^{238}U , ^{234}U , ^{226}Ra , ^{210}Pb , ^{230}Th , ^{232}Th , sulphate, bicarbonate and dissolved inorganic carbon in the sand aquifer originating from the waste rock. Laboratory-determined parameters were applied in two contaminant migration models for simulating the observed frontal positions of the waste-rock-derived radionuclides in the sand aquifer and also for predicting the spread of radionuclide contamination in the future. With the possible exception of ^{238}U , reasonable results were obtained for the simulations of the ^{226}Ra , ^{210}Pb and ^{230}Th mobilities in the sand aquifer.

RÉSUMÉ

Les sites de haldes de stériles provenant des mines d'uranium peuvent nécessiter une surveillance à long terme vu la contamination potentielle due aux radionucléides libérés par les stériles dans l'environnement souterrain. Dans le but d'évaluer les conditions et les mesures de contrôle de la migration dans le réseau d'eaux souterraines de contaminants provenant de stériles, on a étudié une zone de stériles entassés depuis plus de vingt ans sur une couche de sable aquifère à la mine d'uranium abandonnée de Greyhawk, près de Bancroft (Ontario). Les résultats d'une étude hydrologique et radiologique d'une durée de quatre ans menée au site de Greyhawk ont indiqué la présence de zones contaminées par l'uranium 238, l'uranium 234, le radium 226, le plomb 210, le thorium 230, le thorium 232, le sulfate, le bicarbonate et le carbone inorganique dissout dans la couche de sable aquifère en provenance du stérile. On a appliqué des paramètres établis en laboratoire à deux modèles de migration de contaminants afin de simuler la position frontale observée des radionucléides provenant de stériles dans la couche de sable aquifère et afin de prévoir la dispersion de la contamination due aux radionucléides à l'avenir. Compte tenu de l'exception possible de l'uranium 238, on a obtenu des résultats acceptables en ce qui a trait aux simulations de mobilité du radium 226, du plomb 210 et du thorium 230 dans la couche de sable aquifère.

DISCLAIMER

The Atomic Energy Control Board is not responsible for the accuracy of the statements made or opinions expressed in this publication and neither the Board nor the authors assume liability with respect to any damage or loss incurred as a result of the use made of the information contained in this publication.

SUMMARY

This report includes the results and discussion of a four-year investigation on the origin and subsurface migration of radionuclides from waste rock at the abandoned Greyhawk uranium mine site near Bancroft, Ontario. This investigation was initiated at the University of Waterloo under a research agreement initiated in 1978 with the Atomic Energy Control Board.

The objectives of this investigation were (1) to develop an analytical method to enable the sequential determination of ^{238}U , ^{234}U , ^{232}Th , ^{230}Th , ^{226}Ra and ^{210}Pb in groundwater and other environmental samples, (2) to assess the present-day spread of the waste-rock-derived chemical and radioactive contaminants in the sand aquifer at Greyhawk, (3) to assess the factors that affect the release of radionuclides by weathering from waste rock, and (4) to assess the suitability of laboratory-determined parameters and of two contaminant transport models for the simulation of the mobilities of the waste-rock-derived radionuclides in the sand aquifer at Greyhawk.

A method for the determinations of ^{226}Ra , ^{210}Pb and the isotopes of uranium and thorium in environmental samples was developed. Radiochemical separations for this method are achieved by using ion-exchange and solvent extraction techniques. The precision, accuracy and sensitivity for the determinations of the radionuclides of interest have been determined.

A preliminary field investigation (Gillham et al, 1979) at the Greyhawk site began in 1978 with the installation of a few multilevel piezometers in the sand aquifer. The distribution of ^{226}Ra and several chemical constituents in groundwater sampled from these devices were mapped. The results indicated a zone of above-background concentrations of these constituents in groundwater in the vicinity of the waste rock.

During the period from 1978 to 1982, a dense network of groundwater sampling devices for the delineation of the extent of waste-rock-derived contamination was installed in the aquifer. The groundwater velocities in the aquifer progressively decrease from a maximum at 70 m/yr below the waste rock to about 2 m/yr at approximately 125 m downgradient from the waste rock. Waste-rock-derived contaminant plumes of sulphate, bicarbonate, dissolved inorganic carbon, ^{238}U , ^{226}Ra , ^{210}Pb , ^{230}Th and ^{232}Th were identified in the sand aquifer. The maximum zone of groundwater contamination in the sand aquifer, as identified by elevated concentrations of sulphate, bicarbonate and

dissolved inorganic carbon, extends approximately 100 to 125 meters laterally downflow from the piles of waste rock to a swamp nearby. The lateral extent of ^{238}U and ^{234}U contamination downgradient from the waste rock is less than 80 meters, whereas the lateral extent of ^{226}Ra , ^{210}Pb , ^{230}Th and ^{232}Th contamination is less than 20 meters. The highest, reported activities of radionuclides that were found in groundwater below the waste rock in 1979 are 86.90 pCi/l for ^{238}U , 23.6 pCi/l for ^{226}Ra , 9.4 pCi/l for ^{210}Pb , 2.45 pCi/l for ^{230}Th and 1.10 pCi/l for ^{232}Th .

Rock-leaching experiments using artificial solutions that represent rainwater and groundwater from the field site were initiated. The results from these experiments indicated that the pH of the extractant is the most important factor affecting the release of radionuclides from waste-rock weathering. Similarities were drawn between the activities of radionuclides found in the leachates from the rock-leaching experiments and those found in the contaminated groundwater below the waste rock at the Greyhawk site.

The observed frontal positions of ^{238}U , ^{226}Ra , ^{210}Pb and ^{230}Th contamination in groundwater from the waste rock piles were simulated using two transport models, namely the advection-retardation model with uniform groundwater velocity and chemistry and the cell model with non-uniform groundwater velocity and chemistry. Both of these models utilized laboratory-determined parameters, namely: (1) the measured amounts of radionuclides that are extracted from waste rock upon leaching with artificial rainwater and groundwater solutions and (2) distribution coefficients for U(VI), U(IV), Ra(II), Pb(II) and Th(IV). The results from both models indicated good agreement between the analytical and simulated frontal positions of ^{226}Ra , ^{210}Pb and ^{230}Th in the sand aquifer. For the case of the uranium isotopes, the simulated results from the transport models only partly corresponded with that of the analytical results.

Radium-226 was the only radioactive contaminant species in groundwater from this investigation that had been found to exceed the drinking water standards. The spread of ^{226}Ra contamination in the sand aquifer in the future was assessed by predictions based on the transport models. Although the ^{226}Ra contaminated groundwater from the waste rock was predicted to reach the nearby

swamp after 250,000 years, the activity of ^{226}Ra in groundwater after 250,000 years was calculated to be less than the drinking water standard.

The analytical ^{234}U activity in groundwater was found to progressively increase with respect to the analytical ^{238}U activity downflow from the waste rock. That is, the $^{234}\text{U}/^{238}\text{U}$ activity ratios in the relatively-young shallow groundwater increased to as high as 2.05 ± 0.19 from 0.80 ± 0.09 . This distribution pattern of the $^{234}\text{U}/^{238}\text{U}$ activity ratios in the sand aquifer could not be explained on the basis of previously-developed hypotheses on ^{234}U fractionation in groundwater. An explanation was given for this phenomenon based on the different percentages of the (IV) and (VI) oxidation states of the ^{234}U and ^{238}U atoms in the contaminated groundwater. The validity of the explanation was tested with the aid of the cell model and the laboratory-determined parameters.

The findings from this investigation on the subsurface migration of radioactive contaminants from uranium-bearing waste rock at the Greyhawk site were found to be representative of a relatively-simple case. These findings, however, are site specific and cannot be used to draw similarities at other waste-rock sites. Nevertheless, the methodology used for the Greyhawk field problem can be used at other sites for simulating the subsurface migration of radionuclides from waste rock.

ACKNOWLEDGEMENTS

This research was supported by contracts with the Atomic Energy Control Board and by a grant from the National Science and Engineering Research Council and was conducted through a cooperative effort of the Departments of Chemistry and Earth Sciences at the University of Waterloo. The authors gratefully acknowledge the assistance in the field from Bill Clarke, Dan Reynolds, Diane Germain, Paul Johnson, Munawwar Sajjad and Rob Blair. David Mohamed of McMaster University and Kate (MacIntosh) Klie of the University of Waterloo provided the radioanalytical assistance in the 1978-1979 analyses of rock, soil and groundwater. Dr. R.G.V. Hancock provided the irradiation facilities at the Slowpoke Reactor at the University of Toronto.

Thanks are also due to Lynda Lang and Marilyn Bisgould for typing the report; to Nadia Bahar for drafting the diagrams; and to Peter Fischer for the photographic reductions.

TABLE OF CONTENTS

	Page
CHAPTER 1	
INTRODUCTION	1
1.1 Objective and Scope	1
CHAPTER 2	
LITERATURE SURVEY	8
2.1 Transport Models on Radionuclide Migration	8
2.1.1 Advection-Dispersion-Retardation Model	8
2.1.2 Advection-Retardation Model	12
2.1.3 Cell Model	13
2.2 Isotopic Disequilibria in the Uranium-238 Series	16
2.2.1 Introduction	16
2.2.2 Disequilibria in Hydrogeological Systems	16
2.2.3 Theories on Fractionation of Elements in the Uranium-238 Series	17
2.3 Previous Studies at the Field Site	19
CHAPTER 3	
RADIOANALYTICAL METHOD	24
3.1 Analytical Scheme	24
3.2 Accuracy and Reproducibility Tests	38
3.3 Summary	48
CHAPTER 4	
HYDROGEOLOGY OF THE FIELD SITE	49
4.1 Methods of Investigation	49
4.2 Hydrostratigraphy	54
4.3 Hydraulic Gradients and Groundwater Flow Direction	56
4.4 Oxygen-18 as an Indicator of the Groundwater Source	66
4.5 Tritium as an Indicator of the Groundwater Age	72
4.6 Methods of Groundwater Velocity Analysis	76
4.7 Summary	80

	Page
CHAPTER 5	
RADIONUCLIDES AND CHEMICAL CONSTITUENTS IN GROUNDWATER	82
5.1 Sampling and Analytical Procedures	82
5.2 Spatial Distributions of Chemical Constituents	85
5.3 Spatial Distributions of Radionuclides	112
5.4 Temporal Variation in Radionuclide Activities	123
5.5 Summary	126
CHAPTER 6	
LABORATORY STUDIES OF WASTE ROCK, PYRITE AND SAND LEACHING	128
6.1 Waste Rock Characteristics	129
6.1.1 Mineralogical Description	129
6.1.2 Chemical Analysis	129
6.1.3 Radiochemical Analysis	130
6.2 Leachability of Radionuclides from Waste Rock	132
6.2.1 Materials	133
6.2.2 Description of Batch Experiments	134
6.2.3 Description of Column Experiments	136
6.2.4 Results from Batch Experiments	136
6.2.5 Results from Column Experiments	149
6.2.6 Interpretations	153
6.3 Pyrite Leaching Experiments	165
6.3.1 Description of Batch Experiments	165
6.3.2 Results and Interpretation	166
6.4 Acid Neutralization in Sand	168
6.4.1 Description of Column Experiments	169
6.4.2 Results and Interpretation	169
6.5 Summary	173
CHAPTER 7	
RADIONUCLIDE PARTITIONING IN AQUIFER MATERIALS	175
7.1 Materials for Batch K_d Experiments	176
7.2 Description of Batch K_d Experiments	178
7.3 Results	181
7.4 Interpretations	195
7.5 Summary	202

	Page
CHAPTER 8	
MODELLING OF CONTAMINANT BEHAVIOUR IN THE SAND AQUIFER	204
8.1 Waste Rock Weathering	204
8.2 Transport Processes of the Waste-Rock-Derived Radionuclides	209
8.3 Geochemical Models on Radionuclide Migration	228
8.4 Application of Transport Models	233
CHAPTER 9	
DISEQUILIBRIA IN THE URANIUM-238 SERIES IN GROUNDWATER	265
9.1 Spatial Distributions of $^{234}\text{U}/^{238}\text{U}$, $^{226}\text{Ra}/^{238}\text{U}$ and $^{210}\text{Pb}/^{238}\text{U}$ in Groundwater	265
9.2 Fractionation of ^{234}U , ^{226}Ra and ^{210}Pb in Leachates from Waste Rock Leaching Experiments	271
9.3 Evaluation of the ^{234}U Fractionation in Groundwater	273
CHAPTER 10	
SUMMARY AND CONCLUSIONS	279
REFERENCES	285

LIST OF TABLES

Table	Page
3.1 Accuracy and Reproducibility Tests with ^{238}U Standard	40
3.2 Accuracy and Reproducibility Tests with ^{232}Th Standard	41
3.3 Accuracy and Reproducibility Tests with ^{210}Pb Standard	42
3.4 Accuracy and Reproducibility Tests with ^{226}Ra Standard	43
3.5 Accuracy and Reproducibility Tests with ^{226}Ra Standard	44
3.6 Reproducibility Tests with Groundwater Sample A-5.8	45
3.7 Reproducibility Tests with Groundwater Sample L	46
4.1 Hydraulic Head Elevations at Representative Sites M14, M16, M7 and M9	65
4.2 Variation in ^{18}O and ^3H in Swamp Water During the Months of July and September in 1979	67
4.3 Spatial Variation of ^{18}O and ^3H in Groundwater in the Sand Aquifer Near the Swamp	69
4.4 Spatial Variation of ^{18}O and ^3H in Groundwater in the Immediate Vicinity of the Waste Rock	70
4.5 Spatial Variation of ^{18}O , ^2H and ^3H in Deep Groundwater	71
4.6 Spatial Variation of ^3H in Groundwater in the Central Section of the Study Area	74
5.1 Comparison of the Inorganic Solute Composition of Groundwater from Sites K, O and Y and the Drinking Water Standards	90
5.2 Variation in the Chemical Composition of Groundwater Along Traverse GR9-GR11	94
5.3 Variation in the Chemical Composition of Groundwater Along Traverse L-GR6	95
5.4 Chemical Analysis of the 1982 Groundwater from sites M5, M16 and M9	109
5.5 Temporal Variation in ^{226}Ra and ^{210}Pb activities in Groundwater at sites A, U and R	124

Table	Page
6.1 Results of the Chemical and Radiochemical Analysis of the Pegmatitic and Gabbroic Waste Rock	131
6.2 Comparison of the Amounts of Radionuclides Leached from Fresh and Used Pegmatite Grains in Batch Reactors After 40 Days	147
6.3 Effect of the Sulphate Ion Concentration on the Amounts of Radionuclides Released in Solution from the Leaching of Unweathered Pegmatite Grains with the pH4 HCl Solution After 40 Days	151
6.4 Comparison of the Amounts of Radionuclides Leached from Unweathered Grains of Pegmatite and Gabbro Using the Batch and Column Leach Techniques	152
6.5 Composition of Leachate with Time from the Infiltration of pH3 H_2SO_4 Through a Column Bed of Unweathered Grains of Pegmatite and Gabbro	154
6.6 Composition of Leachate with Time From the Infiltration of Deionized Water Through a Column Bed of Unweathered Grains of Pegmatite and Gabbro	155
6.7 Composition of Leachate with Time from the Infiltration of the pH7 Bicarbonate Solution through a Column Bed of Unweathered Grains of Pegmatite and Gabbro	156
6.8 Chemical and Radionuclide Composition in the Acidic and Neutral pH Leachates from the Leaching of Unweathered Pegmatite after 40 days	158
6.9 Saturation Indices of Various Mineral Phases in the Acidic and Neutral pH Leachates	160
6.10 Equations Pertaining to the Breakdown of Primary Aluminum Silicate Minerals to Clay Minerals	161
6.11 Summary of the Results from the Waste Rock Leaching Experiments and the Composition of the Two Types of Zone D Groundwater	164
7.1 Composition of Initial Equilibrating Solutions	177

Table	Page
7.2 Equilibration time study of $^{238}\text{U}(\text{VI})$ and $^{226}\text{Ra}(\text{II})$ batch K_d determinations	182
7.3 Comparison of K_d values for $^{238}\text{U}(\text{IV})$ and $^{238}\text{U}(\text{VI})$ as a function of pH	192
7.4 Effect of liquid - solid ratio on the $^{226}\text{Ra}(\text{II})$ and $^{238}\text{U}(\text{VI})$ batch K_d values	193
7.5 Comparison amongst the field, batch and column K_d values for ^{238}U , ^{232}Th and ^{226}Ra	194
7.6 Effect of background ^{238}U activities on the $^{238}\text{U}(\text{VI})$ batch K_d values	197
7.7 Effect of background ^{232}Th activities on the $^{232}\text{Th}(\text{IV})$ batch K_d values	198
7.8 Concentration comparisons between major cations and UO_2^{2+} and Th^{4+} in the equilibrating solutions	201
8.1 Comparisons between the chemical compositions of the zone D groundwater and water computed from mineral weathering reactions	207
8.2 Saturation indices of some minerals in groundwater samples along the NE flow line, M16-M19	226
8.3 Comparisons between the calculated and observed frontal positions along the M16-M19 flow line	236
8.4 Comparisons between the calculated and observed frontal positions along the L-M10 flow line	238
9.1 Examples of ^{234}U fractionation in groundwater from various aquifers	268
9.2 Comparison of activity ratios of $^{234}\text{U}/^{238}\text{U}$, $^{226}\text{Ra}/^{238}\text{U}$ and $^{210}\text{Pb}/^{238}\text{U}$ in waste rock leachates after 40 days of equilibration	272

LIST OF ILLUSTRATIONS

Figure	Page
1.1 Canadian nuclear fuel cycle	2
2.1 Regional topography and site location	20
2.2 Map of study area showing surficial features	21
3.1 Analytical Scheme Stage 1: Sample preparation	25
3.2 Stage 2: Preconcentration of elements on cation exchange resin	27
3.3 Stage 3: Separation of U, Th, Ra and Pb	28
3.4 Stage 4: Thorium purification and radioanalytical technique	30
3.5 Alpha-particle spectrum of thorium isotopes	31
3.6 Stage 5: Uranium separation and radio-analytical technique	33
3.7 Alpha-particle spectrum of uranium isotopes	34
3.8 Stage 6: Radium-226 and lead-210 determinations	36
3.9 Alpha-particle spectrum of ^{226}Ra and daughters	39
4.1 Map of the study area showing the locations of instruments installed at the site	50
4.2 Location of multi-level piezometers	51
4.3 Schematic illustration of a typical multi-level groundwater sampling installation	53
4.4 Hydrostratigraphic cross sections X-X, and Y-Y,	55
4.5 Water-table map, June 1, 1979	57
4.6 Variations in the water table elevations between May 26, 1979 and September 5, 1979	58
4.7 Water-table map, June 7, 1982	60
4.8 Distribution of hydraulic head values from multi-level sampling points at sites O, R, T, U, V and Y, on April 23, 1980	61
4.9 Equipotential contour diagram, May 12, 1982	63
4.10 Equipotential contour diagram, June 7, 1982	64

Figure	Page
4.11 Tritium distribution in groundwater along cross sections B-B' and C-C'	75
4.12 Analyses of groundwater velocity along cross sections A-A'--C-C' and B-B'--C-C'	77
5.1 A three-dimensional representation of the spatial distribution of bicarbonate concentrations in groundwater in 1979	86
5.2 Profile of electrical conductance, pH, HCO_3 , SO_4 , Ca, Mn, Fe, Zn and ^{18}O in groundwater from multi-level sites K, O and Y	87
5.3 Map illustrating the locations of the different types of waste rock deposits at the study site	88
5.4 Schematic representation of chemical analyses of groundwater from four apparent zones in the sand aquifer	92
5.5 Schematic cross sectional diagram representing the spatial variations in the electrical conductance values in groundwater downflow from site B	97
5.6 Schematic cross sectional diagram representing the spatial variations in the dissolved oxygen values in groundwater downflow from site B	98
5.7 Schematic cross sectional diagram representing the spatial variations in the pH and pe values in groundwater downflow from site B	99
5.8 Schematic cross sectional diagram representing the spatial variations in the concentrations of Ca, Mg, Na and K in groundwater downflow from site B	100
5.9 Schematic cross sectional diagram representing the spatial variations in the concentrations of SO_4 , HCO_3 and DIC in groundwater downflow from site B	101

Figure	Page
5.10 Correlation coefficients between calcium and sulphate concentrations in the deep groundwater, shallow groundwater and waste-rock-influenced groundwater	103
5.11 Distribution of electrical conductance values in groundwater along cross sections A-A', B-B' and C-C'	104
5.12 Distribution of sulphate concentrations in groundwater along cross sections A-A', B-B' and C-C'	105
5.13 Distribution of bicarbonate concentrations in groundwater along cross sections A-A', B-B' and C-C'	106
5.14 Distribution of dissolved inorganic carbon concentrations in groundwater along cross sections A-A', B-B' and C-C'	107
5.15 pH distribution in groundwater along cross sections A-A', B-B' and C-C'	108
5.16 Spatial variation in the activity and concentration vs. depth profiles of radionuclides and chemical constituents in groundwater downflow from piezometer L to multilevel piezometer GR6	113
5.17 Spatial variation in the activity and concentration vs. depth profiles of radionuclides and chemical constituents in groundwater downflow from multilevel piezometer GR9 to multilevel piezometer GR11.	114
5.18 Activity vs. depth profiles of radium-226 in groundwater downflow from site B	116
5.19 Activity vs. depth profiles of ^{234}U and ^{238}U in groundwater downflow from site B	117
5.20 Distribution of radium-226 activity in groundwater along cross sections A-A', B-B' and C-C'	119

Figure	Page
5.21 Distribution of lead-210 activity in groundwater along cross sections A-A', B-B' and C-C'	120
5.22 Distribution of uranium-238 activity in groundwater along cross sections A-A', B-B' and C-C'	121
5.23 Longitudinal activity profiles of (a) uranium-238 and (b) radium-226 in the zone of contamination	125
6.1 Results of pegmatite leaching experiment	137
6.2 Plot of the ^{238}U activity released into solution during the leaching of pegmatite as a function of time	139
6.3 Plot of the ^{234}U activity released into solution during the leaching of pegmatite as a function of time	140
6.4 Plot of the ^{226}Ra activity released into solution during the leaching of pegmatite as a function of time	141
6.5 Plot of the ^{210}Pb activity released into solution during the leaching of pegmatite as a function of time	142
6.6 Plot of the ^{230}Th activity released into solution during the leaching of pegmatite as a function of time	143
6.7 Plot of the ^{232}Th activity released into solution during the leaching of pegmatite as a function of time	144
6.8 Plot of the ^{228}Th activity released into solution during the leaching of pegmatite as a function of time	145
6.9 Effect of grain size on the amount of radionuclides extracted in solution from the leaching of unweathered pegmatitic grains with deionized water after 40 days	148
6.10 Effect of the solid:liquid ratio on the amount of radionuclides extracted in solution from the leaching of unweathered pegmatitic grains with deionized water after 40 days	150

Figure	Page
6.11 Solubility diagram of the mineral thorianite, $\text{ThO}_2(\text{s})$, in equilibrium with the thorium(IV) - hydroxy species at 25°C	162
6.12 Results of pyrite leaching experiments	167
6.13 Results of pyrite leaching experiments	167
6.14 pH variation of the column leachate as a function of time	170
7.1 Sorption isotherms of ^{226}Ra (II)	184
7.2 Sorption isotherms of ^{210}Pb (II)	185
7.3 Sorption isotherms of ^{238}U (VI)	186
7.4 Sorption isotherms of ^{232}Th (IV)	187
7.5 Distribution functions of ^{226}Ra (II) and ^{210}Pb (II)	188
7.6 Distribution functions of ^{238}U (VI) and ^{232}Th (IV)	189
8.1 Zones of the maximum extent of SO_4 , ^{238}U , ^{226}Ra , ^{210}Pb and ^{230}Th contamination from the waste rock in the sand aquifer.	210
8.2 Activities and concentrations of dissolved radionuclides and chemical species along the proposed NW flow line, L-M10	211
8.3 Activities and concentrations of dissolved radionuclides and chemical species along the proposed NE flowline, M16-M19	212
8.4 Comparison between the measured sulphate concentration profile in groundwater along the L-M10 flowline in 1982 and the computed profiles	215
8.5 Molar ratios of (a) $\text{SO}_4/^{238}\text{U}$ and (b) $\text{SO}_4/^{226}\text{Ra}$ in groundwater samples along the NW flowline, L-M10 in 1982	218
8.6 pH variation in groundwater at site L with time	221
8.7 Mole percent distribution of dissolved U(VI), U(IV), Th(IV), Ra(II) and Pb(II) species along the proposed NW flowline, L - M10	224

Figure	Page
8.8 Saturation indices of minerals along the NW flow line from sites L to M10.	225
8.9 Schematic cross sectional diagram illustrating the sequence of geochemical events on the production and migration of waste-rock-derived leachate in the sand aquifer	230
8.10 Schematic diagram of the cell model	240
8.11 Mass balance equations	242
8.12 Activities of ^{238}U , ^{234}U , ^{226}Ra , ^{210}Pb and ^{230}Th in pegmatite/gabbro leachates as a function of pH	246
8.13 Progression of the acid front in groundwater downflow from site L in the sand aquifer as a function of time	247
8.14 K_d values of ^{226}Ra (II), ^{232}Th (IV) and ^{210}Pb (II) versus pH	248
8.15 K_d values of ^{238}U (VI) and ^{238}U (IV) versus pH	249
8.16 Longitudinal profiles of simulated and analytical activities of radium-226 in groundwater along the L-M10 flow line	251
8.17 Longitudinal profiles of simulated and analytical activities of lead-210 in groundwater along the L-M10 flow line	252
8.18 Longitudinal profiles of simulated and analytical activities of thorium-230 in groundwater along the L-M10 flow line	253
8.19 Comparison amongst the simulated longitudinal activity profiles of ^{230}Th , ^{210}Pb and ^{226}Ra at 25 years and 31 years along the L-M10 flow line	254
8.20 Longitudinal profiles of simulated and analytical activities of uranium-238 in groundwater along the L-M10 flow line	255
8.21 Longitudinal profiles of simulated and analytical activities of uranium-238	257

Figure		Page
8.22	Analytical and simulated uranium-238 longitudinal activity profiles downflow from site L	258
8.23	Effect of the number of cells on the simulation of ^{238}U (VI) and ^{226}Ra (II) activities in groundwater for a period of 25 years	260
9.1	Spatial distribution of the $^{234}\text{U}/^{238}\text{U}$ activity ratios (A.R.'s) in groundwater along cross sections A-A', B-B' and C-C'	266
9.2	Longitudinal profiles of the analytical activity ratios for $^{234}\text{U}/^{238}\text{U}$, $^{226}\text{Ra}/^{238}\text{U}$ and $^{210}\text{Pb}/^{238}\text{U}$ in groundwater in 1982 along the L-M10 flow line	270
9.3	Longitudinal profiles of simulated and analytical activity ratios (A.R.'s) of $^{234}\text{U}/^{238}\text{U}$ in groundwater along the L-M10 flow line	277

CHAPTER I

INTRODUCTION

1.1 Objective and Scope

Nuclear power is becoming a major source of energy. Almost 30 percent of the electricity that is generated in Ontario today comes from nuclear-power stations and it is projected that the use of nuclear power will increase even more in the future. One of the reasons for this is that the natural uranium fuel that is used in these power stations, is readily available from the Elliot Lake and Bancroft uranium mining districts in Ontario.

A schematic diagram of the Canadian nuclear fuel cycle is shown in Figure 1.1. As nuclear power production increases, there becomes a need for further development in the management and disposal of the ever-increasing volumes of radioactive wastes that are produced from the nuclear fuel cycle. In particular, research is needed to examine the long-term effects of the disposal of radioactive wastes on the environment. The production of radioactive wastes from the fuel cycle include very low-level wastes that are derived from the mining and milling operations of natural uranium ore, the low and medium level wastes from nuclear reactor operations and the high-level waste consisting of spent nuclear fuel. In comparison to the extensive research that is devoted to the disposal of spent nuclear fuel and associated low and medium level reactor wastes (Tomlinson, 1982), only a limited amount of research has been directed at assessing the effects on the environment of surface-deposited uranium mill wastes (e.g. Blair et al., 1980; Morin et al., 1982). No investigation of the release and subsurface migration of radionuclides from waste rock have been reported in the literature.

Waste rock from uranium mines generally has very low levels of radioactivity but commonly occurs in large volumes that are abandoned on terrain neighbouring the mine chutes. Unlike other forms of radioactive wastes, uranium mine wastes are not managed, as no precautions are imposed to shelter the waste rock from natural weathering. The weathering of waste rock in the

CANADIAN NUCLEAR FUEL CYCLE

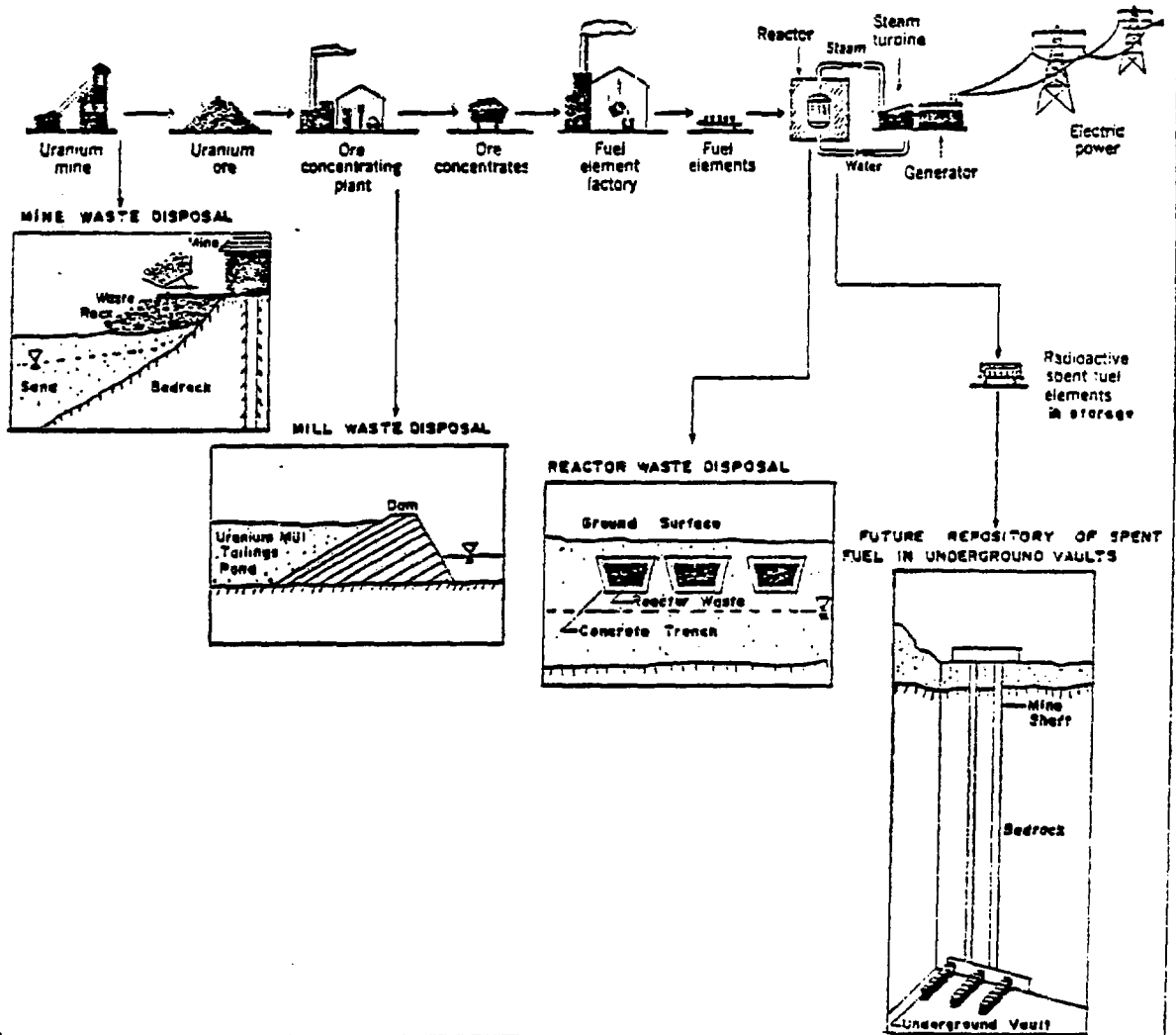


Figure 1.1 Canadian nuclear fuel cycle.

open atmosphere can result in the release of some long-lived and potentially hazardous radionuclides belonging to the natural uranium-238, uranium-235 and thorium-232 decay series (Veska, 1983) to the subsurface through the agency of groundwater.

The objectives of this investigation are: (1) to develop a radioanalytical method to enable the sequential determination of ^{238}U , ^{234}U , ^{232}Th , ^{230}Th , ^{226}Ra and ^{210}Pb in groundwater and other environmental samples, (2) to assess the present-day spread of chemical and radioactive contaminants that have been derived from waste rock in groundwater, (3) to assess the factors that affect the release of radionuclides by weathering from waste rock, and (4) to assess the suitability of laboratory-determined parameters in contaminant migration models for the simulation of the mobility of waste-rock-derived radionuclides in shallow groundwater in a sand deposit.

A field site was chosen for this study at an abandoned uranium mine site near Bancroft, Ontario, where waste rock was left on an unconsolidated sand deposit during the 1956-1959 period. The piles of the uranium-bearing waste rock have been undisturbed by man since 1960. It was expected that during the period of 1957 to 1982, weathering of waste rock had continually produced a leachate that contained radioactive and non-radioactive constituents. Because of the uncertainty as to the magnitude of the waste rock piles accumulated in 1956 in comparison to that in 1959, 1957 was chosen as the date for the initial production of the waste-rock-derived contaminants. For the past 25 years from 1957 to 1982, the leachate was carried downward into the shallow groundwater zone in a sand aquifer below the waste rock. Groundwater in the sand moves laterally from the waste rock towards a wetland about 125 meters away. An investigation of the distribution of radionuclides in this zone of primarily lateral flow provided a basis for comparison of actual radionuclide distributions with distributions simulated using laboratory-measured parameters and geochemical concepts. The radionuclides that are considered in this study are ^{238}U , ^{234}U , ^{230}Th , ^{226}Ra and ^{210}Pb of the natural ^{238}U decay chain and ^{232}Th . A general review of the physical and chemical behaviour of uranium, thorium, radium and lead in the environment is given in Veska (1983).

The factors that affect the natural release of radionuclides from waste rock were assessed in the laboratory as a means of characterizing the initial hydrogeochemical events in the migration of the waste-rock-derived radionuclides to the subsurface environment. Some of these factors include the surface area of the rock grains, the solid-liquid ratio, the mineralogical composition of the rock, the weathered and the unweathered types of rock surfaces and the interaction of rock with solutions of rainwater and groundwater from the field site. The effect of each of these factors on the degree of dissolution of radionuclides from the rock was determined by a batch leach procedure. Because the dissolution rate of radionuclides by a batch leach procedure was expected to be higher than that which occurs in nature, waste rock was also gradually leached by a column leach procedure. The combined results from the batch and column leach procedures were used in part to explain the present-day distribution of the chemical and radioactive constituents in groundwater found beneath and beyond the waste rock.

As radioactive contaminants in groundwater migrate laterally from the waste rock in the sand deposit, some radionuclides are strongly influenced by adsorption whereas other radionuclides are influenced by several geochemical processes, such as oxidation-reduction, precipitation-dissolution, complexation, ion pairing and adsorption-desorption. For the simulation of the present-day distribution of radionuclides in groundwater, two transport models, that have incorporated the effects of geochemical processes on the migration of radionuclides from waste rock in groundwater, were applied to the Greyhawk field problem. These two models were the advection-retardation model and the cell model. Both of these models are described in Chapter 2. The advection-retardation model is normally used when the geochemical effects on solute migration can be described by simple adsorption and/or ion exchange processes. The cell model is normally used when these and/or other geochemical processes are effective. In the application of both of these models to contaminant migration problems, the K_d parameter is utilized. K_d , known as the distribution coefficient, is a valid representation of the partitioning of a radioactive solute between the liquid and solid phases only if the reactions

that cause the partitioning are fast and reversible and only if the resulting sorption isotherm is linear. At the field site, linear sorption isotherms were expected for radionuclide species released from the waste rock to the underlying water table because of the low ionic-strength water produced from the natural weathering of the waste rock.

If equilibrium geochemical conditions exist for contaminant migration in the sand deposit along the flow path from the waste rock, then a constant K_d for a radionuclide can be applied in the advection-retardation model. If, however, the groundwater along the flow path from the waste rock is in dynamic chemical evolution, the K_d for a radionuclide is then expected to vary from one location to the next over a period of time (Reardon, 1981) and thus a constant K_d cannot be used in the advection-retardation model. In this type of situation, the cell model is more effective in the simulation of dynamic changes in the groundwater chemistry during flow.

Early in the field investigation, two major groundwater flow paths from the waste rock were identified. Along one flow path, the groundwater is predominantly a calcium-bicarbonate water that is relatively-pH constant. Because the K_d for a radionuclide is not expected to change significantly with distance along this flow path, the advection-retardation model was applied. The groundwater in the other flow path evolves from a pH 3.0 calcium-sulphate water beneath the waste rock to a calcium-bicarbonate water at a pH of 7.0 downflow from the waste rock. In this situation, the K_d for a radionuclide is not considered to be constant throughout the sand deposit. The relative mobility of the waste-rock-derived radionuclides along the latter flow path was simulated by a cell model that accounted for the variations in K_d with respect to changes in pH and the chemical composition of groundwater downflow from the waste rock.

The ^{234}U activity in groundwater was shown from the field investigation to increase progressively with respect to the ^{238}U activity downflow from the waste rock. The observed $^{234}\text{U}/^{238}\text{U}$ activity ratios in groundwater increased

to as high as 2.05 ± 0.19 from 0.80 ± 0.09 . Explanations for this phenomena in the relatively-young shallow groundwater could not be obtained from previous case studies dealing with ^{234}U fractionation in old groundwaters in deep confined aquifers (Chapter 2). Therefore, several mechanisms to explain the ^{234}U -enriched groundwater at Greyhawk were put forward and were tested. One test involved the application of K_d values of U(IV) and U(VI) in the cell model in the evaluation of the preferential migration of ^{234}U in comparison to ^{238}U due to differences in the distribution of the oxidation states of each atom. This particular test was considered important with regard to the assessment of the applicability of the K_d concept.

The objectives of this investigation were implemented by performing five main tasks, namely: (1) the development of a radio-analytical method to enable the sequential determination of ^{238}U , ^{234}U , ^{232}Th , ^{230}Th , ^{226}Ra and ^{210}Pb from a single sample of water, soil or rock; (2) the estimation of groundwater flow rates and the delineation of the spread of chemical and radioactive contaminants derived from waste rock in the groundwater zone at the field site; (3) the description of the contaminant release from the source material by rock leaching experiments; (4) the determination of the radionuclide partitioning between soil and groundwater by laboratory experiments; and (5) the assessment of the suitability of the laboratory-determined parameters in contaminant migration models for the simulation of the relative mobility of waste-rock-derived radionuclides in groundwater at the field site. The effort expended in each of the five tasks is briefly outlined below. Because no single comprehensive methodology was found for the analyses of the given suite of radionuclides, an analytical method for task 1 was developed from a combination of procedures described in the literature. The most common radioanalytical procedures that are found in the literature, are summarized in Veska (1983). Task 2 was accomplished by drilling holes in the granular overburden in areas downflow from the waste rock, by installing multilevel piezometers and water table wells in the drill holes and by

analysing the water pumped from the multilevel devices for natural and waste-rock-derived chemical and radioactive constituents. The experiments of task 3 entailed the leaching of waste rock with artificial solutions that represent rainwater and groundwater from the field site. For task 4, samples of uncontaminated soil from the field site and three types of simulated groundwater were equilibrated individually with known amounts of a radioactive standard for the determination of the batch K_d values. Laboratory batch K_d values were determined for uranium (IV), uranium (VI), thorium (IV), radium (II) and lead (II). The fifth task assessed the use of the laboratory-determined parameters in the transport models. These parameters included batch K_d values and the measured activities of extracted radionuclides in leachates from the rock leaching experiments. The assessments were made by comparing the simulated distances travelled by radionuclides downflow from the waste rock after 25 years with those found in the sand aquifer in 1982.

CHAPTER 2

LITERATURE SURVEY

2.1 Transport Models of Radionuclide Migration

The advection-dispersion equation is most widely used for the prediction of solute migration in the subsurface. For the case of a one-dimensional flux of a single solute through a saturated homogeneous granular porous medium, the equation is expressed as

$$\frac{\partial C}{\partial t} = \frac{\partial C}{\partial x} (D_0 \frac{\partial C}{\partial x}) - \bar{V}_0 \frac{\partial C}{\partial x} \quad (2.1)$$

where C is the concentration of the solute in solution, t is time, x is the space coordinate, D_0 is the hydrodynamic dispersion coefficient and V_0 is the average linear groundwater velocity. The advection-dispersion equation is particularly applicable to the migration of non-reactive solutes in porous media. For the migration of reactive radioactive solutes in porous media, several transport models have included a reaction term for geochemical mass transfer processes in the advection-dispersion equation. These models include the advection-dispersion-retardation model, the advection-retardation model and the cell model. Each of the three transport models are discussed in the following subsections.

2.1.1 Advection-Dispersion-Retardation Model

The one-dimensional form of the advection-dispersion-retardation model for homogeneous media is expressed as

$$\frac{\partial C}{\partial t} = \frac{\partial C}{\partial x} (D_0 \frac{\partial C}{\partial x}) - \bar{V}_0 \frac{\partial C}{\partial x} - \frac{\rho}{n} \frac{\partial S}{\partial t} \quad (2.2)$$

where $\frac{\partial S}{\partial t}$ is the rate at which the solute is absorbed in the porous medium, ρ is

the bulk density, η is the porosity and the other parameters have already been defined above. The three solute transport terms in equation 2.2 are advection ($\bar{V}_0 \frac{\partial C}{\partial x}$), hydrodynamic dispersion ($\frac{\partial C}{\partial x} (D_0 \frac{\partial C}{\partial x})$) and chemical reaction ($\frac{\rho}{\eta} \cdot \frac{\partial S}{\partial t}$).

Advection and hydrodynamic dispersion constitute the physical transport processes in the model for a migrating solute. Advection is referred to as plug or piston flow in porous medium that results from the bulk motion of flowing groundwater. Hydrodynamic dispersion influences the shape of the advecting solute front by a spreading phenomenon that results in a sigmoid-shaped front. This spreading phenomenon or dilution effect results from mechanical mixing due to microscopic processes and molecular diffusion (Freeze and Cherry, 1979). The hydrodynamic dispersion coefficient, D_0 , in equation 2.2, is determined from the relation,

$$D_0 = \alpha \bar{V}_0 + D^* \quad (2.3)$$

where α is the dispersivity of the porous medium and D^* is the coefficient of diffusion. Diffusion is considered important in equation 2.3 only at low velocities.

The chemical reaction term includes geochemical mass transfer processes that affect the amount of partitioning of a solute between liquid and solid phases in groundwater flow systems. Solute partitioning between liquid and solid phases is commonly derived from a series of batch equilibrium experiments under isothermal conditions and is expressed in the form of a sorption isotherm on a logarithmic graph paper. The isotherm defines the relationship of the solute concentration in solution, C , versus the solute concentration on the solids, S . From the reaction term in equation 2.2, it follows that

$$\frac{\rho}{\eta} \cdot \frac{\partial S}{\partial t} = \frac{\rho}{\eta} \cdot \frac{\partial S}{\partial C} \cdot \frac{\partial C}{\partial t} \quad (2.4)$$

where $\frac{\partial S}{\partial C}$ represents the solute partitioning between the liquid and solid phases

and is the slope of the isotherm. The isotherm shapes that are commonly encountered and their mathematical relationships are discussed by Golubev and Garibyants (1971) and Smith (1970). The most common isotherm found to successfully match experimental data by empirical means is the Freundlich isotherm as expressed by the equation,

$$S = KC^a \quad (2.5)$$

where K and a are empirical constants and S and C have previously been defined. The constant a, represents the slope of a log-log plot of S versus C. The Freundlich relation can be used to describe three different isotherm shapes. For example, when a is less than 1, the S/C ratio decreases with increasing C. When a is greater than 1, the S/C ratio increases with increasing C. In the case of a linear isotherm when $a=1$, the S/C ratio is constant and equilibrium conditions exist between the adsorption and desorption reactions.

A plot of the slope of the sorption isotherm from experimental data versus C is used as a means to examine further the solute distribution between the solid and solution phases. This plot is known as the distribution function, K_f . Differentiating equation 2.5 with respect to C,

$$K_f = \frac{dS}{dC} = KaC^{a-1} \quad (2.6)$$

and thus the equation for the Freundlich distribution function simplifies to

$$K_f = KaC^{a-1} \quad (2.7)$$

When $a=1$, the sorption isotherm is linear and K_f is represented as a horizontal line with respect to the C axis on a K_f versus C plot. For this special case, K_f is equal to an equilibrium constant for the solute reactions between the solid and solution phases. This constant is commonly known as the distribution coefficient, K_d .

Sorption isotherms are generally linear (eg. $a=1$) for trace levels of radioactive solutes. Wahlberg and Fishman (1962) applied the law of mass-action (or chemical equilibrium) of ion exchange to prove that the sorption isotherm is linear when the solute concentrations added in batch reactors are small compared to that of the concentration of the competing cation. Non-linear sorption isotherms were observed by Wahlberg and Fishman only when the concentration of the solute in solution far exceeded that of the competing cation concentration and when the amount of the adsorbed solute approached the cation exchange capacity of the soil.

In situations where the K_d concept is applicable in equation 2.2, the advection-dispersion-retardation model is modified as

$$\frac{\partial C}{\partial t} = \frac{\partial C}{\partial x} \left(D_0 \frac{\partial C}{\partial x} \right) - \bar{v}_0 \frac{\partial C}{\partial x} - \frac{\rho}{n} K_d \frac{\partial C}{\partial t} \quad (2.8)$$

Analytical solutions for this model and its related two- and three-dimensional forms are given by Baetslé (1967,1969) and Cleary (1978). The applicability of the advection-dispersion-retardation model to real systems was reviewed by Gillham and Cherry (1982). They found that accurate predictions have not been made by this model for the migration of reactive solutes in saturated laboratory columns of porous, homogeneous geological materials. The applications of this mathematical model to field-related problems, that have the added complexity of heterogeneity in the system, were expected to be entirely empirical (Gillham and Cherry, 1982). Although there are several limitations to the model, the alternative models for contaminant migration are either empirical and unrepresentative of the actual field conditions or more sophisticated but in the early stages of development (Gillham and Cherry, 1982).

2.1.2 Advection-Retardation Model

The advection-retardation model is becoming a widely-used transport model by hydrogeologists for the evaluation of contaminant migration in groundwater. This model is derived from the advection-dispersion-retardation equation by assuming negligible dispersion in the porous medium and the applicability of the K_d concept. The advection-dispersion-retardation equation, or equation 2.8, is rearranged to yield,

$$\frac{\partial C}{\partial t} = \frac{\partial C}{\partial x} \left(D \frac{\partial C}{\partial x} \right) - \bar{v} \frac{\partial C}{\partial x} \quad (2.9)$$

where

$$D = \frac{D_0}{1 + \frac{\rho}{n} \cdot K_d} \quad (2.10)$$

and

$$\bar{v} = \frac{\bar{v}_0}{1 + \frac{\rho}{n} \cdot K_d} \quad (2.11)$$

Equation 2.11 is known as the retardation equation and also the equation for the advection-retardation model. The advection-retardation model determines the retardation of the 50 percentile concentration point on a contaminant front emanating from a continuous source in porous medium. In some situations, a source can be discontinued and thus the flushing of low concentration groundwater through the previously-contaminated zone causes the contaminants to move as a cloud or slug through the flow system (Pickens and Lennox, 1976). For these situations, the advection-retardation model determines the retardation of the centre of the contaminant cloud or slug moving from the point source while undergoing processes of adsorption and desorption (Baetsle, 1969). A few

examples of the applicability of this simple model for the prediction of contaminant migration in subsurface environments are given by Higgins (1959), Baetsle (1967, 1969) and Grisak and Jackson (1978). The accuracy of the predictions made by these investigators was found to be dependent on the validity of the following assumptions: (1) that the dispersive process was negligible and (2) that the K_d was representative of the interactions between the solute and the porous medium.

2.1.3 Cell Model

Models that simulate the migration of a reactive solute in a flow regime with respect to dynamic changes in the groundwater chemistry are in the early stages of development. Because the advection-retardation model cannot be used to simulate accurately solute migration as a function of reaction progress in a flow regime, a conceptual model called the cell model has been developed for this purpose. Simpson (1973) defined the finite state cell model as a conceptual array of one or more interconnected mixing cells that represent a flow system by a sequence of finite states. For the case of a single mixing cell, there is a single input and single output. At each iteration, the injection of a given volume of input solute solution into the influent end of the cell causes the expulsion of an equal volume of the previous cell solution out of the effluent end of the cell. Simpson (1973) stated that the conservation of mass must be obeyed in each cell for each iteration. That is, the solute concentration within the cell at the present iteration is equal to the solute concentration within the cell from the previous iteration, plus the solute concentration entering the cell at the present iteration, minus the solute concentration leaving the cell at the present iteration. A time interval between the successive iterations is assigned to the model in order to relate the solute concentrations in each of the cells to time (Simpson, 1973).

Solute dispersion and retardation are also programmable into a cell model (Simpson, 1973). Dispersion is accounted for by assigning a fraction of the solute concentration in any one cell to be instantaneously placed downflow into the next cell. The fraction size depends on the dispersivity and the water

velocity in the porous medium. As for the effects of solute retardation in the porous medium, various fractions of the solute concentrations are assigned in the sorbed and solution states. These fractions are determined from the sorption isotherms for a particular solute.

The testing and application of a cell model in the simulation of solute transport through a laboratory soil column are given by Reynolds (1978). Reynolds had arranged the cells in a series that paralleled the column's flow path, with two impermeable cell boundaries for each cell normal to the flow lines. A set of recursive equations was used to perform a solute mass balance in each cell, i.e. beginning with the first cell and serially working downflow to the last cell. One of the main recursive equations was that for the sorption term as,

$$C = \frac{W}{R_f} \quad (2.12)$$

where C = mass of solute in solution in a given cell

W = total mass of solute in the cell (eg. the summation of the sorbed solute mass and the solution solute mass).

R_f = retardation factor, where $R_f = 1 + \frac{\rho}{n} \cdot K_d$

Reynolds (1978) tested the behaviour of the cell model by varying the number of cells, the retardation factor, dispersion factor and groundwater velocity. The more cells that were assigned in the model, the more the slope of the simulated breakthrough curve was found to increase and converge to a particular shape and degree of symmetry. Reynolds reported that the number of cells employed directly affected the degree of approximation of the answer. The accuracy of the approximation increased with the number of finite units employed until a certain end point was reached; thereafter, any increase caused model

breakdown. (Carberry and Bretton (1958) and Banks (1974) have developed equations for the determination of the number of cells and the length of each cell that are required to simulate a flow domain). The influence of the magnitude of the retardation factor (R_f) and the dispersion factor on the cell model was also investigated. For high values of R_f and K_d , the influence of dispersion on the shape of the breakthrough curve was negligible. As the R_f and K_d values decreased, the shape and position of the breakthrough curve were controlled by the dispersion factor. Different flow rates were found to have no effect on the shape of the breakthrough curves.

Reynolds (1978) also tested the results from the cell model with respect to the results from three solutions of the advection-dispersion-retardation model in the simulation of solute transport. These solutions were the finite difference model, the finite element model and an analytical solution. The main difference between the four models was that the cell model treated solute sorption separately from dispersion. For example, if the K_d 's for the solute were high, then dispersion and advection had little influence on solute movement. For the other three solutions, the velocity and dispersion terms were found to exert the controlling influence on the tracer migration in the porous medium, regardless of the magnitude of K_d .

The cell model developed by Grove and Wood (1979) was different from that developed by Reynolds (1978). The difference was that the Grove and Wood model employed equilibrium chemical routines of various mass transfer reactions and calculated values of ion-exchange selectivity coefficients from laboratory batch experiments. The K_d parameter was not included in the Grove and Wood model. Their model provided acceptable results for the prediction of solute migration in laboratory column experiments. Other successful applications of the cell model using continuous simulation modelling programmes to simulate experimental and field data are given by Van Beek and Pal (1978) and Dance and Reardon (1980).

2.2 Isotopic Disequilibria in the Uranium-238 Series

2.2.1 Introduction

Geological materials in closed systems older than ten million years contain activity ratios of $^{234}\text{U}/^{238}\text{U}$, $^{230}\text{Th}/^{238}\text{U}$, $^{226}\text{Ra}/^{238}\text{U}$ and $^{210}\text{Pb}/^{238}\text{U}$ that are equal to unity. This means that the daughter products of the uranium-238 series (Veska, 1983) are not fractionated from the parent, ^{238}U , and that a condition of secular equilibrium is attained within the system. Such equilibrium conditions exist ideally in permanently dry environments, such as on the moon (Fleisher, 1980). If, however, geological materials are brought out of the closed system and into a surficial environment, the material becomes exposed to weathering processes and to surface water and groundwater. This would cause the activity ratios of $^{234}\text{U}/^{238}\text{U}$, $^{230}\text{Th}/^{238}\text{U}$, $^{226}\text{Ra}/^{238}\text{U}$ and $^{210}\text{Pb}/^{238}\text{U}$ to depart from unity in the rock as well as in the resulting leachate. In other words, a state of disequilibria would exist amongst the members of the uranium-238 series. Once disequilibria in the uranium-238 series is attained in some material and then returned back into a closed system, the required time interval for equilibrium to be achieved again is approximately 2.5 million years.

2.2.2 Disequilibria in Hydrogeological Systems

Disequilibrium activity ratios (abbrev. as A.R.'s) of $^{234}\text{U}/^{238}\text{U}$ in nature were first noted by Cherdynstev et al. (1955). Since then, $^{234}\text{U}/^{238}\text{U}$ disequilibrium activity ratios in natural systems have been used for studies involving hydrogeology, age dating, marine chemistry and geochemical exploration (Thurber, 1962; Rosholt, 1958; Dooley et al. 1966; Osmond et al. 1974; Cowart et al. 1978; Cowart and Osmond, 1977; Titayeva and Veksler, 1977; Levinson and Coetzee, 1978; Kronfeld, 1974; Chalov and Merkulova (1969); Asikainen, 1981; Hussain and Krishnaswami, 1980). A review of the fractionation of ^{234}U in hydrologic systems is given by Osmond and Cowart, 1976. In comparison to the extensive literature on $^{234}\text{U}/^{238}\text{U}$ disequilibrium in groundwater regimes, little is reported on the disequilibria of $^{230}\text{Th}/^{238}\text{U}$, $^{226}\text{Ra}/^{238}\text{U}$ and $^{210}\text{Pb}/^{238}\text{U}$ in a similar environment.

Isotopic disequilibrium between ^{234}U and ^{238}U has been found in the hydrosphere to vary from 0.8 to 2.5 in terrestrial surface waters and between 0.5 to 12.0 in groundwaters (Osmond and Cowart, 1976). The extreme fractionation of ^{234}U that ranges from 4.0 to 12.0 in groundwater is generally found in old groundwater regimes in deep confined aquifers (Kronfeld 1974; Cowart and Osmond 1974). Previous investigations on these high $^{234}\text{U}/^{238}\text{U}$ A.R. in deep groundwaters on a regional hydrogeological scale have revealed that ^{234}U can serve as a natural isotopic tracer and hold the potential of defining groundwater movement, deep-water mixing and time transit (Szabo, 1982). In contrast, little or no attention has been given in the past to ^{234}U fractionation in relatively-young groundwater from an uranium source on a local hydrogeological scale.

2.2.3 Theories on the Fractionation of Elements in the Uranium-238 Series

With the exception of ^{234}U , the fractionation of the decay products in the uranium-238 series can be explained by the different chemical and physical properties in comparison to the parent, ^{238}U . In the case of ^{234}U , both ^{234}U and ^{238}U atoms behave the same chemically, and it would not be expected for fractionation of ^{234}U to occur. However, natural enrichments in ^{234}U rather than ^{238}U are normally found in water in contact with weathered uranium minerals (Cherdyntsev, 1971). In most case studies, the enriched ^{234}U water had left the rocks through which it had flowed, depleted in ^{234}U (Fleischer and Raabe, 1978). The common hypothesis for ^{234}U enrichment in water from surficial weathering of uranium minerals is by the decay-related oxidation theory (Cherdyntsev, 1971; Rosholt et al., 1965; Osmond and Cowart, 1976). Two different views on this theory are taken by Cherdyntsev (1971) and Rosholt et al., (1965). Cherdyntsev (1971) stated that some of the ^{234}U atoms were removed from the original positions in the uranium mineral by recoil during geological time and were relocated into crystal defects and microcracks, where it was liable to become more readily eliminated out of the mineral than the parent isotope, ^{238}U . Because of the selective exposure of the dislocated ^{234}U atoms in the mineral, ^{234}U became more readily oxidized

than ^{238}U under oxidizing conditions in the surface layers of the earth. In contrast, Rosholt et al. (1965) suggested another mechanism. For example, hexavalent ^{234}U atoms have been formed by the stripping of two electrons from recoil and bond breakage in the rock during geological time, and later, some of these atoms have been reduced back to U(IV) atoms by insitu reduction.

Regardless of the mechanism for ^{234}U fractionation in rocks, Kolodny and Kaplan (1970) have determined that approximately one-third of the decay-generated ^{234}U atoms within unweathered rocks is in the (VI) oxidation state, whereas the remaining two-thirds is in the (IV) oxidation state. These investigators have also determined that ^{238}U atoms in unweathered rocks are predominantly in the (IV) oxidation state. In a laboratory study, Chalov and Merkulova (1969) carefully separated U(IV) from U(VI) in secondary minerals by chemical means and found that the U(VI) fraction had a higher $^{234}\text{U}/^{238}\text{U}$ A.R. than the U(IV) fraction. Also, Chalov and Merkulova found that the external oxidation of uranium in the microscopic dislocations caused the $^{234}\text{U}/^{238}\text{U}$ A.R. to increase in the aqueous extract. The leaching experiments of uranium ore with various extractants by Umemoto (1973) showed a high $^{234}\text{U}/^{238}\text{U}$ A.R. at 1.357 in the leachate. With increased leaching time and fractional extraction of uranium in solution, the activity ratio in the leachate decreased to 0.886. Umemoto (1973) explained the high $^{234}\text{U}/^{238}\text{U}$ A.R. during the first set of extractions as being due to the leaching of the more easily extractable hexavalent ^{234}U atoms from the crystal lattice.

The degree of ^{234}U fractionation in water that can be explained by selective leaching of ^{234}U atoms from rocks are in the order of a few tens of percent. However, deep groundwaters such as the groundwater in the Trinity Aquifer in Texas, contain ^{234}U fractionation as great as 1200% (Kronfeld, 1974). Kronfeld (1974) explained the excess ^{234}U in the deep groundwater as the result of the production of ^{234}U atoms from the decay of the entrapped ^{234}Th and ^{238}U atoms in the sediments over geological time. Kronfeld's explanation was based on the experiments from Kigoshi (1971), who found that uranium separation could occur independent of leaching. Kigoshi suggested from his findings that the alpha-recoil ^{234}Th atoms that were ejected into groundwater from ^{238}U decay, had produced the excess ^{234}U .

2.3 Previous Studies at the Field Site

A survey was conducted on twelve mine waste disposal sites in the Bancroft uranium mining district in 1977 by the Department of Earth Sciences of the University of Waterloo. The purpose of this survey was to locate possible waste-rock sites for the study of migration of long-lived radionuclides in unconsolidated sand deposits (Gillham et al, 1978). The investigation revealed that the conditions at the abandoned Greyhawk mine site appeared to be the most favourable. The rationale for the selection of this site is because it contains two types of waste rock that vary in degrees of radioactivity and that have been exposed to weathering processes since 1956. Although the mine has been abandoned since 1960, the continuation of weathering of the waste debris to the present time has served as a natural source of radionuclides to the subsurface environment. The mine waste is situated on a sand aquifer that has desirable hydrogeological features for a study on the subsurface migration of the waste-rock-derived radionuclides.

The Greyhawk mine is situated on a large intrusive batholith, that consists mainly of pegmatitic granite and intruding gabbro (Lang et al, 1962). This batholith, which is located in the Grenville Province of the Canadian Shield, is of Precambrian age (i.e. an approximate age of 0.9-1.2 billion years (Woodford, 1965)).

At the field site, pegmatite is the major radioactive rock type, containing uraninite and uranothorite as the ore minerals (Lang et al, 1962). In fact, the Bancroft area contains the only deposits in Canada of the pegmatitic type that have produced uranium (Hewitt, 1978; Lang et al, 1962). Gabbro, the other predominant rock type at Greyhawk, contains visible pyrite grains and negligible amounts of radioactivity. No ore is generally found in the gabbro except in contact with the pegmatitic rock (Lang et al, 1962; Morse, 1971). A detailed description of the regional geology of the area is reported by Hewitt (1957, 1959) and Lang et al, (1962).

The regional topography and site location are shown in Figure 2.1 and the detailed surficial features of the study area are shown in Figure 2.2. The sand

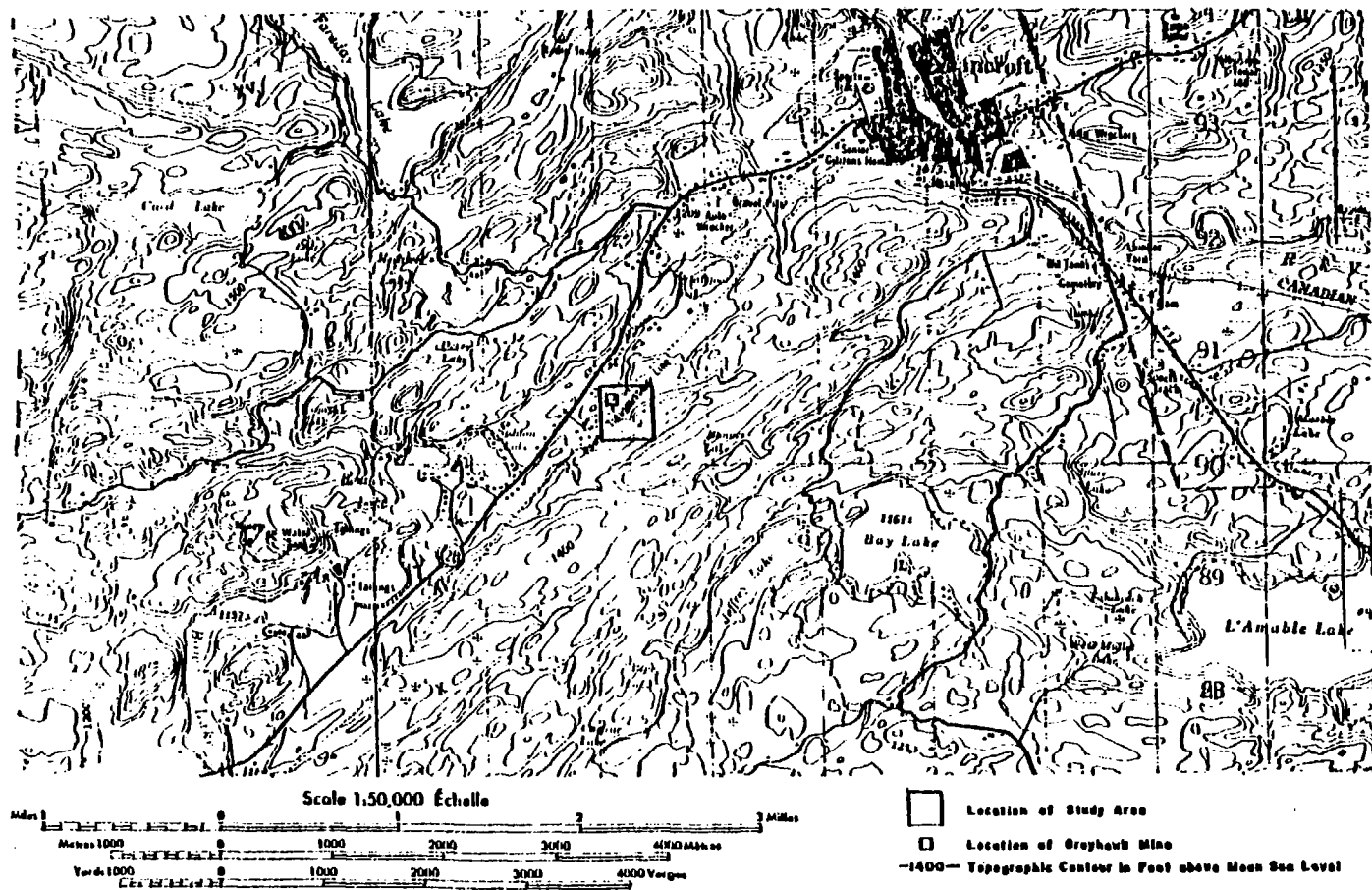


Figure 2.1 Regional topography and site location.

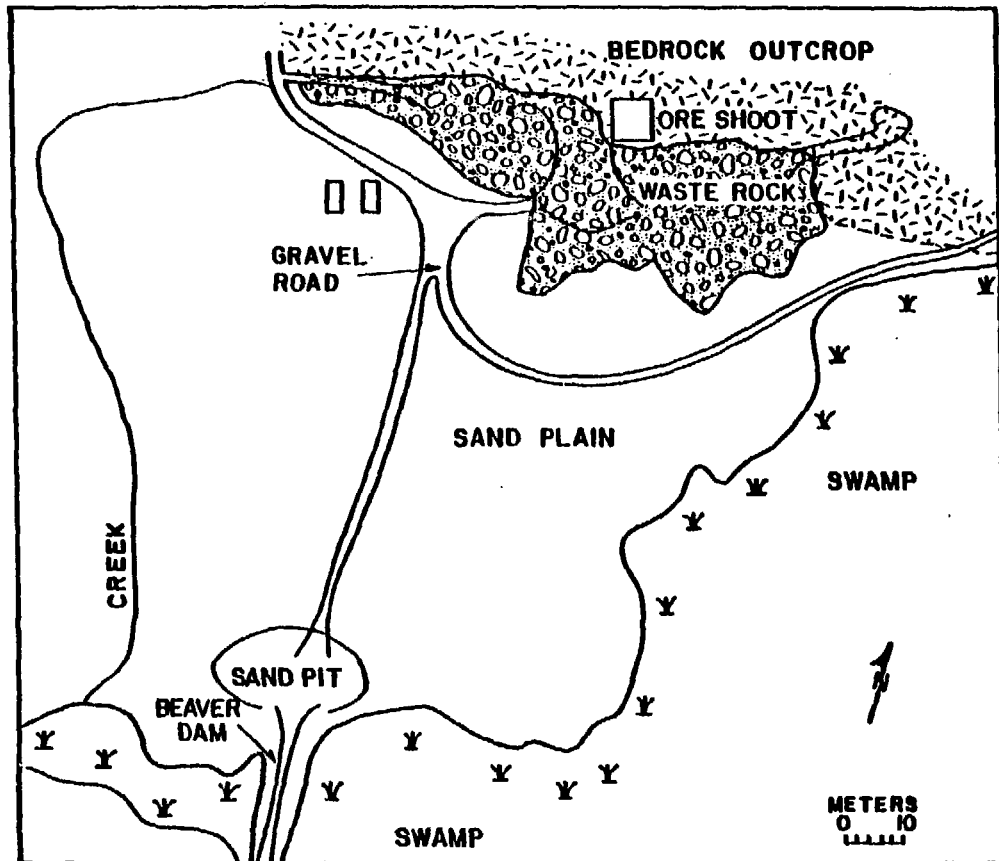


Figure 2.2 Map of study area showing surficial features. The ore shoot represents the location of the Greyhawk mine.

plain in Figure 2.2 is the principal geologic feature of relevance to the present study. The plain, with a surficial area of approximately 2.0 hectares, is bounded on the north by the waste rock and outcrop, on the east and south by the swamp and in the west by a small creek. The topography of the sand plain is generally of low relief, with a gentle slope towards the swamp area, which is the only major surface drainage feature in the study area. Because there was no visible evidence of surface channels caused by surface runoff and because the soil is quite permeable, it is reasonable to expect that nearly all of the precipitation that falls on the sand plain, except for water lost by evapotranspiration, recharges the groundwater zone in the sand deposit.

Uranium ore averaging 0.095 percent U_3O_8 , was removed from the Greyhawk mine from 1956 to 1959 and was transported to a nearby processing facility. The mine waste at Greyhawk, consisting entirely of pegmatitic and gabbroic waste rocks deficient in U_3O_8 (i.e. less than 0.01 percent), was dumped over the side of the bedrock outcrop onto the sandy plain. The piles of waste rock range from approximately three to five meters in total height. In addition, waste rock was discharged into the swamp at a point north-east of the study area and was also used in the construction of the gravel road across the sand plain (Figure 2.2).

Weathering of the waste rock at the site had been expected to effect the chemical composition of the underlying groundwater, as well as the surface water in the creek and swamp. Although the distributions of radionuclides in groundwater at the study area have not been previously investigated, the distributions of ^{226}Ra and uranium in the bottom sediments of the surface drainage system at the Greyhawk site have been investigated by Morse (1971). Morse found the ^{226}Ra activities and the uranium concentrations in the bottom sediments of the creek draining southwards from the waste rock (Figure 2.2), to decrease with distance from 7 to 4.5 pCi/g and from 33 to 12 ug/g, respectively.

With the exception of the Greyhawk site, Chamberlain (1964) investigated the distribution of uranium concentrations in surface waters adjacent to several uranium-mine waste dump sites in the Bancroft area. Chamberlain found high concentrations of uranium in surface waters in the vicinity of the waste dumps, as high as 720 ug/l, and less than two ug/l in surface waters downstream from the dumps.

The hydrogeochemistry of ^{226}Ra in the Bancroft area is reported in Ontario Water Resources (1965). Ontario Water Resources (1965) stated the mean ^{226}Ra activity in surface water at less than 3 pCi/l. ^{226}Ra activities as high as 106 pCi/l were found in some uranium mine-influenced groundwater samples.

CHAPTER 3

RADIOANALYTICAL METHOD

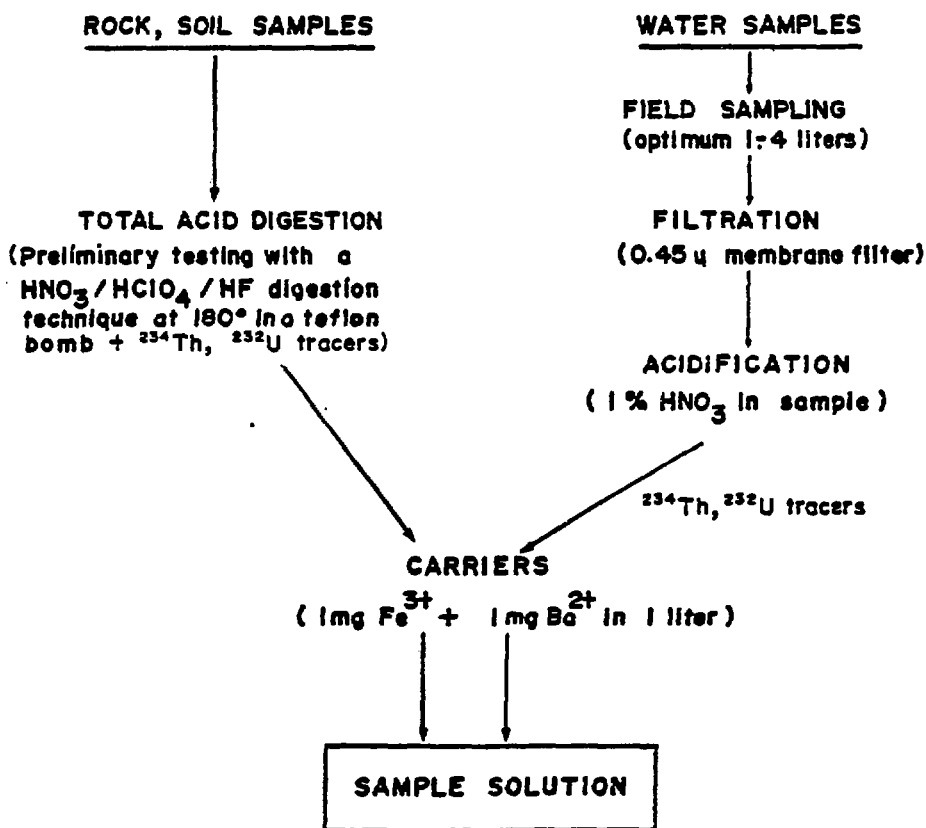
In order to map the activities of ^{238}U , ^{234}U , ^{232}Th , ^{230}Th , ^{226}Ra and ^{210}Pb in groundwater in the sand aquifer, it became desirable to develop a method for the sequential determination of these nuclides from a single groundwater sample. The literature contains several methods of analysis for each radionuclide of interest, as summarized in Veska (1983), and even methods for the sequential determination of two or more of these radionuclides (Sill, 1969; Sill, 1977; Thompson, 1973; Percival and Martin, 1974). However, no single comprehensive methodology could be found for the sequential determination of these radionuclides with the desired chemical recovery, accuracy, precision and sensitivity. Therefore, an effort has been made to develop such an analytical method.

3.1 Analytical Scheme

A method for the sequential determination of ^{238}U , ^{234}U , ^{232}Th , ^{230}Th , ^{226}Ra and ^{210}Pb in environmental samples has been formulated from a combination of various procedures that are given in the literature. The analytical scheme for this method is presented in stages in Figures 3.1, 3.2, 3.3, 3.4, 3.6 and 3.8. The scheme includes sample preparation techniques, radiochemical separation techniques of U, Th, Ra and Pb and then finally, radioanalytical determinations of each of the radionuclides of interest. The method is described in stages below.

The first stage includes the sample preparation techniques for groundwater, rock and soil samples as outlined in Figure 3.1. Because of the trace levels of activities of radionuclides that are generally found in groundwater, large volumes of filtered water are usually collected from a field site. After filtration of water through a $0.45\ \mu$ membrane filter, concentrated nitric acid along with 1 mg ferric and 1 mg barium carriers are added as preservatives to the sample. Enough nitric acid is added to decrease the pH of the water to pH

ANALYTICAL SCHEME



N.B. Acidified water samples stored for more than 30 days to ensure $^{210}\text{Pb}/^{210}\text{Bi}$ equilibrium

Figure 3.1 Stage 1: Sample preparation.

1.0. ^{234}Th and ^{232}U , as tracers, are added to the sample for monitoring the chemical recoveries of thorium and uranium. The acidified sample solution is stored for more than 30 days to ensure $^{210}\text{Bi}/^{210}\text{Pb}$ equilibrium within the sample. The reason for the storage time is that bismuth compounds tend to precipitate in the pH range of most natural waters and thus tends to create $^{210}\text{Bi}/^{210}\text{Pb}$ disequilibrium.

In the rock and soil sample preparation technique, solid samples are digested with a $\text{HNO}_3/\text{HClO}_4/\text{HF}$ mixture (5:5:10) along with ^{234}Th and ^{232}U tracers in a 75-ml volume teflon bomb at 180°C . After the digestion, the solution is evaporated to near dryness under a heat lamp to remove the $\text{HF}(\text{g})$ and $\text{SiF}_4(\text{g})$ gases. The contents are then dissolved in a solution containing dilute HCl and ferric and barium carriers. The recoveries of uranium and thorium from the bomb method range from 60 to 90%. Other digestion techniques are available in the literature but they have neither been tested nor applied in this investigation.

Next is the preconcentration stage for all the radioelements of interest as outlined in Figure 3.2. The sample solution is adjusted to pH of 3.0 by the addition of NH_4OH and is passed through a 1.7 cm x 10.0 cm cation exchange resin column with Dowex 50x8 resin (200-400 mesh), at a flow rate of 1.5 ml/min. All radionuclides of interest are retained in the column. Because the total cation exchange capacity in the 1.7 cm x 10.0 cm resin column is equal to 39 milliequivalents, the total amount of cations in the sample solution must be restricted to under 39 milliequivalents or a larger amount of resin must be taken. The exchange reactions that display the equilibria between the hydrogen ion and each of the radionuclides of interest are given in Figure 3.2.

After the adsorption of radionuclides on the cation exchanger, the following stage, as shown in Figure 3.3, consists of techniques for the separation of U, Th, Ra and Pb. A solution of 200 ml 12 M HCl is added to the cation exchange resin column to elute U, Ra, Pb and Bi. Thorium is not eluted by the 12 M HCl solution. Instead, thorium is subsequently eluted from the column with 200 ml of 0.5 M oxalic acid (Hyde, 1960). The exchange reaction of thorium in the presence of oxalic acid is shown in Figure 3.3.

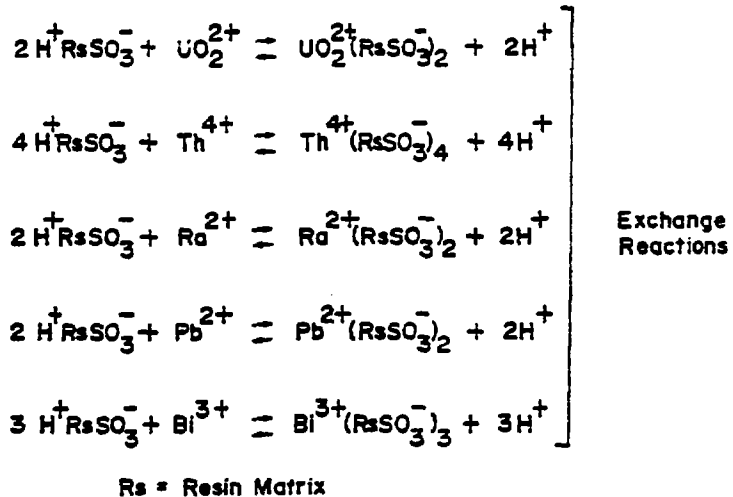
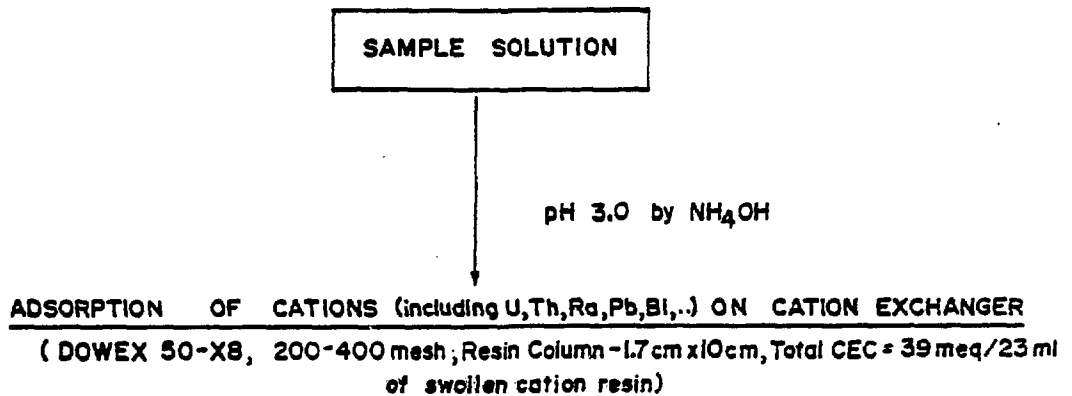


Figure 3.2 Stage 2: Preconcentration of elements on cation exchange resin.

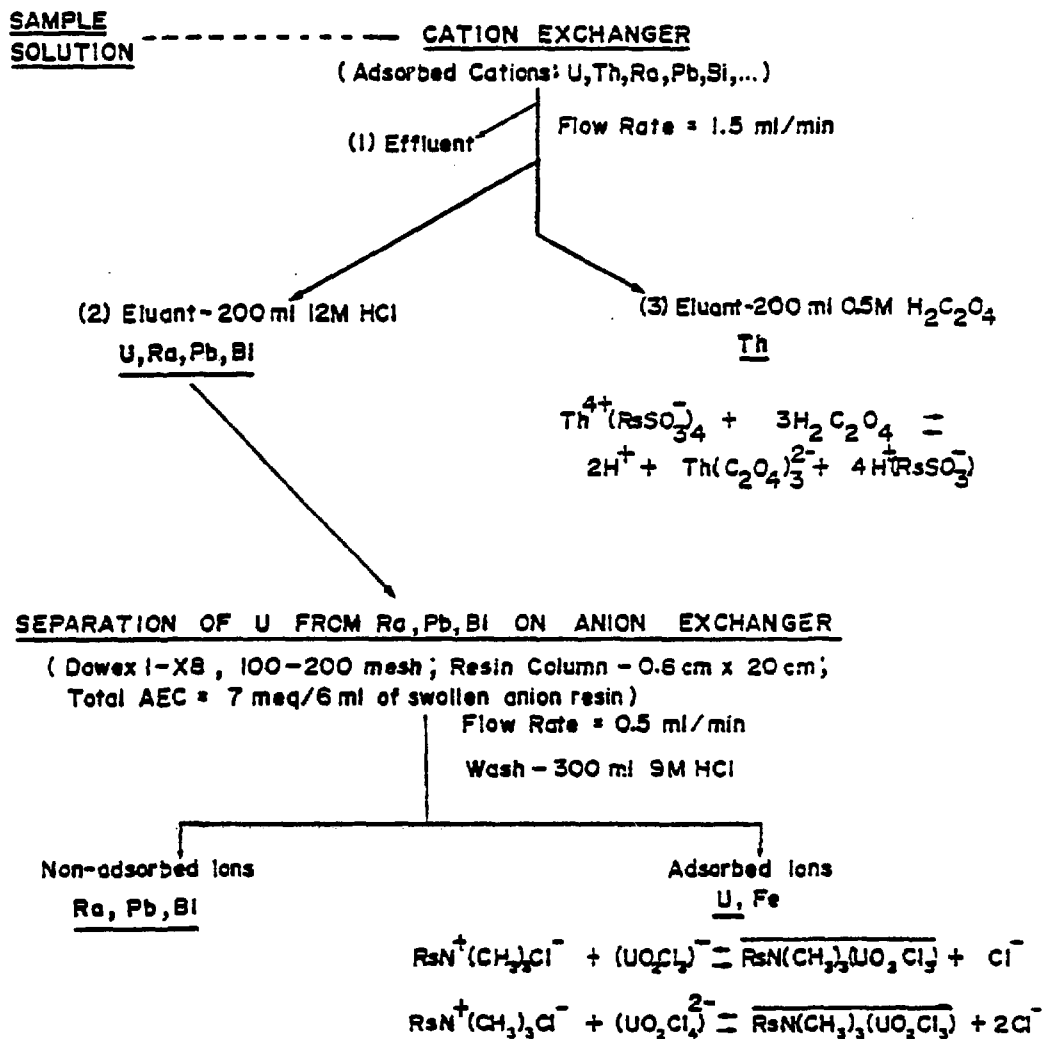


Figure 3.3 Stage 3: Separation of U, Th, Ra and Pb.

Because uranium exists as an anionic species in the concentrated HCl eluant and because these complexes are strongly adsorbed on anion exchange resins (Korkisch, 1969), uranium can be separated from Ra, Pb, Bi and other elements with the help of anion exchange resins. The solution containing U, Ra, Pb and Bi in the 12 M HCl eluant is passed through a 0.6 cm x 20.0 cm column that is pre-packed with Dowex 1-X8 (100-200 mesh) anion exchange resin. The column is then washed with 300 ml of 9N HCl. Uranium is retained on the resin in the form as shown in the exchange reaction in Figure 3.3. Ra, Pb, Bi and other ions, on the other hand, are eluted through the column at such high concentration of HCl. Ions such as Fe, Mn and Co, form anionic chloride complexes and are also retained in the resin along with uranium (Korkisch, 1969).

Stage 4 in the analytical scheme, as shown in Figure 3.4, is the purification and the radioanalytical determination of thorium. For the purification step of thorium, the solution containing the thorium oxalate eluant from the cation exchanger in stage 3 is repetitively oxidized with a mixture of nitric and perchloric acids and heat. Sodium bisulphate is added to the solution so as to prevent hydrolysis of Th^{4+} prior to evaporation of water from the sample. The residue is dissolved in 20 ml of 0.1 M HNO_3 and the pH of the resulting solution is adjusted to 1.5. Thorium is extracted from the pH 1.5 solution by shaking the solution with 20 ml of 0.25 M thenoyltrifluoroacetone (TTA) in benzene in a 125 ml separatory funnel for five minutes (Smithson et al., 1979). The reaction for this extraction is shown in Figure 3.4. Subsequently, the remaining thorium in the aqueous layer is extracted twice with additional 20 ml portions of the 0.25 M TTA-benzene extractant. The combined organic extracts containing the thorium complex are washed twice with 20 ml of 0.03 M HNO_3 . The time of shaking is two minutes for each wash. The thorium in the organic layer is then back extracted three times by contacting it with 20 ml of 2 M HNO_3 . The time of shaking is five minutes for each back extraction.

The preparation of a purified thorium source from the solution is carried out by electrodeposition using the Puphal and Olson (1972) technique. The thorium solution is evaporated to dryness with sodium bisulphate. The residue is then dissolved in 1.0 ml of 6 M HCl and a few drops of 1.0 M ammonium

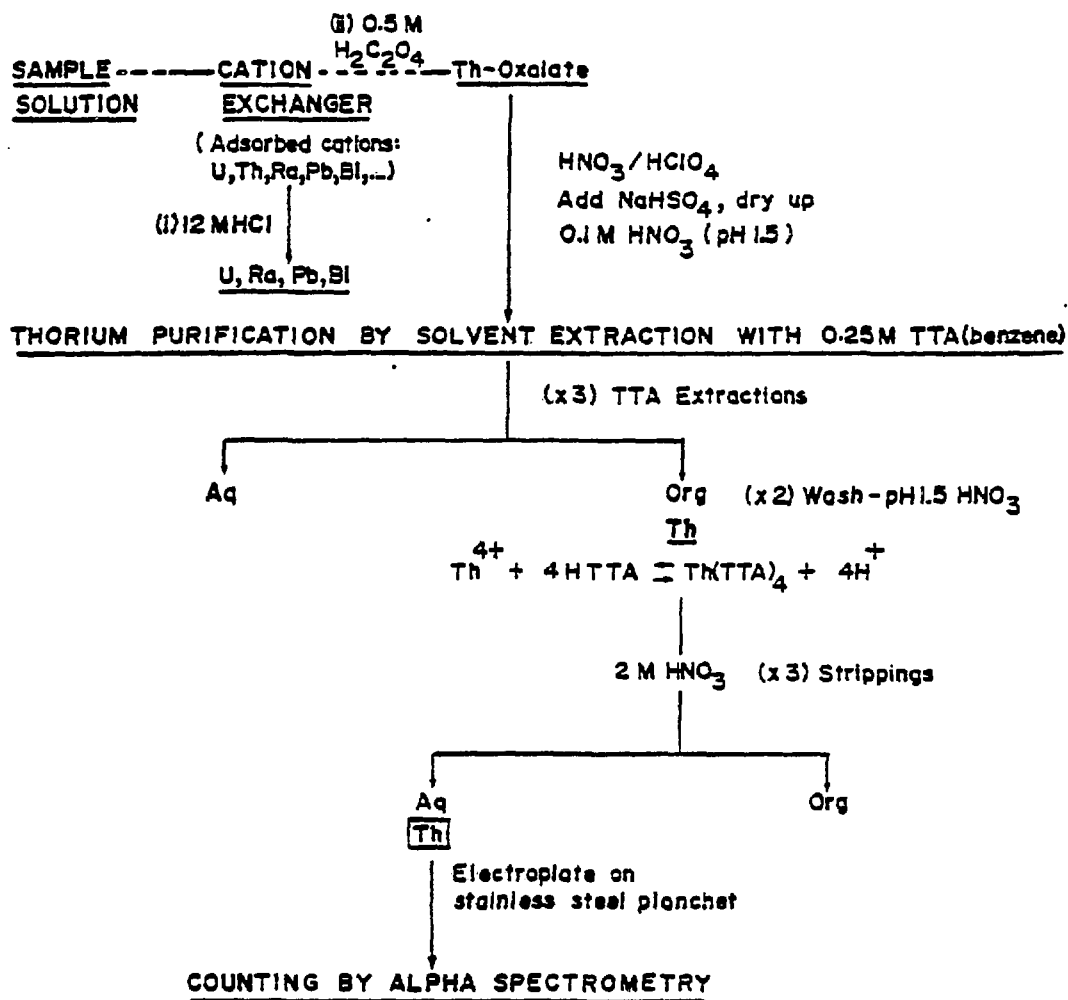


Figure 3.4 Stage 4: Thorium purification and radioanalytical technique.

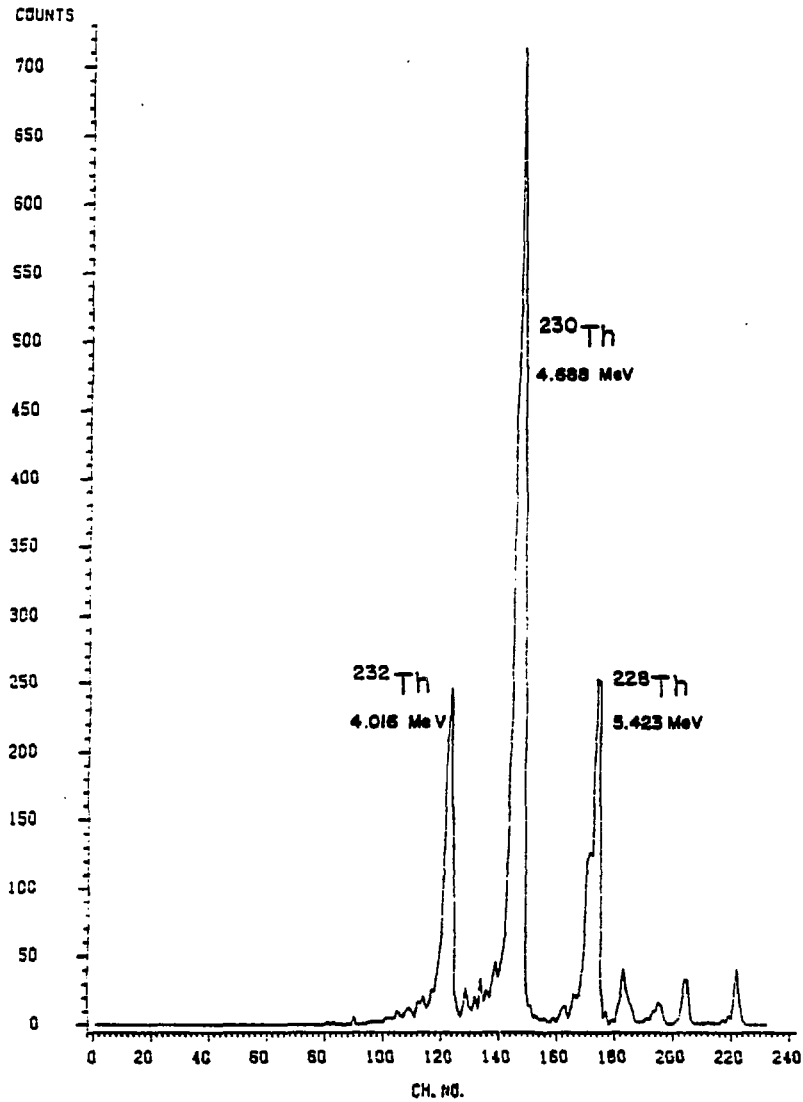


Figure 3.5 Alpha - particle spectrum of thorium isotopes;
alpha energy in million electron volts (MeV).

diethylenetriaminepentaacetate. The thorium solution is transferred to a electrodeposition cell containing a mixed oxalate-chloride electrolyte and a few drops of saturated hydroxylamine hydrochloride. Methyl red is used as an indicator for the pH adjustment of the solution to a pH of about 4.0. After the pH adjustment of the solution, the electrodeposition is started. Thorium hydroxide is deposited on a 3.0 cm diameter stainless steel planchet at 7.0 volts and at a current of about 1.5 amperes for two hours at room temperature.

The alpha activity of the plated sample due to ^{232}Th and ^{230}Th is assayed radioanalytically by alpha spectrometry. Alpha spectrometry is based upon the measurement of the energy of alpha particles emitted by radionuclides. For example, ^{232}Th emits 4.016 MeV alpha particles and ^{230}Th emits 4.688 MeV alpha particles. An example of a spectrum of alpha particles from thorium is shown in Figure 3.5. The alpha particles of each radionuclide are detected by an Ortec EA-21-45-100 partially-depleted silicon surface barrier detector with an active surface area of 450 mm². The detector gave a counting efficiency of 30%. The detector is connected to an Ortec 142-B preamplifier, and an Ortec 210 power supply, an Ortec 440 amplifier and a Nuclear Data Model 60 multichannel pulse height analyzer with 512 channels. The resolution of the alpha peaks from the spectrometer generally ranges from 50 to 150 KeV. The number of events due to alpha particles in the alpha particle energy spectrum is read by a Model 743 teletype terminal printer. The beta activity due to the ^{234}Th tracer in the plated sample is assayed with a Geiger Muller counter. The measurement of the ^{234}Th activity provides data for estimating the chemical recovery of thorium.

The procedure for the isolation of uranium is given in Figure 3.6. Uranium present in the anion-exchange column is eluted with 300 ml of 0.1 M HCl. The dilute hydrochloric acid solution also elutes iron. The concentration of iron in environmental samples is often high and therefore its presence in the sample would lead to a thick deposit upon evaporation, which is considered unsuitable

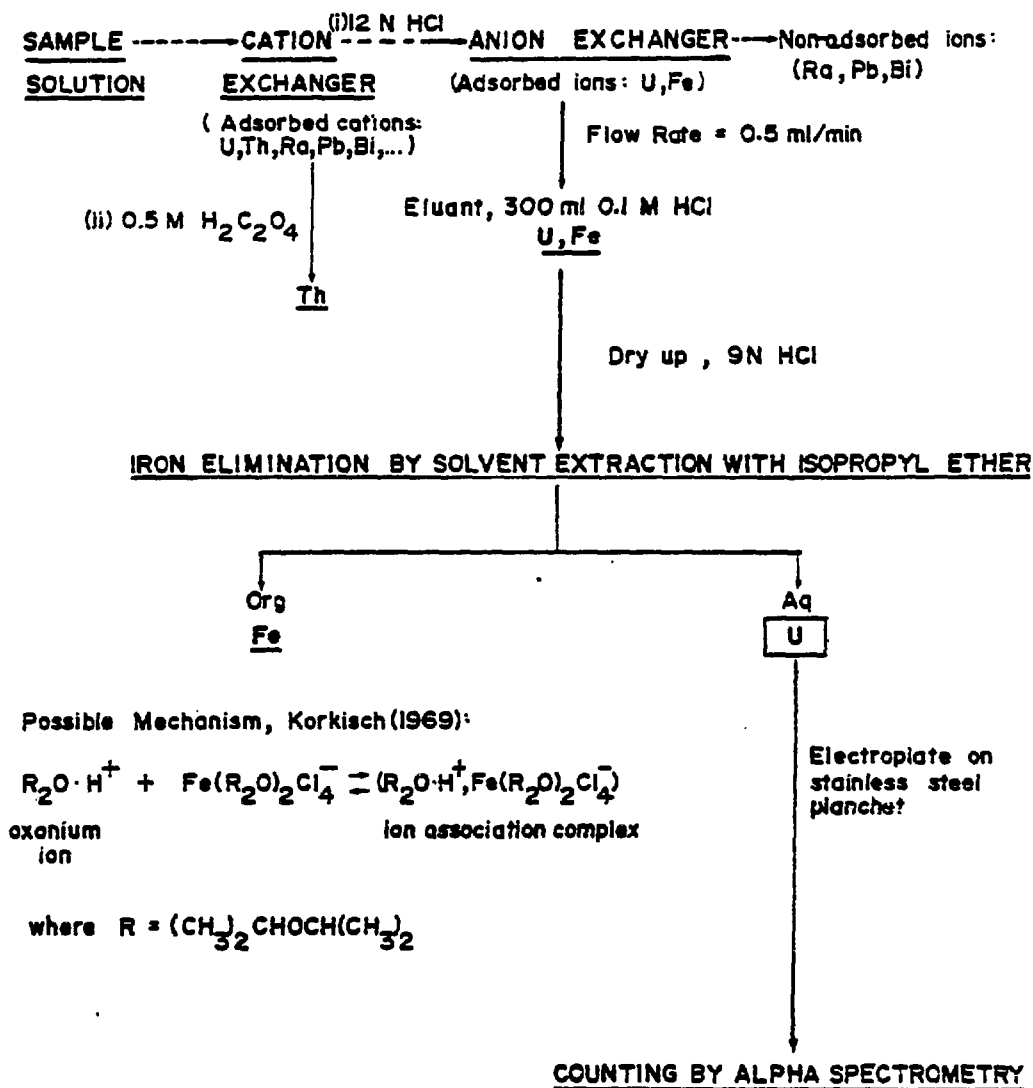


Figure 3.6 Stage 5: Uranium separation and radioanalytical technique.

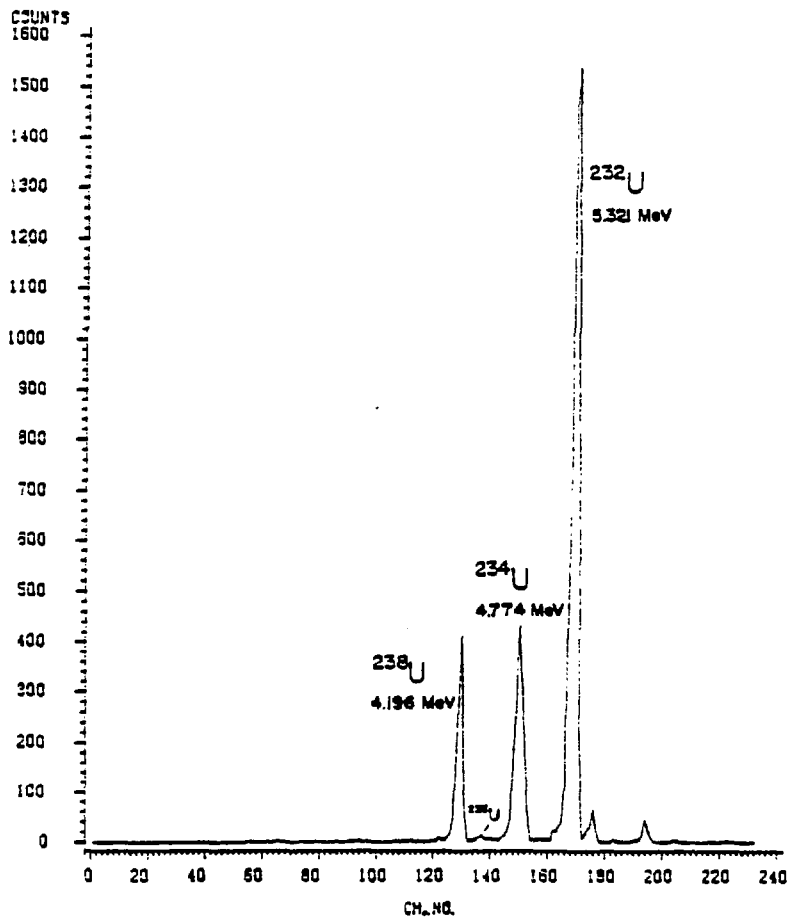


Figure 3.7 Alpha-particle spectrum of uranium isotopes; alpha energy in million electron volts (MeV). Alpha energy of ^{235}U = 4.401 MeV.

for alpha spectrometry. For example, the presence of iron in the assay of a source of uranium by alpha spectrometry results in a thick source which is considered unsuitable for resolving peaks of alpha particles from ^{238}U , ^{234}U and ^{232}U . Iron, therefore, is removed by extracting it from the aqueous solution by isopropyl ether. First, the 0.1 M HCl eluant from the anion exchange column is evaporated to near dryness, and subsequently, 30 ml of 9 N HCl is added. Fe(III) is extracted into 3 x 30 ml aliquots of isopropyl ether by contacting it for two minutes in a 250 ml separatory funnel. The extraction technique is in accordance with the procedure outlined by Thompson (1973). The organic layer containing Fe(III) is discarded. A possible mechanism for the elimination of Fe(III) into the ether layer as an ion association complex is given in Figure 3.6 by Korkisch (1969).

The uranium in the aqueous solution is evaporated to near-dryness after the addition of sodium bisulphate and then is transferred, along with a few drops of 1.0 M ammonium diethylenetriaminepentaacetate, to the electrodeposition cell containing a mixed oxalate-chloride electrolyte and a few drops of saturated hydroxylamine hydrochloride (Puphal and Olsen, 1972). The pH of the solution in the cell is adjusted to about 4.0 and subsequently, uranium is plated as a hydroxide on a 3.0 cm diameter stainless steel planchet at 7.0 volts and at a current of about 1.5 amperes for two hours at room temperature. The alpha activity of the plated sample due to ^{238}U , ^{234}U and ^{232}U is assayed using alpha spectrometry. An example of an uranium spectrum is shown in Figure 3.7. The alpha activity due to the ^{232}U tracer present in the plated sample, provides information for the estimation of the chemical recovery of uranium.

The steps for the separation of Ra from Pb and Bi are shown in Figure 3.8. The 12 M HCl solution after the passage through the anion-exchange column, contains Ra, Pb and Bi. The solution is evaporated from about 500 ml to approximately 30 ml and is subsequently diluted to 60 ml. This procedure results in having 3 M HCl in the solution. One microgram of inactive lead

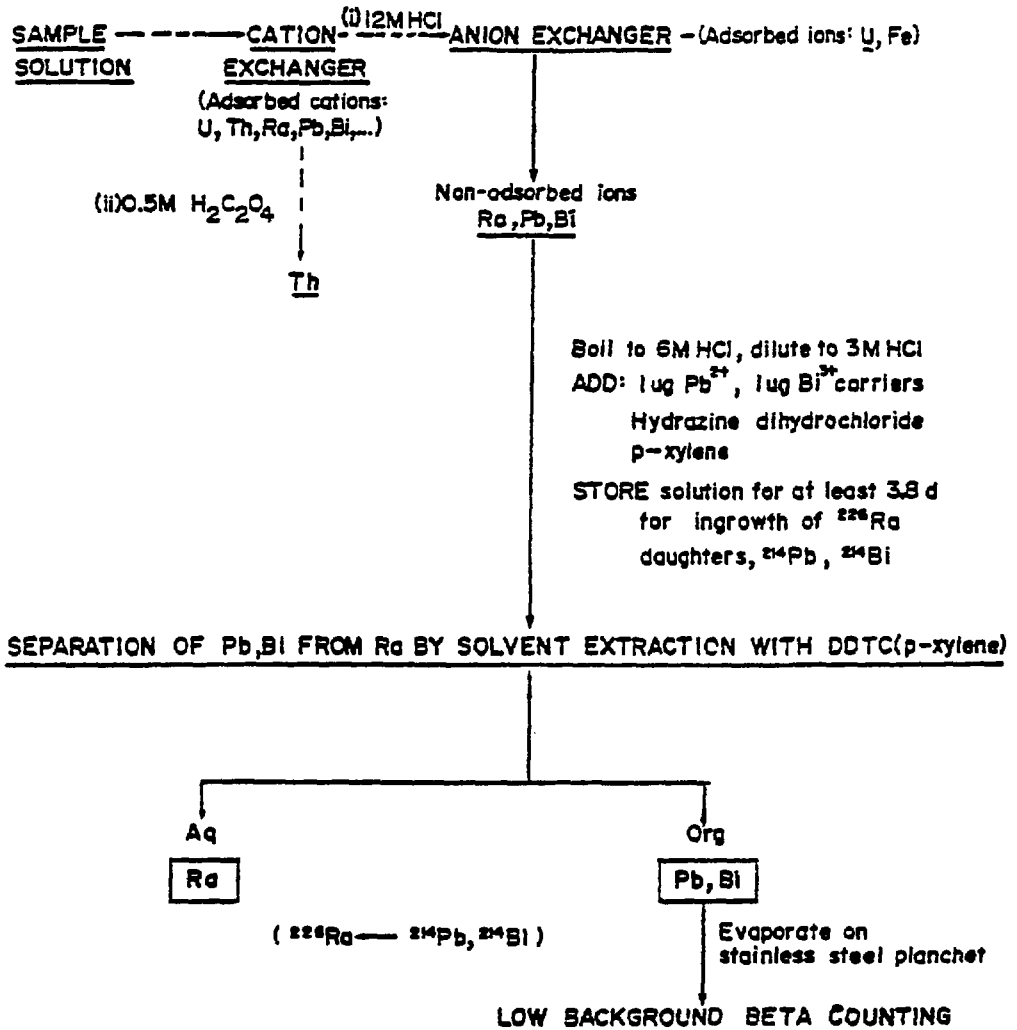


Figure 3.8 Stage 6: Radium-226 and lead-210 determinations.

carrier and one microgram of inactive bismuth carrier, along with hydrazine dihydrochloride and about 1.0 ml of p-xylene are added to this solution. The solution is stored for approximately one week in a sealed container. After the ingrowth period of one week or more, lead and bismuth in the stored solution are extracted in diethylammonium diethyldithiocarbamate (DDTC), leaving radium in the aqueous phase. The organic fraction containing ^{214}Pb , ^{214}Bi , ^{210}Pb and ^{210}Bi , is evaporated on a planchet and is counted within 20 minutes after the initial separation of lead and bismuth from radium. The elapsed time between the initial time of extraction and the initial time of counting is recorded. The total beta activity due to ^{214}Pb , ^{214}Bi , ^{210}Pb and ^{210}Bi on the planchet, is counted using the Canberra Model 2200 ultra low background proportional counter. The detector efficiency of the counter is approximately 30%. Four hours after the end of the DDTC solvent extraction, the same planchet is again counted using the proportional counter. At this time, the activity due to the short-lived isotopes of ^{214}Pb and ^{214}Bi has decayed away, leaving ^{210}Pb and ^{210}Bi on the sample. The activity of ^{226}Ra in the sample is determined by following the decay and growth equations. The details on the ^{226}Ra and ^{210}Pb calculations are summarized below and also in Veska (1983).

The principle of the calculations in the determination of ^{226}Ra involves the ingrowth of its daughters, ^{222}Rn , ^{218}Po , ^{214}Pb and ^{214}Bi . The details of the calculations are outlined in equations 3.1.1 to 3.1.7 inclusively in Veska (1983). The value of A_T , representing the decay of ^{214}Pb plus the decay of ^{214}Bi plus the production of ^{214}Bi from the decay of ^{214}Pb , is integrated from the time elapsed to the time elapsed plus the time of counting in equation 3.1.1. After integration and assuming $^{214}\text{Bi}/^{214}\text{Pb}$ equilibrium, the activity due to ^{226}Ra can be determined from the activity of ^{214}Pb and the time of ingrowth. The ^{226}Ra activity in the sample is obtained by multiplying the ^{226}Ra activity by a constant value representing the chemical recovery of radium in this procedure (eg. 90-100%). Similarly, the activity of ^{210}Pb is calculated by multiplying the ^{210}Pb activity by a constant value representing the chemical recovery of ^{210}Pb in this procedure (eg. 90-100%).

3.2 Accuracy and Reproducibility Tests

The analytical scheme in the determination of the activities of uranium, thorium, radium and lead isotopes in environmental samples was tested for accuracy and reproducibility. Standard solutions of ^{238}U , ^{232}Th , ^{210}Pb and ^{226}Ra were made separately into one liter volumes of 0.1 N HCl. Aliquots from these solutions were evaporated on stainless-steel planchets and analyzed radiometrically. Activities of ^{238}U , ^{232}Th and ^{226}Ra on the planchets were analyzed by alpha spectrometry whereas the planchet with the ^{210}Pb activity was analyzed by the proportional counter, ie. assuming $^{210}\text{Bi}/^{210}\text{Pb}$ equilibrium. An example of the alpha spectrum of ^{226}Ra is given in Figure 3.9. The procedures of the analytical scheme were followed through for each of the radionuclide determinations in aliquots taken from the standard solutions. After the completion of the analyses, values of the mean, standard deviation, coefficient of variation and relative error were calculated for each group of determinations. These calculated values for the ^{238}U , ^{232}Th , ^{210}Pb and ^{226}Ra determinations are given in Tables 3.1, 3.2, 3.3 and 3.4, respectively. The standard deviation, σ , is defined from the equation,

$$\sigma = ((1/(N-1)) \sum_{i=1}^N (x_i - \bar{x})^2)^{1/2} \quad 3.1$$

where, N = number of measurements

x_i = observed measurement

\bar{x} = mean of a number of observed measurements

The reproducibility, R, is related to the precision of the determination and is expressed here as the coefficient of variation at the 95% confidence level, as

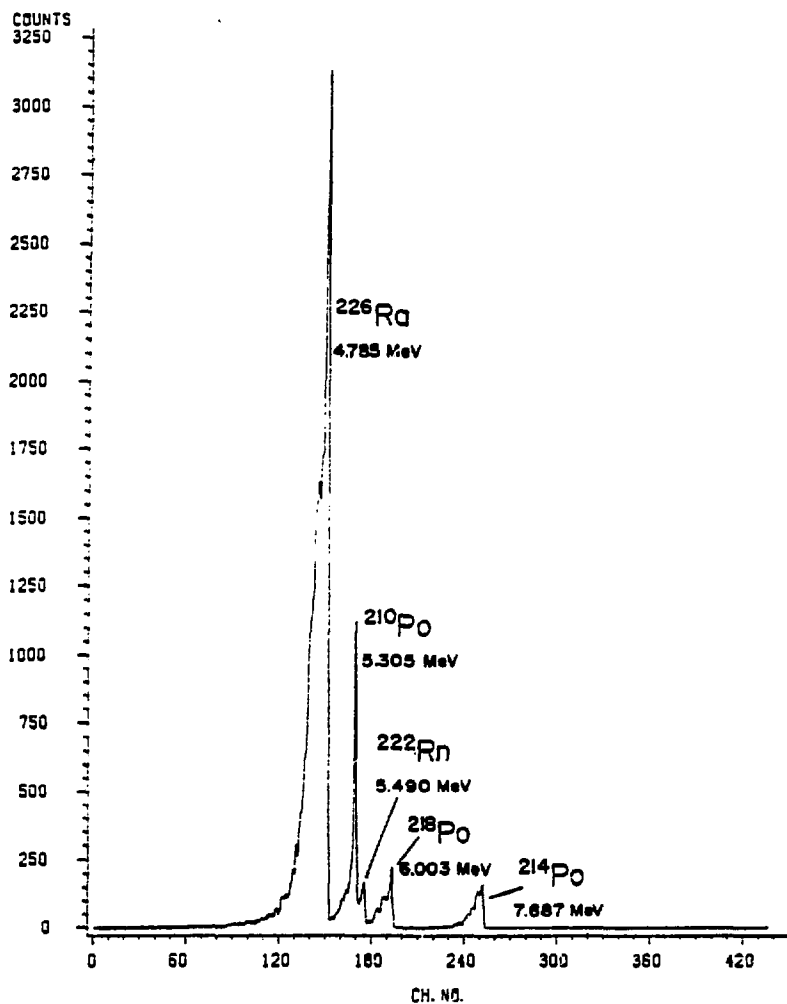


Figure 3.9 Alpha-particle spectrum of ^{226}Ra and daughters; alpha energy in million electron volts (MeV).

TABLE 3.1
ACCURACY AND REPRODUCIBILITY TESTS WITH ^{238}U STANDARD

Sample Number	^{238}U Added ,ug	^{232}U Recovery ,%	^{238}U Recovered ,ug	Percentage ^{238}U Recovery
1	109.0 \pm 2.1	41	104.2 \pm 3.2	96%
2	109.0 \pm 2.1	89	102.5 \pm 2.2	94%
3	109.0 \pm 2.1	74	97.4 \pm 2.4	89%
4	109.0 \pm 2.1	71	103.1 \pm 2.5	95%
5	109.0 \pm 2.1	89	94.0 \pm 2.1	86%

MEAN = 100.2 ug

STANDARD DEVIATION = 4.4 ug

REPRODUCIBILITY @ 95% CONFIDENCE = 9%

RELATIVE ERROR = -8%

TABLE 3.2ACCURACY AND REPRODUCIBILITY TESTS WITH ^{232}Th STANDARD

Sample Number	^{232}Th Added ,ug	^{234}Th Recovery ,%	^{232}Th Recovered ,ug	Percentage ^{232}Th Recovery
1	258.5 \pm 2.0	38	251.5 \pm 6.5	97%
2	258.5 \pm 2.0	36	226.6 \pm 6.4	88%
3	258.5 \pm 2.0	14	254.3 \pm 10.7	98%
4	258.5 \pm 2.0	27	234.1 \pm 7.4	91%

MEAN = 241.6 ug

STANDARD DEVIATION = 13.4 ug

REPRODUCIBILITY @ 95% CONFIDENCE = 11%

RELATIVE ERROR = -7%

TABLE 3.3
ACCURACY AND REPRODUCIBILITY TESTS WITH ^{210}Pb STANDARD

Sample Number	^{210}Pb Added , pCi	^{210}Pb Recovered , pCi	Percentage ^{210}Pb Recovery
1	68.5 ± 1.4	61.7 ± 1.3	90%
2	68.5 ± 1.4	66.1 ± 1.4	97%
3	68.5 ± 1.4	65.6 ± 1.4	96%

MEAN = 64.47 pCi

STANDARD DEVIATION = 2.41 pCi

REPRODUCIBILITY @ 95% CONFIDENCE = 8%

RELATIVE ERROR = -6%

TABLE 3.4ACCURACY AND REPRODUCIBILITY TESTS WITH ^{226}Ra STANDARD

Sample Number	^{226}Ra Added , pCi	^{226}Ra Recovered , pCi	Percentage Recovery	^{226}Ra
1	24.5 ± 1.0	23.8 ± 1.5	98%	
2	24.5 ± 1.0	24.4 ± 1.5	100%	
3	24.5 ± 1.0	24.0 ± 1.5	98%	

MEAN = 24.07 pCi

STANDARD DEVIATION = 0.31 pCi

REPRODUCIBILITY @ 95% CONFIDENCE = 3%

RELATIVE ERROR = -2%

TABLE 3.5
ACCURACY AND REPRODUCIBILITY TESTS WITH ^{226}Ra STANDARD

Sample Number	^{226}Ra Added , pCi	^{226}Ra Recovered , pCi	Percentage ^{226}Ra Recovery
1	135.0 \pm 1.9	133.8 \pm 1.5	99%
2	135.0 \pm 1.9	122.0 \pm 1.8	90%
3	135.0 \pm 1.9	129.0 \pm 1.6	96%

MEAN = 128.3 pCi

STANDARD DEVIATION = 5.93 pCi

REPRODUCIBILITY @ 95% CONFIDENCE = 9%

RELATIVE ERROR = -5%

TABLE 3.6

REPRODUCIBILITY TESTS WITH GROUNDWATER SAMPLE A-5.8

	^{226}Ra pCi/l	^{210}Pb pCi/l	^{238}U pCi/l	^{234}U pCi/l	$^{234}\text{U} / ^{238}\text{U}$ A.R.
x_1	3.4 ± 0.4	<0.5	2.09 ± 0.08	2.15 ± 0.08	1.03 ± 0.05
x_2	3.7 ± 0.4	<0.5	2.33 ± 0.08	2.71 ± 0.09	1.16 ± 0.06
x_3	3.3 ± 0.4	<0.5	2.51 ± 0.08	2.52 ± 0.09	1.00 ± 0.05
x_4	3.5 ± 0.4	<0.5	2.26 ± 0.08	2.37 ± 0.09	1.05 ± 0.05
x_5	3.2 ± 0.4	<0.5	2.10 ± 0.08	2.27 ± 0.09	1.08 ± 0.06
\bar{x}	3.4	-	2.26	2.40	1.06
σ	0.19	-	0.17	0.22	0.06
C.V.	11%	-	15%	18%	12%

where $x_1, x_2 \dots$ sample numbers

\bar{x} mean

σ standard deviation

C.V. coefficient of variation at the
95% confidence level

TABLE 3.7
REPRODUCIBILITY TESTS WITH GROUNDWATER SAMPLE L

	^{226}Ra , pCi/l	^{210}Pb , pCi/l	^{238}U , pCi/l	^{234}U , pCi/l	$^{234}\text{U} / ^{238}\text{U}$ A.R.	^{232}Th , pCi/l	^{230}Th , pCi/l
x_1	12.5 ± 1.6	14.4 ± 1.1	39.11 ± 1.45	38.11 ± 1.47	0.98 ± 0.05	0.42 ± 0.17	2.47 ± 0.39
x_2	11.6 ± 1.7	15.2 ± 1.1	34.89 ± 1.16	32.01 ± 1.14	0.92 ± 0.05	0.48 ± 0.14	2.19 ± 0.29
x_3	11.3 ± 1.7	15.0 ± 1.1	36.00 ± 2.80	32.18 ± 2.65	0.90 ± 0.10	0.52 ± 0.12	2.37 ± 0.26
x_4	10.2 ± 1.7	14.9 ± 1.1	30.90 ± 1.15	29.49 ± 1.16	0.95 ± 0.05	0.47 ± 0.12	2.33 ± 0.26
x_5	11.3 ± 1.7	13.2 ± 1.1	35.50 ± 1.90	35.30 ± 2.10	0.99 ± 0.08	0.55 ± 0.09	2.21 ± 0.19
\bar{x}	11.38	14.5	35.28	33.42	0.95	0.49	2.31
σ	0.82	0.81	2.94	3.34	0.04	0.05	0.12
C.V.	14%	12%	16%	20%	8%	20%	10%

where x_1, x_2, \dots sample numbers

\bar{x} mean

σ standard deviation

C.V. coefficient of variation at the
95% confidence level

$$R = (2\sigma/x)100\%$$

3.2

The accuracy of each determination is referred to as the relative error, E, where

$$E = ((\bar{x} - \text{True } x)/\text{True } x)100\%$$

3.3

The values of relative error for ^{238}U , ^{232}Th , ^{210}Pb and ^{226}Ra are listed in Tables 3.1 to 3.4 inclusively at -8%, -7%, -6% and -2% respectively. A relative error value at 0% for both ^{238}U and ^{232}Th was expected because of the ^{232}U and ^{234}Th tracers which were added to monitor the chemical recoveries. The variations between the added amounts and the recovered amounts for ^{238}U and ^{232}Th in Tables 3.1 and 3.2 can be explained due to counting statistics. The coefficient of variation values for ^{238}U , ^{232}Th , ^{210}Pb and ^{226}Ra , as shown in Tables 3.1 to 3.4, are 9%, 11%, 8%, and 3%, respectively. Values of the coefficient of variation and relative error appear to be the lowest in the case of the ^{226}Ra determination. However, in another ^{226}Ra reproducibility and accuracy test, an increase in the original, initial amount of the ^{226}Ra was found to increase the values of the coefficient of variation to 9% and the relative error to -5%. These results are shown in Table 3.5.

Reproducibility tests were also carried out for the determinations of ^{226}Ra , ^{210}Pb , ^{232}Th , ^{230}Th , ^{238}U , ^{234}U and the $^{234}\text{U}/^{238}\text{U}$ A.R. in aliquots of natural groundwater samples taken from the field site. Two groundwater sample types that contained high and low activities of radionuclides were chosen from the site, i.e. samples L and A5.8, respectively. The reproducibility results for each determination are given in Tables 3.6 and 3.7. The coefficient of variation values from each of the radionuclide determinations show no significant difference between the two groundwater types in these tables. For example, the values of the coefficient of variation for ^{226}Ra , ^{238}U , ^{234}U and $^{234}\text{U}/^{238}\text{U}$ A.R. are 11%, 15%, 18%, and 12% in sample A5.8 and 14%, 16%, 20% and 8% in sample L. The values of the coefficient of variation for ^{210}Pb , ^{232}Th and ^{230}Th in sample L are 12%, 20% and 10%.

The detection limits for the determination of the uranium isotopes, thorium isotopes, ^{226}Ra and ^{210}Pb in groundwater were calculated. The equation used to calculate these detection limits is given by Smithson et al.(1979) as follows:

$$\text{LLD} = 4.66 \frac{(N)^{1/2}}{t} \quad 3.4$$

where LLD = lower limit of detection (cpm)

N = total number of background counts in time, t (min)

The detection limits for the analyses of ^{238}U , ^{234}U , ^{232}Th , ^{230}Th , ^{226}Ra and ^{210}Pb in natural waters by this analytical scheme are 0.1, 0.1, 0.1, 0.1, 0.5 and 0.5 pCi, respectively.

3.3 Summary

An analytical method, formulated from a combination of previous-reported procedures, has been proven successful in the sequential determination of ^{238}U , ^{234}U , ^{232}Th , ^{230}Th , ^{226}Ra and ^{210}Pb from a single sample of natural water, soil or rock. For the determination of these radionuclides in natural waters, the relative error is less than 10% for activities greater than 20 pCi/l and the coefficient of variation ranges from approximately 5% to a maximum of 20% for activities greater than 2 pCi/l. The detection limit for the isotopes, ^{238}U , ^{234}U , ^{232}Th , ^{230}Th , is 0.1 pCi. The detection limit for ^{226}Ra and ^{210}Pb is 0.5 pCi.

CHAPTER 4

HYDROGEOLOGY OF THE FIELD SITE

The first major stage in the delineation of the spread of waste-rock-derived contaminants in the groundwater was an investigation of the site hydrogeology. This investigation took place during the period from 1978 to 1982. This chapter describes the hydrogeological findings during the four year period, including the instrumentation, the hydrostratigraphy, the directions and velocity estimates of groundwater flow and the identification of groundwater sources and age. The directions and velocity estimates of groundwater flow provided the necessary components of input for the contaminant analyses and modelling in Chapters 8 and 9.

4.1 Methods of Investigation

To determine the directions of groundwater flow in the sand aquifer and to provide means for groundwater sampling at the site, a network of water-table monitoring wells and multilevel sampling devices was installed in the sand deposit. During 1978 to 1979, 44 water-table wells, 11 deep piezometers and 28 multilevel samplers were placed in the sand aquifer at locations shown in Figure 4.1. An additional 19 multilevel samplers, as indicated by the M-series (ie. from sites M1 to M19) in Figure 4.2, were installed in May 1982.

Each water table well consisted of 3.2 cm ID, Schedule 40 PVC pipe, with the bottom 0.3 m slotted and wrapped with nylon screen and masking tape. Because of the shallow depth to the water table, the wells were installed in holes that were augered by hand to a depth of about 3.0 m to the water table. The water-table wells were used to determine the general direction of shallow groundwater flow in the sand deposit.

A CME Model 55, truck-mounted auger drill was used to drill holes in the sand aquifer in order to determine the depth to bedrock, to obtain split-spoon samples and to install deep piezometers and multilevel samplers. Split-spoon

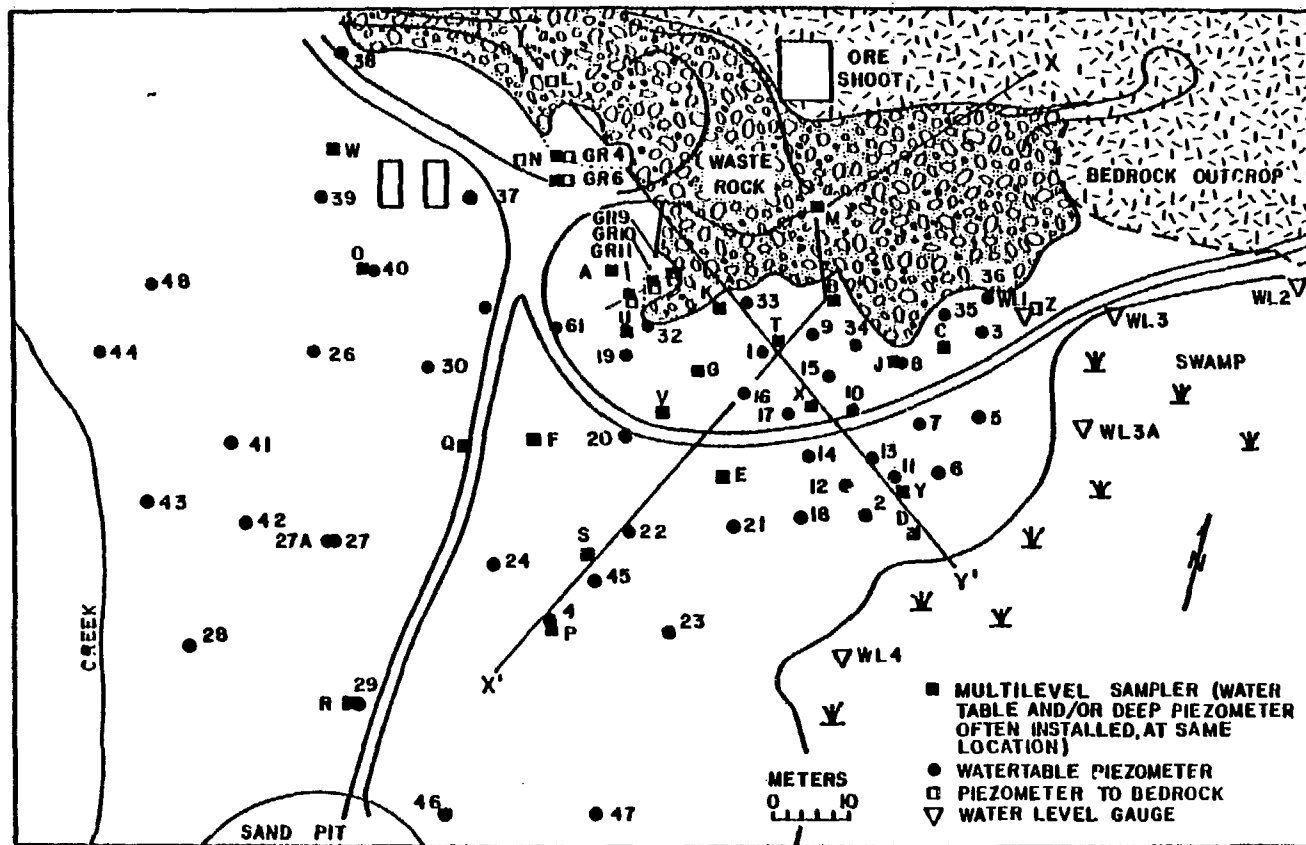


Figure 4.1 Map of the study area showing the locations of instruments installed at the site.

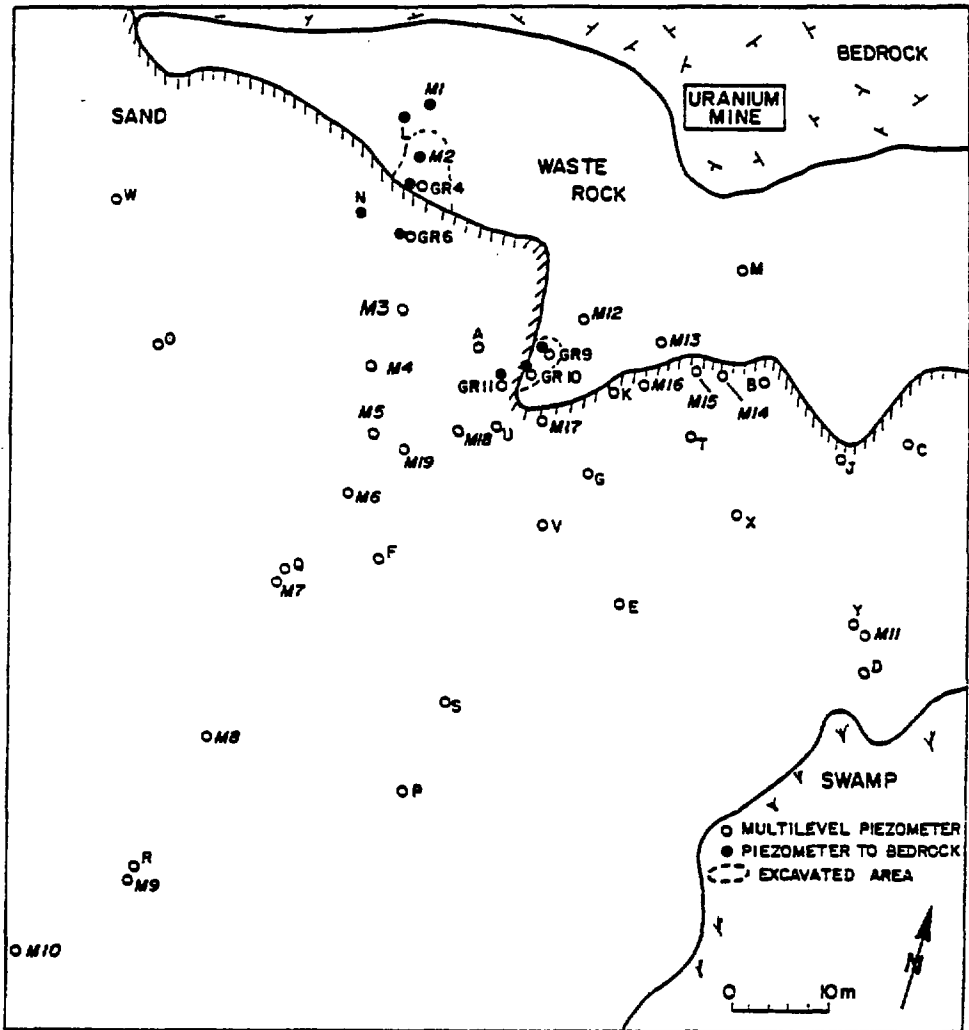


Figure 4.2 Location of multi-level piezometers. The M-series piezometers from sites M1 to M19, inclusively, were installed in 1982.

samples were collected at vertical intervals of 1.5 m at some sites for visual inspection of the stratigraphy of the sand deposit. The deep piezometers consisted of 3.2 cm ID, Schedule 40 PVC pipe with the bottom 0.3 m section slotted and wrapped with nylon screen and tape. These deep sampling points ranged in depth from 15 to 25 meters below ground. During the 1978 to 1979 installation period, the multilevel samplers consisted of a 6.1 m centre tube of 1.27 cm ID Schedule 80 PVC pipe. The bottom 0.2 m of the pipe was perforated with holes and wrapped with nylon screen and masking tape. Eight to ten lengths of 0.64 cm ID Tygon tubing were taped to the centre tube and each tube was terminated at a different depth to give a vertical sampling interval of approximately 0.5 m. Each tube was fitted with a screened sampling tip approximately 9 cm in length. Before installation, most multilevel samplers had moist bentonite packed around the sampling tubes between successive sampling tips. The bentonite was held in place by wrapping with a coarse fabric material. This was to prevent vertical circulation of groundwater along the sampling device. In 1982, multilevel samplers of a different type were installed. Each of these consisted of eight to ten lengths of 0.95 cm I.D. polyethylene tubing instead of the 0.64 cm I.D. Tygon tubing. The tubes were taped around the 1.27 cm I.D. PVC pipe. The length of PVC pipe was selected to equal the maximum depth of drilling for that site. Each 0.95 cm I.D. polyethylene tube was terminated at a different depth to give vertical sampling intervals equally spaced between the water table and the maximum depth of drilling. The deepest piezometer installed in 1982 was 27.5 m below ground surface. Bentonite packings were not used in the 1982 multilevel installations. A typical multilevel installation is shown in Figure 4.3. The multilevel devices and the deep sampling points were used to obtain water samples for field geochemical measurements, to obtain water samples for laboratory analysis and to provide measurements of the hydraulic head.

Groundwater and sand samples were also collected below the waste rock. A bulldozer was brought onto the site in September, 1979, to excavate the waste

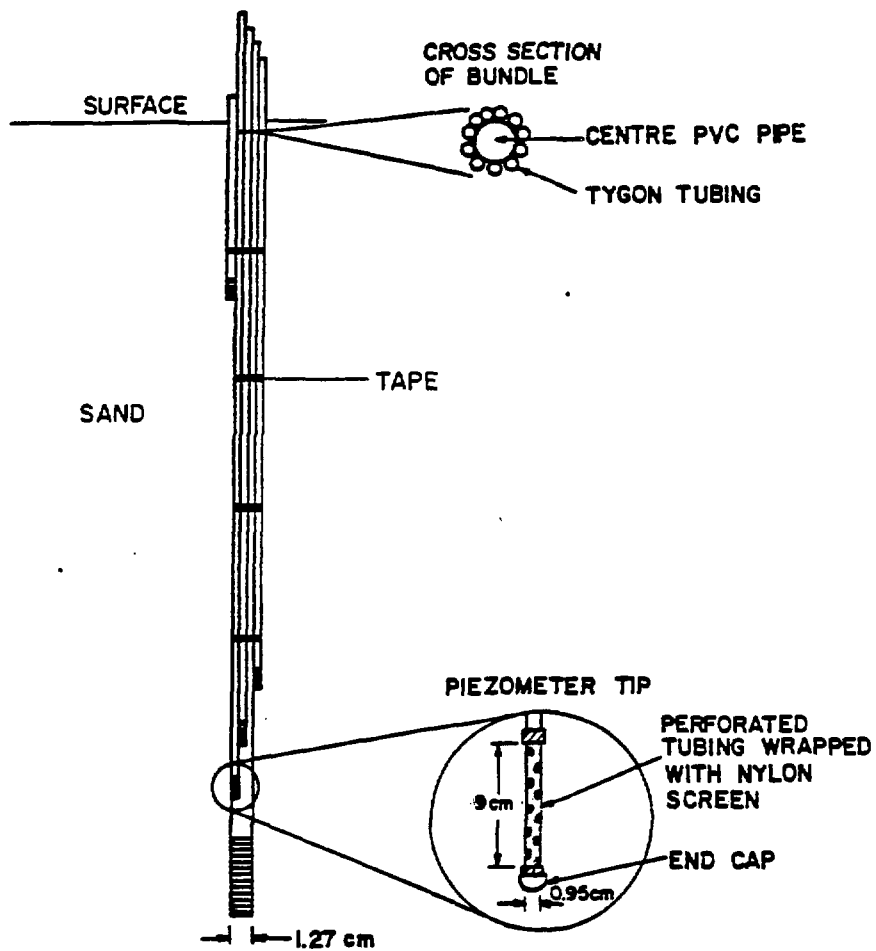


Figure 4.3 Schematic illustration of a typical multi-level groundwater sampling installation.

rock from two locations. One location was in an area of pegmatitic and gabbroic rock near piezometer L (Figure 4.1), while the other was in an area of pegmatitic rock near piezometer A (Figure 4.1). The excavations exposed the top of the sand deposit for a lateral distance of about 5 m inward from the original outer edge of the rock pile. Continuous core samples were collected from the ground surface to bedrock. Cores were obtained in aluminum tubes driven into the sand, followed by removal with the use of jacks. To prevent the core material from falling out of the tube, suction was applied to the top of the tubes when the tubes were jacked out of the ground. Multilevel groundwater sampling devices and piezometers were installed at core-sampling locations GR9, GR10, GR11, GR4 and GR6 (Figure 4.1).

4.2 Hydrostratigraphy

Two hydrostratigraphic cross sections, X-X' and Y-Y', in Figure 4.4, the locations of which are shown in plan view in Figure 4.1, show the depths of some of the multilevel and deep samplers and give an indication of the slope of the bedrock surface towards the swamp. The depth to bedrock surface increases rapidly with distance from the bedrock outcrop, being in excess of 21 m at a distance of about 60 m from the outcrop.

In most of the study area, medium to fine-grained sand extends from the maximum depth of drilling to the ground surface. The upper part of the sand unit (about 1.0 m) was light yellow to light brown in colour, whereas at greater depths the sand was uniformly dark grey. The change in colour occurred near the water table and undoubtedly reflects a change in the redox condition with depth. Examination of the split-spoon and core samples showed the sand to be very heterogeneous, with distinct horizontal layers. The horizontal layering was believed to represent a complex array of lenses rather than continuous layering. The medium to fine sands were found to grade to a silty-fine sand in the north-west sector of the study area. The silty-fine sand in this sector showed considerable heterogeneity in the vertical direction. The sand aquifer

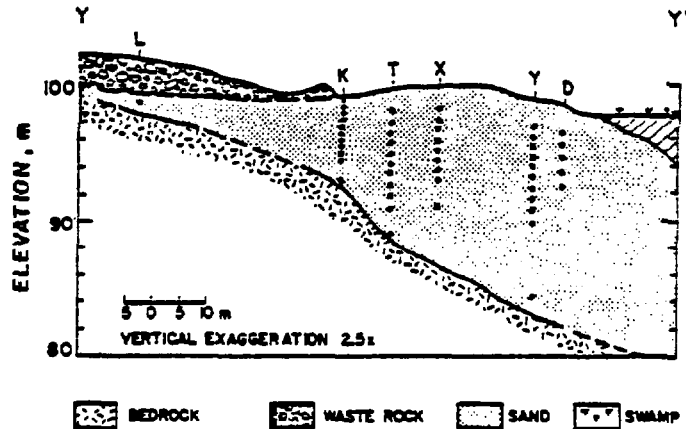
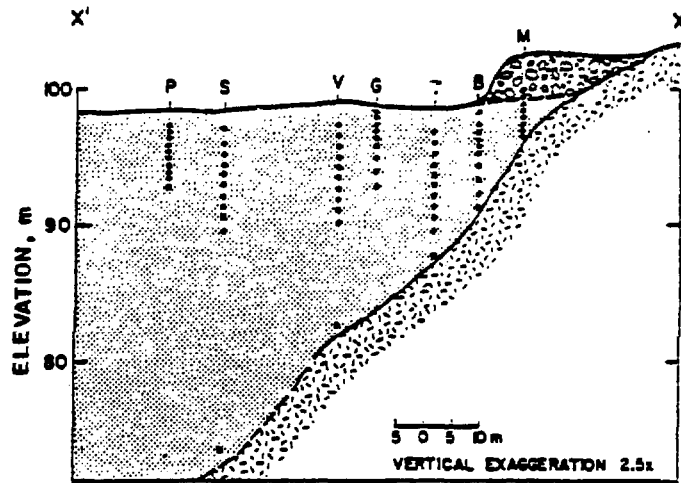


Figure 4.4 Hydrostratigraphic Cross Sections X-X' and Y-Y'.

is believed to be glacial fluvial in origin.

Measurements of hydraulic conductivity in the aquifer have been made by single piezometer response tests using the Hvorslev (1951) method. The tests were performed by Clarke (1980) in the medium to fine sands of the central region of the study area. Hydraulic conductivity values determined from these slug tests ranged from a low of $1.91 \times 10^{-4} \text{ cms}^{-1}$ to a high of $1.61 \times 10^{-3} \text{ cms}^{-1}$.

4.3 Hydraulic Gradients and Groundwater Flow Direction

The general direction of groundwater flow was derived from the measurement of the water-level elevations in the water-table wells. Water-level measurements with an accuracy of $\pm 0.2 \text{ cm}$ were made on June 1, 1979 using an Ott electric contact gauge. The elevations were measured with respect to an arbitrary 100 m datum established above the ground surface. Contours of equal elevation or equal hydraulic head are shown in Figure 4.5. The direction of groundwater flow can be evaluated by constructing perpendiculars to these equipotential contours in the direction of the maximum potential gradient. There are two major groundwater flow domains as shown in Figure 4.5. One flow domain originates to the northeast of the site whereas a second flow domain appears to originate to the north northwest of the study area. Both flow domains converge to the center of the study area and appear to exist in parallel near the access road toward the sand pit. The curvature of the water-table contour lines from both flow domains suggests that a significant amount of recharge occurs as infiltration through the waste rock or runoff from the bedrock outcrop.

Water table elevations from the water-table wells were monitored from May to September of 1979. The measured values of equal hydraulic head from the water-table wells on May 29, June 1, August 16 and September 5 of 1979, were plotted and contoured as four, separate water table maps (Figure 4.6). From May to August, the contours are found to narrow progressively toward the centre

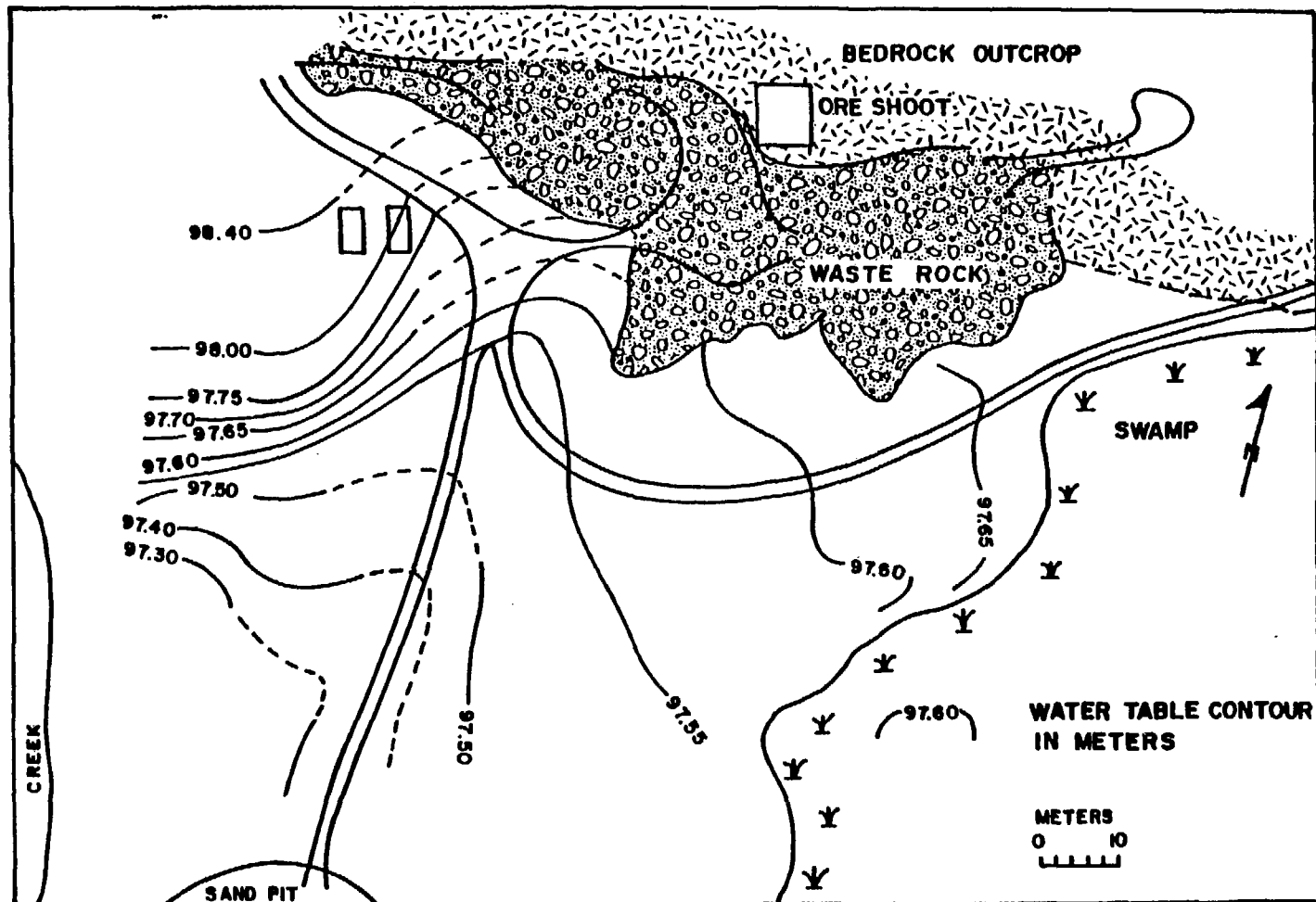


Figure 4.5 Water-Table Map, June 1, 1979.

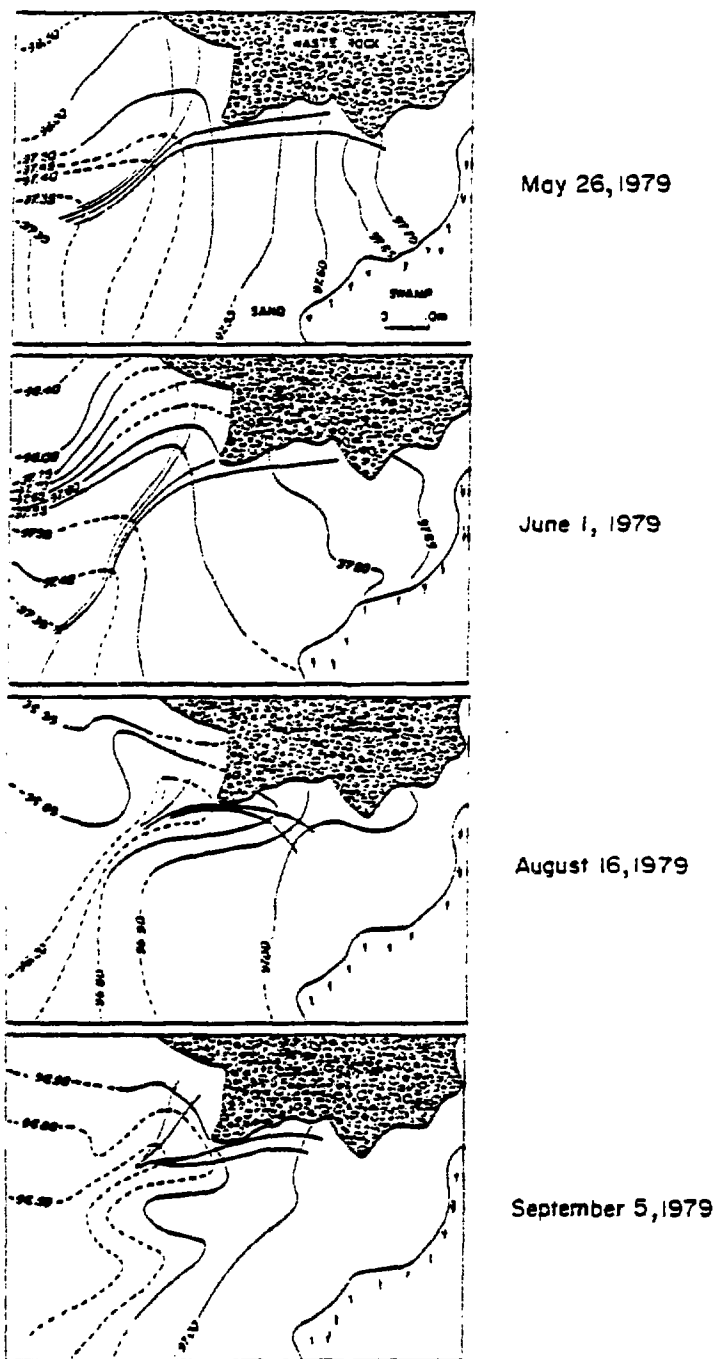


Figure 4.6 Variations in the water-table elevations between May 26, 1979 and September 5, 1979. The units of the water-table contours are in meters. Representative streamlines from the waste rock are shown at right angles to the water-table contours.

of the site. That is, the water-table declines more sharply with time during this period by approximately 0.7 meters. From August to September, the acute shape of the contours in the centre of the site widens, corresponding to an increase in the water-table level.

Water-table elevations in the same water-table wells were remeasured three years later on June 7th, 1982. Water-table elevations were also measured from the newly-installed piezometers, M1, M2, M12, M13, underlying the waste rock on the same date. Measurements were taken with a Roctest electric contact gauge. The equipotential contours from the 1982 water-level measurements are displayed in the water-table map in Figure 4.7. Similar to the water-table maps in Figures 4.5 and 4.6, Figure 4.7 shows the existence of two major flow regimes originating from the northwest and from the northeast. However, a difference does exist between the water table elevations measured on June 1, 1979 and on June 7, 1982. For example, the hydraulic head measurements are approximately 0.75 m lower in June 1982 than in June 1979. Possible reasons for this decrease in hydraulic-head values during the three year period include: (1) a dry season and (2) the slow draining process of the swamp, which is in direct hydraulic connection with the groundwater in the study area.

Vertical hydraulic head profiles were obtained from each of the multilevel bundles. Elevations of the hydraulic head were made relative to the 100 m datum located above the ground surface. Head measurements were first taken on April 23, 1980 with a specially-constructed 0.5 cm diameter electric contact gauge. The values are tabulated in Veska (1983) and are displayed in Figure 4.8 as graphs of hydraulic head vs. depth on a plan view map of the study area. From the distribution of hydraulic head values in Figure 4.8, the values decrease with depth and with flow downgradient from the NE and NW recharge areas.

In 1982, hydraulic head values were measured in a detailed network of multilevel sampling points that paralleled the two major groundwater flow paths. The measurements were made with a Roctest electric contact gauge on May

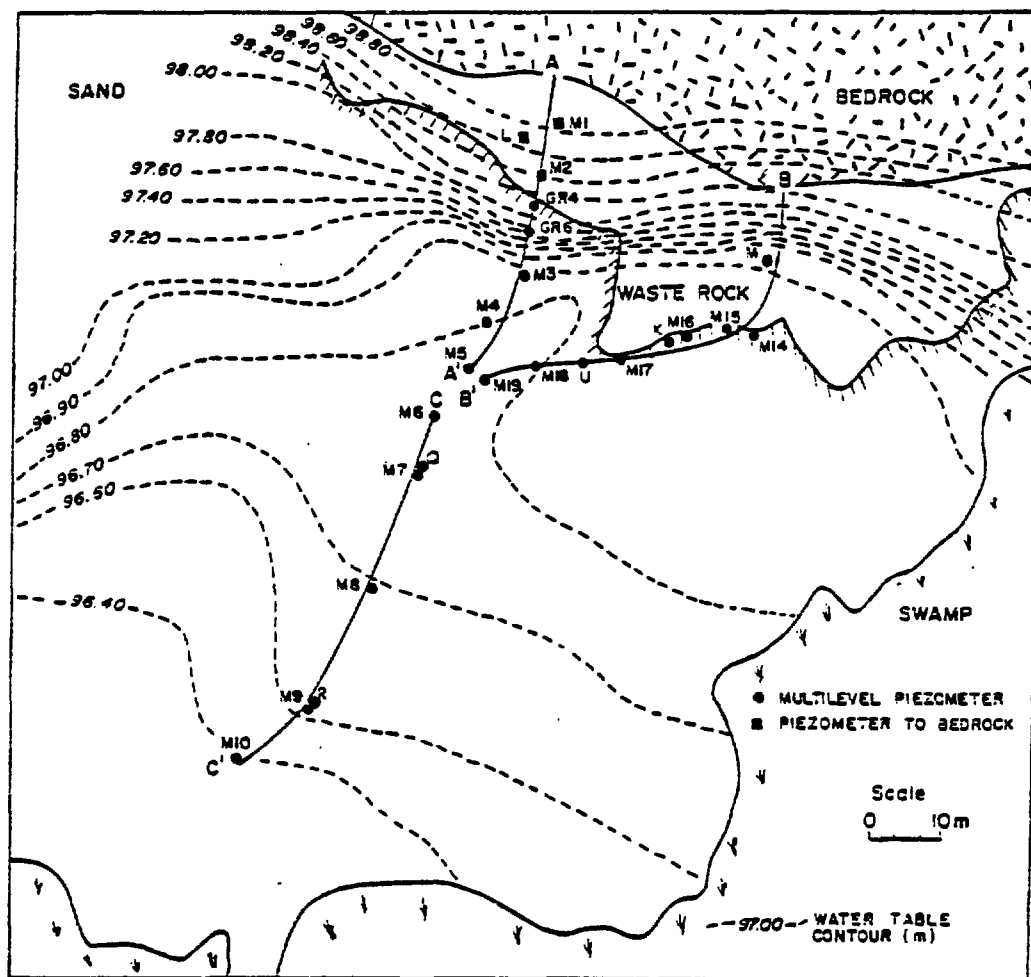


Figure 4.7 Water table map, June 7, 1982. Superimposed are cross sections A-A', B-B' and C-C' and the locations of the piezometers and multi-level piezometers that either intersect or are adjacent to the traverses of these cross sections.

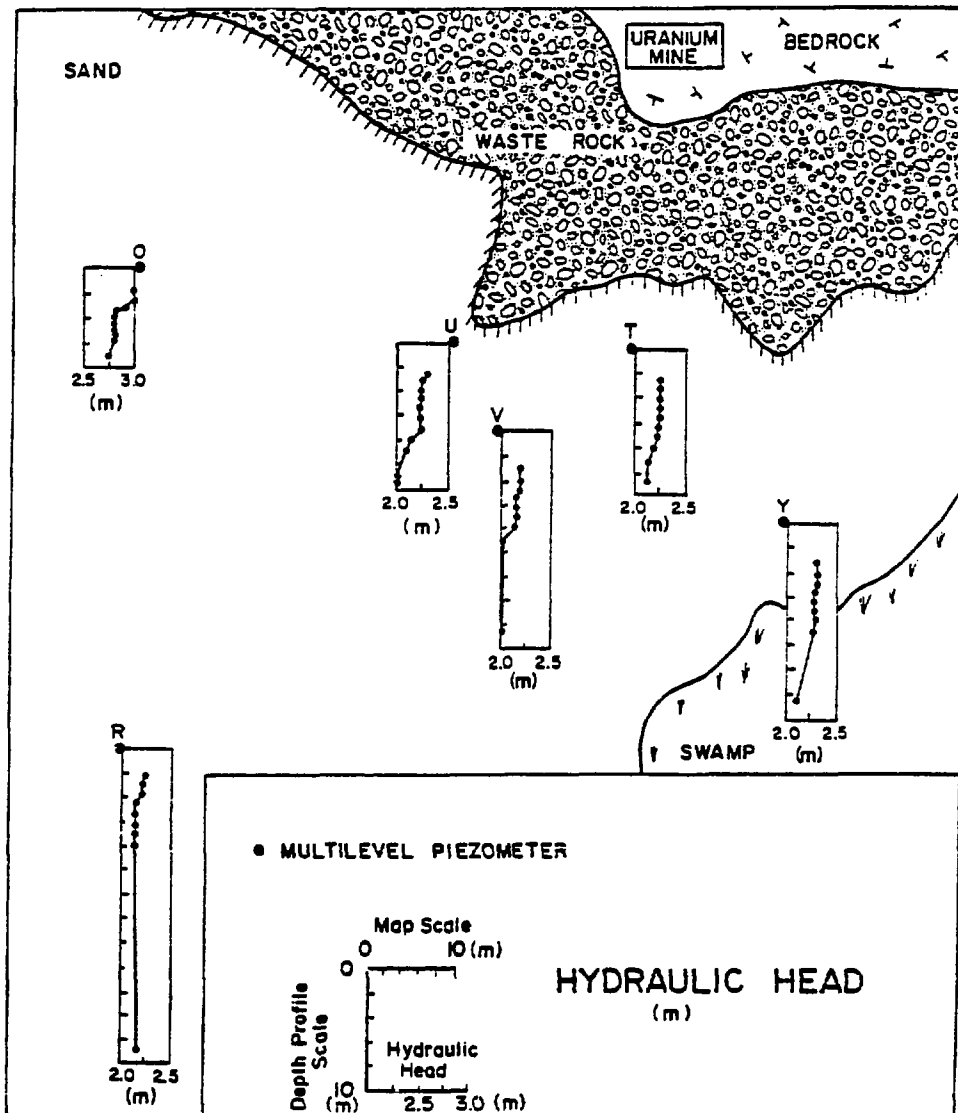
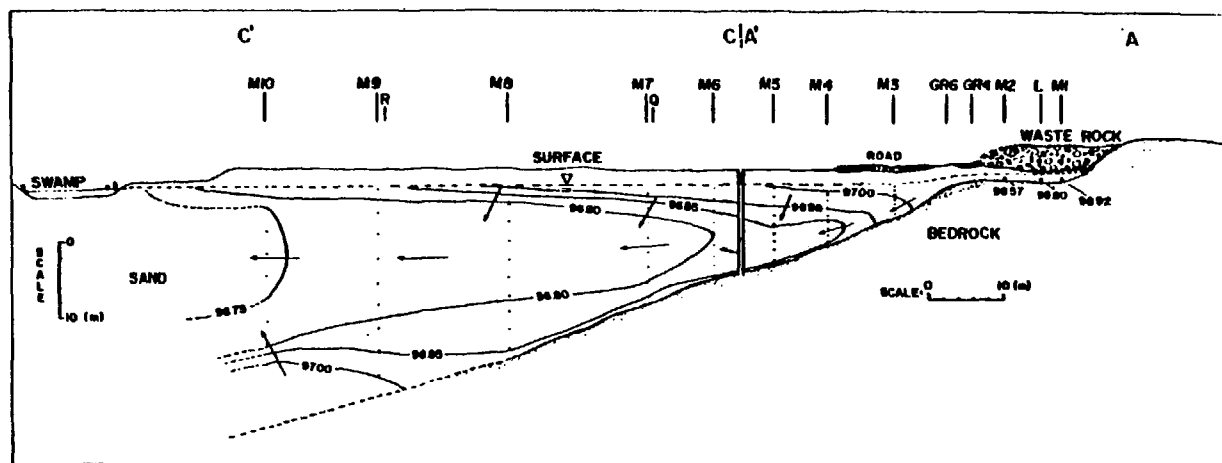


Figure 4.8 Distribution of hydraulic head values from multi-level sampling points at sites O, R, T, U, V and Y, in April 23, 1980.

12, 1982 and June 7, 1982. These measured values, that indicate a downward component in the hydraulic gradients at each site, are recorded in Veska (1983) and are contoured along cross sections A-A'-C-C' and B-B' in Figures 4.9 and 4.10. The plan-view locations of cross sections, A-A'-C-C' and B-B', are shown in Figure 4.7. Cross sections A-A' and B-B' are oriented perpendicular to the water-table contours, and therefore, it is likely that they are situated generally along groundwater flow paths. Cross section C-C' represents the general groundwater flow direction from the centre of the study area towards the swamp, along multilevels, M6, M7, M8, M9 and M10. It is at the centre of the study area where the NW and NE flow regimes converge. This convergence has been shown to be present at various times of the year by the streamline patterns in the water-table contour maps in Figure 4.6. Sample elevation readings of the hydraulic head from the 1982 measurements, that are representative of the data in Figures 4.9 and 4.10, are given for a few of the multilevels in Table 4.1. It is noted in Table 4.1 that the elevations in June are lower than that in May by approximately 20 cm.

From the equipotential contours in Figures 4.9 and 4.10, the groundwater flow direction, as represented by the arrows, was estimated. Below the waste rock along A-A', the recharge water enters the water-table zone and flows laterally from the vicinity of site L towards site M3. The hydraulic gradient in the zone between sites L and M3 is large, approximately 0.05. The groundwater flow from sites M3 towards M4 occurs under the influence of a smaller hydraulic gradient, approximately 0.01. From sites M4 to M7, the hydraulic gradient is approximately 0.005 and further downflow from site M7 toward site M10, the gradients decline to 0.001. The hydraulic gradients along the B-B' flow path are approximately a factor of 10 less than the gradients along the A-A' flow path. For example, the hydraulic gradients from sites M15 to M17, from sites M17 to M18 and from sites M18 to M6 are 0.0063, 0.0046 and 0.0044, respectively. Both cross sections indicate large hydraulic gradients in the vicinity of the waste rock and progressively smaller gradients downflow from the waste rock. These lateral gradients decrease only slightly with decrease in the water table from May to June in 1982.



EQUIPOTENTIAL CONTOURS

MAY 12, 1982

- Waste rock deposited on terrain from 1956 to 1959
- Section of waste rock excavated in September 1979
- Water table
- Water level measurements:
 - Piezometer tip
 - Bundle piezometer tip
- 96.80 — Equipotential line (meters, in reference to the 100m datum)
- Estimated groundwater flow direction

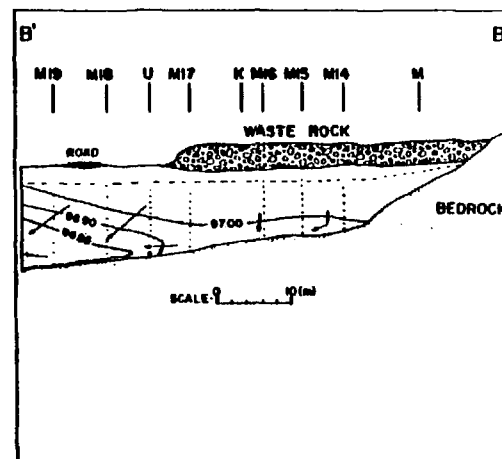
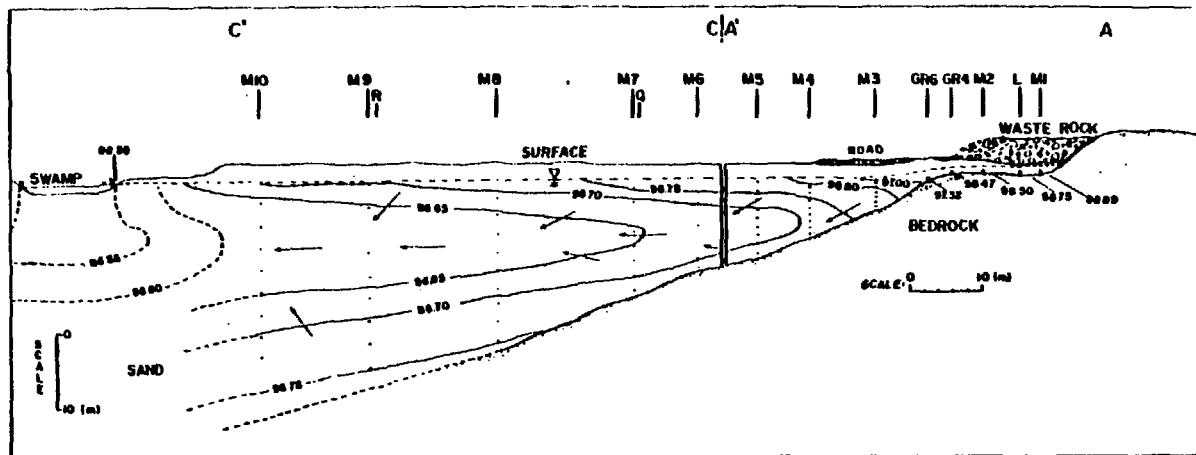





Figure 4.9 Equipotential contour diagram, May 12, 1982. Contours are plotted along cross sections A-A', B-B' and C-C'.



EQUIPOTENTIAL CONTOURS

JUNE 7, 1982

-  Waste rock deposited on terrain from 1906 to 1959
-  Section of waste rock excavated in September 1979
-  Water table
- Water level measurements:
 - Piezometer tip
 - Bundle piezometer tip
- 96.50— Equipotential line (meters, in reference to the 100m datum)
- Estimated groundwater flow direction

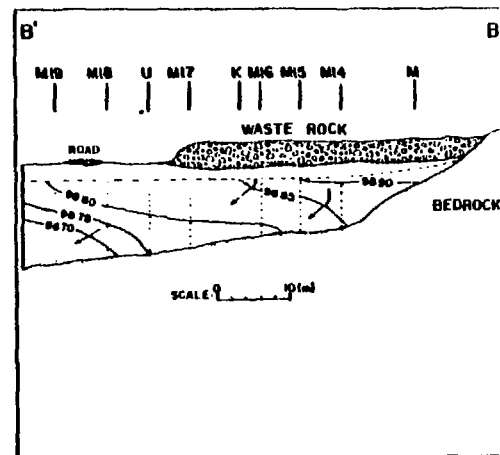


Figure 4.10 Equipotential contour diagram, June 7, 1982. Contours are plotted along cross sections A-A', B-B' and C-C'.

TABLE 4.1

HYDRAULIC HEAD ELEVATIONS AT REPRESENTATIVE SITES M14, M16, M7, M9

Sample Depth at Site M14, m	Elevation, m	
	May 1982	June 1982
3.53	97.05	96.88
4.55	97.05	96.87
5.46	97.02	96.87
6.37	97.02	96.87
7.28	97.01	96.86
8.07	96.98	96.85
9.07	96.98	96.84

Sample Depth at Site M16, m	Elevation, m	
	May 1982	June 1982
2.14	97.05	96.85
3.06	97.02	96.85
3.94	97.02	96.85
4.84	97.02	96.84
5.75	97.01	96.83
6.65	97.01	96.83
7.57	97.00	96.82
8.47	96.94	96.79
9.38	96.93	96.77

Sample Depth at Site M7, m	Elevation, m	
	May 1982	June 1982
3.21	96.95	96.76
5.18	96.82	96.69
7.19	96.79	96.66
9.19	96.79	96.64
11.20	96.80	96.65
13.10	96.79	96.66
15.17	96.81	96.67
17.13	96.85	96.72

Sample Depth at Site M9, m	Elevation, m	
	May 1982	June 1982
3.00	96.82	96.67
6.06	96.77	96.65
9.09	96.77	96.65
12.17	96.77	96.64
15.25	96.77	96.63
18.21	96.78	96.66
21.58	96.82	96.71
24.45	96.85	96.72
27.47	96.95	96.73

The hydraulic-head pattern between sites M6 and M10 in Figures 4.9 and 4.10 indicates a deep, upward component of flow from the bedrock and a shallow downward component of flow from the water table. Both components of flow are directed towards the middle of the sand aquifer. According to the equipotential contours in both figures, the groundwater from the middle of the sand aquifer moves laterally to areas of apparent discharge into the swamp.

4.4 Oxygen-18 as an Indicator of the Groundwater Source.

To determine whether the groundwater in the sand aquifer has zones of distinctly different origin, a group of water samples from some of the multilevel sampling devices and from the swamp were analyzed for concentrations of ^{18}O . The samples were collected on July 5, 1979, September 5, 1979 and October 19, 1981 and were analyzed in the isotope geochemistry laboratory at the University of Waterloo. What follows is a discussion of the ^{18}O results as they relate to the interpretations of the groundwater flow patterns based on the hydraulic-head data.

Oxygen-18 offers the potential to identify zones of groundwater derived from various sources of recharge. The two main sources are the infiltration of rain and snowmelt and the lateral seepage from the swamp. The ^{18}O composition of groundwater generally represents an average of precipitation that falls throughout the year. If groundwater originates as swamp water, the groundwater should then reflect the ^{18}O composition of the swamp instead of that of local precipitation. Because the swamp is a slow-draining water body, evaporation should cause the swamp water to be considerably enriched in ^{18}O .

Oxygen-18 concentrations in the swamp water are shown in Table 4.2. The swamp water in the month of July, 1979 was particularly high in ^{18}O values, which ranged from -4.7 to -5.1 ‰. These values indicate that significant evaporation had occurred. During September 1979, the ^{18}O values decreased to a range of -7.5 to -8.5 ‰. These seasonal ^{18}O variations in surface water can be compared to those found by Welhan (1974) in Perch Lake, a small lake located approximately 120 km northwest of Bancroft. Welhan (1974) found ^{18}O values in surface water at approximately -8 ‰ in the summer months of June and July and

TABLE 4.2VARIATION IN ^{18}O and ^3H IN SWAMP WATER DURINGTHE MONTHS OF JULY AND SEPTEMBER IN 1979

Location of Swamp Water Sample	^{18}O , $\frac{0}{00}$ July 5, 1979	^{18}O , $\frac{0}{00}$ Sept. 5/1979	^3H ,T.U. Sept. 5/1979
WL3	-4.8	-7.5	54
WL6	-4.7	-8.2	63
WL9	-5.1	-8.5	72

progressively decreasing ^{18}O values towards the fall (eg. approximately $-10^0/00$) and the spring months (e.g. about $-13^0/00$). This decrease in ^{18}O values in lake or swamp water during fall and spring is expected because fall and winter precipitation is isotopically much lighter than summer precipitation.

In order to determine if the swamp water recharges the sand aquifer, fifteen groundwater samples collected on September 5, 1979 were analyzed for ^{18}O from multilevels Y, S and R, located 10, 30 and 60 meters respectively from the swamp. The ^{18}O results in ‰ are tabulated in Table 4.3. The overall uncertainty in each determination is $\pm 0.2^0/00$. ^{18}O values similar to those of the swamp are found in the shallow groundwater at multilevels S and Y. For example, the shallow groundwater from 2.52 m to 4.06 m below ground surface at site S, ranges in ^{18}O values from -6.4 to $-7.6^0/00$. The deep water at 25 m below ground surface at site S is lower in ^{18}O at $-11.42^0/00$ and therefore the latter value probably represents water that is not derived from the swamp. At site Y, the ^{18}O concentration is relatively constant at $-11.2^0/00$ in groundwater below the water table to the three meter depth and also in groundwater between the five and fifteen meter depths below ground surface. Between the three and five meter depths at site Y, the ^{18}O concentrations in groundwater, ranging as high as 9.9 ‰, are close to those values found in the swamp water. The range of ^{18}O values in groundwater between the three and five meter depths is probably a result of mixing because the values are between those obtained from the swamp water and those from the shallow and deep groundwater.

Twenty groundwater samples collected at multilevels B, K, U, GR9, GR10 and GR4 on September 5, 1979 were analyzed for ^{18}O in order to determine the dominant source of recharge in the immediate vicinity of the waste rock. The ^{18}O results are tabulated in Table 4.4. The ^{18}O values range from -11.5 to $-13.7^0/00$. One exceptional value at $-15.1^0/00$ is found in groundwater at 1.72 m below the ground surface at site K. Although the ^{18}O values in Table 4.4 show considerable variation in groundwater with depth, no distinct trends with depth are found. No indication of the presence of swamp water is detected in the shallow groundwater at these sites.

TABLE 4.3

SPATIAL VARIATION OF ^{18}O AND ^3H IN GROUNDWATER* IN THE
SAND AQUIFER NEAR THE SWAMP

SAMPLE NUMBER	DEPTH BELOW GROUND, m	^{18}O ‰	^3H T.U.
Y-2.52	2.52	-11.2	-
Y-3.29	3.29	-10.8	-
Y-4.06	4.06	-10.5	-
Y-4.83	4.83	- 9.9	-
Y-5.60	5.60	-11.0	-
Y-6.37	6.37	-11.3	-
Y-7.14	7.14	-11.2	-
Y-7.91	7.91	-11.2	-
Y-8.89	8.89	-11.3	-
Y-14.45	14.45	-11.4	-
S-2.52	2.52	- 6.7	72
S-3.29	3.29	- 7.6	81
S-4.06	4.06	- 6.4	72
S-4.83	4.83	-	75
S-5.60	5.60	-	60
S-6.37	6.37	-	65
S-7.14	7.14	-	73
S-7.91	7.91	-	60
S-8.89	8.89	-	99
S-25.05	25.05	-11.42	61
R-8.89	8.89	-	56
R-25.05	25.05	-11.7	25

*Samples collected on September 5, 1979

TABLE 4.4

SPATIAL VARIATION OF ^{18}O AND ^3H IN GROUNDWATER* IN THE IMMEDIATE
VICINITY OF THE WASTE ROCK

SAMPLE NUMBER	DEPTH BELOW GROUND, m	^{18}O , ‰	^3H , T.U.
B-2.2	2.2	-	55
B-2.7	2.7	-	53
B-3.7	3.7	-	52
B-4.7	4.7	-	72
B-5.7	5.7	-	66
B-7.7	7.7	-	51
K-1.72	1.72	-15.1	-
K-2.22	2.22	-12.7	-
K-2.72	2.72	-13.3	-
K-3.22	3.22	-12.5	-
K-3.72	3.72	-13.7	-
K-4.22	4.22	-13.2	-
K-4.60	4.60	-11.5	-
K-8.03	8.03	-11.9	-
U-2.52	2.52	-13.7	39
U-4.06	4.06	-12.6	65
U-5.60	5.60	-12.0	62
U-7.14	7.14	-11.8	77
U-8.89	8.89	-12.7	44
U-11.80	11.80	-	94
GR9-2.32	2.32	-12.9	-
GR9-2.57	2.57	-12.7	-
GR10-2.35	2.35	-13.0	-
GR10-2.90	2.90	-11.8	-
GR4-0.89	0.89	-11.6	-
GR4-1.14	1.14	-11.8	-
GR4-1.64	1.64	-11.7	-

* Samples collected on September 5, 1979

TABLE 4.5SPATIAL VARIATION OF ^{18}O , ^2H AND ^3H IN DEEP GROUNDWATER*

SAMPLE NUMBER	DEPTH BELOW GROUND, m	^{18}O ‰	^2H ‰	^3H T.U.
T-10.72	10.72	-11.3	-82	+64
U-11.80	11.80	-11.6	-87	+68
V-16.59	16.59	-11.8	-84	+71
S-24.77	24.77	-11.4	-82	+68
R-25.05	25.05	-11.4	-84	<0

* Samples collected in October 19, 1981

Oxygen-18 and deuterium (^2H) were analyzed in groundwater from five deep piezometers in the general study area on October 19, 1981. The analytical results are given in Table 4.5. The ^{18}O values are spatially consistent and range from -11.3 to -11.8 0 /oo. Similar to the ^{18}O findings, the deuterium results show no indication of seepage from the swamp water. The overall uncertainty in the deuterium analysis by the isotope geochemistry laboratory at the University of Waterloo is $\pm 5^0$ /oo.

In conclusion, the shallow and deep groundwater in the immediate vicinity of the waste rock is the result of infiltration of rain and snowmelt. Approximately 80 meters downflow from the waste rock, shallow groundwater from the water table to five meters below the ground surface, represents a mixture of the swamp seepage and the infiltration from rain and snowmelt. The deeper water is not derived from seepage of the swamp water.

4.5 Tritium as an Indicator of the Groundwater Age

Tritium in groundwater has been analyzed because the measurements can give information on the age of the water in the aquifer. Tritium analyses were performed by the isotope geochemistry laboratory at the University of Waterloo. Tritium values that are below the detection limit of about 20 T.U., indicate that very little water younger than 30 years is present. Water of tritium content above about 20 T.U. is of recent origin, since the tritium content of atmospheric precipitation increased as a result of thermonuclear testing after 1953 (Brown, 1961). Therefore, ^3H values in groundwater from the study area can be used as an indicator to discriminate between the shallow groundwater zone influenced by young precipitation sources and the deeper groundwater zone influenced by a possibly older precipitation source. This discrimination between two groundwater types of different age would aid in the delineation of the maximum extent of travel of the recharge water that infiltrated through the waste rock from 1957 to 1982.

The tritium content in 25 groundwater samples that were collected in September 1979 is represented in Tables 4.3 and 4.4. At levels above 20 T.U., the precision of the ^3H measurements is ± 8 T.U. The tritium values in groundwater range from 39 to 99 T.U., suggesting groundwater of recent origin. The exception is the value of 27 T.U. in groundwater at 25 m below ground surface at site R. The latter value is near the detection limit of 20 T.U. which suggests that water at this point is in the transition zone between young and older water. There is a possibility that the tritium content in this transition zone was masked by some drilling effects, since groundwater was sampled for ^3H analysis shortly after the installation of the piezometers.

Additional sampling of groundwater for ^3H determinations was made on October 19, 1981 and June 11, 1982 to provide more conclusive evidence of the age of the deep groundwater. Tritium results for these samples are given in Tables 4.5 and 4.6, respectively. The tritium values of groundwater from deep piezometers, T, U, V, S and R in Figure 4.5, indicate that this groundwater is younger than about 30 years in age. An exception occurs at the 25 m depth at site R, where no detectable tritium is found. Tritium values in Table 4.6 represent the analysis of 19 groundwater samples from multilevel bundles at sites M6, Q, M7, M8, R, M9 and M10. With the exception of groundwater samples without tritium (M8-24.19, R-25.05, M9-27.47 and possibly M10-26.18), the ages of the groundwater in the other 15 samples are less than 30 years.

The tritium values from Tables 4.4 and 4.6 are displayed on a cross sectional diagram along B-B' and C-C' in Figure 4.11. This figure shows a deep bomb tritium boundary at approximately 25m below the ground surface. The boundary represents the 20 T.U. detection limit for ^3H in groundwater and marks the division between pre-1953 recharge water and post-1953 recharge water. Identification of the zone in which tritium occurs is significant because it is within this zone where waste-rock-derived contaminants can occur.

TABLE 4.6SPATIAL VARIATION OF ^3H IN GROUNDWATER* IN THE CENTRAL
SECTION OF THE STUDY AREA

<u>SAMPLE NUMBER</u>	<u>DEPTH BELOW GROUND, m</u>	<u>^3H ,T.U.</u>
M6-9.99	9.99	+91
Q-2.65	2.65	+47
Q-5.15	5.15	+86
Q-15.43	15.43	+93
M7-9.19	9.19	+80
M7-13.10	13.10	+75
M7-17.13	17.13	+55
M8-14.59	14.59	+91
M8-21.73	21.73	+97
M8-24.19	24.19	<0
R-25.05	25.05	<0
M9-9.09	9.09	+80
M9-15.25	15.25	+44
M9-21.58	21.58	+84
M9-27.47	27.47	+10
M10-14.30	14.30	+113
M10-20.38	20.38	+113
M10-23.45	23.45	+81
M10-26.18	26.18	+26

* Samples collected in June 11, 1982

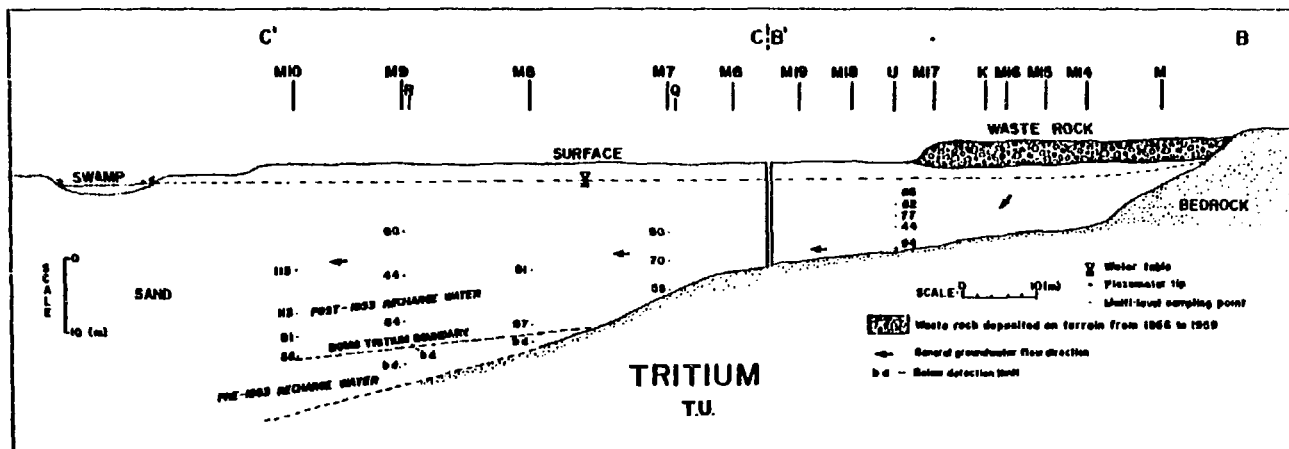


Figure 4.11 Tritium distribution in groundwater along cross sections B-B' and C-C'.

4.6 Methods of Groundwater Velocity Analysis

Three independent methods have been used for the determination of groundwater velocities along two extended cross sections, A-A' to C-C' and B-B' to C-C'. The three methods of groundwater velocity analysis include: (1) the trial and error calculations that are based on the maximum extent of sulphate contamination and on the hydraulic-head gradients; (2) velocity calculations that are based directly on the Darcy equation; and (3) the borehole dilution technique.

The first method is based on an estimate of the lateral maximum extent of sulphate contamination in the aquifer. It is believed that most of the sulphate in the sand aquifer has originated by geochemical weathering of the waste rock since 1957. The lateral extent of an identifiable plume of sulphate in groundwater was estimated to be approximately 100 m from the waste rock. The data upon which this estimate is based are presented in Chapter 5. From the hydraulic head data collected during the summer of 1982, groundwater velocities between multilevel piezometers were calculated in a successive manner on a trial and error basis until a match was reached between the calculated 25 year groundwater travel position and the observed lateral extent of travel of sulphate contamination from the waste rock. The results of this kind of velocity analysis along the A-A' to C-C' cross section and the B-B' to C-C' cross section are given in Figure 4.12. Along the A-A'-C-C' cross section, the groundwater velocities decrease from 70 to 69 m/yr at sites L to M3, from 15 to 6.4 m/yr at sites M3 to M7 and from 4.4 to 1.6 m/yr at sites M7 to M10. In comparison, the groundwater velocities along the B-B'-C-C' profile show less pronounced decreases. For example, the velocities decrease from 10 m/yr to 7 m/yr downflow from site M15 to site M7 and from 4.4 m/yr to 1.8 m/yr downflow from site M7 to site M10.

Since it is possible that the actual sulphate front, although not detectable, is somewhat farther than 100m from the waste rock, the above velocity estimates may be somewhat smaller than the true values. This statement is supported by the following interpretation of the tritium distribution in groundwater in Figure 4.11. Sulphate and tritium are considered to be both non-reactive constituents in groundwater in this field investigation. Tritium

used in the first method. Maximum and minimum values of measured hydraulic conductivities in the sand aquifer were used to represent the K parameter in equation 4.1. An estimated value of 0.33 was used to represent the porosity of the sand. The results of the calculated average linear velocities are displayed in Figure 4.12, but only from sites L to M2 along A-A' and from sites M15 to M17 along B-B'. Although other velocities downflow from these sites have been calculated, the average linear velocity values given in Figure 4.12 are sufficient to make comparisons with the velocities determined from the first method. The groundwater velocity range of flow from sites L to M2 is between 9 m/yr and 74 m/yr, as calculated from the respective minimum and maximum hydraulic conductivity values. The groundwater velocity range from sites M15 to M17 is between 1.1 m/yr and 10 m/yr, as calculated from the respective minimum and maximum hydraulic conductivities. Comparing the first two methods of groundwater velocity analysis, the velocity calculated by the first method corresponds well to the maximum velocity calculated from the second method.

The third method of groundwater velocity analysis was the borehole dilution technique. The application of this technique to the field site on June 29, 1982, involved the injection of a mild sodium chloride tracer solution into an isolated segment of driven well point. The isolated well segment was installed approximately 30 cm below the water table. Lateral groundwater flow continually mixed and removed the tracer from the well screen. From direct measurements of the electrical conductance of the diluted tracer in the well with time, the groundwater velocity (V_f) in the sand was calculated from the equation given by Grisak et al. (1977), where

$$V_f = (-V/(\alpha A t)) \ln C/C_0 \quad 4.2$$

The parameters in equation 4.2 are identified as the following: t = time; C_0 = injection concentration at $t = 0$; C = concentration at time, t , after the tracer was injected; V = volume in which dilution occurs; A = cross-sectional area of flow; and α = correction factor (2.5). An average linear groundwater velocity for the sand aquifer was calculated by dividing V_f by the value for porosity. The porosity of the sand was assumed at 0.33 (Freeze and Cherry, 1979).

Borehole dilutions were carried out at two sites in the study area. One site is located approximately one meter downflow from site M3 and the other site is located approximately two meters adjacent to site M16. The locations of these test sites and the measured groundwater velocities at these sites are given in Figure 4.12. The measured groundwater velocity at the site downflow from site M3 is 15 m/yr, which is equal to the calculated value of 15 m/yr by the first method. In comparison, the measured groundwater velocity at the site adjacent to site M16 is 42 m/yr or approximately a factor of four greater than the calculated value by the first method. The accuracy of the 42 m/yr value is in doubt because problems were encountered in the installation of the well point adjacent to site M16. That is, the isolated well segment was exposed to groundwater flow at only 15 cm below the water table instead of the usual 30 cm depth exposure.

Hydraulic conductivities (K) from the first and third methods of groundwater velocity analysis are calculated and are compared in Figure 4.12 to those values of K measured at the field site. The calculated values of K for the first and third methods along cross section A-A' are considered to be equal. These calculated K values are similar to the maximum measured value of K (i.e. 1.6×10^{-3} cm/s). In comparison, the calculated K values from the first and third methods along the B-B' cross section differ by a factor of four. However, the calculated K value from the first method at 1.7×10^{-3} cm/s along cross section B-B' corresponds with the maximum measured K value for the study area. The arithmetic mean value of K estimated from the calculated and measured K values along both cross sections in the sand aquifer is 1.6×10^{-3} cm/s.

4.7 Summary

Two major groundwater flow domains exist in the sand aquifer. That is, recharge water in the vicinity of the waste rock piles in the northeast and in the northwest converge towards the south of the study area and discharge below the swamp. The groundwater velocities progressively decrease from about 70 m/yr below the waste rock in the northwest section of the study area to about two m/yr at approximately 100 m downgradient from the waste rock in the south. To a smaller extent, the groundwater velocities decrease from about 10 m/yr below the

waste rock in the northeast sector to about 2 m/yr in the south near the swamp. Good agreement in the analysis of groundwater velocity was found amongst three independent methods. The arithmetic mean hydraulic conductivity for the sand was estimated at 1.6×10^{-3} cm/s.

The ^{18}O data confirmed the sources of various types of groundwater in the sand aquifer. For example, the shallow and deep groundwater in the immediate vicinity of the waste rock are the result of the infiltration of recharge water from atmospheric precipitation. Approximately 80 meters laterally downflow from the waste rock along the NE flow regime, the shallow groundwater from the water table to five meters below the ground surface, represents a mixture of swamp seepage and the infiltration from rain and snowmelt. Also, the ^{18}O data helped to indicate that the deeper water was not derived from seepage of the swamp water.

The absence of detectable tritium in groundwater deeper than approximately 25 meters below the ground surface and beyond approximately 70 meters downflow from the waste rock indicates water older than 30 years. The water at shallower depth in the sand aquifer has detectable tritium and has therefore entered the aquifer since tritium fallout from the atmosphere began in 1953. The waste rock was deposited on the sand unit from 1956 to 1959. Therefore, the tritium zone in the sand aquifer is a zone in which contaminants leached from the waste rock may occur.

CHAPTER 5

RADIONUCLIDES AND CHEMICAL CONSTITUENTS IN GROUNDWATER

The spread of radioactive contaminants (^{228}U , ^{234}U , ^{232}Th , ^{230}Th , ^{226}Ra and ^{210}Pb) from the uranium-bearing waste rock in groundwater was assessed by groundwater sampling and subsequent radiochemical analyses during the period from 1978 to 1982. Although the main focus of the Greyhawk study is on the leaching and movement of radionuclides, the geochemical conditions within the sand aquifer have also been investigated. The chemical composition of the groundwater can, in favourable circumstances, provide an indication of the zone of influence of waste-rock-derived leachate.

5.1 Sampling and Analytical Procedures

A geochemical reconnaissance of the study area from 1978 to 1980 involved field measurements of pH, alkalinity, electrical conductance and temperature of groundwater samples from multilevel devices at sites A, B, C, D, E, F, G, J, K, N, O, P, Q, T, U, V, X, GR9, GR10, GR11, GR6 and GR4. The locations of these sites are shown in Figure 4.1. The field measurements were made immediately upon withdrawal of water from the sampling tubes using a battery-powered peristaltic pump. Similar measurements were also made in groundwater at piezometers L and M, which were installed through the waste rock into the underlying sand aquifer. It was thought that the water chemistry found beneath the waste rock piles could be used to represent the input of contaminants to the sand aquifer. The field geochemical measurements were done primarily to obtain a rapid and inexpensive preliminary indication of the position of the zone of contamination from the waste rock.

The 1978/1980 geochemical reconnaissance also entailed the determination of the concentrations of chemical constituents in groundwater at the field site.

Groundwater samples from sites GR9, GR10, GR11, GR6, GR4 and L in the excavated waste rock areas were analyzed for sulphate in the laboratory by the turbidimetric method (Rand, 1975). Water samples for chemical analyses of major ions and trace elements were collected from all of the sample tubes at sites K, O and Y in order to give complete vertical profiles of the hydrogeochemistry of the sand aquifer. Additional samples were collected from several sampling devices, located at sites GR4, GR9, B and Q. These samples were filtered in the field through 0.45 micron filter paper. The filtered samples for the analysis of heavy metals and other trace constituents were collected in 500-ml polyethylene bottles with ultrapure HNO_3 added as a preservative to maintain low pH. The samples were analyzed for Al, As, Cd, Cu, Cr, Fe, Mo, Mn, Ni, Pb and Zn by the water quality laboratory at the Ontario Ministry of the Environment. Additional 500-ml groundwater samples from the same sampling devices, which were not acidified, were collected for the analyses of Ca, Mg, Na, K, SO_4 , Cl, HCO_3 , NO_3 , F, P and SiO_2 . These samples were also analyzed by the Ontario Ministry of the Environment.

An investigation of the distribution of radionuclides in groundwater in 1979 and 1980 involved the collection of four-liter groundwater samples from multilevel sites, A, B, C, G, J, K, L, M, O, P, Q, R, S, T, U, V, X, Y, GR4, GR6, GR9, GR10 and GR11. A total of 110 water samples were collected in 4.5-litre polyethylene bottles at these sites. The samples were filtered in the field and then were acidified with nitric acid. To further avoid adsorption of radioactive species on the polyethylene bottles, barium and ferric ions were added to the water samples. The bottles were transported to the radiochemistry laboratory at the University of Waterloo for the determination of radionuclides, ^{238}U , ^{234}U , ^{232}Th , ^{230}Th , ^{226}Ra and ^{210}Pb . During 1979, the analyses of ^{238}U and ^{234}U in groundwater samples were done by the radiochemistry laboratory at McMaster University. After 1979, the uranium isotopes, along with the thorium isotopes, ^{226}Ra and ^{210}Pb , in all of the groundwater samples were determined at the University of Waterloo.

The preliminary investigations revealed zones of high concentrations of chemical constituents and high activities of radionuclides in groundwater beneath the waste rock and also in groundwater at greater depths below the ground surface downflow from the waste rock. This led to a follow-up sampling program in October 1981 at sites B, T, V, R, L, GR4, GR6, A, GR9, GR10, GR11, U and Q. Field measurements of pH, Eh, dissolved oxygen, alkalinity and electrical conductance in groundwater were taken from 37 sample points from these multilevel sites. For Eh measurements, a calomel ($\text{Hg-Hg}_2\text{Cl}_2$) reference electrode and a platinum electrode were placed in the spillover chamber of a flow cell. The cell was connected by tubing to a piezometer. A pump was used to draw groundwater through the cell at a low flow rate. After 15 minutes of groundwater flow through the cell, the potential difference in millivolts between the two electrodes was measured by a Corning Model 610A Expanded Scale pH-Eh meter. A Zobell solution of known Eh was used as an instrument check prior to Eh measurements. The dissolved oxygen content in groundwater was measured by the Winkler technique, which has a detection limit of 0.1 mg/l.

As part of the October 1981 sampling program, groundwater samples from 8 sample devices were analysed at the University of Waterloo for dissolved inorganic carbon (DIC) determinations by the head-space gas chromatographic technique. The DIC measurements were to provide a method of comparison with the calculated DIC values obtained from the pH and alkalinity measurements in groundwater. In addition, groundwater was obtained in October 1981 from 18 sample devices for analysis of Ca, Mg, Na, K, HCO_3 , SO_4 , Cl, SiO_2 , Al, Fe and Mn in the geochemistry laboratory at the University of Waterloo and from 17 sample devices for the analyses of ^{238}U , ^{234}U , ^{226}Ra and ^{210}Pb in the radiochemistry laboratory at the University of Waterloo.

A detailed geochemical and radiochemical investigation of the groundwater chemistry along the two major flow paths in the study area was conducted in June 1982. Groundwater from 267 sample points was analyzed for pH, alkalinity and electrical conductance in the field. Unacidified, filtered groundwater samples

were taken to the laboratory for the analyses of sulphate in 200 samples, electrical conductance in 267 samples and major ions in 9 samples. A total of 65 acidified, filtered groundwater samples were analysed for ^{238}U , ^{234}U , ^{226}Ra and ^{210}Pb .

5.2 Spatial Distributions of Chemical Constituents

The results of the field measurements of electrical conductance, pH, alkalinity and the calculated DIC values for the 1978/80 reconnaissance sampling program are tabulated in Veska (1983). With the exception of some areas beneath and in the immediate vicinity of the waste rock, the pH of the groundwater in the sand aquifer is generally between 5.0 and 7.5. The highest pH values generally occur in groundwater at the deep sampling points, corresponding to the high alkalinity, DIC and electrical conductance. The sampling points with lowest pH are beneath or near the waste rock in the northwest sector of the study area. The lowest pH is observed at site L (pH = 3.4). The electrical conductance at this site (1950 uS) is the highest in the study area.

The measured alkalinity values in groundwater are reported as bicarbonate concentrations in Veska (1983). The bicarbonate concentrations in groundwater range from less than 10 to 295 mg/l, where the higher values generally correspond to deeper sampling points and higher pH. This trend is observed in the three-dimensional diagram in Figure 5.1, representing the spatial distribution of bicarbonate concentrations in groundwater at the field site.

The calculated dissolved inorganic carbon (DIC) values in groundwater range from about 7.6 to 74.5 mg/l, with the higher values generally corresponding to high values of alkalinity and pH in the deeper water (Veska, 1983). This trend did not occur at all of the sampled sites.

Detailed vertical profiles of the chemical constituents and the ^{18}O distribution in groundwater, as represented by the chemical and isotopic data of groundwater from the three multilevel sampling sites, Y, K and O, are given in Figure 5.2 and Veska (1983). The locations of the three sites are

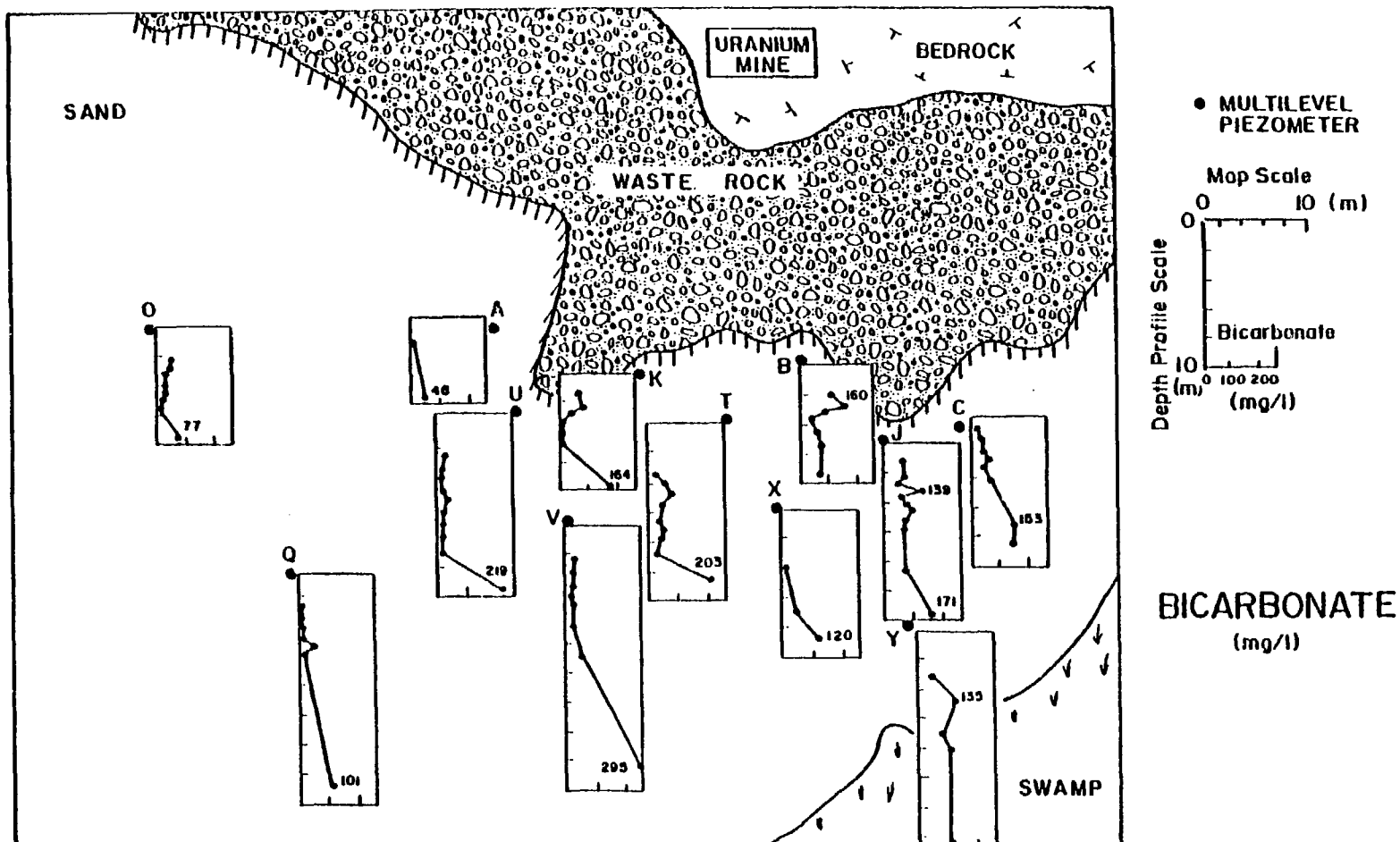


Figure 5.1 A three-dimensional representation of the spatial distribution of bicarbonate concentrations in groundwater in 1979.

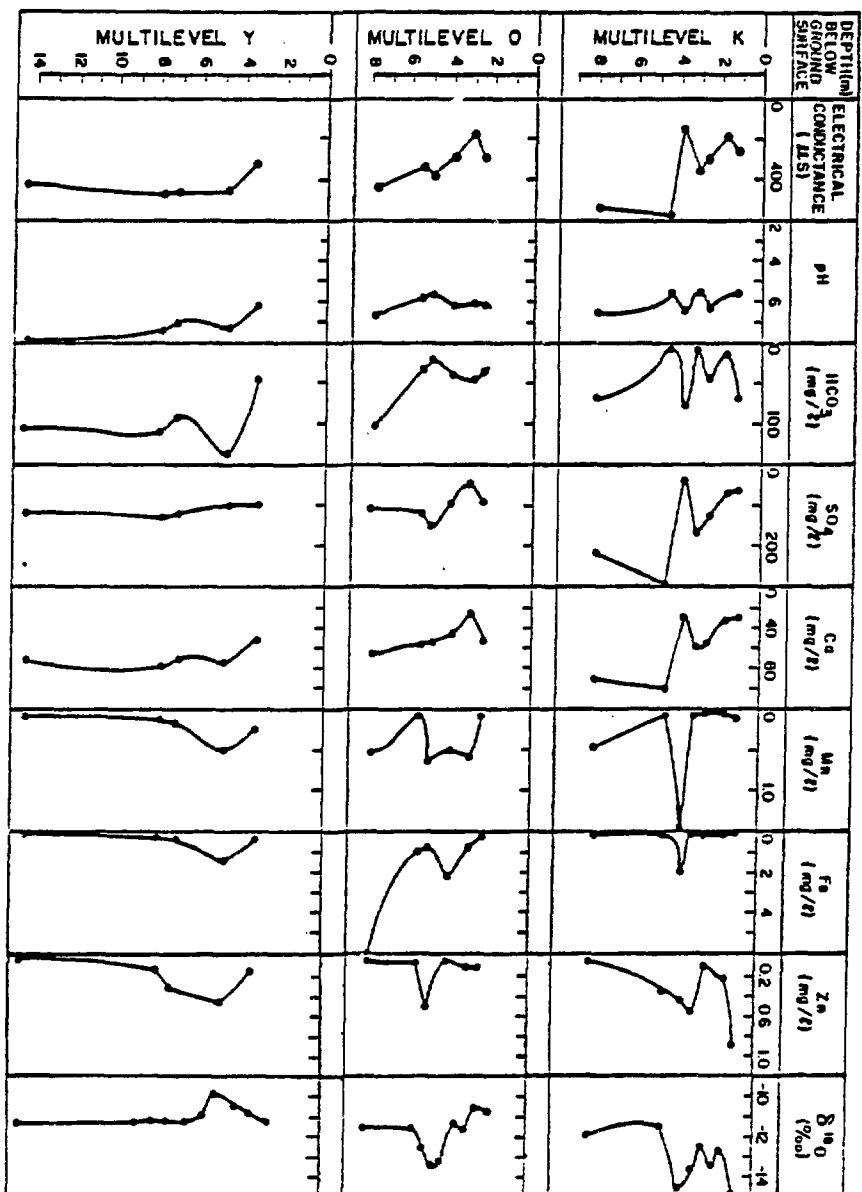


Figure 5.2 Profiles of electrical conductance, pH, HCO_3^- , SO_4 , Ca, Mn, Fe, Zn and $\delta^{18}\text{O}$ in groundwater from multilevel sites K, O and Y.

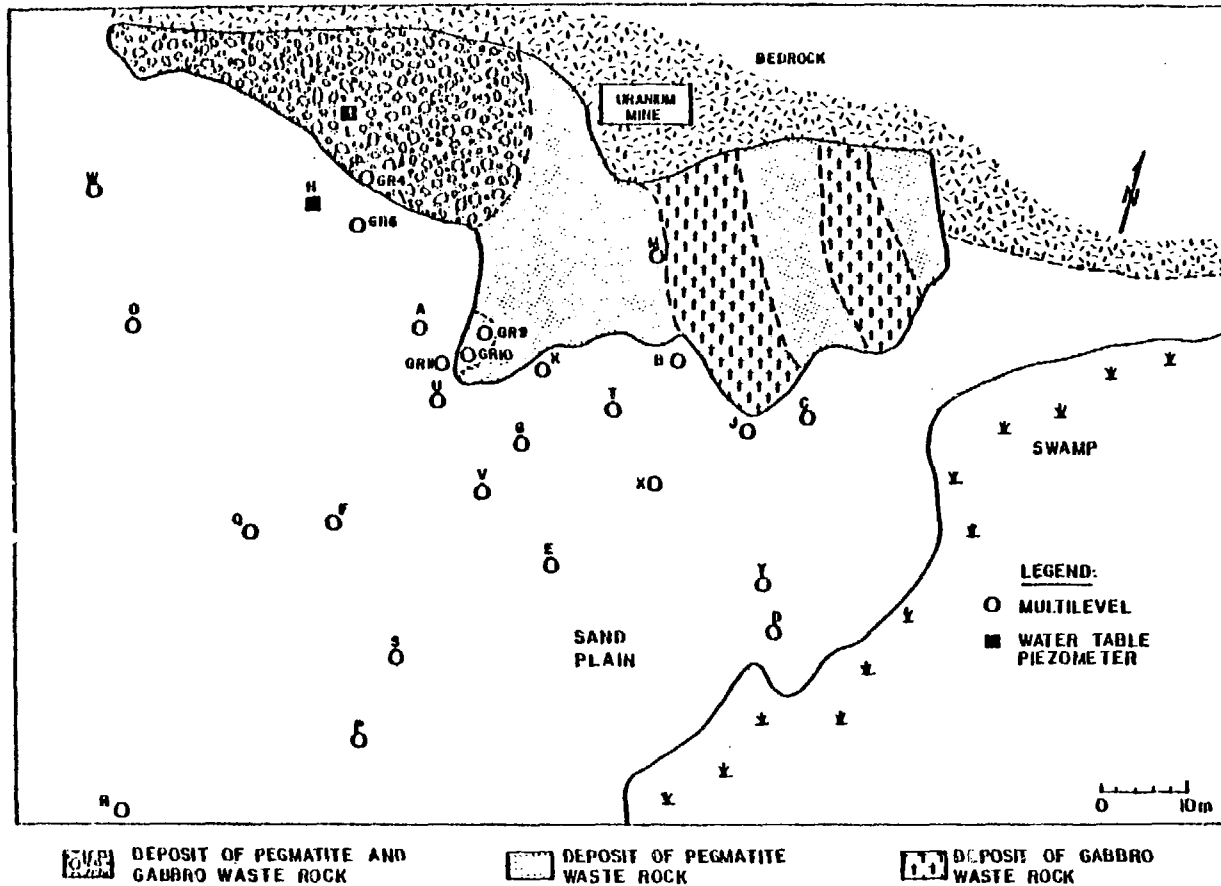


Figure 5.3 Map illustrating the locations of the different types of waste rock deposits at the study site.

shown in Figure 5.3. Site Y is located about 10 metres from the swamp and is considered to be unaffected by contamination from waste rock which is adjacent to the mine shaft. Site K is within a meter of the pegmatitic waste rock and is influenced by recharge from the northeast groundwater flow regime. Site O is located approximately 30 meters downflow from the pegmatite-gabbro waste rock and is influenced by the northwest groundwater flow regime.

The hydrogeochemical profiles of sites K and O are quite complex (Figure 5.2). In general, progressively increasing concentrations of Ca, Mg, Na, SO_4 , HCO_3 , DIC and Mn as well as increasing values of pH and electrical conductance occur in the groundwater with depth. A similarity exists in the trends amongst the Ca and SO_4 concentrations and the electrical conductance values in the groundwater at sites K and O.

Compared to sites K and O, the groundwater chemistry at site Y is fairly uniform with depth, except between the four to five meter depth interval below the ground surface. At this depth interval, increased concentrations of dissolved HCO_3 , DIC, Mn, Fe and Zn as well as pH and ^{18}O occur in the groundwater (Figure 5.2). The groundwater composition at this interval is influenced by the nearby swamp water flowing through the aquifer, as deduced by the ^{18}O distributions in groundwater in Chapter 4. The geochemical evidence shown here further supports the view based upon the ^{18}O data that the shallow groundwater near the swamp receives recharge from the swamp.

The concentrations of dissolved Cl, K, Na, Al, showed little variability in groundwater with depth for sites K, O and Y. The trace constituents which showed no variability in concentration in groundwater amongst the three sites were Pb, Ni, Cu, Cr, Cd, As, Mo, F and P. All of these trace constituents had concentrations in groundwater approaching the analytical detection limits and were found to be below the respective maximum permissible concentration limits for drinking water (Health and Welfare Canada, 1978). Table 5.1 compares the concentration range of various chemical constituents in groundwater from sites K, O and Y with that of the drinking water standard, which serves as a convenient reference scale. Table 5.1 shows that the concentrations of Fe and

TABLE 5.1

COMPARISON OF THE INORGANIC SOLUTE COMPOSITION OF
GROUNDWATER FROM SITES K, O AND Y AND THE DRINKING WATER STANDARDS

CHEMICAL CONSTITUENT	CONCENTRATION RANGE IN GROUNDWATER FROM SITES K, O AND Y (mg/l)	ANALYTICAL DETECTION LIMIT + (mg/l)	MAXIMUM PERMISSIBLE CONCENTRATION LIMIT* (mg/l)
Ni	< 0.02	0.02	N
Cu	< 0.01	0.01	1.0
Cr	< 0.02	0.02	0.05
Cd	< 0.005	0.005	0.005
As	< 0.001	0.001	0.05
Mo	< 0.04	0.04	N
Pb	< 0.03 - 0.08	0.03	0.05
Zn	0.03 - 0.56	0.01	5
Fe	< 0.04 - 6.4	0.04	0.3
Mn	< 0.02 - 1.7	0.02	0.05
Al	< 0.02 - 0.04	0.02	N
Cl	0.7 - 6	0.1	250
NO ₃	< 0.1 - 5.3	0.1	10
SO ₄	36 - 290	0.1	500
F	< 0.1	0.1	1.5
P	< 0.001 - 0.008	0.001	N

- Approximate detection limits taken from the Ontario Ministry of the Environment.

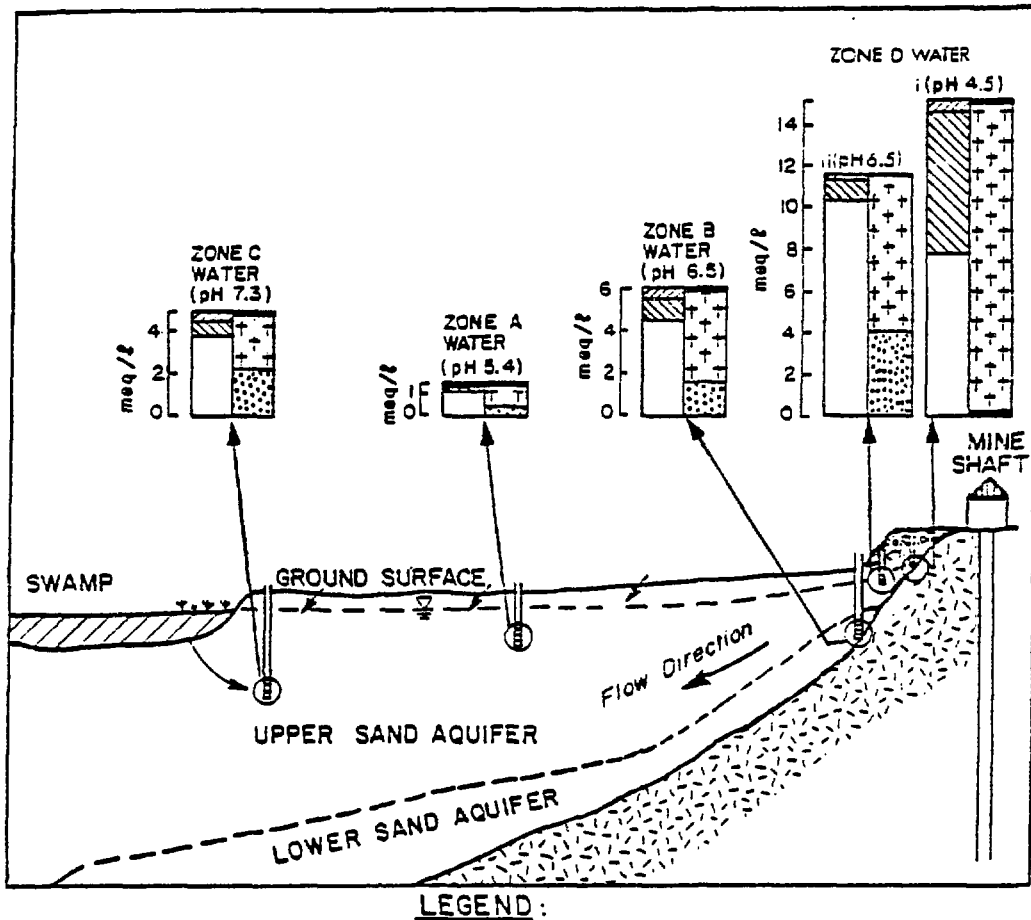
* Source of drinking water standards: Health and Welfare Canada, 1978.

N - No limit available because of the low oral toxicity of the constituent.

Mn in groundwater in certain parts of the sand aquifer are above recommended limits for drinking water.

Besides site K, other sites adjacent to the waste rock piles contained groundwater with high concentrations of chemical constituents, namely; sites GR4, GR9 and B. Site GR4 is located in the excavated pegmatite-gabbro waste rock area (Figure 5.3); site GR9 is located in the excavated pegmatite waste rock area (Figure 5.3); and site B is at the periphery of the gabbroic waste rock pile (Figure 5.3). The chemical analyses of groundwater from these sites are given in Veska (1983). The groundwater at site GR4 is a low pH, calcium-magnesium-sulphate water with notably high values of Al and Ni. The groundwater at site GR9 is a pH 5.0 calcium-sulphate water whereas the groundwater at site B is a neutral pH calcium-bicarbonate-sulphate water. In comparison to the high ionic strength groundwater at these three sites, the composition of the shallow groundwater at site Q, at approximately 50 meters downflow from the waste rock piles, is a dilute calcium-sulphate water (Veska,1983).

From the results of the preliminary geochemical sampling program, the groundwater in the sand aquifer can be divided, for convenience of discussion, into four hydrochemical zones. The boundaries of these zones are gradational and not all water samples in a particular zone are different from samples in a neighboring zone. These four zones are identified in Figure 5.4 as the following: zone A, the upper zone of the sand aquifer; zone B, the lower zone of the sand aquifer; zone C, the zone influenced by swamp water; and zone D, the zone influenced by waste rock. Each hydrochemical zone in Figure 5.4 is schematically represented by bar graphs, which reflect the characteristic major-ion composition in groundwater in milliequivalents per liter. The bar graphs for zones A, B and C in Figure 5.4 are represented by chemical analyses of the groundwater samples Q-2.65, K-8.03 and Y-4.83, respectively. The bar graphs for zone D are represented by the chemical analysis of samples B-2.2 and GR4-1.64.



CLASSIFICATION OF GROUNDWATER ZONES:

- ZONE A - UPPER ZONE OF SAND AQUIFER
- ZONE B - LOWER ZONE OF SAND AQUIFER
- ZONE C - ZONE INFLUENCED BY SWAMP WATER
- ZONE D - ZONE INFLUENCED BY WASTE ROCK

Figure 5.4 Schematic representation of chemical analyses of groundwater from four apparent zones in the sand aquifer.

Zone D in Figure 5.4, is of key significance to this study because it represents the effect on water quality in groundwater underlying the waste rock as a result of leaching processes. The leachate-influenced water in zone D is characterized by two types of groundwater chemistry at the site. The two types of groundwater are represented in Figure 5.4 as the low pH calcium-magnesium-sulphate water in the northwest sector and the neutral pH calcium-bicarbonate-sulphate water in the northeast sector.

In the endeavour to delineate the zone D boundary in the northwest flow regime, the groundwater compositions in the two excavated waste rock areas in the northwest sector were investigated along traverses from sites L to GR6 and from sites GR9 to GR11. Both traverses, approximately 10 meters in length, are in the shallow sand aquifer and follow apparent groundwater flow paths as deduced from the water table maps in Chapter 4. The GR9-GR11 traverse passes through a disturbed pile of pegmatitic rock whereas the L-GR6 traverse passes through a disturbed pile of gabbro and pegmatite. The variations in the values of pH, alkalinity, DIC, electrical conductance and sulphate in groundwater along these two traverses are given in Tables 5.2 and 5.3. The trends observed in the groundwater chemistry along traverse GR9-GR11 are similar to the spatial trends in the groundwater chemistry along traverse L-GR6. That is, the groundwater downflow from the waste rock in both traverses shows progressive decreases in values of electrical conductance and sulphate and progressive increases in values of pH, alkalinity and DIC.

The calculated DIC values in groundwater at sites L and GR4 in Table 5.3 were not included because of the negligible alkalinity values determined during the preliminary survey. From the follow-up geochemical survey in 1981, groundwater was measured for pH and alkalinity in the field and also sampled for laboratory determination of DIC. Calculated and measured values of DIC in the 1981 groundwater samples are compared in Veska (1983). The agreement between the DIC values by the two different methods is within approximately 20%.

TABLE 5.2VARIATION IN THE CHEMICAL COMPOSITION OF GROUNDWATER⁺ ALONG
TRAVERSE GR9-GR11

SAMPLE NUMBER	DEPTH BELOW GROUND ,m	ELECTRICAL CONDUCTANCE ,uS	pH	ALKALINITY as HCO ₃ ,mg/l	DIC ,mg/l	SO ₄ ,mg/l
GR9-2.07	2.07	210	6.1	23	15	80
GR9-2.32	2.32	240	5.2	<10	-	105
GR9-2.57	2.57	245	5.5	<10	-	120
GR9-2.82	2.82	500	3.2	<10	-	80
GR10-2.15	2.15	280	5.9	<10	-	70
GR10-2.35	2.35	220	5.6	16	26.4	60
GR10-2.65	2.65	210	5.2	<10	-	160
GR10-2.90	2.90	360	5.8	<10	-	180
GR11-2.35	2.35	150	5.9	16	14.8	30
GR11-2.65	2.65	120	5.9	31	28.7	20
GR11-2.90	2.90	150	6.2	31	17.5	20

+ - sampled in November 1979

TABLE 5.3

VARIATION IN THE CHEMICAL COMPOSITION OF GROUNDWATER⁺ ALONG
TRAVERSE L-GR6

SAMPLE NUMBER	DEPTH BELOW GROUND ,m	ELECTRICAL CONDUCTANCE ,uS	pH	ALKALINITY as HCO ₃ ,mg/l	DIC ,mg/l	SO ₄ ,mg/l
L-3.53	3.53	1400	3.4	<10	-	760
GR4-1.14	1.14	760	4.8	<10	-	420
GR4-1.64	1.64	750	5.0	<10	-	470
GR6-1.89	1.89	590	5.5	12	24.5	350
GR6-2.14	2.14	420	5.4	<10	-	235
GR6-2.39	2.39	450	5.5	15	30.4	220

+ - sampled in November 1979

To delineate the zone D boundary in the northeast flow regime, variations in the vertical profiles of electrical conductance, dissolved oxygen, pH and pe, major cations and major anions in groundwater amongst multilevel sites B, K, U, Q and R in Figures 5.5, 5.6, 5.7, 5.8, and 5.9 are examined. Data from sites B, K, U, Q and R are represented in these figures because these sites are located approximately along a flow line at 1, 16, 29, 55 and 90 meters, respectively, downflow from the gabbroic waste rock pile (Figure 5.3). The chemical analyses of groundwater from the follow-up geochemical survey in 1981, as reported in Veska (1983) have been used in these vertical profiles. Because major-ion data of the 1981 groundwater from some of the sites were lacking, chemical data of the 1979 groundwater from sites B, K and Q have been used in Figures 5.8 and 5.9 to provide complete vertical profiles.

Along the cross section of electrical conductance profiles from sites B to R in Figure 5.5, the values in groundwater decrease from 690 uS near the water table beneath the waste rock to 30 uS in the shallow aquifer at site R and to 340 uS in the deep aquifer at site R. High electrical conductance values are seen to originate from site B and to decrease in a downward direction towards site U.

The dissolved oxygen profiles in groundwater in the vicinity of the waste rock in Figure 5.6 indicate values at 4.5 mg/l at approximately 3 meters below the ground surface and values below the detection limit (0.1 mg/l) at depths greater than 10 meters. Downflow from the waste rock at site R, the dissolved oxygen content in groundwater is less than one mg/l in the shallow aquifer. The decrease in the dissolved oxygen content in groundwater with depth is reflected by the decrease in p with depth in the sand aquifer as shown in Figure 5.7. An inverse relation between pH (hydrogen-ion activity) and pe (relative electron activity) in groundwater with depth is shown in Figure 5.7.

The spatial distribution of the concentrations of the major cations in groundwater in Figure 5.8 indicates that calcium is dominant throughout the aquifer. The concentration distribution of the SO_4 , HCO_3 and DIC in groundwater

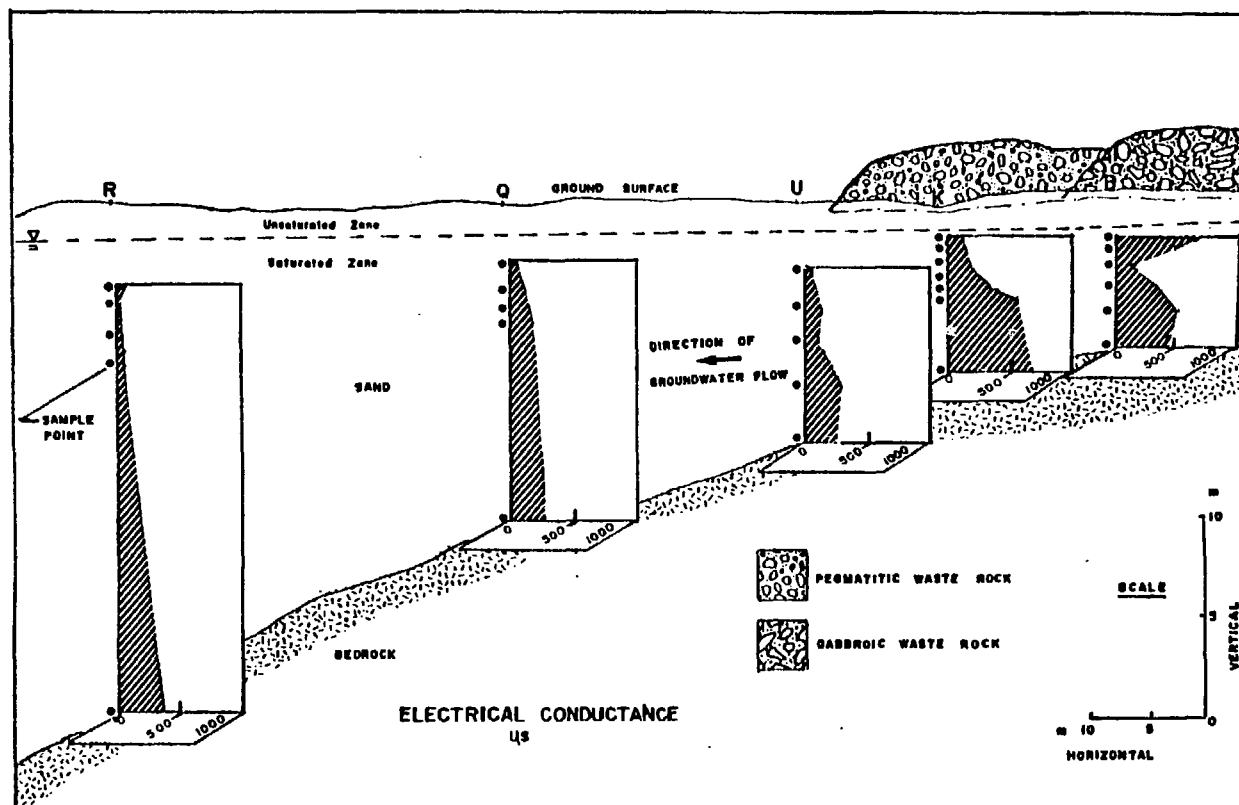


Figure 5.5 Schematic cross sectional diagram representing the spatial variations in the electrical conductance values in groundwater downflow from site B.

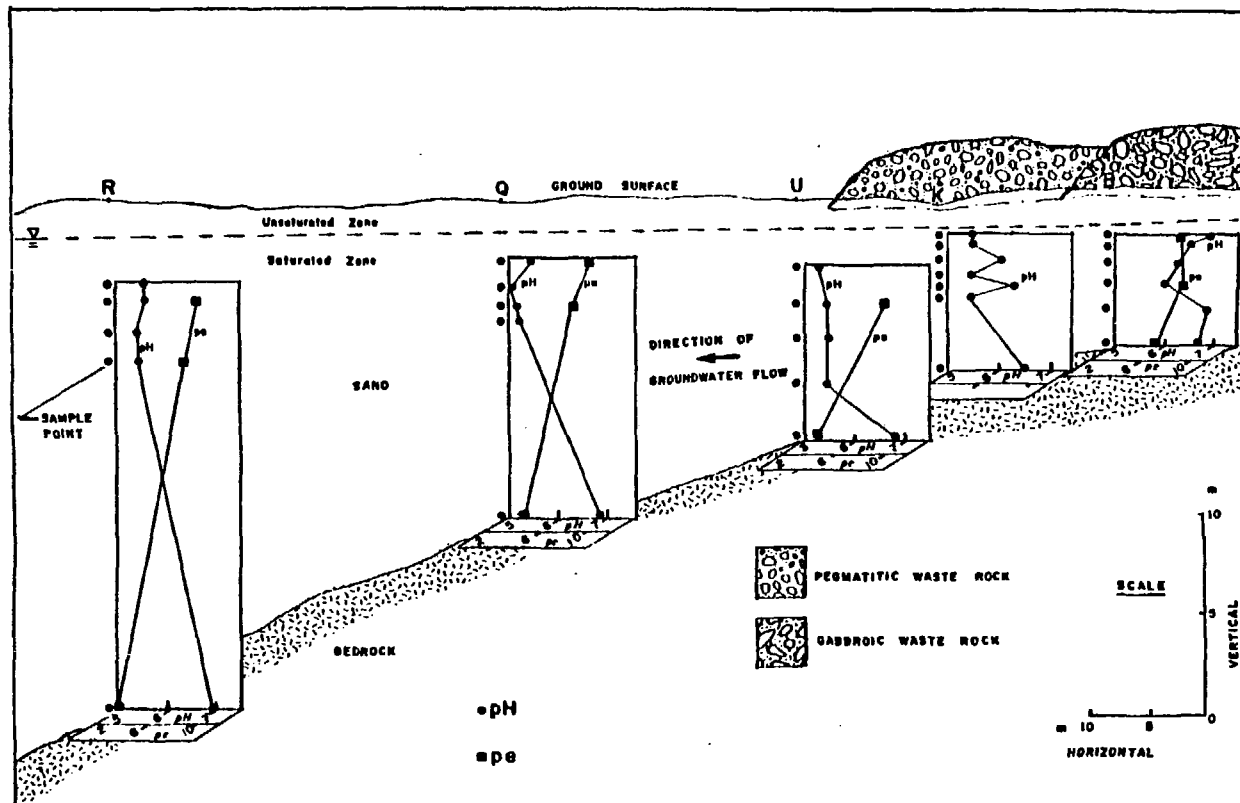


Figure 5.7 Schematic cross sectional diagram representing the spatial variations in the pH and pe values in groundwater downflow from site B.

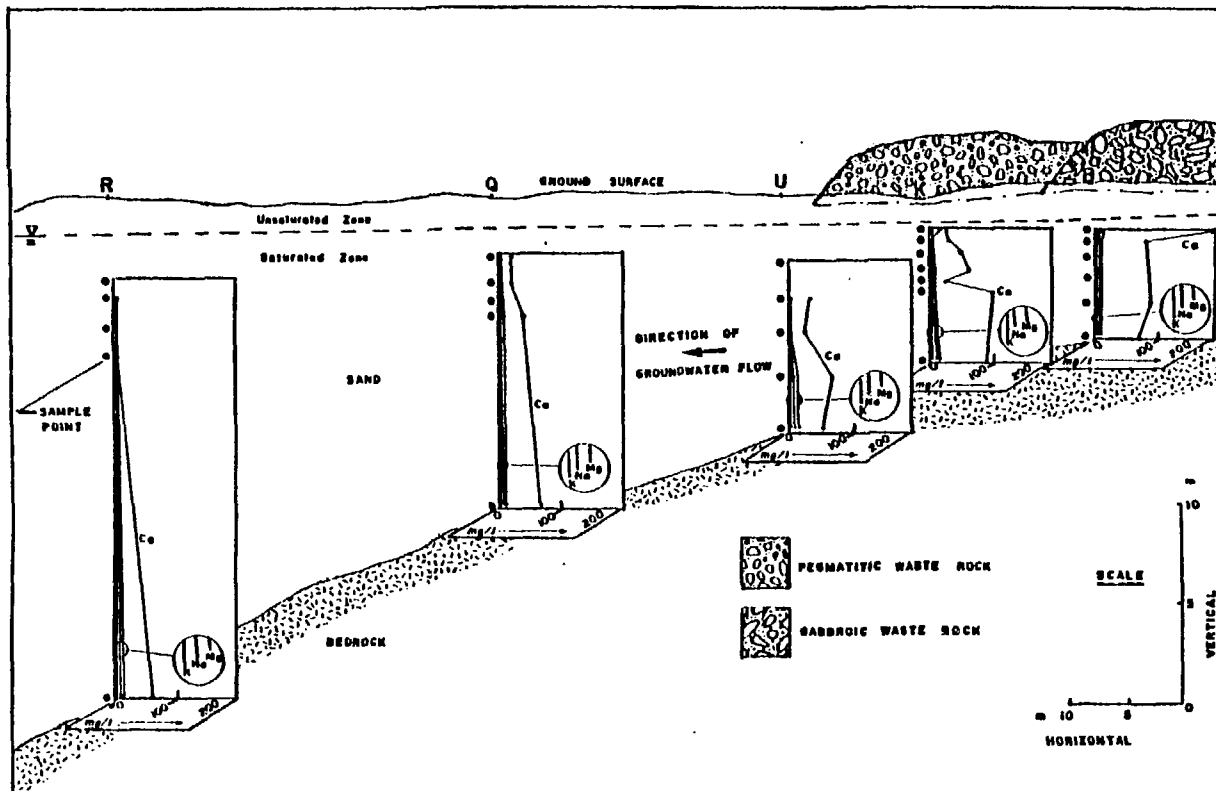


Figure 5.8 Schematic cross sectional diagram representing the spatial variations in the concentrations of Ca, Mg, Na and K in groundwater downflow from site B.

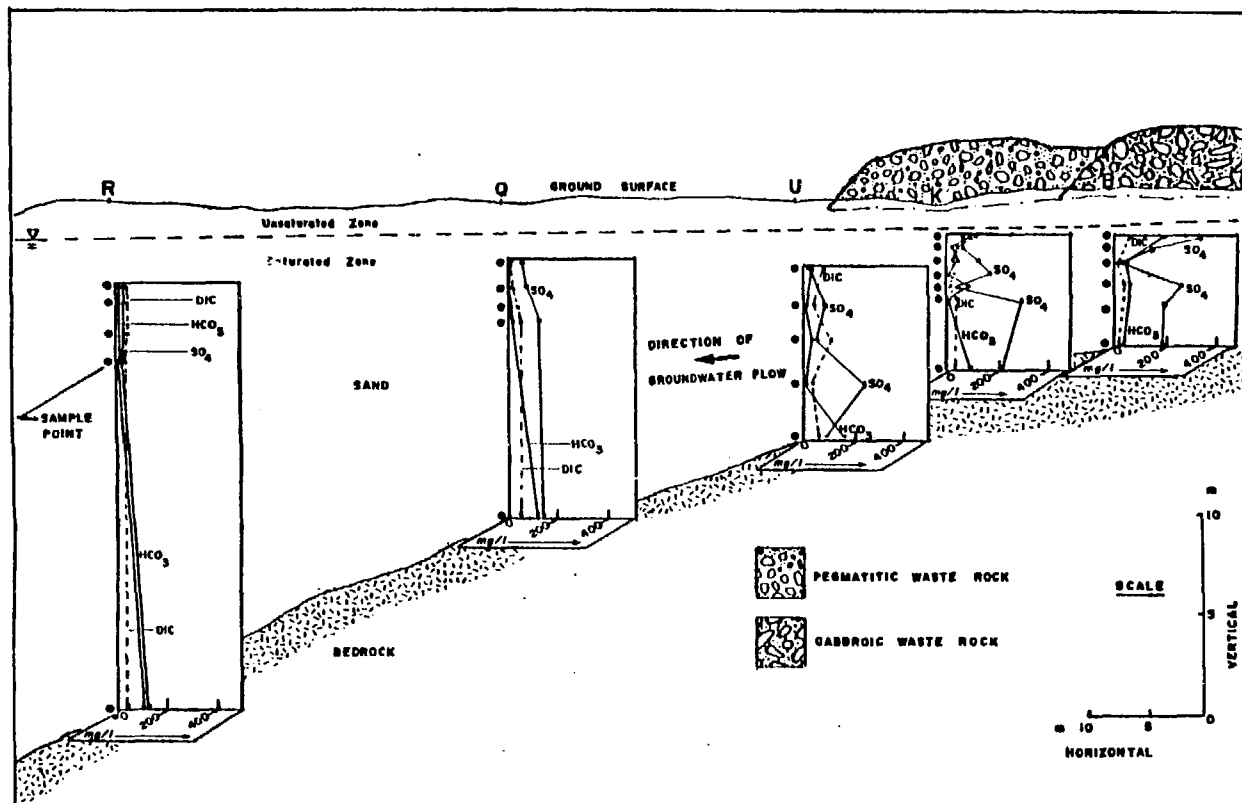


Figure 5.9 Schematic cross sectional diagram representing the spatial variations in the concentrations of SO_4 , HCO_3 and DIC in groundwater downflow from site B.

in Figure 5.9 indicates that sulphate is the predominant anion below the waste rock and that bicarbonate predominates progressively downflow from the waste rock at greater depths. To elaborate further on these empirical observations, statistical correlations between calcium and sulphate concentrations and between calcium and bicarbonate concentrations in the waste-rock-influenced groundwater (zone D), the shallow groundwater (zone A) and the deep groundwater (zone B), were determined by SAS, a statistical analysis computer program at the University of Waterloo. From 44 chemical analyses of groundwater samples in the sand aquifer, the correlation coefficients between calcium and sulphate concentrations in groundwater zones D, A and B are 0.87, 0.98 and 0.08, respectively as shown in Figure 5.10. In the same order of groundwater zones, the correlation coefficients between calcium and bicarbonate concentrations in groundwater are 0.08, 0.64 and 0.82. Based on these findings, the waste-rock-influenced groundwater and the shallow groundwater can both be characterized to a large degree as calcium-sulphate water and the deep groundwater as calcium-bicarbonate water.

Because of the lack of detailed sampling points at greater depths in the 1978 and 1979 instrumentation, the preliminary and follow-up geochemical surveys could not provide an accurate description of the spread of the zone D groundwater. From the installation of the detailed network of multilevel sampling points in 1982, groundwater was analyzed for electrical conductance, sulphate, alkalinity and pH from 267 sample points. The results of the chemical analyses from these samples are given in Veska (1983). These results are represented in the detailed contour mappings of electrical conductance, sulphate, bicarbonate, DIC and pH in groundwater along cross sections A-A'-C-C' and B-B' in Figures 5.11, 5.12, 5.13, 5.14 and 5.15. To inspect the accuracy of the generalized contours in Figures 5.11-5.15 inclusive, values of each of the five constituents from several sample multilevel bundles are given in Table 5.4. Cross sections A-A'-C-C' and B-B' were chosen in order to map the spread of the waste-rock-derived contaminants in the zone D groundwater because of the

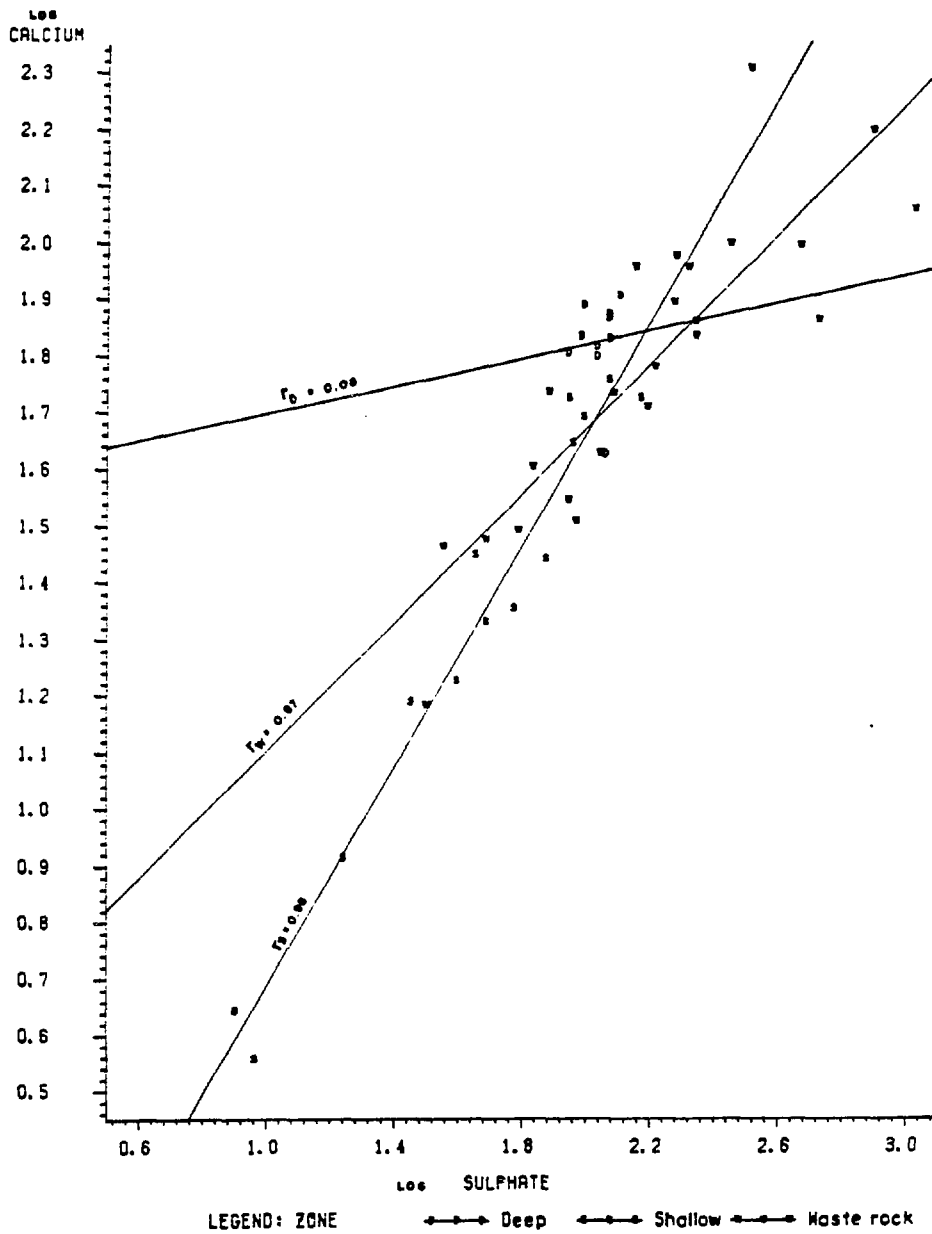
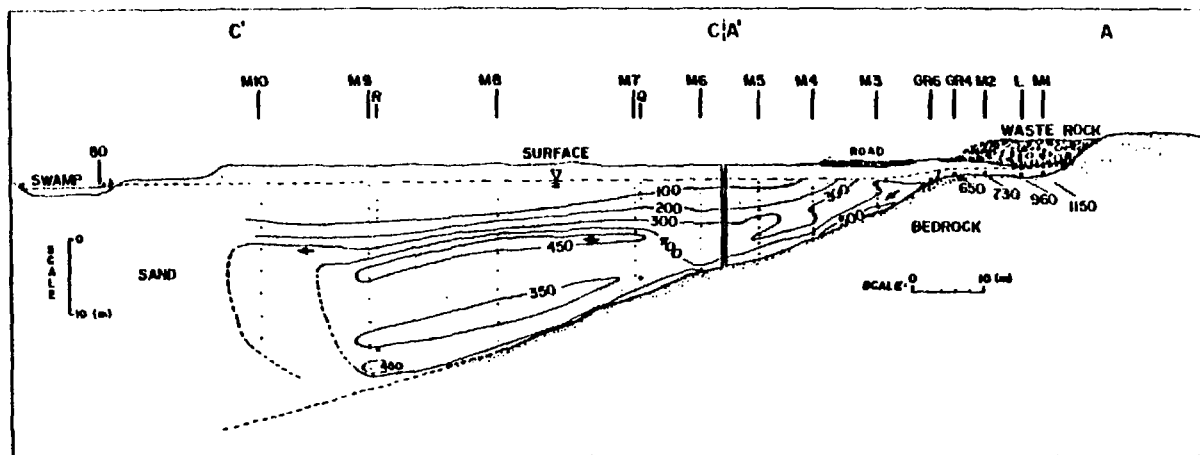


Figure 5.10 Correlation coefficients between calcium and sulphate concentrations in the deep groundwater, shallow groundwater and waste-rock-influenced groundwater.



ELECTRICAL CONDUCTANCE

uS

 Waste rock deposited on terrain from 1906 to 1959

 Section of waste rock excavated in September 1979

 Water table, June 7, 1982

• Piezometer tip

• Multi-level sampling point

→ General groundwater flow direction

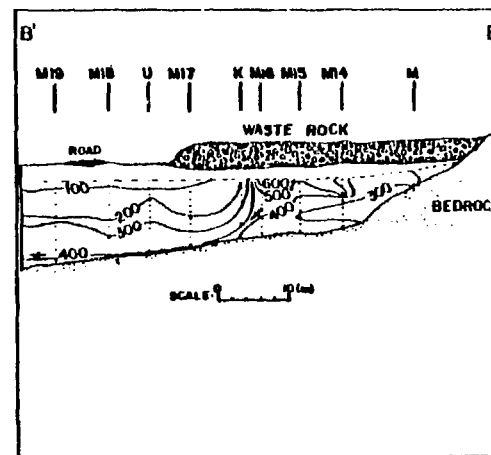
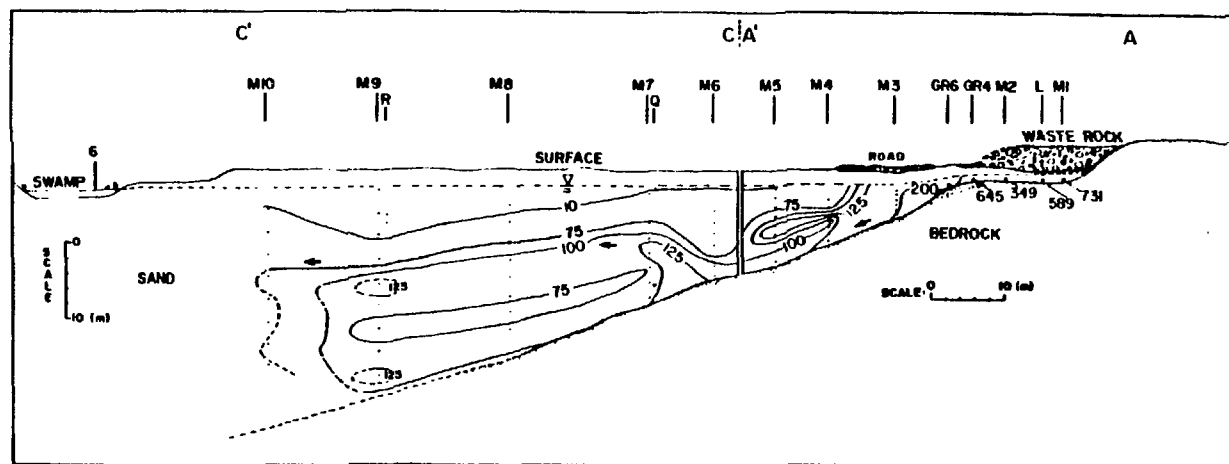








Figure 5.11 Distribution of electrical conductance values in groundwater along cross sections A-A', B-B' and C-C'.



SULPHATE
mg/l

-  Waste rock deposited on terrain from 1956 to 1959
-  Section of waste rock excavated in September 1979
-  Water table, June 7, 1982
-  Piezometer tip
-  Multilevel sampling point
-  General groundwater flow direction

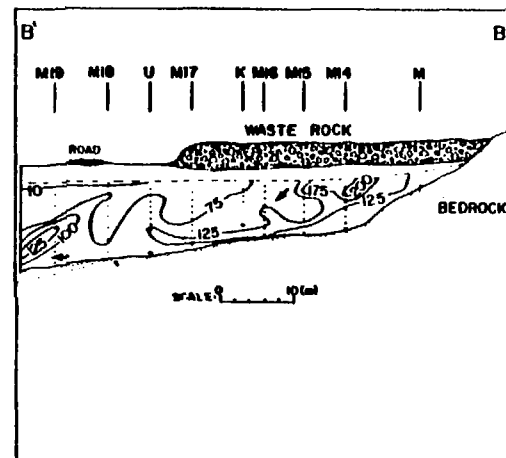
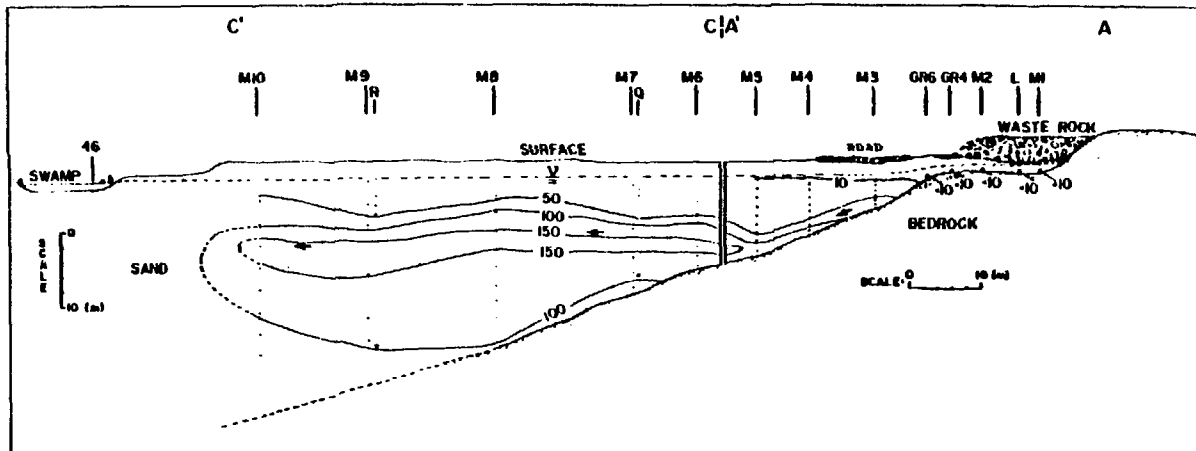


Figure 5.12 Distribution of sulphate concentrations in groundwater along cross sections A-A', B-B' and C-C'.



BICARBONATE mg/l

- Waste rock deposited on terrain from 1956 to 1959
- Section of waste rock excavated in September 1979
- Water table, June 7, 1982
- Piezometer tip
- Multilevel sampling point
- General groundwater flow direction

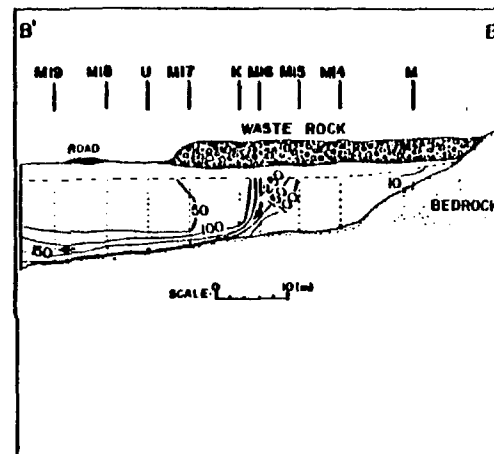
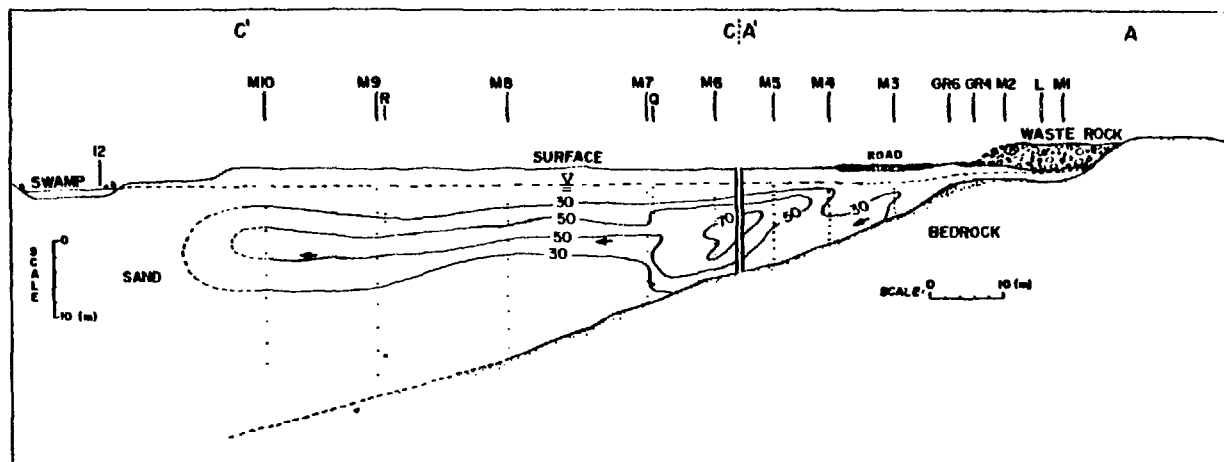


Figure 5.13 Distribution of bicarbonate concentrations in groundwater along cross sections A-A', B-B' and C-C'.



DISSOLVED INORGANIC CARBON

mg/l



Waste rock deposited on terrain from 1906 to 1959



Section of waste rock excavated in September 1979



Water table, June 7, 1982



Piezometer tip



Multilevel sampling point



General groundwater flow direction

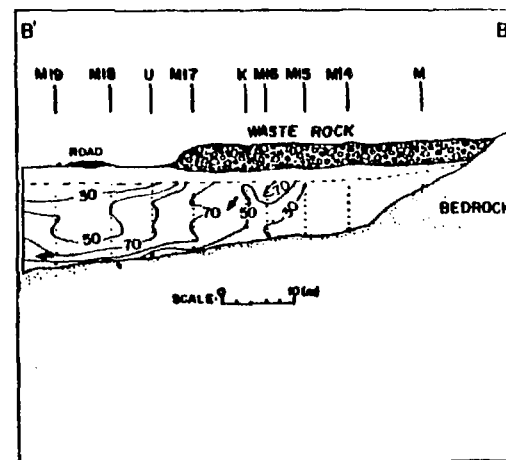
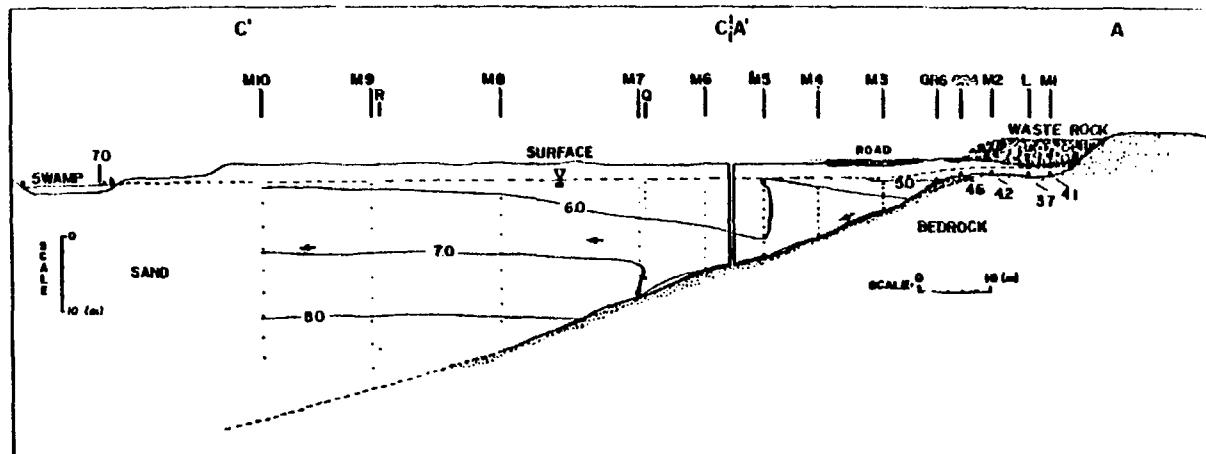


Figure 5.14 Distribution of dissolved inorganic carbon concentrations in groundwater along cross sections A-A', B-B' and C-C'.



pH

 Waste rock deposited on terrain from 1956 to 1959

 Section of waste rock excavated in September 1979

 Water table, June 7, 1982

 Piezometer tip

 Multilevel sampling point

 General groundwater flow direction

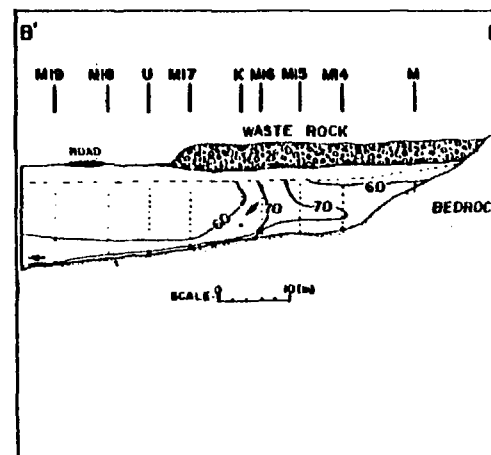


Figure 5.15 pH distribution in groundwater along cross sections A-A', B-B' and C-C'.

TABLE 5.4

CHEMICAL ANALYSIS OF THE 1982 GROUNDWATER
FROM SITES M5, M16 and M9

SAMPLE NUMBER*	LABORATORY ELECTRICAL CONDUCTANCE, uS	SULPHATE ,mg/l	BICARBONATE ,mg/l	DIC ,mg/l	pH
M5-2.44	94	10.5	33	15.8	6.3
M5-3.80	128	44.7	25	49.5	5.5
M5-4.92	124	75.8	20	60.6	5.3
M5-6.13	246	90.8	20	53.9	5.4
M5-7.34	360	154	26	51.5	5.5
M5-8.37	390	171	28	25.5	5.9
M5-9.78	298	100	45	41.0	5.9
M5-11.00	360	101	97	36.1	6.5
M5-12.21	428	116	132	35.0	6.9
M16-3.06	600	108	277	62.3	7.3
M16-3.94	580	109	272	70.7	7.0
M16-4.84	490	92.1	234	62.0	6.9
M16-5.75	460	116	163	46.3	6.8
M16-6.65	480	134	154	48.4	6.7
M16-7.57	390	108	103	43.3	6.4
M16-8.47	360	125	54	14.0	7.0
M16-9.38	370	127	60	33.0	6.2
M9-3.00	66	4.6	30	27.9	5.9
M9-6.06	74	5.5	40	26.4	6.1
M9-9.09	134	3.9	79	37.9	6.3
M9-12.17	330	56.7	170	43.4	7.0
M9-15.25	430	142	152	31.9	7.6
M9-18.21	368	86.3	119	24.2	7.9
M9-21.58	378	51.2	108	21.9	8.0
M9-24.45	330	81.7	100	20.0	8.0
M9-27.47	490	160	94	19.1	8.0

* The numbering system is given for groundwater samples with their respective locations and depths. The individual depths at which the groundwater samples were taken from multilevel devices are given in meters.

intersections made with the 1982 instrumentation sites and because of the approximate alignment with the two major groundwater flow directions. No other cross sections could have been made along the two major flow regimes that would have contained as many sample points from the water table to the bedrock surface, as that for cross sections A-A'-C-C' and B-B'.

The distribution of the values of laboratory-measured electrical conductance in groundwater in Figure 5.11 shows high values below the waste rock, ranging from 600 to 1150 uS. Approximately 100 meters downflow from the waste rock to site M10, the conductance values decrease to approximately 300 uS. The trend in the decrease in electrical conductance values in groundwater downflow from the waste rock follows the general trend in the directions of groundwater flow. Downflow from the waste rock, the plume of electrical conductance in groundwater is bordered at the top by shallow groundwater with values below 100 uS and at the bottom by the bomb tritium boundary. Below this lower boundary, pre-1953 recharge water flows upward towards the center of the sand aquifer.

In order to determine the degree of retardation of radionuclides in the aquifer, it is necessary to know the extent of migration of non-retarded contaminants and/or the groundwater velocity. Early in the investigation, groundwater sampling indicated that sulphate was the best waste-rock-derived constituent to use as a non-retarded tracer of waste-rock contamination. Sulphate emanates from the waste rock into the aquifer, mainly because of the weathering of sulphide minerals, such as pyrite, in the rock. The sulphate distribution in groundwater for 1982 is shown in Figure 5.12. The highest sulphate concentrations in groundwater are found below the waste rock, ranging from 200 to 731 mg/l. Downflow from the waste rock to site M10, the values decrease to a low of 63.2 mg/l in the middle of the aquifer. Similar to the electrical conductance plume, the plume of sulphate contamination from the waste rock follows the general groundwater flow directions in the sand aquifer. The sulphate plume is bordered by an upper boundary in the shallow aquifer that contains sulphate in groundwater below 10 mg/l. This low concentration range of

sulphate in groundwater is indicative of background sulphate, resulting from soil-water interactions from the infiltration of recharge water by precipitation. The low sulphate content in the shallow groundwater is considered to represent conditions of no waste-rock contamination because there is no evidence of waste rock deposition on the ground surface along cross section C-C'. The lower boundary for the sulphate plume in the deep aquifer is the bomb tritium boundary. The bomb tritium boundary marks the deepest limit possible within the sand aquifer for the travel of the 1957 recharge water that has infiltrated the waste rock near the mine. Although the sulphate concentrations in groundwater were not determined downflow from site M10, it is reasonable to estimate from Figure 5.12 that the extent of the sulphate plume is between site M10 and the swamp, or 100 to 120 meters downflow from the waste rock.

Plumes of DIC and bicarbonate concentrations in groundwater are observed in Figures 5.13 and 5.14. There exists a resemblance between the shapes of the two plumes, as both plumes follow the general direction of groundwater flow. The highest concentrations of DIC at 70 mg/l, and bicarbonate, at 250 mg/l, appear to originate in groundwater beneath the waste rock along the B-B' cross section. Approximately 100 meters downflow from the waste rock in the center of the sand aquifer, the DIC and bicarbonate concentrations decrease to less than 30 mg/l and less than 100 mg/l, respectively.

The pH distribution of groundwater is shown in Figure 5.15. Two different types of pH profiles in groundwater are observed along cross sections, A-A' and B-B'. Along cross section A-A', the progression of a low-pH front in the sand aquifer is evident from the pH 3.7 groundwater at site L downflow to the pH 5.0 groundwater at site GR6 and further downflow to the pH 6.5 groundwater at site M4. Conversely, the pH is fairly constant between 6.0 and 7.0 in groundwater along cross sections B-B' and C-C'.

5.3 Spatial Distributions of Radionuclides

The hydrochemical patterns in the sand aquifer indicated the presence of a contaminant zone (zone D) that was derived from the weathering of the uranium-bearing waste rock. This zone may also have some influence on the activity distribution of radionuclides found in groundwater.

The radiochemical results for ^{238}U , ^{234}U , ^{226}Ra , ^{210}Pb , ^{230}Th and ^{232}Th in the groundwater samples that have been obtained from various sites in the aquifer from 1979 to 1980 are recorded in Veska (1983). From these analyses, activity versus depth profiles of radionuclides in groundwater are given and are described in detail in Veska (1983). From the findings in Veska (1983), a zone of generally above-background activities of radionuclides in groundwater is delineated near and around the piles of the uranium-bearing waste rock. This zone overlaps with the hydrochemical zone D. With the exception of ^{226}Ra , the activities of ^{238}U , ^{234}U , ^{230}Th , ^{232}Th and ^{210}Pb in the contaminated groundwater in the vicinity of the waste rock are below the maximum permissible concentrations for drinking water as prescribed by the International Committee on Radiological Protection (ICRP) (i.e. ^{238}U at 600 pCi/l, ^{234}U at 30,000 pCi/l, ^{210}Pb at 100 pCi/l, ^{230}Th at 2000 pCi/l and ^{232}Th at 2000 pCi/l, ICRP, 1979). The ^{226}Ra activities in water in certain parts of the sand aquifer are greater than the maximum acceptable limits for drinking water, i.e. at 10 pCi/l (ICRP, 1979) and at 27 pCi/l (Health and Welfare Canada, 1978). The target limit or the objective limit set by the Canadian Government for ^{226}Ra in drinking water is 2.7 pCi/l (Health and Welfare, 1978).

To investigate the effect of the emanation of radioactive and chemical constituents from the waste rock on the natural aquifer conditions in the northwest flow regime, the spatial variations of these constituents along traverses L-GR6 and GR9-GR11 are described using the 1979/1980 data. The activities of radionuclides and concentrations of chemical constituents in groundwater along traverse L-GR6 are plotted in Figure 5.16. Along traverse L-GR6, decreases are seen in the activities of the radioactive constituents in groundwater for ^{238}U from 86.90 pCi/l to 1.84 pCi/l, for ^{234}U from 43.45

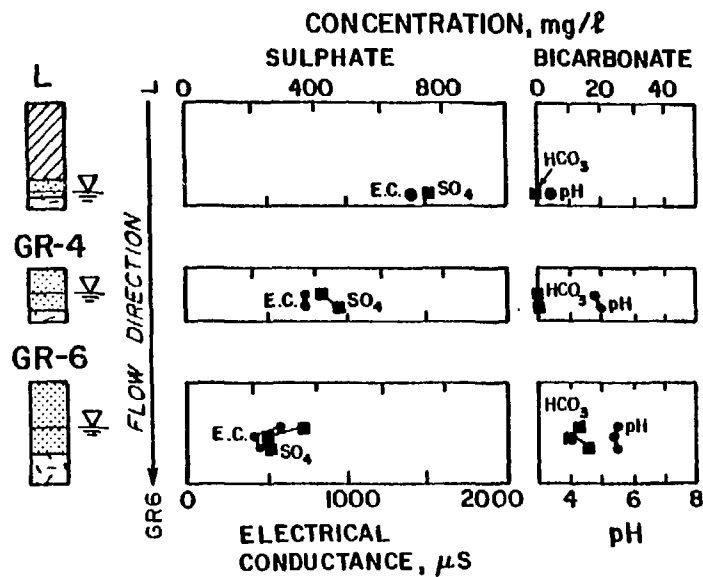
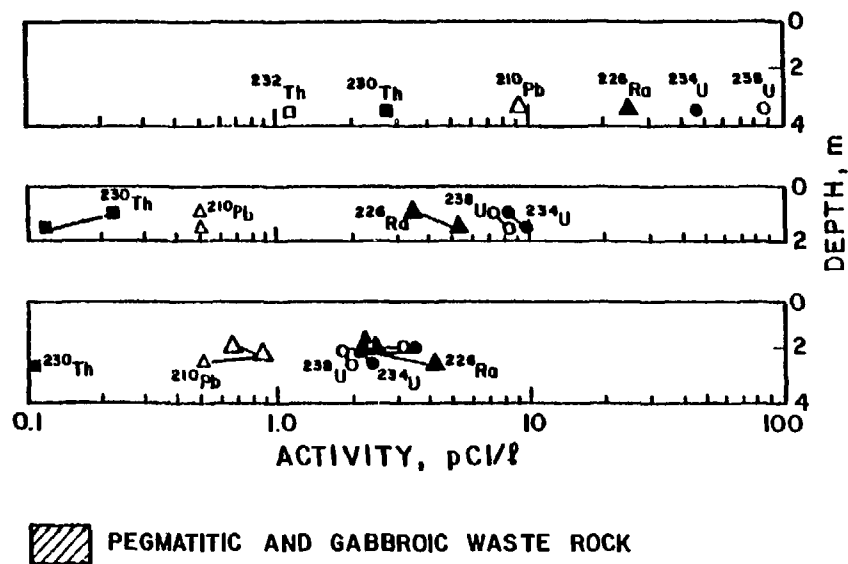


Figure 5.16 Spatial variation in the concentration vs. depth profiles of radionuclides and chemical constituents in groundwater downflow from piezometer L to multilevel piezometer GR-6.

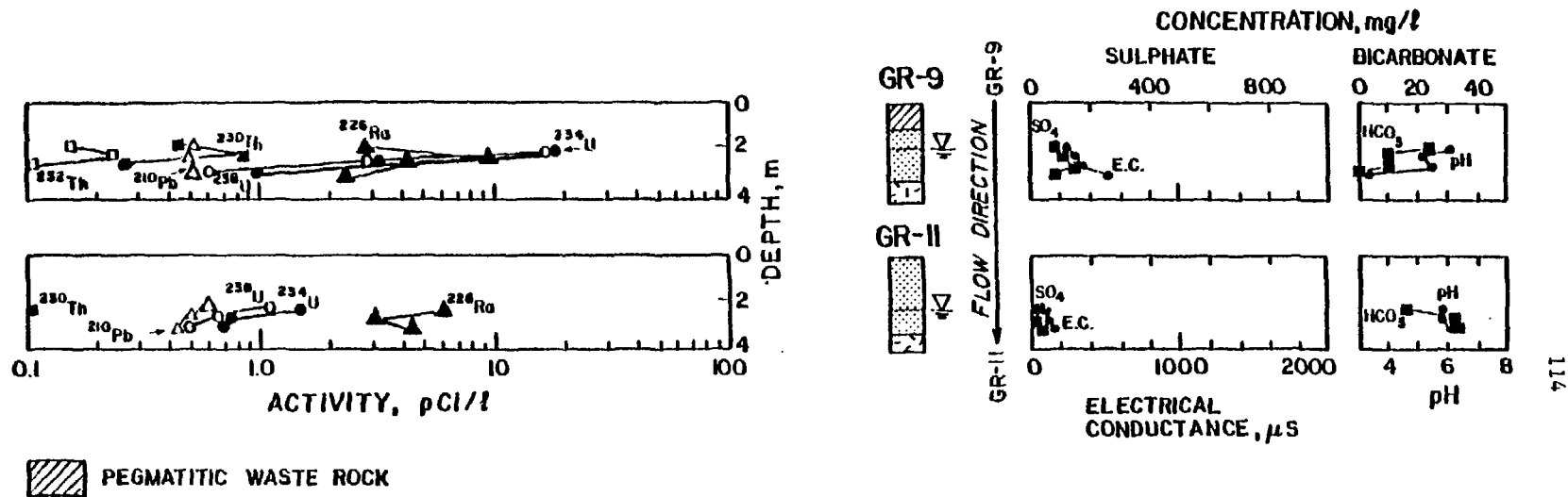


Figure 5.17 Spatial variation in the activity and concentration vs. depth profiles of radionuclides and chemical constituents in groundwater downflow from multilevel piezometer GR-9 to multilevel piezometer GR-11.

pCi/l to 2.07 pCi/l, for ^{226}Ra from 23.6 pCi/l to 2.4 pCi/l, for ^{210}Pb from 9.4 pCi/l to 0.9 pCi/l, for ^{230}Th from 2.45 pCi/l to less than 0.1 pCi/l and for ^{232}Th from 1.10 pCi/l to less than 0.1 pCi/l. These strong decreasing trends are similar to those of the decreasing trends in the values of sulphate and electrical conductance in groundwater along traverse L-GR6. Conversely, the values of bicarbonate and pH show an increasing trend in groundwater along traverse L-GR6.

Similar radionuclide and chemical trends are evident in water samples along traverse GR9-GR11 in Figure 5.17. The radionuclide composition of groundwater along this 10 meter traverse shows a decrease in the activities of ^{238}U from 16.82 pCi/l to 0.69 pCi/l, ^{234}U from 18.00 pCi/l to 0.74 pCi/l, ^{226}Ra from 9.4 pCi/l to 3.1 pCi/l, ^{230}Th from 0.84 pCi/l to less than 0.1 pCi/l and ^{232}Th from 0.24 pCi/l to 0.1 pCi/l. Superimposed with the radionuclide profiles are the profiles of the sulphate and electrical conductance values, which show a similar decreasing trend along this traverse. Conversely, an increasing trend in the values of bicarbonate and pH is observed with distance from site GR9 (Figure 5.17).

To investigate the influence of radionuclide contamination from the waste rock in the northeast flow regime, the spatial variations of the activities of radionuclides in groundwater along the flow path that joins sites B, K, U, Q, and R, are described using the 1979/1980 radiochemical data. Along the B-R traverse, the variations in the distributions of ^{226}Ra and ^{238}U activities in groundwater are displayed by three-dimensional activity verses depth profiles in Figures 5.18 and 5.19. The variations in the ^{210}Pb , ^{230}Th and ^{232}Th activities in groundwater have not been assessed in a similar manner because the activities of these radioisotopes are either near or at the respective detection limits.

The distribution of ^{226}Ra activities in groundwater as depicted in Figure 5.18 shows the highest activities below the waste rock, ranging from 1.9 to 19.5 pCi/l. The ^{226}Ra activity in groundwater at site R, approximately 100 meters downflow from the waste rock, decreases to levels that approach 1.5 pCi/l. A strong downward trend in the profiles of activities of ^{226}Ra in groundwater below the waste rock exists along the direction of groundwater flow.

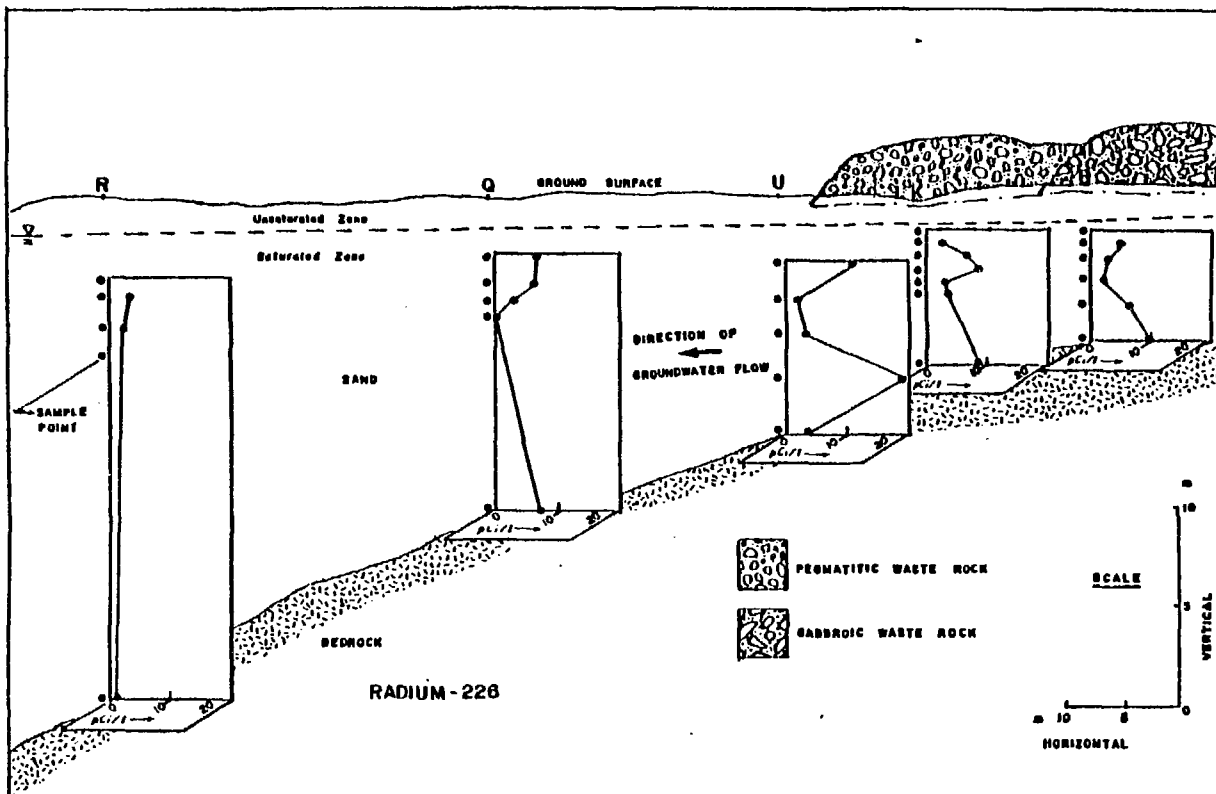


Figure 5.18 Activity vs. depth profiles of radium-226 in groundwater downflow from site B.

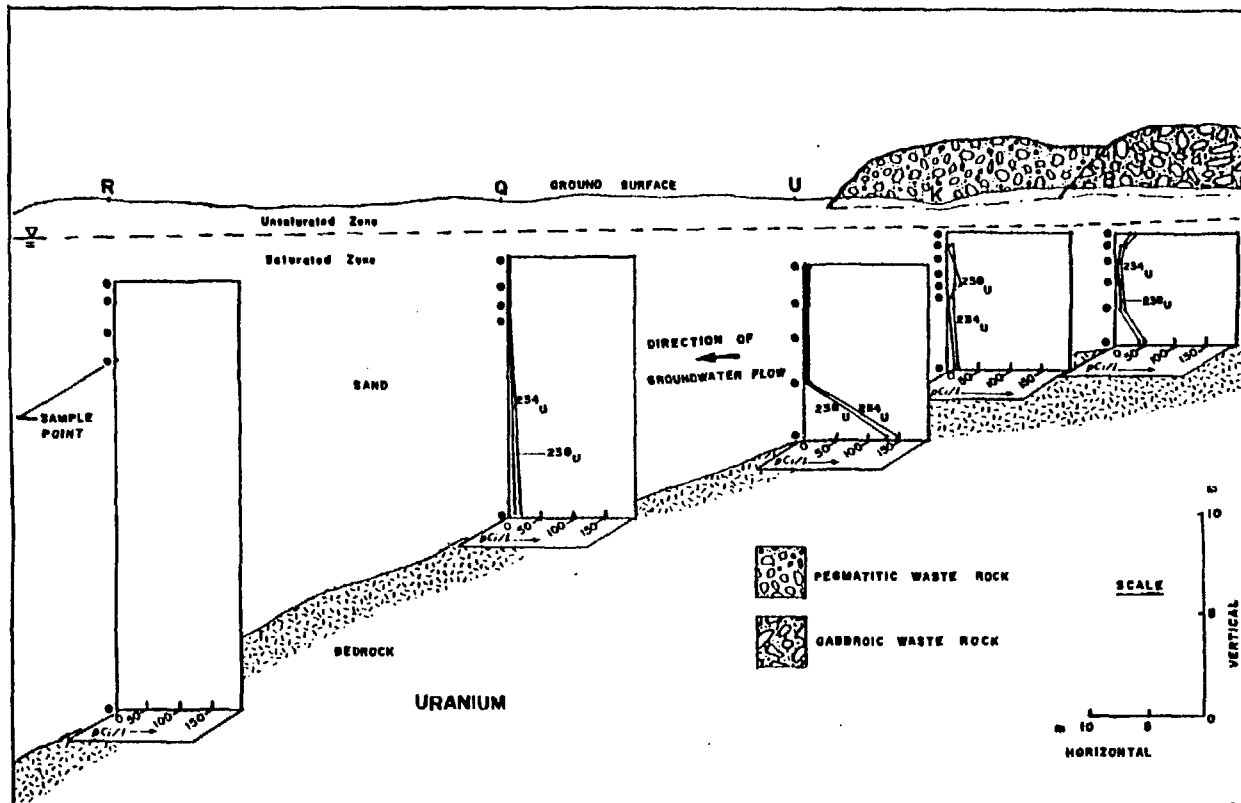


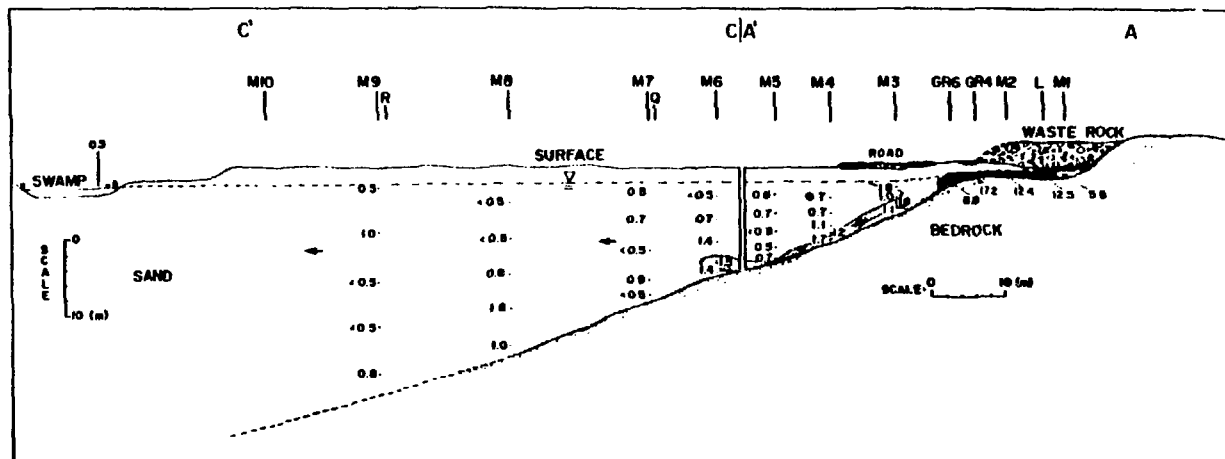
Figure 5.19 Activity vs. depth profiles of ^{234}U and ^{238}U in groundwater downflow from site B.

A trend in increasing ^{238}U activities in groundwater with depth downflow from the waste rock exists (Figure 5.19). The ^{238}U activity in groundwater is relatively high at 27.90 pCi/l near the water table at site B and increases to 128.06 pCi/l in deep groundwater downflow from the waste rock at site U. The activity of ^{238}U in groundwater decreases downflow from site U to site Q, with values ranging from 1.30 to 9.11 pCi/l in groundwater at site Q.

The radiochemical analyses of groundwater collected in 1981 from sites L, GR4, GR6, A, U, T, Q, R and Y are given in Veska (1983). The activity ranges of radionuclides in the 1981 groundwater are shown to be slightly lower than those which were analyzed for in the 1979/80 preliminary survey. A discussion of the temporal variation in radionuclide activities in groundwater from sampling devices will be discussed in the next section of this Chapter.

For a more accurate delineation of the extent of ^{226}Ra , ^{210}Pb and ^{238}U contamination from waste rock in groundwater, the 1982 activity distributions for each of these constituents are plotted in detail at numerous sampling points along cross sections A-A'-C-C' and B-B' in Figures 5.20, 5.21 and 5.22. The 1982 radiochemical data for each of these radioactive constituents in groundwater are given in Veska (1983).

The spatial distribution of the ^{226}Ra activities in groundwater in Figure 5.20 indicates that ^{226}Ra contamination in groundwater originates from the waste rock, in particular, below the pegmatite-gabbro waste rock along cross section A-A'. From sites L to GR6 along cross section A-A', the ^{226}Ra activities in this low pH groundwater zone range from 8.8 to 17.2 pCi/l. Approximately seven meters downflow from site GR6, or 20 meters downflow from site L, the ^{226}Ra activities decrease to between 0.5 and 1.8 pCi/l at site M3. It is reasonable to estimate from Figure 5.20, that site M3 represents the lateral extent of the ^{226}Ra plume in groundwater from the pegmatite-gabbro waste rock. In comparison to the ^{226}Ra activities in groundwater along cross section A-A', the highest ^{226}Ra activities below the pegmatite waste rock along cross section B-B' range from 2.5 to 5.0 pCi/l, i.e. at approximately



RADIUM-226

pCi/l

7.5 - 20

2.5 - 7.5

1.5 - 2.5

< 1.5



Waste rock deposited on terrain from 1956 to 1959



Section of waste rock excavated in September 1979



Water table, June 7, 1982



Piezometer tip



Multilevel sampling point



General groundwater flow direction

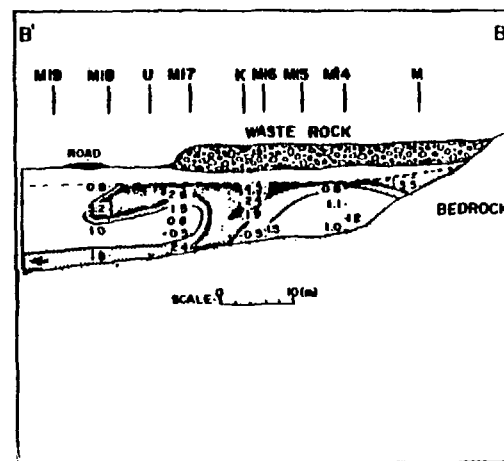
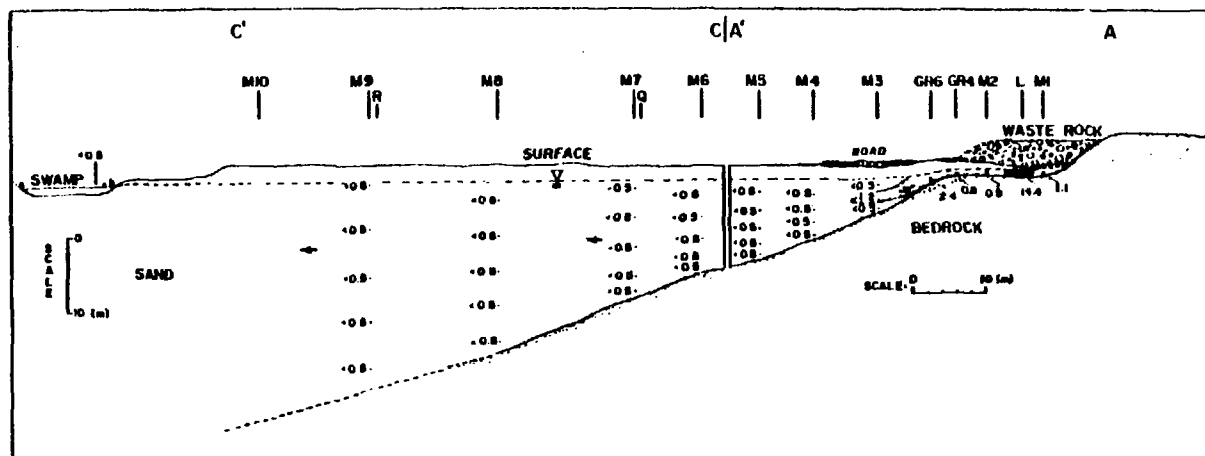


Figure 5.2.0 Distribution of radium-226 activity in groundwater along cross sections A-A', B-B' and C-C'.



LEAD-210

pCi/l

25-150

05-25

<05



Waste rock deposited on terrain from 1956 to 1959

Section of waste rock excavated in September 1979



Water table, June 7, 1982



Piezometer tip



Multilevel sampling point



General groundwater flow direction

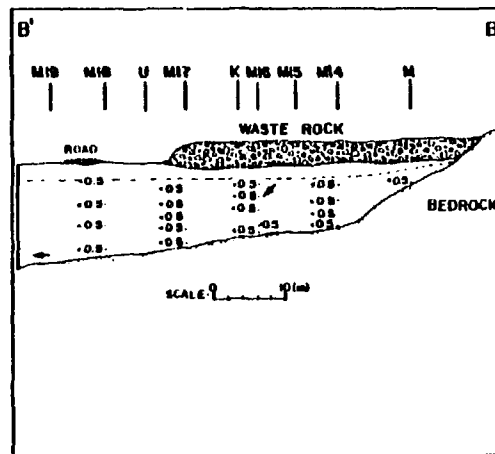


Figure 5.21 Distribution of lead-210 activity in groundwater along cross sections A-A', B-B' and C-C'.

two meters below the water table. Below this point, the radium activities decrease to a range between 1.0 to 2.5 pCi/l. The only exceptions are the 3.2 pCi/l value at 5.54 meters below ground surface at site M18 and the 2.4 pCi/l value at 10.79 meters below the ground surface at site M17.

For most of the sand aquifer, the ^{210}Pb activities in groundwater in Figure 5.21 are below the detection limit at 0.5 pCi/l. The only noticeable activities of ^{210}Pb in groundwater are found in the low pH zone beneath the pegmatite-gabbro waste rock along cross section A-A'. The highest ^{210}Pb value in groundwater, at 14.4 pCi/l, is found at site L. The values of ^{210}Pb in groundwater drastically decrease to less than 1.0 pCi/l at four meters upflow and downflow from site L. Downflow from site L, ^{210}Pb activities greater than 1.0 pCi/l exist in groundwater at site GR6 at 2.4 pCi/l and at site M3 at 1.2 pCi/l. These values can possibly be derived from radioactive decay of ^{226}Ra in groundwater along cross section A-A' for the past 25 years. Indeed, the amount of ^{210}Pb activity in groundwater that can be produced from ^{226}Ra decay in a closed system for a 25 year ingrowth period is equivalent to 55% of the ^{226}Ra activity in groundwater.

Although the 1982 samples were not analyzed for thorium isotopes, the distribution of dissolved thorium in the sand aquifer is expected to be similar to that of ^{210}Pb . For example, from the preliminary 1979/80 findings, the only notable activities of ^{230}Th and ^{232}Th in the groundwater were confined to the acid front zone below the waste rock. Beyond the periphery of the waste rock, the activities of the thorium isotopes in the groundwater were below the detection limit.

Uranium is the most mobile of all the radionuclides of interest in the sand aquifer, as can be observed from the spatial distribution of the ^{238}U activities in groundwater in Figure 5.22. The activity of ^{238}U is high in groundwater at site L at 39.1 pCi/l. Downflow from site L along cross section A-A', the ^{238}U activities in groundwater decrease to 8.3 pCi/l at site GR6. Downflow from site GR6 and approximately 30 meters from site L along cross section A-A', the ^{238}U activities in groundwater increase to 121.1 pCi/l at

site M4. Downflow from site M4 along cross section A-A'-C-C', the ^{238}U activities decrease to levels near the detection limit at approximately 80 meters from site L. The shape of the ^{238}U plume along A-A'-C-C' follows the direction of groundwater flow, as deduced from the equipotential contours in Figures 4.9 and 4.10. The shape of the ^{238}U plume is also similar to the shapes of the plumes for bicarbonate, DIC, electrical conductance and sulphate in groundwater. The ^{238}U activities in groundwater are also high below the waste rock along cross section B-B'. The highest ^{238}U activities are found near the bedrock surface at 101.56 pCi/l at site M17, at 36.74 pCi/l at site M14 and at 99.95 pCi/l at site M13 and also near the water table at site M16, i.e. between 39.83 and 86.59 pCi/l. Along the general direction of the ^{238}U plume beyond the waste rock along cross section B-B', the high activities of ^{238}U in groundwater decrease to 7.5 pCi/l at site M18.

5.4 Temporal Variation in Radionuclide Activities

Several of the 1979/80 samples at multilevel sites downflow from the waste rock contained higher activities of ^{226}Ra and ^{210}Pb (Veska 1983) than normal background values for those areas. In particular, water samples from sample numbers A-5.8, U-8.89, R-7.14 and R-7.91 contained anomalously-high activities of ^{226}Ra and ^{210}Pb in groundwater. Samples of groundwater from these four sampling points were resampled on October 31, 1979 and October 20, 1981 and analyzed for ^{226}Ra and ^{210}Pb to check the earlier reported results. Samples of water were also taken from seven multilevel devices along the 12 meter depth profile at site U in order to observe any change in the radionuclide profiles with depth and time. The results are listed in Table 5.5. The original high ^{226}Ra and ^{210}Pb activities in groundwater samples, A-5.8, U-8.89, R-7.14 and R-7.91, decrease with time of sampling from 1979 to 1981. With the exception of sample U-8.89, the activities of ^{226}Ra and ^{210}Pb in six of the water samples from multilevel piezometer U are nearly the same for the September 1979, October 1979 and October 1981 sampling dates. The

TABLE 5.5

TEMPORAL VARIATION IN ^{226}Ra AND ^{210}Pb ACTIVITIES IN GROUNDWATER
AT SITES A, U AND R

SAMPLE NUMBER	SEPTEMBER 17, 1979		OCTOBER 31, 1979		OCTOBER 20, 1981	
	^{226}Ra , pCi/l	^{210}Pb , pCi/l	^{226}Ra , pCi/l	^{210}Pb , pCi/l	^{226}Ra , pCi/l	^{210}Pb , pCi/l
A- 5.8	67.3 ± 5.9	< 0.5	4.6 ± 0.3	< 0.5	3.5 ± 0.4	< 0.5
U- 4.06	5.0 ± 0.4	< 0.5	3.6 ± 0.3	< 0.5	-	-
U- 4.86	1.9 ± 0.2	< 0.5	5.3 ± 0.3	1.1 ± 0.2	2.3 ± 0.3	< 0.5
U- 5.60	4.2 ± 0.3	< 0.5	3.2 ± 0.2	< 0.5	-	-
U- 7.14	5.5 ± 0.7	< 0.5	4.8 ± 0.3	< 0.5	-	-
U- 7.91	8.7 ± 0.4	< 0.5	4.1 ± 0.3	< 0.5	-	-
U- 8.89	19.5 ± 1.7	< 0.5	4.1 ± 0.3	< 0.5	1.6 ± 0.3	< 0.5
U-11.80	3.7 ± 0.3	0.9 ± 0.2	2.5 ± 0.4	< 0.5	1.6 ± 0.3	< 0.5
R- 7.14	7.7 ± 0.5	< 0.5	0.7 ± 0.3	< 0.5	-	-
R- 7.91	44.6 ± 3.4	7.7 ± 3.5	1.1 ± 0.5	1.4 ± 0.4	0.6 ± 0.3	< 0.5

anomalously-high activities of ^{226}Ra and ^{210}Pb in the September 1979 groundwater samples can possibly be explained by experimental errors in the early development period of the analytical procedure or by cross-contamination from other radioactive sources within the radiochemistry laboratory. Whatever the reason(s), it is believed that the measured ^{226}Ra and ^{210}Pb activities in these four groundwater samples in September 1979 are not representative of the activities in groundwater at the Greyhawk field site at the time of sampling.

The temporal and spatial variations in ^{238}U and ^{226}Ra activities in groundwater at site L and also at sites located along cross section A-A'-C-C' are shown in Figure 5.23. The selected sample points along cross section A-A'-C-C' in Figure 5.23 are located in the zones of uranium and radium contamination in the sand aquifer. Large variations are seen in the radionuclide activities in groundwater at site L with time. However, these variations with time become very small downflow from the waste rock, as noticed at site Q. The large variations in the activities of radionuclides in groundwater at site L are probably affected by variations in the mineral-weathering reaction rates in the waste rock mass and by variations in the rates and frequencies of infiltration through the waste rock.

5.5 Summary

Three natural hydrochemical zones were identified in the sand aquifer. One of these zones contains an appreciable percentage of water derived by seepage from the nearby swamp. A second zone occurs in the deep part of the sand and possibly represents water derived from outside the local area. The third zone occurs at shallow depth in the sand and represents water from local infiltration that has not passed through the waste rock and has not been influenced by seepage from the swamp. The boundaries between the various hydrochemical zones are indistinct because of mixing and probably because of variations in the source concentrations.

Superimposed on the natural aquifer conditions is the contamination of the sand aquifer beneath and beyond the waste rock. For more than two decades,

water from rain and snow that has infiltrated through the waste rock piles, has transported the waste-rock-derived leachate to the water table. The radionuclide and chemical composition of the waste-rock-impacted groundwater is different along the two dominant flow regimes (ie. NW and NE). Along the NW flow regime below the waste rock, the contaminated groundwater zone contains a low pH calcium-magnesium-sulphate water with relatively high activities of ^{238}U , ^{234}U , ^{226}Ra , ^{210}Pb , ^{232}Th and ^{230}Th . The contaminant groundwater zone below the waste rock along the NE flow regime contains a neutral pH, calcium-bicarbonate-sulphate water with high activities of ^{238}U and ^{234}U and moderately-high activities of ^{226}Ra . Significant ^{210}Pb , ^{230}Th and ^{232}Th contamination in groundwater beneath the waste rock in the NE flow regime was not evident.

The maximum lateral extent of contamination of the waste-rock-derived contaminants in the sand aquifer for the past 25 years was delineated at approximately 100 meters from the waste rock. The general directions of the plumes of the waste-rock-derived contaminants in groundwater follow the direction of groundwater flow in the sand aquifer. The plumes of electrical conductance, sulphate, bicarbonate, DIC and ^{238}U from the waste rock piles are bordered by an upper and a lower boundary in the sand aquifer. Above the upper boundary, the groundwater is low in total dissolved solids and its chemical composition is the result of soil-water interactions from the infiltration of recharge water by precipitation. The lower boundary is the bomb tritium boundary at approximately 25 meters below the ground surface. The bomb tritium boundary marks the deepest limit possible within the sand aquifer for the travel of the 1957 recharge water that had infiltrated the waste rock 25 years ago. There is also hydrogeological evidence that the deeper groundwater below the 25 meter depth boundary, flows upwards towards the center of the sand aquifer.

The plume of uranium in groundwater was found to extend further out from the waste rock than that for ^{226}Ra , ^{210}Pb or any of the thorium isotopes. The lateral extent of the uranium plume is approximately 70 meters from the waste rock. The extent of contamination of ^{226}Ra , ^{210}Pb , ^{230}Th and ^{232}Th in groundwater is confined either below or around the periphery of the waste rock.

CHAPTER 6

LABORATORY STUDIES OF WASTE ROCK, PYRITE AND SAND LEACHING

The source of uranium, thorium, radium and lead isotopes in groundwater was delineated in that part of the sand aquifer below the piles of waste rock. In order to better understand the occurrence and the distribution of these isotopes in the contaminated groundwater lying below the waste rock piles, three different types of experiments were carried out in the laboratory. These experiments involved the separate leachings of waste rock, pyrite and sand. Waste rock leaching experiments were carried out to describe the leaching behaviour of radionuclides from waste rock, to compare the radionuclide compositions of leachates from the laboratory experiments with that of the contaminated groundwater below the waste rock piles and to apply the activities of the extracted radionuclides in leachates from the laboratory experiments as parameters in the transport models.

The second experiment is centered on the leaching of pyrite under aerobic conditions. Pyrite is an iron sulphide mineral which exists in the gabbroic rock at the site. The rationale behind this experiment is to determine whether pyrite oxidation within the waste rock mass is responsible for the zone D type of groundwater chemistry at site L. Generally, the effects of pyrite oxidation on the composition of a solution in contact with pyrite are that of low pH and high sulphate ion concentration. At site L in 1979, the groundwater had a pH of 3.4 and values of sulphate that approached 1000 mg/l, as well as relatively high activities of uranium, thorium, radium and lead isotopes.

The last experiment entails the leaching of the sand from the field site with a low pH sulphate solution using a column technique. This column experiment simulates the migration of the low pH sulphate groundwater downflow from site L in the sand aquifer. The purpose of the experiment was to determine the degree of acid front retardation in the sand column. The applicability of a

modified, one-dimensional retardation equation is assessed in the calculation of the acid front velocity in the sand column.

6.1 Waste Rock Characteristics

During the operation of the mine from 1956 to 1959, the ore grade within the pegmatite ranged from 0.01% to 0.1% U_3O_8 . Crushed pegmatite and gabbro from the mine that were deficient in U_3O_8 (ie. less than 0.01%) were considered to be waste rock at that time and were dumped over the side of the bedrock outcrop. What follows below are descriptions of the characteristics of the two types of waste rock.

6.1.1 Mineralogical Description

The mineralogical descriptions of the gabbroic and pegmatitic rocks at the site are described by Lang et al. (1962) and Hewitt (1959). A summary of these descriptions is given as follows. The gabbroic rocks, largely gneissic in texture include minerals such as, anorthosite, olivine, magnetite, ilmenite, pyrite and bands of gneissic dolomite and crystalline limestone. The pegmatitic rocks on the other hand, contain all of the radioactive minerals, predominantly uraninite and uranothorite, and non-radioactive minerals such as quartz, microcline, andesine, chlorite, magnetite, hematite, tourmaline and zircon.

6.1.2 Chemical Analysis

Large individual samples of pegmatite and gabbro, ranging from 20 to 30 cm in diameter, have been collected by a grab method in order to obtain a representative distribution of the two rock types from the waste rock piles. Each type of rock specimen was crushed and sieved below 1.0 mm in particle diameter. The less than 1.0 mm fraction of rock grains was subsampled for various chemical tests including major element assay, total sulphur and carbonate determinations, as well as radiochemical analysis for uranium and thorium.

The prepared specimens of crushed pegmatite and gabbro were sent to McMaster University for an assay of the major elements by x-ray fluorescence. The results are tabulated in Table 6.1 and are normalized to 100% for the first ten chemical constituents. The chemical assay of the two types of waste rock reveals that pegmatite is more silica rich, whereas gabbro contains higher amounts of iron, calcium, magnesium, manganese and titanium.

The total sulphur content in the waste rocks was determined at the University of Waterloo by the combustion method. A sample is placed in a LECO furnace, SO_2 gas evolves from the combustion of sulphur in the sample and is then analyzed by an iodate titration technique using a LECO DB-64 Model 765-100 sulphur titrator. The overall uncertainty of this method is approximately $\pm 2\%$. The sulphur results are given in Table 6.1. Gabbro contains more sulphur than pegmatite, which is consistent with the mineralogical description indicating that the gabbro contains pyrite (FeS_2). It may also be possible that gabbro contains some soluble sulphate minerals (eg. gypsum).

Subsamples of the prepared waste rocks were also submitted for carbonate analysis. Samples were weighed into a plastic syringe, acidified and the evolved CO_2 gas measured by a head-space gas chromatographic technique. This technique, as recently developed at the University of Waterloo, was carried out with a Fisher-Hamilton model 29 gas partitioner equipped with a thermal conductivity detector. The accuracy of this method is $\pm 5\%$. The carbonate results are given in Table 6.1 and are reported as wt. % CaCO_3 . The gabbro contains more carbonate than pegmatite. The high carbonate value for gabbro is due to the presence of dolomite and limestone within the gabbro matrix.

6.1.3 Radiochemical Analysis

Subsamples of the prepared specimens of the waste rock were analyzed for uranium and thorium. The results are given in Table 6.1. Pegmatite contains higher percentages of uranium and thorium than those found in gabbro, which is consistent with the mineralogical description. For comparative purposes,

TABLE 6.1

RESULTS OF THE CHEMICAL AND RADIOCHEMICAL ANALYSIS OF THE
PEGMATITIC AND GABBROIC WASTE ROCK

CHEMICAL CONSTITUENT	PEGMATITE	GABBRO
SiO ₂	74.19%	45.28%
Al ₂ O ₃	14.71%	13.92%
Fe ₂ O ₃	0.59%	12.87%
MgO	0.56%	6.77%
CaO	1.73%	14.17%
Na ₂ O	7.64%	4.34%
K ₂ O	0.49%	0.57%
TiO ₂	0.05%	1.81%
MnO	0.02%	0.25%
P ₂ O ₅	0.02%	0.03%
S (total)	0.02%	1.22%
CaCO ₃	0.01%	4.20%
U ₃ O ₈	0.013%	0.001%
ThO ₂	0.004%	0.0001%

subsamples of pegmatite were also sent to McMaster University for uranium and thorium analysis by neutron activation (N.A.A.). The results by the N.A.A. method gave 31.97 ug/g for uranium and 23 ug/g for thorium. These N.A.A. values for uranium and thorium in pegmatite are close to those of the alpha spectrometric results, i.e. 36.4 ug/g of uranium and 30.4 ug/g of thorium. The advantage of using the alpha spectrometric technique for this investigation instead of the N.A.A. technique is that various isotopic activity ratios of the natural uranium series can be determined within a sample. For example, considering the alpha spectrometric results for the same pegmatite sample, the $^{234}\text{U}/^{238}\text{U}$ isotopic activity ratio has been measured as 0.99 ± 0.06 .

The radiochemical analyses of the two rock types have shown that pegmatite is higher in radioactivity in comparison to gabbro. A surficial field survey of each of the individual waste rock piles at the field site as located and outlined in Figure 5.3, was conducted with a survey meter. The activity that is measured by this meter represents the total activity from both beta and gamma rays that are emitted by the rock. The pegmatite waste rock located by piezometer GR9 gave high activity, in the order of 1000 to 3000 counts per minute (cpm). The pegmatite and gabbroic waste rock near piezometer L and to the west of piezometer GR9, exhibited lower surficial activity, in the order of 400 to 800 cpm. In addition, the surficial activity readings for the principally gabbroic waste rock located near piezometers B and J and to the east of piezometer GR9 were even lower than the latter site by approximately 200 cpm.

6.2 Leachability of Radionuclides from Waste Rock

Various batch-type leaching experiments have been carried out on pegmatitic grains in order to investigate the factors that affect the amounts of radionuclides released in solution upon leaching. The factors that have been investigated include solution composition, weathered and unweathered grain surfaces, fresh and pre-leached grains, grain size and solid-liquid ratio. Only pegmatite was chosen for this particular investigation because of its higher radioactive content.

Leaching experiments with pegmatitic and gabbroic grains were carried out by both batch and column techniques in the laboratory. The purpose was to determine the range in activities of radionuclides released in solution from the two different leach techniques, to compare the laboratory results with the field results and to apply the activities of the extracted radionuclides in leachates from the leaching experiments as parameters in the transport models. For all of the rock leaching experiments, the rock grains were leached aerobically. Rock grains have been leached under aerobic conditions because the waste rock mass at the site is in a relatively open system with respect to oxygen and carbon dioxide.

6.2.1 Materials

Specimens of pegmatite and gabbro were collected at the study site by a grab method from the waste rock piles. The collection was restricted to two size ranges, 0.5 - 3.0 cm in diameter and 20-30 cm in diameter. The former size range represented the weathered material and the latter, when crushed and mixed, represented the unweathered material. Freshly crushed specimens of rock were used in order to represent the conditions that existed in the rock approximately 25 years ago before weathering occurred. Weathered, as well as unweathered specimens, were crushed in a jaw-crusher and subsequently passed through a series of sieves ranging in particle diameter from 1 mm to 5 mm. For the crushing of the weathered grains, the amount of exposed, freshly-crushed surfaces was considered to be small in comparison to the original amount of weathered surfaces.

Three different types of extractants were prepared for the waste rock leaching experiments in order to represent the range of the observed chemical compositions in water at the field site. Deionized water in equilibrium with the atmosphere at a pH of 5.7 was chosen as one of the extractants in order to represent the action of rainwater and snow upon the rock surfaces. The pH of rainwater can be lower than 5.7 in some areas due to the acidity produced from

the presence of $\text{SO}_2(\text{g})$ and other gases in the atmosphere. The second extractant was dilute sulphuric acid at a pH of 3.0. This extractant represents the low pH sulphate groundwater in zone D underlying the waste rock, as found at site L in the northwest sector of the field site. The third extractant contained 250 mg/l of bicarbonate at pH 7.0. This solution represented the neutral pH bicarbonate zone D groundwater underlying the waste rock in the northeast sector of the field site. The bicarbonate solution was made from NaHCO_3 and adjusted to pH 7.0 with $\text{H}_2\text{SO}_4/\text{NH}_4\text{OH}$.

6.2.2 Description of Batch Experiments

The leaching method of Nathwani and Phillips (1979) was carried out with some minor variations. What follows is a description of this modified procedure in the leaching of waste rock:

- (a) Fifty grams of freshly-crushed, 1-3 mm unweathered pegmatite grains were placed in ten-275 ml capacity polyethylene bottles with tightly fitting screwcaps, to which 100 ml of deionized water at a pH of 5.7 was added such that a constant solid to solution ratio of 1:2 (weight/volume) was obtained.
- (b) A blank was prepared by adding 100 ml of the leaching solution to an empty bottle.
- (c) The sealed containers were then mechanically shaken end-to-end at approximately 120 times a minute for periods ranging from 1 to 1000 hours.
- (d) All of the runs were carried out at room temperature.
- (e) After each reaction period, the bottle was removed from the shaker and the suspension was then filtered through 0.45 μ millipore filters. The filtrate was analyzed for pH, electrical conductance, bicarbonate concentration and sulphate concentration, as well as for activities of ^{238}U , ^{234}U , ^{232}Th , ^{230}Th , ^{226}Ra and ^{210}Pb .

(f) The same pegmatite grains that had been leached with deionized water, were then oven dried and then placed in the clean 275 ml capacity polyethylene bottles. A dilute H_2SO_4 acid solution at pH 3.0 was then placed into each bottle in 100 ml aliquots. Steps (c) to (e) were then repeated. Throughout the leaching procedure, the pH of the acidic leachate was continually monitored with narrow range pH paper and adjusted to $\text{pH } 3.0 \pm 0.5$.

Modifications to the above procedure were made in order to examine the effects of weathered and unweathered grains, fresh and pre-leached grains, grain size, solid-liquid ratio, solution composition and rock type on the amounts of radionuclides extracted from pegmatite. First, steps (a) to (f) were repeated with 1-3 mm weathered grain specimens. Second, the same 50 gram, pre-leached grains after 40 days of leaching from the unweathered pegmatite/water, unweathered pegmatite/pH3 H_2SO_4 , weathered pegmatite/water and weathered pegmatite/pH3 H_2SO_4 systems, were re-leached for another 40 days with new solutions and the leachates were analyzed according to step (e). Third, 50 gram samples of unweathered pegmatite at mean diameter grain sizes, varying from 1.0, 1.2, 2.0 and 4.5 mm, were leached separately with 100 ml aliquots of deionized water for 40 days and step (e) was carried out. Fourth, 50 gram samples of 1-3 mm unweathered pegmatite grains were leached with aliquots of deionized water at solid:liquid ratios varying from 1:0.5, 1:1, 1:2 and 1:5 for 40 days and step (e) was carried out. Because there was a strong trend between the high sulphate ion concentration and the high activities of radionuclides in the low pH groundwater below the waste rock, the fifth experiment involved the increment addition of sulphate ions from a Na_2SO_4 solution to four batch reactors with 100 ml of a pH 4 solution and 50 grams of unweathered pegmatite grains, followed by the leaching of these batch reactors for 40 days. The amounts of sulphate added to the batch reactors were 0, 100, 500 and 1000 mg/l. After 40 days of leaching, the four leachates were analyzed according to step (e). Lastly, 50-gram samples of the 3.5 mm unweathered grains of pegmatite and gabbro

in a 50:50 mixture were leached with deionized water and the pH3 (H_2SO_4) extractant according to steps (a) to (f).

6.2.3 Description of Column Experiments

Freshly-crushed, 3-5 mm unweathered grains of pegmatite and gabbro in a 50:50 mixture were placed in a 3 cm x 60 cm cylindrical glass column. The total weight of the rock grains in the column was equal to 642 grams. A stopcock was fitted to the bottom of the column and a glass joint to the top of the column. Attached to the glass joint, was a 1.0 liter glass reservoir. The pH 3.0 solution was continuously added to the reservoir, which infiltrated the column below at a flow rate at 4.0 ml/min. A set of ten, one liter samples of the column effluent was collected within a 40 day period. Each solution sample was filtered through 0.45 μ millipore filters and was analyzed for values of pH, electrical conductance, ^{238}U , ^{234}U , ^{226}Ra , ^{210}Pb , ^{230}Th and ^{232}Th . The above procedure was repeated with fresh rock samples and with other extractants, such as with deionized water and with the pH 7.0 bicarbonate solution.

6.2.4 Results from Batch Experiments

The chemical compositions of the leachates from the leaching of unweathered pegmatite grains with deionized water and also from the leaching of weathered grains of pegmatite with deionized water, are shown in Figure 6.1. The values of pH and bicarbonate in these leachates increase to a constant level after 30 days, while the values of electrical conductance and sulphate in the leachates similarly increase to a steady level after 15 days. After 40 days, the leachate from the unweathered material has 76 mg/l of HCO_3 , 14 mg/l of SO_4 , an electrical conductance of 40 μS and a pH value at 7.8. In comparison, the leachate composition from the leaching of weathered material after 40 days has 33 mg/l of HCO_3 , 18 mg/l of SO_4 , an electrical conductance of 75 μS and a pH value at 7.7.

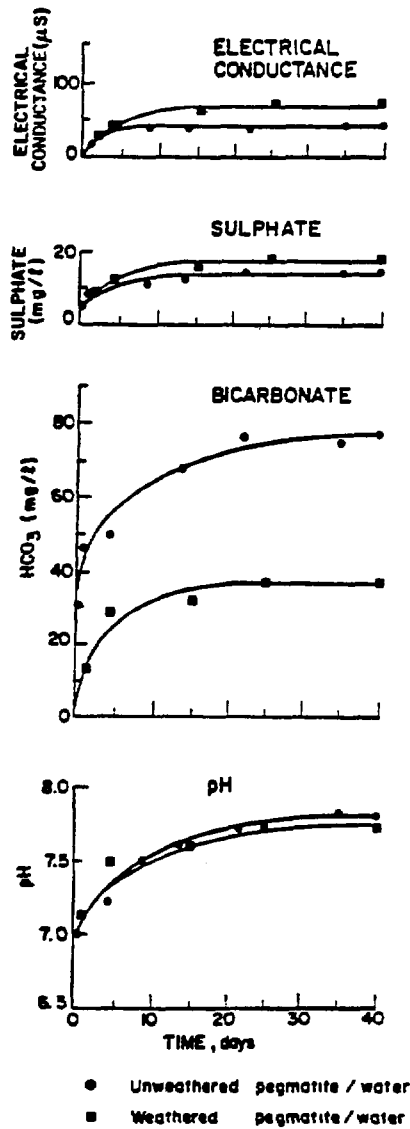


Figure 6.1 Results of pegmatite leaching experiment (50 g of pegmatite in 100 ml deionized water). The values of electrical conductance, sulphate, bicarbonate and pH in solution are plotted as a function of time.

The radionuclide compositions of leachates resulting from the leaching of unweathered pegmatite grains with the deionized water and the pH 3 extractants are tabulated respectively in Veska (1983). The radionuclide compositions of leachates resulting from the leaching of weathered pegmatite grains with the deionized water and the pH3 extractants are tabulated in Veska (1983) . The activities of ^{238}U , ^{234}U , ^{226}Ra , ^{210}Pb , ^{230}Th , ^{232}Th and ^{228}Th released into solution from each of these four types of pegmatite leaching experiments are shown individually as activity versus time graphs in Figures 6.2- 6.8. In almost all of the activity versus time graphs in Figures 6.2-6.8, the activity of the radionuclide increases in the leachate initially with time. After a leaching period ranging from 5 to 15 days, the radionuclide activities reach a plateau or a steady state level. Similar types of plateau shapes were found by Szalay and Samsoni (1969) in the leaching of uranium from crushed magmatic rocks and Nathwani and Phillips (1979) in the leaching of ^{226}Ra from uranium mill tailings. The average activities of radionuclides in leachates, resulting from the leaching of unweathered and weathered pegmatite with deionized water and corresponding to the plateaus in Figures 6.2-6.8, are respectively, 33 and 60 pCi/l for ^{238}U , 50 and 60 pCi/l for ^{234}U , 40 and 60 pCi/l for ^{226}Ra , 14 and 50 pCi/l for ^{210}Pb , 7 and 20 pCi/l for ^{230}Th and below the detection limits for ^{232}Th and ^{228}Th . For all cases, the activities of radionuclides in the leachates from weathered pegmatite are greater than that in the leachates from unweathered pegmatite. The activities of radionuclides that are leached from pegmatite with the pH3 extractant are found to be greater than that leached with deionized water. For example, the average activities of radionuclides in leachates resulting from the leaching of unweathered and weathered pegmatite with the pH3 extractant and corresponding to the plateaus in Figures 6.2-6.8, are respectively, 2400 and 2400 pCi/l for ^{238}U , 2100 and 2100 pCi/l for ^{234}U , 1000 and 700 pCi/l for ^{226}Ra 720 and 850 pCi/l for ^{210}Pb , 800 and 950 pCi/l for ^{230}Th , 260 and 290 pCi/l for ^{232}Th and 300 and 320 pCi/l for ^{228}Th . With the exception of

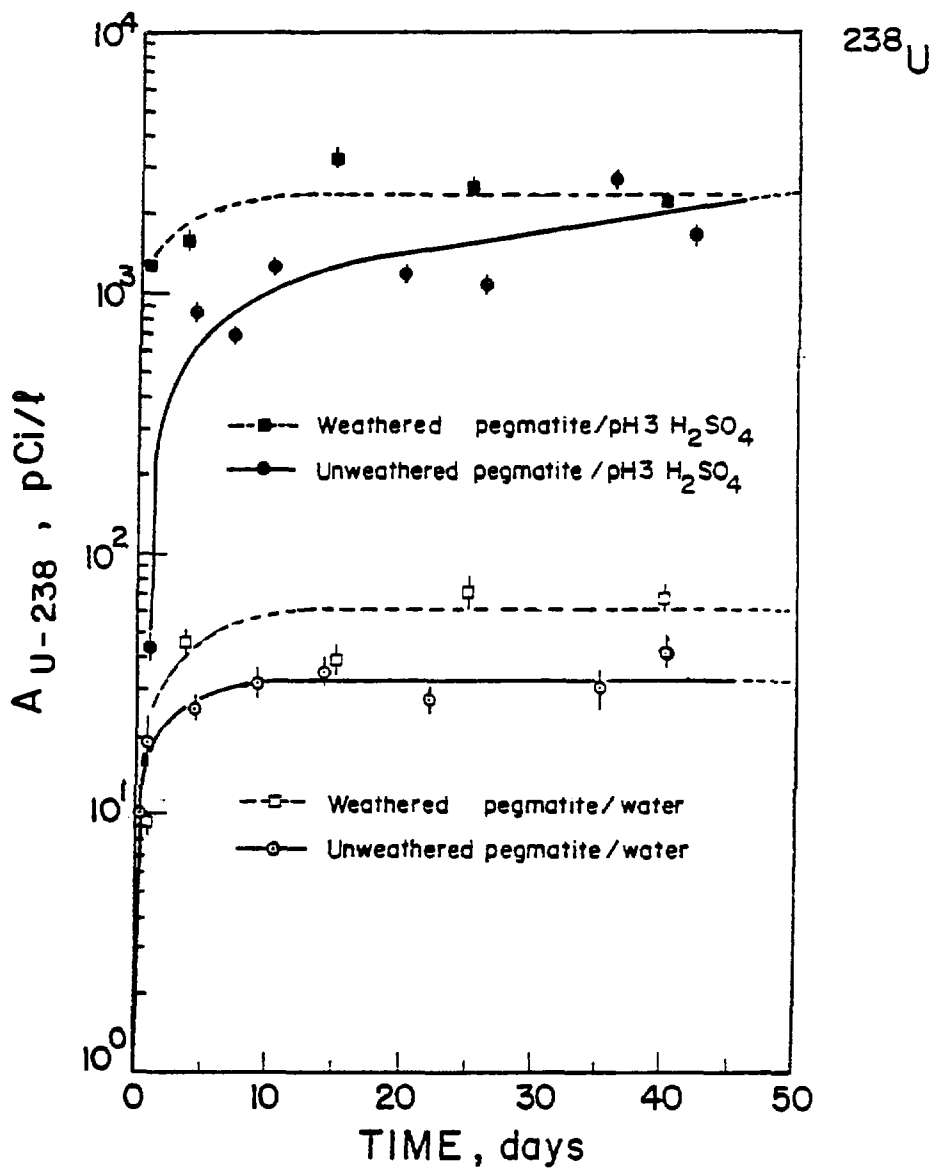


Figure 6.2 Plot of the ^{238}U activity released into solution during the leaching of pegmatite as a function of time. Error bars are incorporated for each activity value.

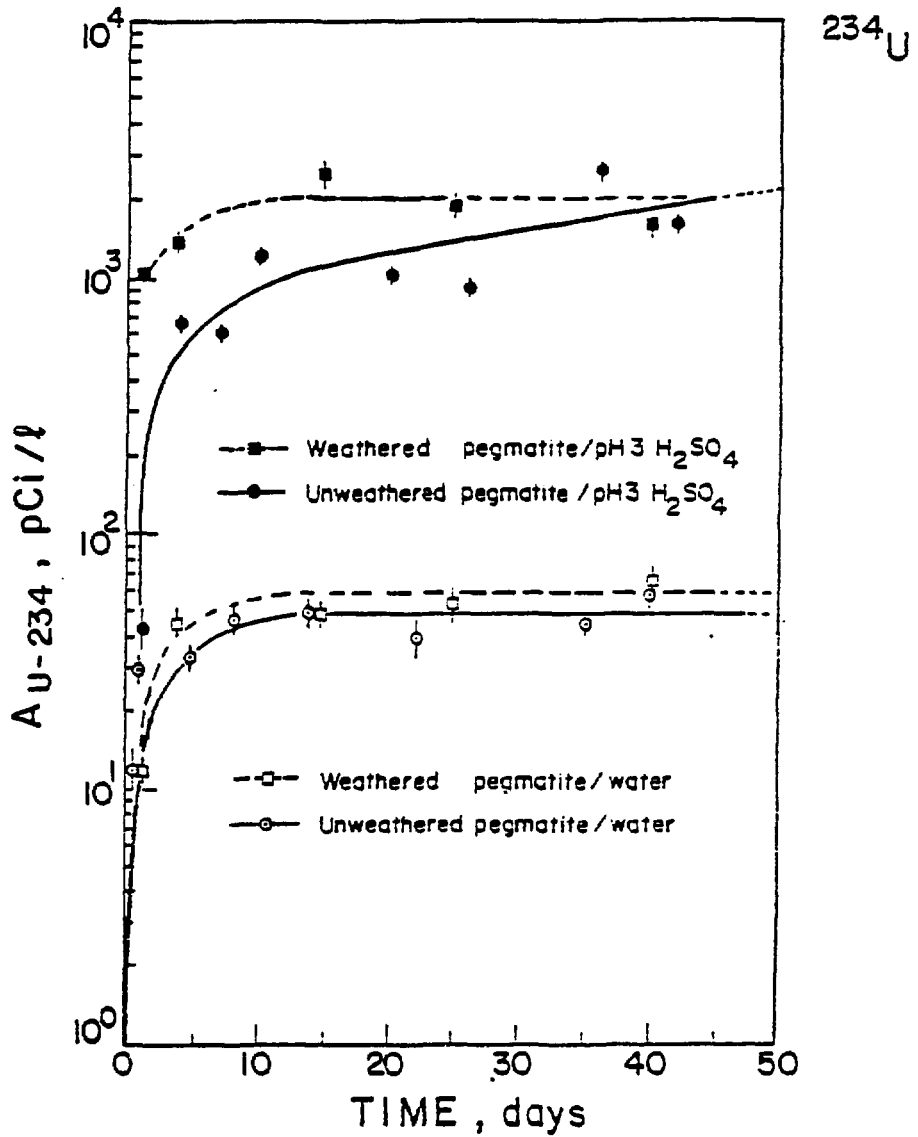


Figure 6.3 Plot of the ^{234}U activity released into solution during the leaching of pegmatite as a function of time. Error bars are incorporated for each activity value.

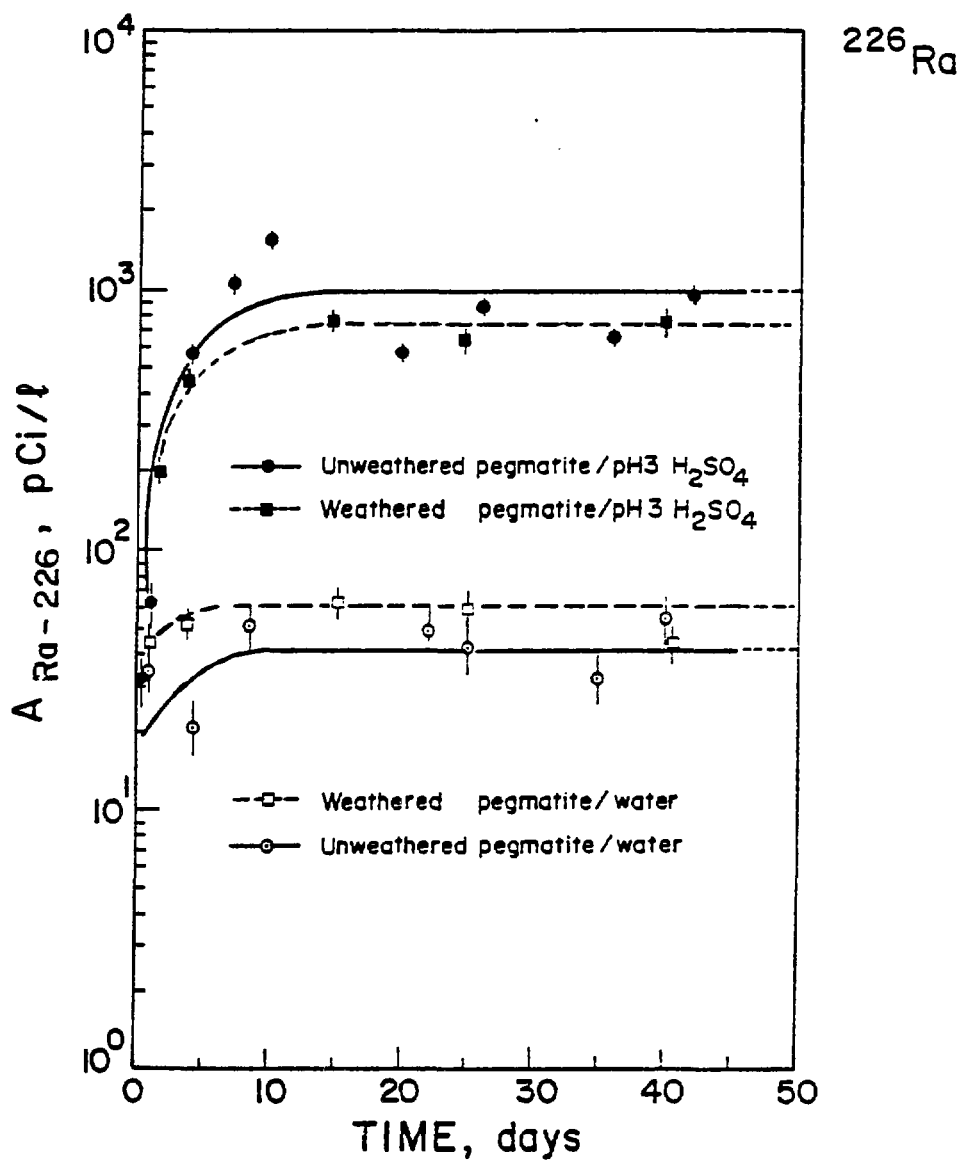


Figure 6.4 Plot of the ^{226}Ra activity released into solution during the leaching of pegmatite as a function of time. Error bars are incorporated for each activity value.

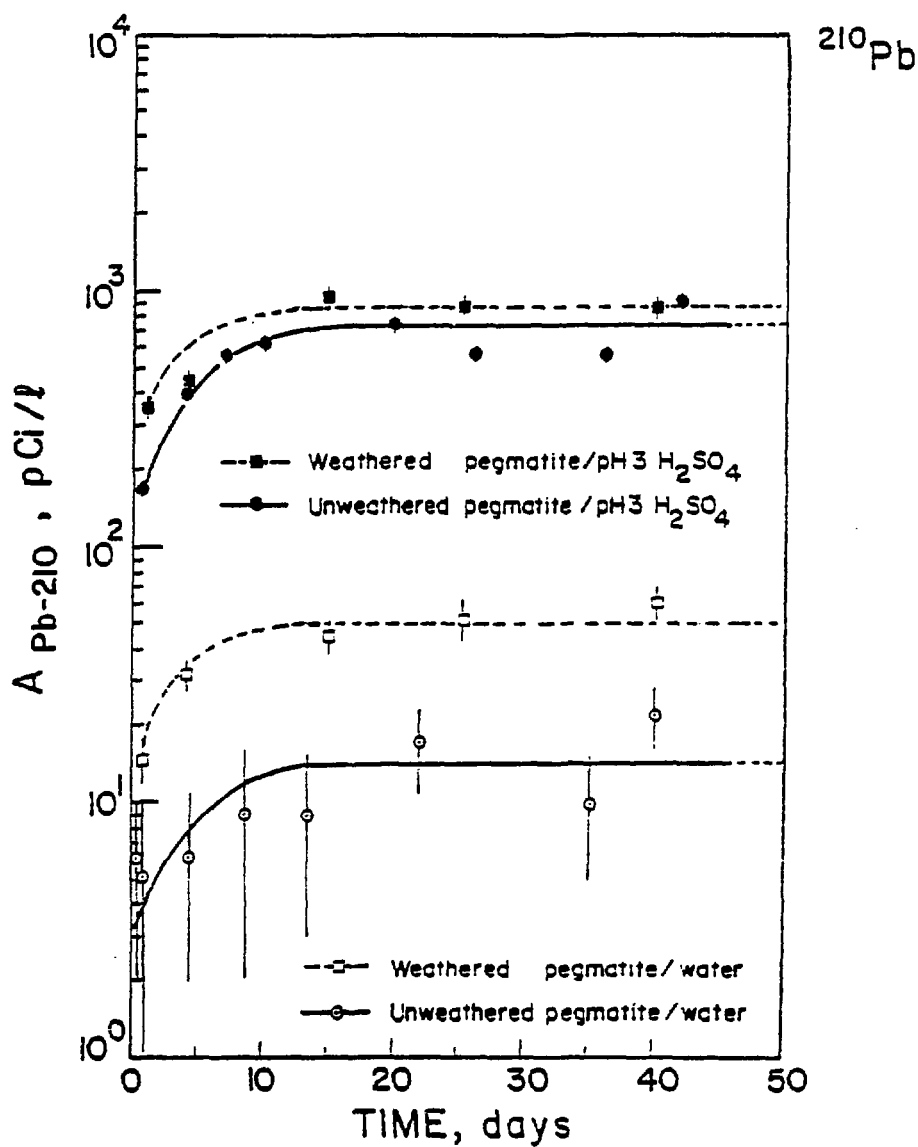


Figure 6.5 Plot of the ^{210}Pb activity released into solution during the leaching of pegmatite as a function of time. Error bars are incorporated for each activity value.

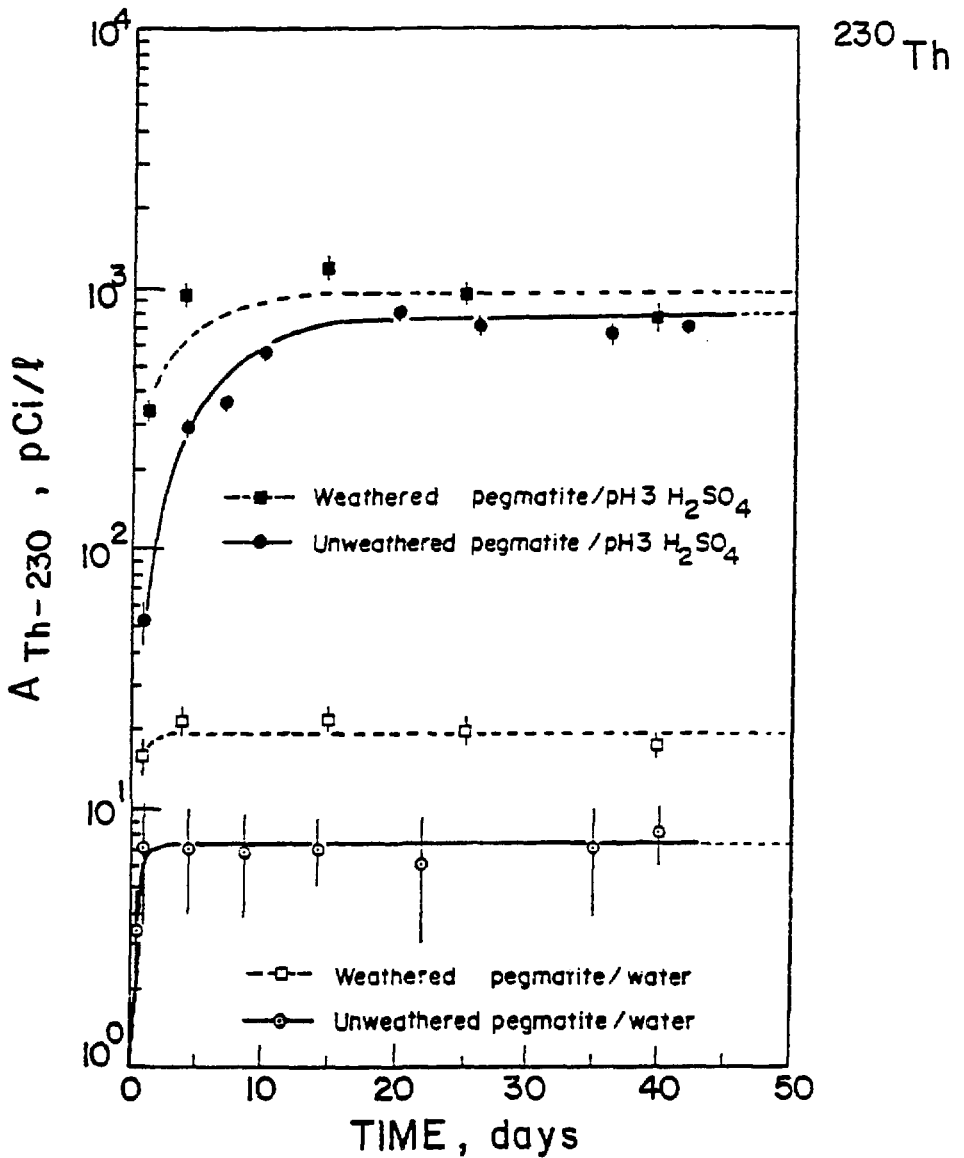


Figure 6.6 Plot of the ^{230}Th activity released into solution during the leaching of pegmatite as a function of time. Error bars are incorporated for each activity value.

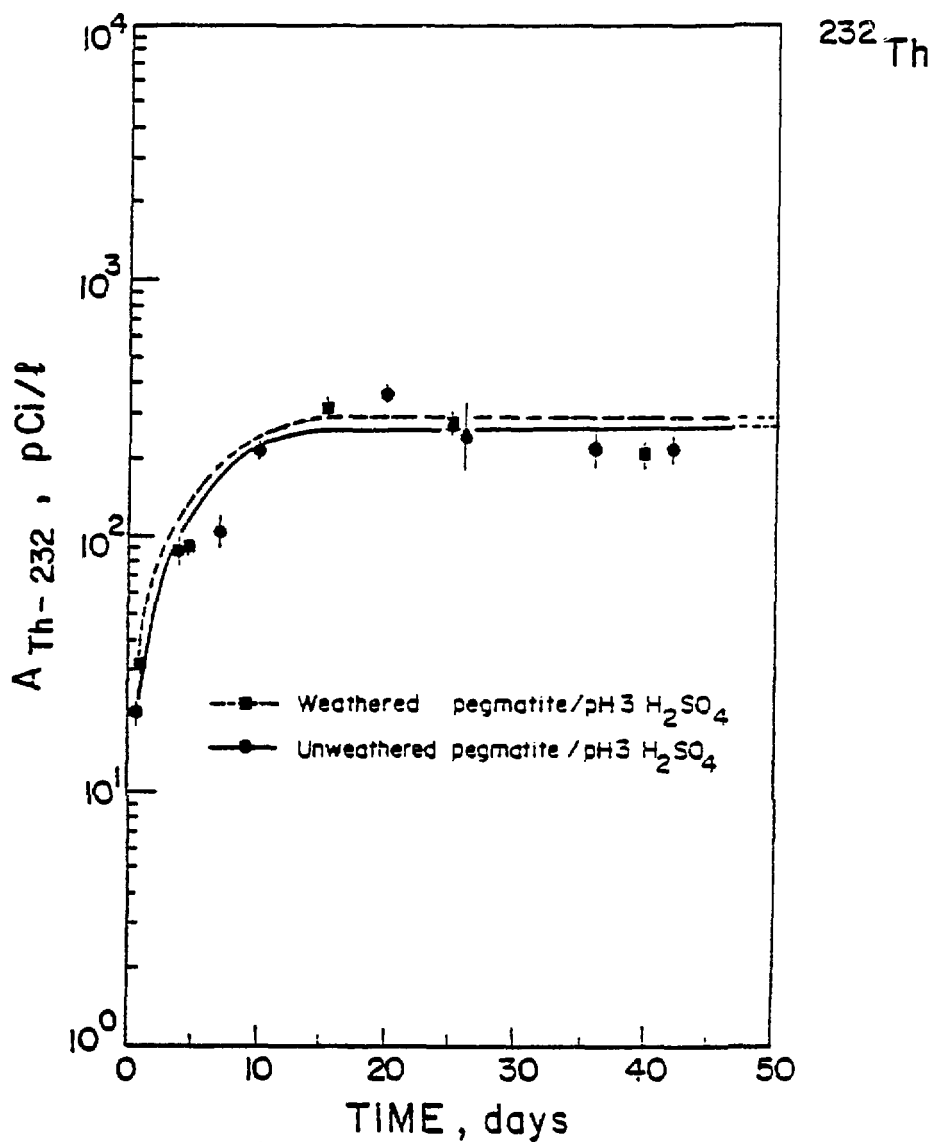


Figure 6.7

Plot of the ^{232}Th activity released into solution during the leaching of pegmatite as a function of time. Error bars are incorporated for each activity value. ^{232}Th values in leachates from the leaching of pegmatite with deionized water were below the detection limit.

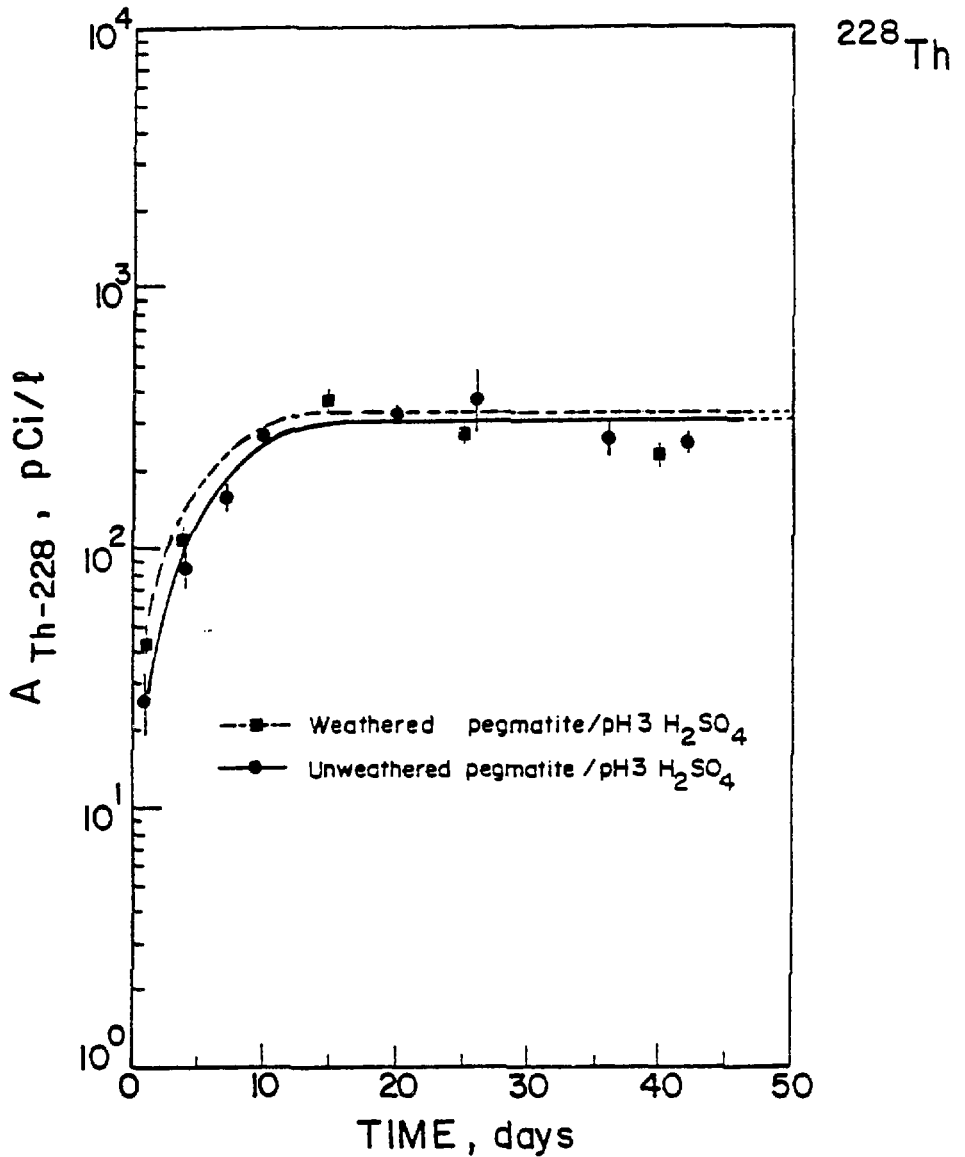


Figure 6.8 Plot of the ^{228}Th activity released into solution during the leaching of pegmatite as a function of time. Error bars are incorporated for each activity value. ^{228}Th values in leachates from the leaching of pegmatite with deionized water were below the detection limit.

^{226}Ra , the activities of radionuclides in leachates from weathered pegmatite are either the same or greater than that in the leachates from unweathered pegmatite.

The unweathered and weathered pegmatite grains, that were pre-leached with water after 40 days and with the pH 3 extractant after 40 days, were re-leached with new solutions for a total period of 40 days. A period of 40 days was chosen as the appropriate duration for the second set of extractions because steady state activities of radionuclides in the leachates were generally well attained at this time. The expression, steady state, does not necessarily represent true thermodynamic equilibrium. The radionuclide compositions in the leachates from the second extractions are given in Table 6.2. Comparisons of the amounts of radionuclides leached from the same pegmatite grains from the first and second extractions are also given in Table 6.2. Each of the four comparisons indicates lower activities of radionuclides in the leachates from the second extractions rather than that from the first extractions.

Fresh samples of unweathered pegmatite grains of mean diameter grain sizes less than 1.0, 1.2, 2.0 and 4.5 mm were leached with deionized water for a total period of 40 days. The composition of the resulting four leachates after 40 days are shown in Figure 6.9 and the data are tabulated in Veska (1983). As the grain size decreases from 4.5 mm to less than 1.0 mm increases are seen in the values of electrical conductance from 20 to 120 μS , ^{238}U from 8.4 to 188.5 pCi/l, ^{234}U from 7.6 to 160.5 pCi/l, ^{226}Ra from 36.1 to 87.5 pCi/l, ^{210}Pb from 24.6 to 68.2 pCi/l and ^{230}Th from 5.6 to 40.2 pCi/l in the leachates. The pH in all of the four leachates is constant at 7.8. A similar trend was found by Megumi (1979) from the leaching of weathered granitic soil with various extractants. Megumi experimentally determined that the activities of ^{238}U , ^{230}Th , ^{226}Ra and ^{210}Pb increased in the leachates as the grain size decreased.

TABLE 6.2

**COMPARISON OF THE AMOUNTS OF RADIONUCLIDES LEACHED FROM FRESH AND USED PEGMATITE GRAINS
IN BATCH REACTORS AFTER 40 DAYS**

TYPE OF GRAINS	TYPE OF GRAIN SURFACE	TYPE OF EQUILIBRATING SOLUTION	^{238}U ,pCi/l	^{234}U ,pCi/l	$^{234}\text{U}/^{238}\text{U}$ A.R.	^{226}Ra ,pCi/l	^{210}Pb ,pCi/l	^{230}Th ,pCi/l	^{232}Th ,pCi/l
Fresh	Unweathered	Water	40.97 ± 2.90	58.63 ± 3.71	1.43 ± 0.14	52.7 ± 8.9	22.0 ± 6.3	8.0 ± 2.0	<0.1
Used	Unweathered	Water	18.23 ± 1.64	24.10 ± 2.05	1.32 ± 0.16	18.0 ± 2.2	9.7 ± 1.5	N A	N A
Fresh	Weathered	Water	69.81 ± 4.09	64.28 ± 4.42	0.92 ± 0.08	42.9 ± 8.2	60.7 ± 6.0	18.1 ± 2.0	<0.1
Used	Weathered	Water	33.03 ± 1.27	38.43 ± 1.43	1.16 ± 0.06	24.5 ± 2.4	24.4 ± 1.7	N A	N A
Fresh	Unweathered	pH3 H ₂ SO ₄	1697 ± 82	1599 ± 82	0.94 ± 0.07	905 ± 25	904 ± 15	707 ± 32	213 ± 17
Used	Unweathered	pH3 H ₂ SO ₄	382 ± 14	329 ± 14	0.86 ± 0.05	104 ± 5	86 ± 3	227 ± 9	92 ± 6
Fresh	Weathered	pH3 H ₂ SO ₄	2034 ± 47	1587 ± 43	0.78 ± 0.03	710 ± 23	855 ± 16	753 ± 10	200 ± 20
Used	Weathered	pH3 H ₂ SO ₄	1731 ± 45	1389 ± 41	0.80 ± 0.03	653 ± 24	434 ± 16	167 ± 3	18 ± 0.9

N A = Not analyzed

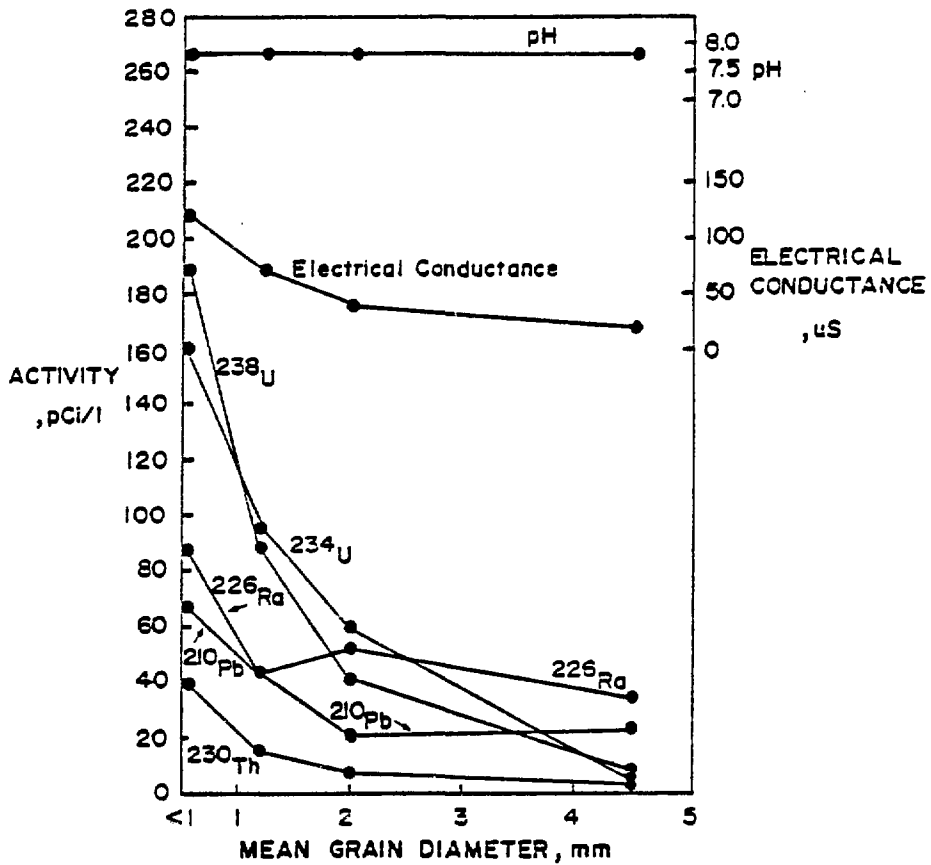


Figure 6.9 Effect of the grain size on the amount of radionuclides extracted in solution from the leaching of unweathered pegmatitic grains with deionized water after 40 days.

Fresh 50 gram samples of 1-3 mm unweathered grains were leached with deionized water for 40 days at solid:liquid ratios at 1:0.5, 1:1, 1:2 and 1:5. The compositions of the resulting four leachates after 40 days are given in Veska (1983) and are shown in Figure 6.10. As the solid:liquid ratio increases from 1:5 to 1:0.5 as shown in Figure 6.10, increases in the leachates are noticed for values of electrical conductance from 28 to 130 μS , ^{238}U from 10.7 to 114.1 pCi/l , ^{234}U from 11.2 to 113.0 pCi/l , ^{226}Ra from 23.3 to 258.6 pCi/l , ^{210}Pb from 20.5 to 277.9 pCi/l and ^{230}Th from 1.2 to 28.3 pCi/l . A pH value at 7.8 is constant in all of the four leachates. A similar trend was observed by Vandergraaf (1981) in studies related to mineral/water interactions. Vandergraaf found increased leach rates for most of the ions studied with increased rock/water ratios.

The results from the leaching of unweathered pegmatite grains with pH 4 HCl and at various sulphate ion concentrations are given in Table 6.3. As the sulphate ion concentration increases from 0 to 1000 mg/l , the activities of ^{238}U , ^{234}U , ^{226}Ra , ^{210}Pb , ^{230}Th and ^{232}Th in the leachates respectively increase from 402.71 to 622.02 pCi/l , from 321.92 to 530.30 pCi/l , from 33.8 to 88.3 pCi/l , from 34.4 to 64.7 pCi/l , from 10.73 to 56.05 pCi/l and from 3.82 to 17.21 pCi/l .

Fresh samples of unweathered grains of pegmatite and gabbro were leached with deionized water and also with the pH3 H_2SO_4 extractant in batch reactors for a period of 40 days. The results of the determination of radionuclides in the leachates from the leaching of pegmatite and gabbro are given in Table 6.4. The amounts of radionuclides extracted from the combined pegmatitic and gabbroic grains with the pH3 H_2SO_4 extractant are much greater than that with the deionized water extractant, but less than that in leachates from the leaching of pegmatite with pH 3 H_2SO_4 extractant.

6.2.5 Results from Column Experiments

Three portions of freshly-crushed unweathered grains of pegmatite and gabbro were leached with the pH3 H_2SO_4 extractant, deionized water and pH 7.0 bicarbonate solutions respectively within a 40 day period using the column

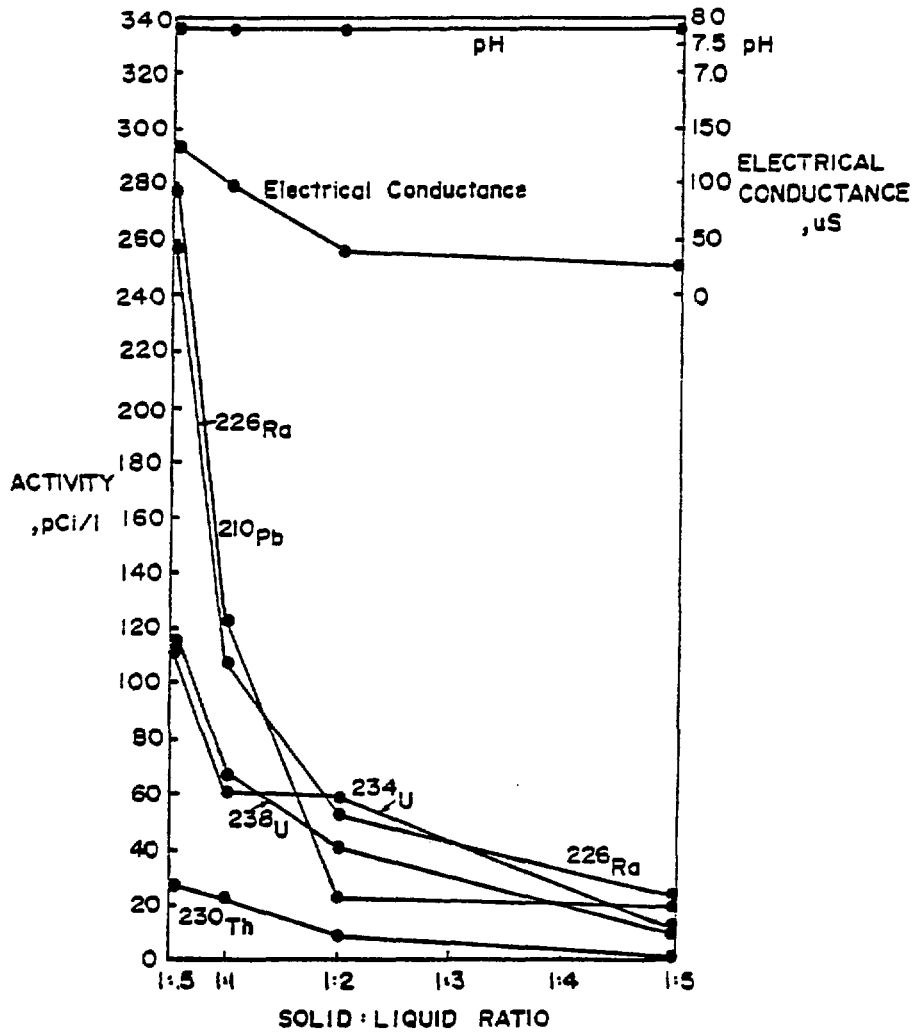


Figure 6.10 Effect of the solid:liquid ratio on the amount of radionuclides extracted in solution from the leaching of unweathered pegmatitic grains with deionized water after 40 days.

TABLE 6.3

EFFECT OF THE SULPHATE ION CONCENTRATION ON THE AMOUNTS OF RADIONUCLIDES RELEASED IN SOLUTION FROM THE LEACHING OF UNWEATHERED PEGMATITE GRAINS WITH pH4 HCl SOLUTION AFTER 40 DAYS

AMOUNT OF SULPHATE ADDED , mg/l	^{238}U , pCi/l	^{234}U , pCi/l	$^{234}\text{U}/^{238}\text{U}$ A.R.	^{226}Ra , pCi/l	^{210}Pb , pCi/l	^{230}Th , pCi/l	^{232}Th , pCi/l
0	402.71 ± 16.23	321.92 ± 15.72	0.80 ± 0.05	33.8 ± 2.2	34.4 ± 1.7	10.73 ± 0.93	3.82 ± 0.65
100	434.67 ± 17.33	335.40 ± 16.17	0.77 ± 0.05	47.0 ± 2.2	39.1 ± 1.8	14.68 ± 1.69	4.39 ± 0.94
500	536.47 ± 26.04	461.47 ± 25.14	0.86 ± 0.06	63.9 ± 2.3	49.2 ± 1.8	28.71 ± 2.48	10.85 ± 1.48
1000	622.02 ± 32.40	530.30 ± 30.05	0.85 ± 0.07	88.3 ± 2.4	64.7 ± 1.8	56.05 ± 5.12	17.21 ± 2.84

TABLE 6.4

COMPARISON OF THE AMOUNTS OF RADIONUCLIDES LEACHED FROM UNWEATHERED GRAINS OF PEGMATITE
AND GABBRO USING THE BATCH AND COLUMN LEACH TECHNIQUES

LEACHING TECHNIQUE	SOLUTION TYPE	pH	SAMPLE TIME ,days	^{238}U ,pCi/l	^{234}U ,pCi/l	$^{234}\text{U}/^{238}\text{U}$ A.R.	^{226}Ra ,pCi/l	^{210}Pb ,pCi/l	^{230}Th ,pCi/l	^{232}Th ,pCi/l
Batch Column	pH3 H_2SO_4	3	40	908.6 \pm 22.8	775.9 \pm 22.2	0.85 \pm 0.03	260.7 \pm 18.1	152.7 \pm 12.3	207.7 \pm 2.3	24.2 \pm 0.8
	pH3 H_2SO_4	3	33	35.68 \pm 1.55	28.37 \pm 1.43	0.80 \pm 0.05	59.2 \pm 2.7	22.1 \pm 1.7	4.96 \pm 0.13	0.58 \pm 0.05
Batch Column	Water	8.2	40	105.0 \pm 5.4	107.2 \pm 5.9	1.02 \pm 0.08	21.8 \pm 7.5	33.0 \pm 5.4	1.2 \pm 0.1	<0.1
	Water	7.8	35	3.46 \pm 0.17	4.67 \pm 0.18	1.35 \pm 0.08	1.0 \pm 0.4	< 0.5	N A	N A
Column	pH7 HCO_3	8.0	35	9.32 \pm 0.28	9.20 \pm 0.27	0.99 \pm 0.04	2.7 \pm 0.4	0.9 \pm 0.4	N A	N A

N A = Not analyzed

technique. The results are tabulated in Tables 6.5, 6.6, and 6.7. The activities of radionuclides in the acidic leachates using the pH 3 H_2SO_4 extractant in Table 6.5 are approximately constant for the first 13 days of leaching. As the pH in the leachates eventually decreases to 3.0 after 30 days of leaching, the activities of radionuclides increase. During the 33 day period of column leaching with the pH 3 H_2SO_4 extractant, the maximum values that have been attained in the leachates are 58.94 pCi/l for ^{238}U , 49.37 pCi/l for ^{234}U , 59.2 pCi/l for ^{226}Ra , 26.0 pCi/l for ^{210}Pb , 12.06 pCi/l for ^{230}Th and 1.55 pCi/l for ^{232}Th .

The activities of radionuclide are much lower in the column leachates using the deionized water and the pH 7.0 bicarbonate extractants, as shown in Tables 6.6 and 6.7. After 35 days, the activities of radionuclides in the leachate from the leaching of waste rock with the deionized water extractant are 3.46 pCi/l of ^{238}U , 4.67 pCi/l of ^{234}U , 1.0 pCi/l of ^{226}Ra and less than 0.5 pCi/l of ^{210}Pb , whereas in the leachate from the leaching of waste rock with the pH 7.0 bicarbonate extractant, the values are 9.32 pCi/l for ^{238}U , 9.20 pCi/l for ^{234}U , 2.7 pCi/l for ^{226}Ra and 0.9 pCi/l for ^{210}Pb . The activities of the extracted radionuclides in leachates from the leaching of pegmatite and gabbro by the batch and column techniques, are shown in Table 6.4 as a comparison. The comparison shows that the amounts of radionuclides leached in solution by the batch technique are much greater than that by the column technique, ie. by a factor of 4 to a factor of 40.

6.2.6 Interpretations

The factors that affect the natural release of radionuclides from waste rock have been assessed in the laboratory by rock leaching experiments using the batch technique. The amounts of radionuclides that are leached from pegmatite in solution are found to increase with: (1) weathered rock grain surfaces rather than with unweathered surfaces (for most cases); (2) first extractions rather than with repeated extractions with the same rock grains; (3) active

TABLE 6.5

COMPOSITION OF LEACHATE WITH TIME FROM THE INFILTRATION OF pH1 H₂SO₄ THROUGH A
COLUMN BED OF UNWEATHERED GRAINS OF PEGMATITE AND GABBRO

TIME , days	pH	ELECTRICAL CONDUCTANCE , μ S	²³⁸ U , pCi/l	²³⁴ U , pCi/l	²³⁴ U/ ²³⁸ U A.R.	²²⁶ Ra , pCi/l	²¹⁰ Pb , pCi/l	²³⁰ Th , pCi/l	²³² Th , pCi/l
1	4.1	275	22.30 \pm 0.46	17.60 \pm 0.43	0.79 \pm 0.03	23.3 \pm 1.0	9.8 \pm 0.7	0.23 \pm 0.05	< 0.1
2	3.5	295	23.50 \pm 0.80	19.58 \pm 0.75	0.83 \pm 0.04	22.6 \pm 1.3	13.5 \pm 0.7	0.47 \pm 0.12	< 0.1
5	3.2	300	24.09 \pm 0.59	21.64 \pm 0.58	0.90 \pm 0.03	10.8 \pm 0.8	10.9 \pm 0.5	0.49 \pm 0.15	< 0.1
6	3.2	345	29.65 \pm 1.67	26.09 \pm 1.75	0.88 \pm 0.07	33.2 \pm 2.2	15.7 \pm 1.5	1.64 \pm 0.26	< 0.1
9	3.2	320	24.02 \pm 2.65	18.35 \pm 2.43	0.77 \pm 0.13	14.0 \pm 2.2	9.8 \pm 1.4	0.99 \pm 0.17	0.12 \pm 0.08
13	3.2	280	20.03 \pm 1.13	16.71 \pm 1.07	0.83 \pm 0.07	29.4 \pm 2.0	10.8 \pm 1.4	1.23 \pm 0.19	0.38 \pm 0.09
30	3.1	700	44.69 \pm 3.06	37.98 \pm 2.94	0.85 \pm 0.09	56.3 \pm 2.4	11.9 \pm 1.5	7.66 \pm 0.18	1.25 \pm 0.08
31	3.0	695	58.94 \pm 3.14	49.37 \pm 2.97	0.84 \pm 0.07	21.8 \pm 2.0	8.5 \pm 1.5	12.06 \pm 0.21	1.55 \pm 1.11
32	3.0	625	32.54 \pm 1.50	27.96 \pm 1.47	0.86 \pm 0.06	32.5 \pm 2.6	26.0 \pm 1.9	10.90 \pm 0.33	1.42 \pm 0.12
33	3.0	650	35.68 \pm 1.55	28.37 \pm 1.43	0.80 \pm 0.05	59.2 \pm 2.7	22.1 \pm 1.7	4.96 \pm 0.13	0.58 \pm 0.05

TABLE 6.6

COMPOSITION OF LEACHATE WITH TIME FROM THE INFILTRATION OF DEIONIZED WATER THROUGH A
COLUMN BED OF UNWEATHERED GRAINS OF PEGMATITE AND GABBRO

TIME ,days	pH	^{238}U ,pCi/l	^{234}U ,pCi/l	$^{234}\text{U}/^{238}\text{U}$ A.R.	^{226}Ra ,pCi/l	^{210}Pb ,pCi/l
1	7.0	3.00 ± 0.10	3.92 ± 0.12	1.31 ± 0.06	< 0.5	< 0.5
5	7.2	1.82 ± 0.15	2.52 ± 0.16	1.38 ± 0.14	0.7 ± 0.4	< 0.5
35	7.8	3.46 ± 0.17	4.67 ± 0.18	1.35 ± 0.06	1.0 ± 0.4	< 0.5

TABLE 6.7

COMPOSITION OF LEACHATE WITH TIME FROM THE INFILTRATION OF pH 7 BICARBONATE SOLUTION
THROUGH A COLUMN BED OF UNWEATHERED GRAINS OF PEGMATITE AND GABBRO

TIME ,days	pH	^{238}U ,pCi/l	^{234}U ,pCi/l	$^{234}\text{U}/^{238}\text{U}$ A.R.	^{226}Ra ,pCi/l	^{210}Pb ,pCi/l
1	7.4	8.51 ± 0.23	7.43 ± 0.23	0.87 ± 0.04	1.6 ± 0.4	< 0.5
5	7.5	7.91 ± 0.25	7.71 ± 0.27	0.98 ± 0.05	3.2 ± 0.4	1.4 ± 0.4
35	8.0	9.32 ± 0.28	9.20 ± 0.27	0.99 ± 0.04	2.7 ± 0.4	0.9 ± 0.4

surface area of rock grains; (4) solid:liquid ratio; (5) hydrogen ion concentration; and (6) sulphate ion concentration.

Two distinctive stages have been observed in the extracted radionuclide activity versus time graphs in Figures 6.2-6.8 from the leaching of pegmatite. A similar two-stage desorption reaction was evident in the leaching of ^{226}Ra from uranium mill tailings by Nathwani and Phillips (1979). From their findings, the first stage involves the fast desorption rate of loosely-held radium atoms, whereas the second stage entails the slow desorption rate of tightly-held radium atoms by diffusion. Fung et al. (1980) have also reported similar shapes in plots of the amounts of extractable constituents in leachates with time from the leaching of feldspars. Feldspars are aluminosilicate minerals and are the principal constituents of granite and other common rocks. Fung et al. (1980) have concluded based on their experimental findings, that: (1) the rapid depletion of major cations in the near-surface layers and the increase in solution pH and major cations during the early times is due to the exchange of hydrogen ions for major cations and (2) the approaching of steady state levels is due to the formation of precipitates, such as clay minerals (eg. kaolinite) and a range of aluminosilicate minerals.

The processes described by these investigators, as well as other processes that may be responsible for the attainment of steady state activities of radionuclides in the pegmatite leachates at latter times are assessed. The neutral and acidic leachates from the leaching of unweathered pegmatite grains with deionized water and the pH3 extractant, after 40 days, have been analyzed for Ca, Mg, Na, K, Cl, HCO_3 , SO_4 , Fe, Mn, and Al. The results of the chemical and radiochemical analysis for the two solutions are given in Table 6.8. The degree of disequilibrium that exists between the ionic species in each of the leachates and various mineralogical species has been evaluated by the computation of saturation indices (S.I.) using two ion speciation and geochemical equilibrium programs, known as WATEQ2 (Ball et al. 1978, 1979) and PHREEQE (Parkhurst et al. 1980). Computed saturation indices, that represent

TABLE 6.8

CHEMICAL AND RADIONUCLIDE COMPOSITION IN THE ACIDIC AND NEUTRAL pH LEACHATES
FROM THE LEACHING OF UNWEATHERED PEGMATITE AFTER 40 DAYS

CONSTITUENT	ACIDIC LEACHATE	NEUTRAL pH LEACHATE
pH	3.0	7.8
Electrical Conductance, uS	40	1300
Ca, mg/l	67.2	1.2
Mg, mg/l	37.4	1.1
Na, mg/l	66.0	32.0
K, mg/l	56.0	8.0
HCO ₃ , mg/l	<5	73.1
SO ₄ , mg/l	1355	6.7
Cl, mg/l	3.5	6.9
SiO ₂ , mg/l	349	40.8
Al, mg/l	146	5
Fe, mg/l	29.3	1.0
Mn, mg/l	0.93	0.06
²³⁸ U, pCi/l	1697 ± 82	40.97 ± 2.92
²³⁴ U, pCi/l	1599 ± 82	58.63 ± 3.71
²³⁴ U/ ²³⁸ U A.R.	0.94 ± 0.07	1.43 ± 0.14
²²⁶ Ra, pCi/l	905 ± 25	52.7 ± 8.9
²¹⁰ Pb, pCi/l	904 ± 15	22.0 ± 6.3
²³⁰ Th, pCi/l	707 ± 32	8.05 ± 1.95
²³² Th, pCi/l	213 ± 17	N D
²²⁸ Th, pCi/l	247 ± 19	N D

N D - not detected

leachates with respect to various mineral phases, are given in Table 6.9. The minerals that are saturated or supersaturated in the acidic leachates are goethite, hematite, $\text{AlOHSO}_4(\text{s})$, quartz and thorianite. The minerals that are saturated or supersaturated in the neutral pH leachates are $\text{Fe}(\text{OH})_3(\text{am})$, goethite, hematite, gibbsite, pyrophyllite, $\text{Al}_4(\text{OH})_{10}\text{SO}_4(\text{s})$, quartz, albite, anorthite, adularia, Na-jarosite, K-jarosite, illite, kaolinite, Ca-montmorillonite and muscovite.

Oxides of iron and aluminum are computed to be present in the acidic and neutral pH leachates. The surfaces of iron and aluminum oxides can provide potential adsorption sites for radionuclides. Other minerals that are computed to be present in the neutral pH leachates in Table 6.9 include primary aluminum silicate minerals (e.g. albite, anorthite, adularia) and related secondary mineral alteration productions (e.g. illite, kaolinite, Ca-montmorillonite, muscovite). These alteration products or clay minerals can provide possible adsorption sites for radionuclides. Primary aluminum silicate minerals generally breakdown to clay minerals and release cations, silicic acid and alkalinity in solution upon weathering. A few examples of these breakdown reactions are given in Table 6.10.

The calculated saturation indices of the acidic and neutral pH leachates with respect to various radioactive mineral phases are given in Table 6.9. All of the Uranium minerals are computed to be undersaturated in both of the leachates. Thorianite ($\text{ThO}_2(\text{s})$), on the other hand, is found to be saturated in the acidic leachates at an S.I. value of + 0.0006. Because the observed ^{232}Th activity in the neutral pH leachate was below the detection limit at 10^{-1} pCi/l, no comparison could be made with the theoretical ^{232}Th activity (i.e. below 10^{-6} pCi/l). A mineral solubility diagram for $\text{ThO}_2(\text{s})$ in Figure 6.11 is generated from the compilation of thermodynamic data into the program, PHREEQE. From the distribution of the respective S.I. values for ThO_2 in the acidic and neutral pH leachates in Figure 6.11, the distribution of the ^{232}Th activities in the pegmatite leachates appears to be primarily solubility controlled.

TABLE 6.9

SATURATION INDICES OF VARIOUS MINERAL PHASES IN THE ACIDIC AND NEUTRAL pH LEACHATES

MINERAL AND CHEMICAL COMPOSITION		SATURATION INDICES:	
		ACIDIC LEACHATE	NEUTRAL pH LEACHATE
Calcite, CaCO_3		- 8.02	- 1.70
Dolomite, $\text{CaMg}(\text{CO}_3)_2$		- 16.01	- 3.20
Gypsum, $\text{CaSO}_4 \cdot 2\text{H}_2\text{O}$		- 0.96	- 4.23
Siderite, FeCO_3		- 6.47	- 3.80
$\text{Fe}(\text{OH})_3$		- 1.78	- 3.44
Goethite, $\text{FeO}(\text{OH})$		1.02	10.38
Hematite, Fe_2O_3		1.63	20.35
Gibbsite, $\text{Al}_2\text{O}_3 \cdot 3\text{H}_2\text{O}$		- 3.87	1.65
Pyrophyllite, $\text{Al}_2\text{Si}_4\text{O}_{10}(\text{OH})_2$		3.67	10.95
AlOHSO_4		0.53	- 5.43
$\text{Al}_4(\text{OH})_{10}\text{SO}_4$		8.40	2.21
Quartz, SiO_2		1.85	0.91
Albite, $\text{NaAlSi}_3\text{O}_8$		- 5.85	1.40
Anorthite, $\text{CaAl}_2\text{Si}_2\text{O}_8$		17.55	0.17
Adularia, KAlSi_3O_8		- 3.53	3.20
Na-Jarosite, $\text{NaFe}_3(\text{SO}_4)_2(\text{OH})_6$		- 8.59	1.08
K-Jarosite, $\text{KFe}_3(\text{SO}_4)_2(\text{OH})_6$		- 5.24	3.91
Illite, $\text{K}_{0.6}\text{Mg}_{0.25}\text{Al}_{2.3}\text{Si}_{3.5}\text{O}_{10}(\text{OH})_2$		- 7.20	6.72
Kaolinite, $\text{Al}_2\text{Si}_2\text{O}_5(\text{OH})_4$		- 2.65	6.52
Ca-Montmorillonite, $\text{Ca}_{0.17}\text{Al}_{2.33}\text{Si}_{3.67}\text{O}_{10}(\text{OH})_2$		3.59	7.17
Muscovite, $\text{KAl}_3\text{Si}_3\text{O}_{10}(\text{OH})_2$		- 10.26	7.51
Uraninite, UO_2		- 13.15	- 20.19
Coffinite, USiO_4		- 10.75	- 18.73
UO_3		- 7.13	- 4.77
$\text{UO}_2(\text{OH})_2$		- 4.92	- 2.56
Uranophane, $\text{Ca}(\text{UO}_2)_2(\text{SiO}_3\text{OH})_2$		- 17.57	- 6.72
U_3O_8		- 67.23	- 53.07
U_4O_9		- 166.82	- 147.93
Thorianite, ThO_2		0.0006	-

TABLE 6.10

EQUATIONS PERTAINING TO THE BREAKDOWN OF PRIMARY ALUMINUM SILICATE MINERALS TO CLAY MINERALS

1. $\text{KAlSi}_3\text{O}_8(\text{s}) + 2\text{H}^+ + 12\text{H}_2\text{O} = 2\text{K}^+ + 6\text{H}_4\text{SiO}_4 + \text{KAl}_3\text{Si}_3\text{O}_{10}(\text{OH})_2(\text{s})$
Microcline Muscovite
2. $3\text{KAlSi}_3\text{O}_8(\text{s}) + 2\text{H}_2\text{CO}_3 + 12\text{H}_2\text{O} = 2\text{K}^+ + 2\text{HCO}_3^- + 6\text{H}_4\text{SiO}_4 + \text{KAl}_3\text{Si}_3\text{O}_{10}(\text{OH})_2(\text{s})$
3. $\text{CaAl}_2\text{Si}_2\text{O}_8(\text{s}) + 2\text{H}^+ + \text{H}_2\text{O} = \text{Ca}^{2+} + \text{Al}_2\text{Si}_2\text{O}_5(\text{OH})_4(\text{s})$
Anorthite Kaolinite
4. $\text{CaAl}_2\text{Si}_2\text{O}_8(\text{s}) + 2\text{H}_2\text{CO}_3 + \text{H}_2\text{O} = \text{Ca}^{2+} + 2\text{HCO}_3^- + \text{Al}_2\text{Si}_2\text{O}_5(\text{OH})_4(\text{s})$
5. $\text{NaAlSi}_3\text{O}_8(\text{s}) + \text{H}^+ + 4.5\text{H}_2\text{O} = \text{Na}^+ + 2\text{H}_4\text{SiO}_4 + 0.5\text{Al}_2\text{Si}_2\text{O}_5(\text{OH})_4(\text{s})$
Albite Kaolinite
6. $\text{NaAlSi}_3\text{O}_8(\text{s}) + \text{CO}_2(\text{g}) + 5.5\text{H}_2\text{O} = \text{Na}^+ + \text{HCO}_3^- + 2\text{H}_4\text{SiO}_4 + 0.5\text{Al}_2\text{Si}_2\text{O}_5(\text{OH})_4(\text{s})$
7. $4\text{Na}_{0.5}\text{Ca}_{0.5}\text{Al}_{1.5}\text{Si}_{2.5}\text{O}_8 + 6\text{H}^+ + 1\text{H}_2\text{O} = 2\text{Na}^+ + 2\text{Ca}^{2+} + 4\text{H}_4\text{SiO}_4 + 3\text{Al}_2\text{Si}_2\text{O}_5(\text{OH})_4(\text{s})$
Andesine Kaolinite
8. $4\text{Na}_{0.5}\text{Ca}_{0.5}\text{Al}_{1.5}\text{Si}_{2.5}\text{O}_8 + 6\text{H}_2\text{CO}_3 + 1\text{H}_2\text{O} = 2\text{Na}^+ + 2\text{Ca}^{2+} + 4\text{H}_4\text{SiO}_4 + 6\text{HCO}_3^- + 3\text{Al}_2\text{Si}_2\text{O}_5(\text{OH})_4(\text{s})$

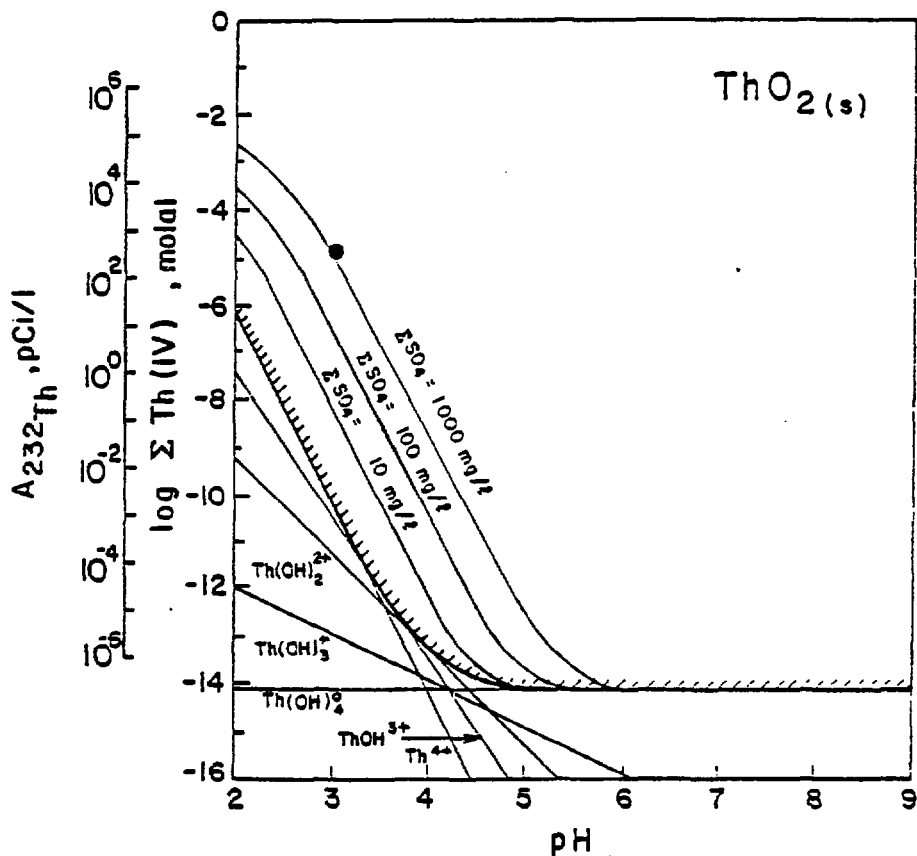


Figure 6.11 Solubility diagram of the mineral thorianite, $\text{ThO}_2(\text{s})$, in equilibrium with the thorium (IV)-hydroxy species at 25°C. The solid line surrounding the hatched area gives the total solubility of Th (IV). Superimposed on the diagram is the effect of thorium (IV)-sulphate complexing on the solubility of $\text{ThO}_2(\text{s})$. ● Symbol for the experimental thorium value in solution after 40 days of pegmatite leaching with pH 3.0 H_2SO_4 . In comparison, the thorium values in solution from the leaching of pegmatite with deionized water were below the detection limit (0.1 pCi/l of ^{232}Th). The source of thermodynamic data for the construction of the diagram was obtained from Langmuir and Herman, 1980.

An explanation for the two stage mechanism in the leaching of radionuclides from pegmatite is suggested based upon the experimental data and related studies by previous investigators. The first stage at early times is dominated by the oxidation and dissolution of the radioactive mineral grains, and subsequently, the release of radioactive species in leachates. The release of these radioactive species in solution is related to hydrogen ion exchange, as suggested from the pH increase with time in Figure 6.1. The steady state level in the second stage at latter times is suggested to be the result of a combination of geochemical mass transfer processes, that include precipitation-dissolution, adsorption-desorption and complexation. Precipitation-dissolution processes here include the dissolution of oxides, silicates and primary aluminosilicate minerals from pegmatite and the formation of thorianite, iron and aluminum oxides, clay minerals and other minerals in the pegmatitic leachates, as determined from the thermodynamic computations. The clay minerals and the oxides of iron and aluminum can offer potential sites for exchange and adsorption of radionuclides.

The data from the pegmatite and the pegmatite-gabbro leaching experiments using the batch and column techniques are summarized in Table 6.11. The radionuclide compositions of the waste-rock-influenced groundwater in zone D, are also listed in Table 6.11 for comparative purposes with the leaching results. With the exception of ^{226}Ra , the activities of ^{210}Pb , ^{238}U and ^{234}U in the low pH zone D water sample at site L are similar to that found in the leachate from the column leaching of pegmatite-gabbro with pH3 H_2SO_4 . The radionuclide activities in leachates resulting from the leaching of pegmatite-gabbro by the batch method are much higher than that found naturally in water sample L. With the exception of the uranium isotopes, the ^{226}Ra and ^{210}Pb activities in water samples M16-4.84 and M13-8.95 in zone D are found to be similar to that found in the neutral pH leachates from the column experiments. The reasons for the discrepancy between the field results and the lab results for all six radionuclides in Table 6.11 can be attributed to various

TABLE 6.11

SUMMARY OF THE RESULTS FROM THE WASTE ROCK LEACHING EXPERIMENTS AND THE COMPOSITION OF THE
TWO TYPES OF ZONE D GROUNDWATER

DESCRIPTION				pH	^{238}U ,pCi/l	^{234}U ,pCi/l	$^{234}\text{U}/^{238}\text{U}$ A.R.	^{226}Ra ,pCi/l	^{210}Pb ,pCi/l	^{230}Th ,pCi/l	^{232}Th ,pCi/l
A. Zone D Groundwater											
(1) Sample L, April 1980				3.4	69.4 ± 1.1	61.9 ± 1.0	0.88 ± 0.02	11.5 ± 1.8	3.7 ± 1.3	0.44 ± 0.06	0.16 ± 0.03
June 1982				3.7	39.1 ± 1.5	38.1 ± 1.5	0.98 ± 0.05	12.5 ± 1.6	14.4 ± 1.1	-	-
(2) Sample B-2.2, July 1979				6.5	27.9 ± 1.9	35.4 ± 2.0	1.27 ± 0.11	-	-	-	-
Sample M16-4.84, June 1982				6.9	86.6 ± 3.1	78.4 ± 3.1	0.91 ± 0.05	2.4 ± 0.3	< 0.5	-	-
Sample M13-8.95, June 1982				6.6	100.0 ± 1.1	94.9 ± 1.1	0.95 ± 0.02	2.2 ± 0.3	< 0.5	-	-
B. Rock Leaching Experiments											
Leach Tech.	Rock*	** Surf.	Solution Type								
Column	P,G	UN	pH3 H ₂ SO ₄	3.0	35.7 ± 1.6	28.4 ± 1.4	0.80 ± 0.05	59.2 ± 2.7	22.1 ± 1.7	4.96 ± 0.13	0.58 ± 0.05
Column	P,G	UN	Water	7.8	3.46 ± 0.17	4.67 ± 0.18	1.35 ± 0.08	1.0 ± 0.04	< 0.5	-	-
Column	P,G	UN	pH7 HCO ₃	8.0	9.32 ± 0.28	9.20 ± 0.27	0.99 ± 0.04	2.7 ± 0.4	0.9 ± 0.4	-	-
Batch	P,G	UN	pH3 H ₂ SO ₄	3.0	909 ± 23	776 ± 22	0.85 ± 0.03	261 ± 18	153 ± 12	208 ± 2	24 ± 0.8
Batch	P,G	UN	Water	8.2	105 ± 5	107 ± 6	1.02 ± 0.08	22 ± 8	33 ± 5	1.2 ± 0.1	< 0.1
Batch	P	UN	pH3 H ₂ SO ₄	3.0	1697 ± 82	1599 ± 82	0.94 ± 0.07	905 ± 25	904 ± 15	707 ± 32	213 ± 17
Batch	P	UN	Water	7.8	41.0 ± 2.9	58.6 ± 3.7	1.43 ± 0.14	52.7 ± 8.9	22.0 ± 6.3	8.0 ± 2.0	< 0.1
Batch	P	UN,R	pH3 H ₂ SO ₄	3.0	382 ± 14	329 ± 14	0.86 ± 0.05	104 ± 5	86 ± 3	227 ± 9	92 ± 6
Batch	P	UN,R	Water	7.8	18.2 ± 1.6	24.1 ± 2.1	1.32 ± 0.16	18.0 ± 2.2	9.7 ± 1.5	-	-
Batch	P	W	pH3 H ₂ SO ₄	3.0	2034 ± 47	1587 ± 43	0.78 ± 0.03	710 ± 23	855 ± 16	753 ± 10	200 ± 20
Batch	P	W	Water	7.7	69.8 ± 4.1	64.3 ± 4.4	0.92 ± 0.08	42.9 ± 8.2	60.7 ± 6.0	18.1 ± 2.0	< 0.1

* Symbols for Rock Type: P - pegmatite, G - gabbro

** Symbols for type of surface: UN - unweathered grains; W - weathered grains; R - released grains

leaching factors and to the selective adsorption of uranium, thorium, radium and lead on the surfaces of the sand particles below the waste rock piles.

The applicability of the activities of the extracted radionuclides from the leaching experiments as parameters in the transport models is given in Chapter 8.

6.3 Pyrite Leaching Experiments

To determine whether pyrite oxidation within the waste rock mass was responsible for the zone D type of groundwater chemistry at site L, grains of pyrite were leached with deionized water using the batch technique and also with a solution of the acidophilic, iron-oxidizing bacterium *Thiobacillus ferrooxidans*. The bacterium was added to the pyrite grains in order to observe its effectiveness as a catalyst in the oxidation of pyrite. The increase in hydrogen ion and sulphate ion concentrations in each of the resulting batch leachates would suggest the occurrence of pyrite oxidation.

Although pyrite is readily found in trace amounts in the gabbroic rock at the site, a large sample of pyrite from Noranda, Quebec was used in the experiments. The sample was crushed and sieved to a particle diameter of approximately 5 mm. The extractants used were deionized water and a solution of *Thiobacillus ferrooxidans*. The bacteria solution was provided by the biology department at the University of Waterloo.

6.3.1 Description of Batch Experiments

The procedure for the leaching of pyrite grains is described below:

- (a) Pyrite grains (5 mm dia.) were sterilized from any trace amounts of bacteria by heat at 200°C for 3 days in an oven.
- (b) Ten grams of the sterilized pyrite grains were added to ten 100 ml polyethylene bottles to which five of the bottles each contained 50 ml deionized water and the remaining five each contained 50 ml of a bacteria solution of *Thiobacillus ferrooxidans*.

- (c) The bottles were sealed and mechanically shaken end-to-end at approximately 120 times a minute for periods ranging from 1 to 1000 hours.
- (d) All of the sample runs were carried out at room temperature.
- (e) After each reaction period, the bottle was removed from the shaker and the suspension was then filtered through 0.45 μ millipore filters. The filtrate was analyzed for values of pH, electrical conductance and sulphate concentration.

6.3.2 Results and Interpretation

The variations in the pH, electrical conductance and sulphate values in the leachates from the leaching of pyrite with time are shown in Figures 6.12 and 6.13. The results of the leaching of pyrite without the influence of bacteria after 40 days show the pH to drop from 5.5 to 3.7, whereas increases in the sulphate concentration from 0 to 260 mg/l and in the electrical conductance from 0 to 450 μ S are observed. The effects on the added bacterium Thiobacillus ferrooxidans to the batch reactor of pyrite and water have increased the sulphate concentration from 1000 to 4560 mg/l and the electrical conductance from 1900 to 4000 μ S, along with a drop in pH from 3.9 to 2.2.

The experimental observations in the solution phase in Figures 6.12 and 6.13 are definitely reflected by the effects of pyrite oxidation. The effects of pyrite oxidation are found to be more pronounced when the bacterium Thiobacillus ferrooxidans has been added to the chemical system. These observations of increased values of hydrogen and sulphate ions and electrical conductance in the leachates are also present in groundwater at site L in the waste-rock influenced zone in the northwest sector of the field site. In fact, the NW waste-rock-influenced groundwater at site L contains higher concentrations of hydrogen and sulphate ions as well as higher activities for most of the radionuclides of interest than that of the NE waste-rock-influenced groundwater. The difference is attributed to the oxidation and dissolution of

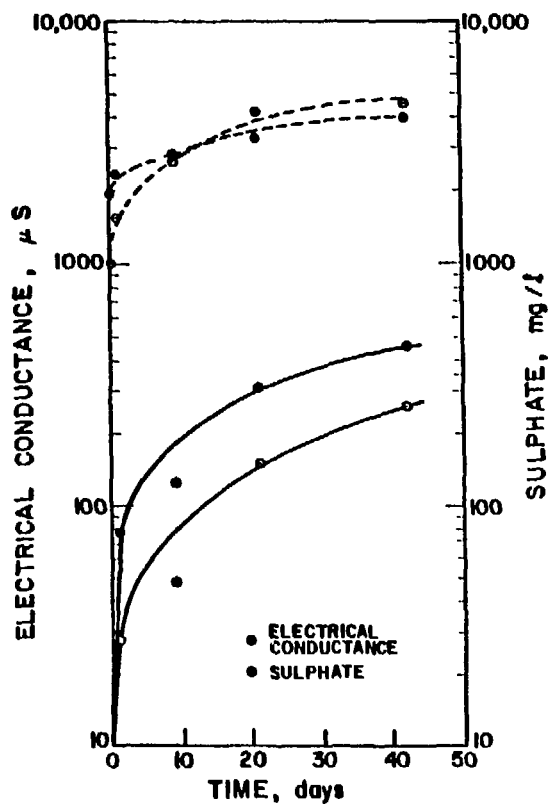


Figure 6.13 Results of pyrite leaching experiment. The values of electrical conductance and sulphate plotted as a function of time. Type of extractant: — deionized water; --- bacterial solution.

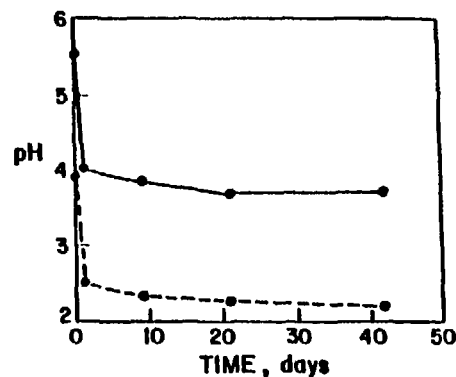


Figure 6.12 Results of pyrite leaching experiment. The values of pH in solution plotted as a function of time. Type of extractant: — deionized water; --- bacterial solution.

the pyrite-containing gabbro and the pegmatitic rock in the pile lying above piezometer L. The rationale for this explanation is based on the locations of the various waste rock piles in the northeast and northwest sectors in Figure 5.3 and on the pyrite leaching results. Although the dissolution of gypsum could also yield high sulphate values in groundwater from site L, it could not explain for the decrease in the pH values.

6.4 Acid Neutralization in Sand

To determine the degree of acid front retardation at the field site, a column experiment was initiated in the laboratory. The column experiment involved the movement of artificial, low pH sulphate groundwater through a column packed with the Greyhawk sand. The experimental conditions were set up as closely as possible to represent the actual field conditions for the neutralization of the low pH sulphate groundwater from site L by the porous medium along the NW flow regime. The artificial groundwater was made by the addition of concentrated H_2SO_4 to 20 liters of deionized water in a nalgene bottle until the pH was equal to 3.5. This is the approximate pH of the groundwater at site L, as measured from 1979 to 1982. Samples of the Greyhawk sand were taken from a core sample within the low pH zone in the excavated pegmatite-gabbro area at site GR1. Site GR1 is approximately 5 meters downflow from site L.

Because numerous investigators (Blair et al., 1980; Morin et al., 1982) have attributed the retardation of acid fronts at tailings impoundments primarily to the neutralization effect that is caused from the dissolution of calcite, soil core samples from sites GR1, GR4, GR7 and GR9, have been examined for carbonate content by the head-space gas chromatographic technique. Prior to carbonate analyses, the soils were oven-dried and then sieved through 2 mm and 1 mm openings. Five grams of the 1-2 mm fractions were used for the carbonate determinations. The analyses of the carbonate content in the sand samples are given in Veska (1983). The values range from 0.010 to 0.113 weight percent as $CaCO_3$; i.e. assuming total carbonate as $CaCO_3$. The carbonate content in the GR1 sand is low, ranging from 0.010 to 0.012%.

6.4.1 Description of Column Experiments

Sand from sample GR1 (1-2 mm grain size) was packed into a 9.7 cm long by 6.4 cm I.D. cylindrical, plexiglass column with removable plexiglass end caps. The weight of the sand in the column was 560 grams. The design of the column and the end caps is given in detail by Reynolds (1978). Prior to the packing of the sand, stainless steel screens were installed in the recessions made on the inside of each of the end caps. In the recessed opening of the influent end cap, a radial system of interconnected 2.5 mm square open channels was recessed even further within the end cap. The radial system was to allow an equal distribution of flow throughout the sand column. The recessed opening of the effluent end cap, on the other hand, consisted of a central 0.8 mm I.D. opening in order to maintain one-dimensional flow near the end of the column. Both influent and effluent end caps contained portals for the passage of solution through the column.

A pH 3.5 solution in a 20 liter nalgene container was passed through the column through 2.5 mm I.D. tygon tubing connected to the influent portal of the column and the outlet of the nalgene container via a variable speed, peristaltic pump. The flow rate of the solution through the sand column was found to be constant at 0.7 ml/min. at the effluent portal. The effluent from the column was continuously monitored for pH by the movement of the column effluent through 2.5 mm I.D. tygon tubing into a flow-through cell in contact with a single combination pH electrode. The pH electrode was connected to a pH meter. The response in pH readings with time was recorded by a chart recorder that was connected to the pH meter. Prior to the initiation of the column experiment, the pH meter was calibrated with pH buffers 4.0 and 7.0.

6.4.2 Results and Interpretation

The pH of the column effluent was equal to 5.6 immediately after the complete saturation of the sand grains with the pH 3.5 solution. A graph of the change in pH of the leachate with time is plotted in Figure 6.14. Three

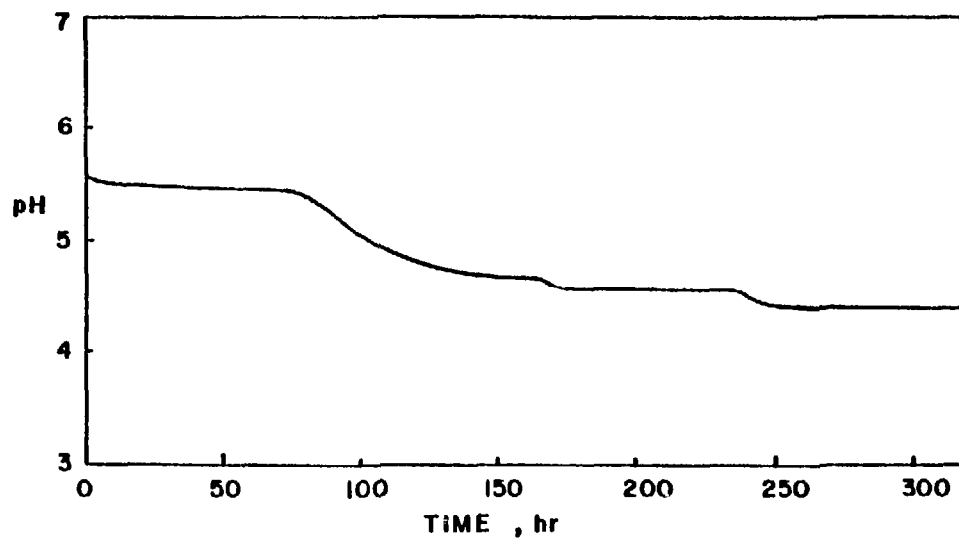


Figure 6.14 pH variation of the column leachate as a function of time.

points of inflection are noticed in the leachate pH versus time plot in Figure 6.14. The first major inflection point is at 102 hours and pH 5.00. The other two inflection points occur at 170 hours and pH 4.60 and at 244 hours and pH 4.45. From 260 to 320 hours, the pH is shown to be constant at 4.40.

The first inflection point at pH 5.00 in Figure 6.14 represents the dissolution of all of the carbonate minerals within the sand. The rationale for this explanation is because calcite has very high buffer capacities at near neutral pH values and rapidly decreases below pH 5.0 (Van Breeman and Wielemaker, I, 1974). The second and third inflection points at pH 4.60 and pH 4.45 in Figure 6.14 can be explained due to the leaching of the aluminosilicate minerals. For example, strong buffering takes place under acid conditions (pH 3.0 to pH 4.0) with the aluminosilicates, kaolinite and montmorillonite, and also under slightly acid conditions (pH 4.5 to pH 6.0) with gibbsite and the aluminosilicates, microcline and illite (Van Breeman and Wielemaker, II, 1974). In addition, the dissolution of primary feldspar minerals within the sand can release bicarbonate ions into solution (refer to Table 6.10) and thus result in an increase in solution pH. Therefore, the leaching of the feldspars in the sand and the added buffering capacities of the clay minerals within the sand are the main reasons why pH values in the leachates after a long period of time do not drop to the same pH as that of the stock solution (i.e. pH 3.5).

The equivalence point for the neutralization of the pH 3.5 sulphate solution by the carbonate content in the sand, as represented by the first inflection point in Figure 6.14, was predicted by cell calculations with a mass-balance approach. The volume of sand within the column or cell was calculated at 206.64 cm^3 from the values of the total weight of the sand (560 g) and the specific gravity of the sand (2.71 g/cm^3). With the assumption of 100% water saturation in the cell, the volume of solution within the column was calculated at 105.4 cm^3 from the values of the cell volume (312 cm^3) and the volume of solids. A porosity of 0.34 was derived directly from the volumes of solids and solution within the cell. From the average calcite content in the GR1 sand at 0.011 weight percent, the number of moles of calcite in 560 grams of sand was calculated at 6.16×10^{-4} moles. In the neutralization reaction,



each CaCO_3 reacts with 2H^+ and the equivalent weight for CaCO_3 becomes 50 g/g-eq. Thus the number of gram-equivalents (g-eq) of CaCO_3 present in the 560 grams of sand is 1.23×10^{-3} g-eq. Because the major source of H^+ ions is from the pH 3.5 H_2SO_4 solution and because the equivalent weight of the sulphuric acid in a neutralization reaction with CaCO_3 in the soil is equal to 49 g/g-eq, the number of gram-equivalents of H_2SO_4 in the 105.4 ml of solution phase is equal to 3.37×10^{-5} g-eq.

The degree of acid front retardation in the sand column is represented by a factor that is equal to

$$\frac{\text{g-eq}_{\text{CaCO}_3}}{\text{g-eq}_{\text{H}_2\text{SO}_4}} = 36.5. \quad (6.2)$$

This factor is used in this experiment for the equivalence point determination of the neutralization of hydrogen ions with CaCO_3 and in the calculation of the acid front velocity. Assuming the acid front within the cell advances by plug displacement, the velocity of the acid front is calculated by dividing the pore water velocity by the acid front retardation factor, as

$$V_A = \frac{V_W}{\frac{\text{g-eq}_{\text{CaCO}_3}}{\text{g-eq}_{\text{H}_2\text{SO}_4}}} \quad (6.3)$$

,where V_A = acid front velocity

V_W = average linear pore water velocity

$\frac{\text{g-eq}_{\text{CaCO}_3}}{\text{g-eq}_{\text{H}_2\text{SO}_4}}$ = acid front retardation factor

It is important to note that equation 6.3 is only valid in the context of a cell conceptualization of one-dimensional plug advancement of an acidic solution that dissolves instantaneously in each cell. Although equation 6.3 is expressed as a modified form of the retardation equation, it cannot be derived from and has nothing to do with the K_d parameter which is used in the normal retardation equation (equation 2.11).

The average linear pore water velocity for equation 6.3 is determined at 3.82 cm/hr from the values of the flow rate ($0.7 \text{ cm}^3/\text{min}$), the cross-sectional area of the column (32.17 cm^2) and the porosity (0.34). From the determined parameters of pore water velocity and retardation factor, the acid front velocity is calculated at 0.105 cm/hr using equation 6.3. Because the length of the sand column is 9.7 cm, the predicted time of arrival of the acid front from the influent portal to the effluent portal is 93 hours. As a comparison, these predicted values for the acid front velocity at 0.105 cm/hr and the equivalence point at 93 hours are close to the respective experimental values at 0.095 cm/hr and 102 hours.

6.5 Summary

The factors that affect the natural release of radionuclides from waste rock have been assessed in the laboratory. These factors include: (1) weathered and unweathered rock surfaces; (2) number of repeated extractions with the same rock grains; (3) active surface area of rock grains; (4) solid:liquid ratio; (5) pH of the extractant; and (6) sulphate ion concentration in the extractant.

The radionuclide compositions of leachates from the waste rock leaching experiments using the column and batch techniques were compared to that of the waste-rock-influenced groundwater in zone D. The matches were found to be good for several of the radionuclides and only fair for all six of the radionuclides of interest.

The increased hydrogen ion and sulphate ion concentrations in the leachates from the pyrite leaching experiments confirmed that pyrite oxidation can occur in the presence of water. The effect of pyrite oxidation was especially noticeable in bacteria solutions that contained *Thiobacillus ferrooxidans*. At the field site, pyrite is found only in the gabbroic waste rock. Because low pH sulphate groundwater was found below the pegmatite-gabbro waste rock pile in the northwest sector of the site, pyrite oxidation was considered responsible for the resulting groundwater composition.

From the acid neutralization column experiments with samples of field sand, the passage of hydrogen ions in the sand column was controlled by the buffering capacities of the calcite and aluminosilicate minerals. The relative velocity of the acid front in the sand column was calculated at a factor of 36.5 less than the average linear pore water velocity. A modified, one-dimensional retardation equation was used to predict the acid front velocity. Good agreement was found between the predicted and the experimentally-derived velocities.

CHAPTER 7

RADIONUCLIDE PARTITIONING IN AQUIFER MATERIALS

The relative mobilities of waste-rock-derived radionuclides in the sand aquifer are assessed by the advection-retardation model and the cell model. The most critical parameter in both of these models is the distribution coefficient, K_d , which is a measure of the partitioning of a particular radionuclide species between the solid and liquid phases of the porous medium. The K_d approach is only applicable if there exists a linear functional relationship between the activities in the solid and solution phases. This equilibrium condition is generally met by fast, adsorption-desorption reactions.

The relationship for the partitioning of uranium, thorium, radium and lead between the solid and liquid phases was determined in the laboratory. Laboratory-determined K_d values can be measured either by the static batch method under steady state conditions or by the column method under dynamic flow conditions (Ames and Rai, 1978). Because the standard K_d determination technique to which all other technique results are compared is the batch technique (Ames and Rai, 1978), only batch experiments have been conducted. The batch experiments in this investigation have involved the equilibration of known amounts of aquifer sand with solutions of varying activities of a radioactive solute under isothermal conditions. Adsorption isotherms are plotted from the results of the batch experiments in order to determine if linear functional relationships exists for each radionuclide between the solution and the solid phases at various solution activities.

The batch K_d values for the radionuclides of interest are compared with those values that are determined by the field technique. The determination of a field K_d for a radionuclide can be done either by injection experiments or by another method involving a knowledge of the radionuclide activities in groundwater and that which is adsorbed on the solid phase. The former method

has not been implemented because it is time-consuming and expensive. Instead, the latter method is used in the determination of field K_d values. The disadvantage of the latter method is the problem of determining the adsorbed activities of the radionuclides on the solid phase. Nonetheless, field K_d values are estimated based upon the activities of radionuclides in groundwater and soil. The groundwater activities of radionuclides are given in Chapter 5. Soil sample GR4-(IV) is used in the field K_d calculations. This soil sample is located in the acid front zone below the waste rock and is spatially related to groundwater sample, GR4-1.14. The activities of ^{238}U and ^{232}Th in the soil have been determined by neutron activation analyses at McMaster University and the ^{226}Ra activity in the soil has been determined by Pon (1980).

7.1 Materials for Batch K_d Experiments

Batch K_d values were determined for the individual partitioning of $^{238}\text{U(IV)}$, $^{238}\text{U(VI)}$, $^{232}\text{Th(IV)}$, $^{226}\text{Ra(II)}$ and $^{210}\text{Pb(II)}$ between uncontaminated sand and three types of equilibrating solutions. The three types of equilibrating solutions are non-radioactive and are representative of the waste-rock-influenced groundwater at three different localities below the waste rock piles. These localities are in the acid front zone (sites L and GR4), site GR9 and site B. These sites are respectively located in the northwest, northcentral and northeast sectors of the field site. The chemical compositions of the equilibrating solutions corresponding to groundwater at the acid front zone, at site GR9 and at site B are given in Table 7.1 under the respective titles, namely: (1) the pH 3.0 calcium-magnesium sulphate solution, (2) the pH 5.5 calcium-sulphate solution and (3) the pH 7.0 calcium-bicarbonate-sulphate solution.

The $^{238}\text{U(IV)}$, $^{238}\text{U(VI)}$, $^{232}\text{Th(IV)}$, $^{226}\text{Ra(II)}$ and $^{210}\text{Pb(II)}$ groundwater solutions were each prepared by the increment addition of the respective radioactive standard to each of the three types of equilibrating solutions. Calibrated solutions of ^{226}Ra and ^{210}Pb were procured from Amersham, U.K. The $^{238}\text{U(VI)}$ and $^{232}\text{Th(IV)}$ solutions were prepared from uranyl nitrate and thorium nitrate. The $^{238}\text{U(IV)}$ standard was prepared by

TABLE 7.1COMPOSITION OF INITIAL EQUILIBRATING SOLUTIONS*

CONSTITUENT	pH 3.0 SOLUTION	pH 5.5 SOLUTION	pH 7.0 SOLUTION
Ca	156.0	53.9	201.0
Mg	82.0	7.4	8.9
Na	7.0	3.4	4.7
K	5.4	1.7	4.8
Mn	1.5	0.04	0.04
Al	16.0	0.57	0.05
Fe	0.5	0.14	0.05
Pb	0.01	0.01	0.01
SO ₄	820.0	161.7	337.0
HCO ₃	< 10	10.6	201.0
Cl	3.0	0.6	1.0
Ionic Strength	0.022 m	0.006 m	0.020 m

* All units in mg/l with the exception of the ionic strength

the elution of a uranyl chloride solution in 0.1M HCl through a 2.0 cm x 6.0 cm lead reductor column for the reduction of the U(VI) species (Rodden, 1950). Unlike other reductors, such as the Jones reductor (zinc amalgam) that reduces U(VI) species to a mixed (III) - (IV) state, the lead reductor reduces the U(VI) species to the (IV) oxidation state only. The lead column was further washed with 3N HCl. The U(IV) solution from both the 0.1 N HCl and the 3N HCl effluents was dark green in color. The green color is characteristic of the uranium tetravalent state, whereas red and yellow are respectively characteristic of the tri- and hexavalent states of uranium in solution. To ensure that the UO_2^{2+} solution was quantitatively reduced to U(IV), an aliquot of the effluent from the reductor was scanned in the 700 to 375 millimicron range with the Beckman 35 scanning spectrophotometer. The adsorption spectrum of the green solution showed only U(IV) peaks.

The uncontaminated solid phase material for the batch K_d determinations was taken from soil core GR7 in an area near the swamp that was not expected to be influenced by contamination from the waste-rock-derived radionuclides. The sand from the core was sampled at approximately three meters below the ground surface in the oxic zone. Grab samples of the sand at this depth were oven dried and sieved through a 2 mm stainless steel screen. The minus 2.0 mm sand fraction was used in the batch experiments.

7.2 Description of Batch K_d Experiments

The batch K_d experiments were carried out with some modifications to the method described by Baetsle (1969). The modified procedure is as follows: (1) approximately 1.00-gram samples of the uncontaminated sand were weighed and were placed in 30 ml capacity polyethylene centrifuge tubes; (2) to the centrifuge tubes, two aliquots of each of the $^{238}\text{U(VI)}$, $^{232}\text{Th(IV)}$, $^{226}\text{Ra(II)}$ and $^{210}\text{Pb(II)}$ tagged groundwater solutions along with a blank were added individually and mixed with known amounts of equilibrating solutions at different ratios such that the solution to solid ratio was kept at 20:1;

(3) step 2) was repeated without the sand in the centrifuge tubes; and with only one aliquot of each of the tagged groundwater solutions. (4) the tubes were sealed and shaken on a ManaWhirl Shaker for 48 hours at room temperature; (5) the suspensions were centrifuged in an I.E.C. centrifuge; (6) two milliliter aliquots were removed from the supernatants.

Supernatant samples of uranium, thorium and radium from the K_d experiments were counted by alpha spectrometry as solid sources. Solid sources were prepared by the evaporation of two milliliter aliquots onto the surfaces of 3.0 cm diameter, stainless steel planchets. As for the ^{210}Pb supernatant samples, only one milliliter aliquots were used in the radiometric analysis of ^{210}Pb . The one milliliter aliquots were placed in 20 milliliter glass scintillation vials that contained 10 ml of a fluor solution (Kobayashi and Mandsley, 1974). The soft beta activity of ^{210}Pb in each vial was counted by the Beckman-133 liquid scintillation system using the tritium window.

The K_d , in units of ml/g was calculated for each determination from the equation,

$$K_d = \bar{C}_e / C_e = \frac{(C_0 - C_e)}{C_e} \cdot \frac{\text{ml of solution}}{\text{g of dry material}} \quad 7.1$$

where C_0 is the initial activity of the nuclide in the equilibrating solution (pCi/ml), C_e is the activity of the nuclide in solution after equilibrium (pCi/ml) and \bar{C}_e is the activity of the adsorbed nuclide after equilibrium (pCi/g).

The time of shaking required for the attainment of constant K_d values at equilibrium was determined experimentally. Four, twenty milliliter aliquots of the pH 5.5, 0.164 pCi/ml $^{238}\text{U(VI)}$ solution and four, twenty milliliter aliquots of the pH 5.5, 20.0 pCi/ml ^{226}Ra solution were added separately to eight centrifuge tubes that contained one gram samples of the uncontaminated

sand. The tubes were sealed and placed on the mechanical shaker and shaken for various time intervals that ranged from two hours to seven days. At the end of each time interval, several tubes were withdrawn from the shaker, centrifuged and the supernatants were analyzed for activities of either $^{226}\text{Ra}(\text{II})$ or $^{238}\text{U}(\text{VI})$.

In the sand aquifer, the solution to solid ratio is estimated at one milliliter of groundwater to five grams of dry soil. Although a similar ratio in the laboratory batch K_d determinations would be desirable, it is virtually impossible under laboratory conditions. Therefore, because the 20:1 solution to solid ratio used in the batch experiments was not ideally representative of the field conditions, the effects of the volume of equilibrating solution to the soil mass ratio on the measured K_d values were examined. To each of two centrifuge tubes that contained 1.0 gram of uncontaminated sand, a five milliliter aliquot of the pH 5.5, 76.8 pCi/ml $^{226}\text{Ra}(\text{II})$ solution was added. The solution to soil ratios in the tubes were adjusted to 5:1 and 10:1 with the pH 5.5 equilibrating solution. Similarly, the same procedure was repeated with 5 milliliter aliquots of the pH 5.5, 5.36 pCi/ml $^{238}\text{U}(\text{VI})$ solution. The samples were shaken for two days. The solution phase, after centrifugation, was radiometrically analyzed for either $^{226}\text{Ra}(\text{II})$ or $^{238}\text{U}(\text{VI})$.

It was necessary to determine the partitioning of the $\text{U}(\text{IV})$ species as well as the $\text{U}(\text{VI})$ species at solution pH's 3.0, 4.0, 5.0, 5.5, 6.0, 7.0 and 8.0 in order to accurately assess the relative mobility of uranium in the sand aquifer. Equilibrating solutions with pH values at 4.0, 5.0, 6.0 and 8.0 were made from the three original solutions at pH's 3.0, 5.5 and 7.0 and adjusted to the correct pH by the addition of H_2SO_4 and NH_4OH .

To seven, 100 ml polyethylene bottles that contained 60 ml aliquots of equilibrating solutions at pH's 3.0, 4.0, 5.0, 5.5, 6.0, 7.0 and 8.0, aliquots of the $^{238}\text{U}(\text{IV})$ solution were added such that the resultant solution activity was approximately 1.5 pCi/ml. To another set of seven, 60 ml aliquots of equilibrating solutions at pH's 3.0, 4.0, 5.0, 5.5, 6.0, 7.0 and

8.0, aliquots of the $^{238}\text{U(VI)}$ solution were added such that the resultant activity was approximately 1.5 pCi/ml in each tube. (From earlier U(VI) K_d results, the activity of $^{238}\text{U(VI)}$ at 1.5 pCi/ml corresponded within the linear section of the adsorption isotherms.) For the batch K_d determinations of $^{238}\text{U(IV)}$ and $^{238}\text{U(VI)}$ at various pH's, three, 20 ml aliquots from each of the 60 ml solutions were added to two, 30 ml polyethylene tubes that contained 1.00 gram of uncontaminated sand and to one 30 ml polyethylene tube with no sand. Including duplicates, a total of 42 tubes were sealed and shaken for 48 hours at room temperature. The pH of the solutions in the batch reactors was monitored and adjusted twice during the 48 hour shaking time. After 48 hours, the tubes were centrifuged. Two milliliter aliquots of the supernatant in each tube were removed, evaporated on a planchet and counted for the activity of ^{238}U by alpha spectrometry.

7.3 Results

The agitation time that was needed to reach constant K_d values in the $^{238}\text{U(VI)}$ and $^{226}\text{Ra(II)}$ time equilibration experiments was greater than one day, as found from the results in Table 7.2. The agitation time for all of the batch K_d experiments in this investigation was kept constant at two days.

The solution pH was measured in several of the batch reactors in order to observe any changes. It was found that the pH of the supernatant from the soil interaction with the pH 3.0 equilibrating solution was equal to 3.5. The 0.5 unit increase in pH was probably due to the dissolution of carbonate minerals as well as other minerals within the sand. No apparent pH increases were found in the supernatants from the soil interaction with the pH 5.5 and the pH 7.0 solutions.

The results of the batch K_d determinations for $^{226}\text{Ra(II)}$, $^{210}\text{Pb(II)}$, $^{238}\text{U(VI)}$ and $^{232}\text{Th(IV)}$ at specified solution compositions at pH's 3.0, 5.5 and 7.0 are tabulated in Veska (1983). These results are displayed graphically as adsorption isotherms (i.e. plots of the activity in the

TABLE 7.2

EQUILIBRATION TIME STUDY OF $^{238}\text{U(VI)}$ AND $^{226}\text{Ra(II)}$
BATCH K_d DETERMINATIONS

TIME	$K_d^{238}\text{U(VI)}$, ml/g	$K_d^{226}\text{Ra(II)}$, ml/g
2 hours	95 ± 36	41 ± 2
1 day	180 ± 47	62 ± 3
2 days	150 ± 24 , 168 ± 27	68 ± 4 , 80 ± 5
7 days	174 ± 32	82 ± 5

solid phase vs. activity in solution for each radionuclide) in Figures 7.1 to 7.4 and as distribution functions (i.e. plots of the K_d vs. initial solution activity for each radionuclide) in Figures 7.5 and 7.6. The replication of the data from the duplicates in these figures appear to show only small variations. These variations are largely due to counting statistics as noticed from the calculated one sigma error bars for the K_d values in the distribution functions of $^{226}\text{Ra}(\text{II})$, $^{210}\text{Pb}(\text{II})$, $^{238}\text{U}(\text{VI})$ and $^{232}\text{Th}(\text{IV})$. The observed shapes of the adsorption isotherms and the distribution functions are described below.

The slopes of the $^{226}\text{Ra}(\text{II})$ adsorption isotherms in Figure 7.1 are equal to unity. These linear adsorption isotherms are reflected by the constant K_d values in the horizontal regions of the distribution functions of ^{226}Ra in Figure 7.5. The average K_d values of ^{226}Ra at pH's 3.5, 5.5 and 7.0 in Figure 7.5 are 20, 88 and 1526 ml/g, respectively.

The shapes of the adsorption isotherms and the distribution functions of $^{210}\text{Pb}(\text{II})$ in Figures 7.2 and 7.5 are similar to those of $^{226}\text{Ra}(\text{II})$. The average K_d values of ^{210}Pb in the horizontal regions of the distribution functions in Figure 7.5 at pH's 3.5, 5.5 and 7.0 are 102, 1239 and 215 ml/g, respectively. The magnitude of the K_d values for ^{210}Pb is greater than that for ^{226}Ra between pH's 3.5 and 5.5, i.e. by a factor greater than 5. However, at pH 7.0, the ^{210}Pb K_d is a factor of 7 less than the ^{226}Ra K_d . The lack of significant changes in the magnitude of the K_d values with increasing solution activities for $^{226}\text{Ra}(\text{II})$ and $^{210}\text{Pb}(\text{II})$ indicates that K_d is independent of the initial solution activity in both cases.

The shapes of the adsorption isotherms and the distribution functions of $^{238}\text{U}(\text{VI})$ at pH's 3.5 and 5.5 in Figures 7.3 and 7.6 are different from those for $^{226}\text{Ra}(\text{II})$ and $^{210}\text{Pb}(\text{II})$. At low solution activities of $^{238}\text{U}(\text{VI})$ in Figure 7.3, the slopes of the adsorption isotherms are at unity. However, at higher activities of $^{238}\text{U}(\text{VI})$ in solution, the slopes after a certain point decrease from unity. The decreasing slope after this point, or break-point in

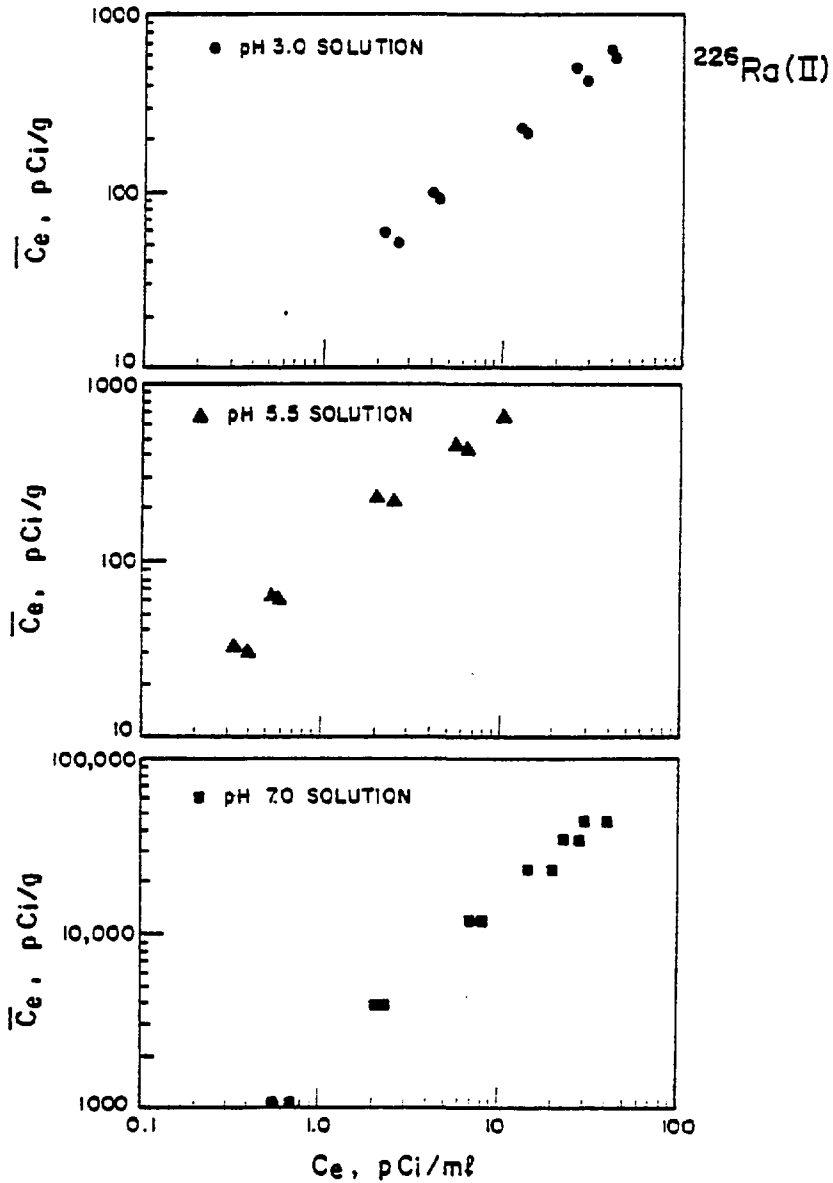


Figure 7.1 Sorption isotherms of $^{226}\text{Ra}(\text{II})$. Three equilibrating solutions were used: (1) pH 3.0 Ca-SO_4 ; (2) pH 5.5 Ca-SO_4 and (3) pH 7.0 $\text{Ca-HCO}_3\text{-SO}_4$.

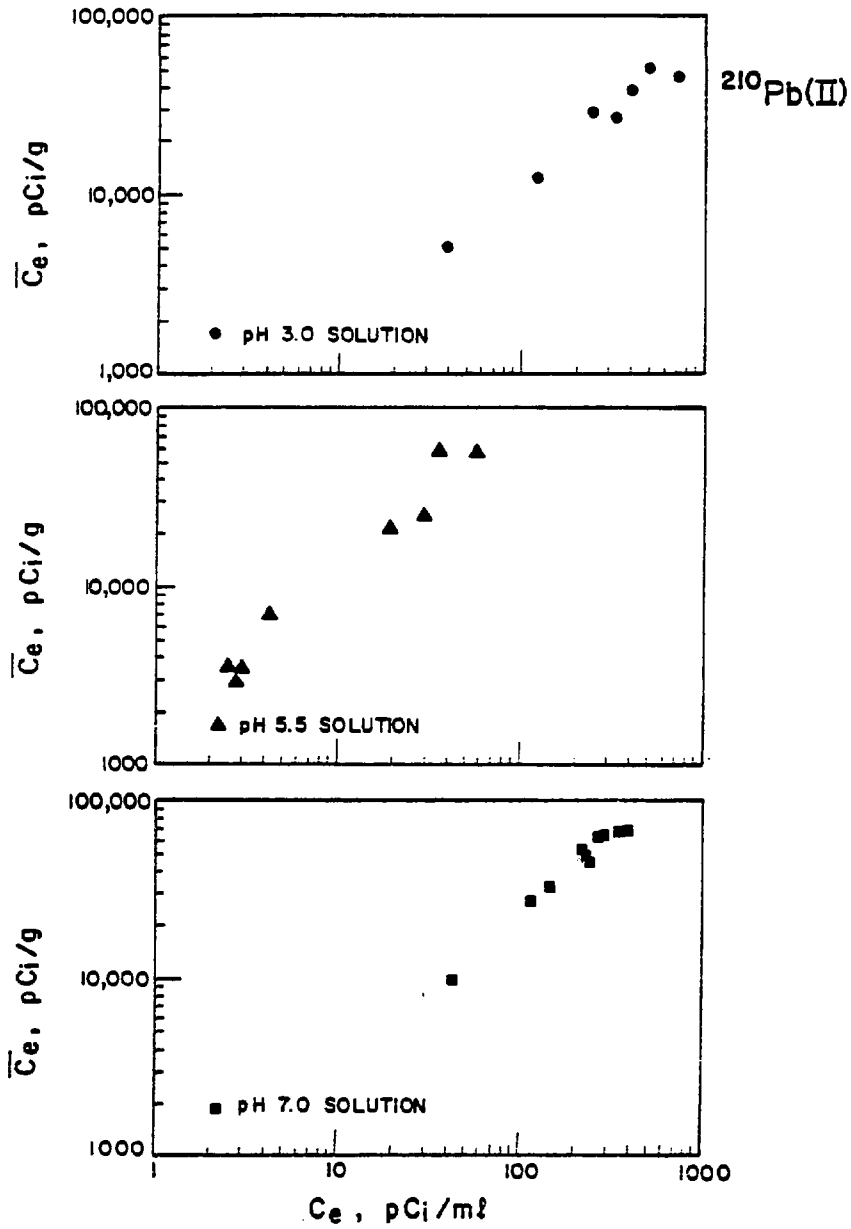


Figure 7.2 Sorption isotherms of $^{210}\text{Pb(II)}$. Three equilibrating solutions were used: (1) pH 3.0 Ca-SO_4 ; (2) pH 5.5 Ca-SO_4 and (3) pH 7.0 $\text{Ca-HCO}_3\text{-SO}_4$.

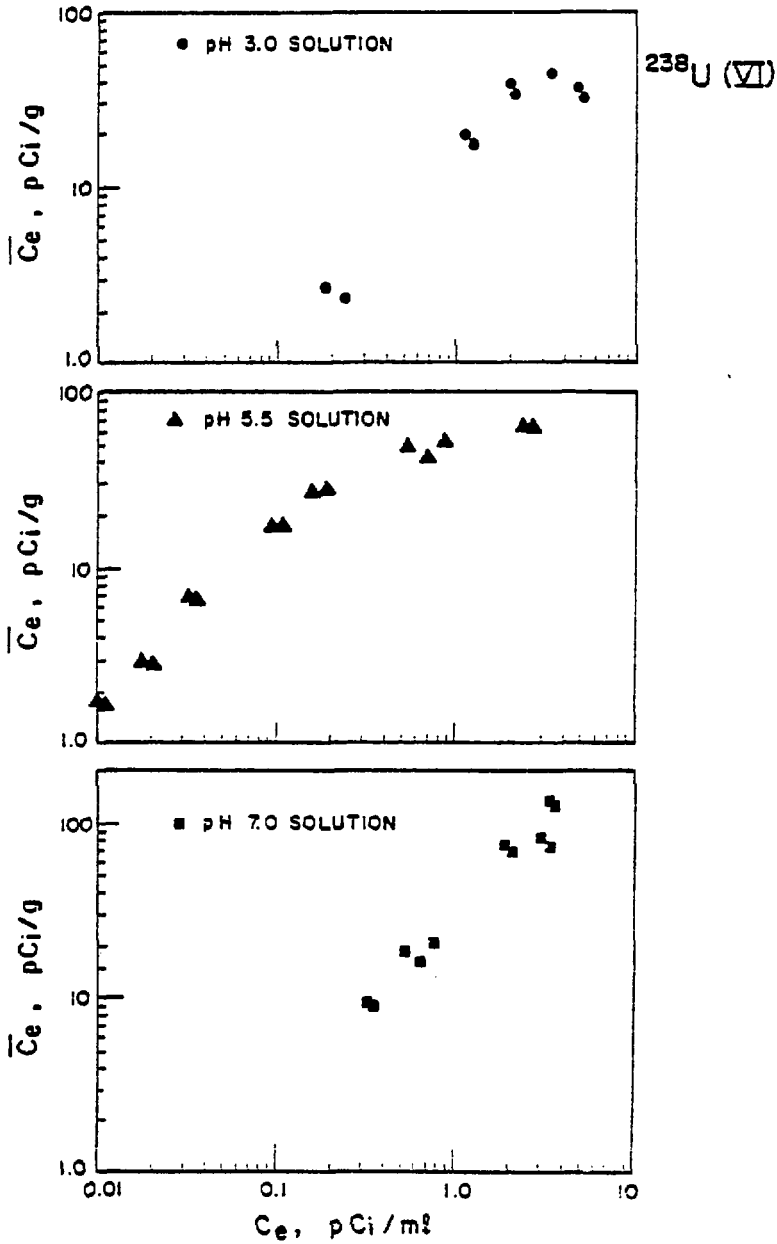


Figure 7.3 Sorption isotherms of $^{238}\text{U(VI)}$. Three equilibrating solutions were used: (1) pH 3.0 Ca-SO_4 ; (2) pH 5.5 Ca-SO_4 and (3) pH 7.0 $\text{Ca-HCO}_3\text{-SO}_4$.

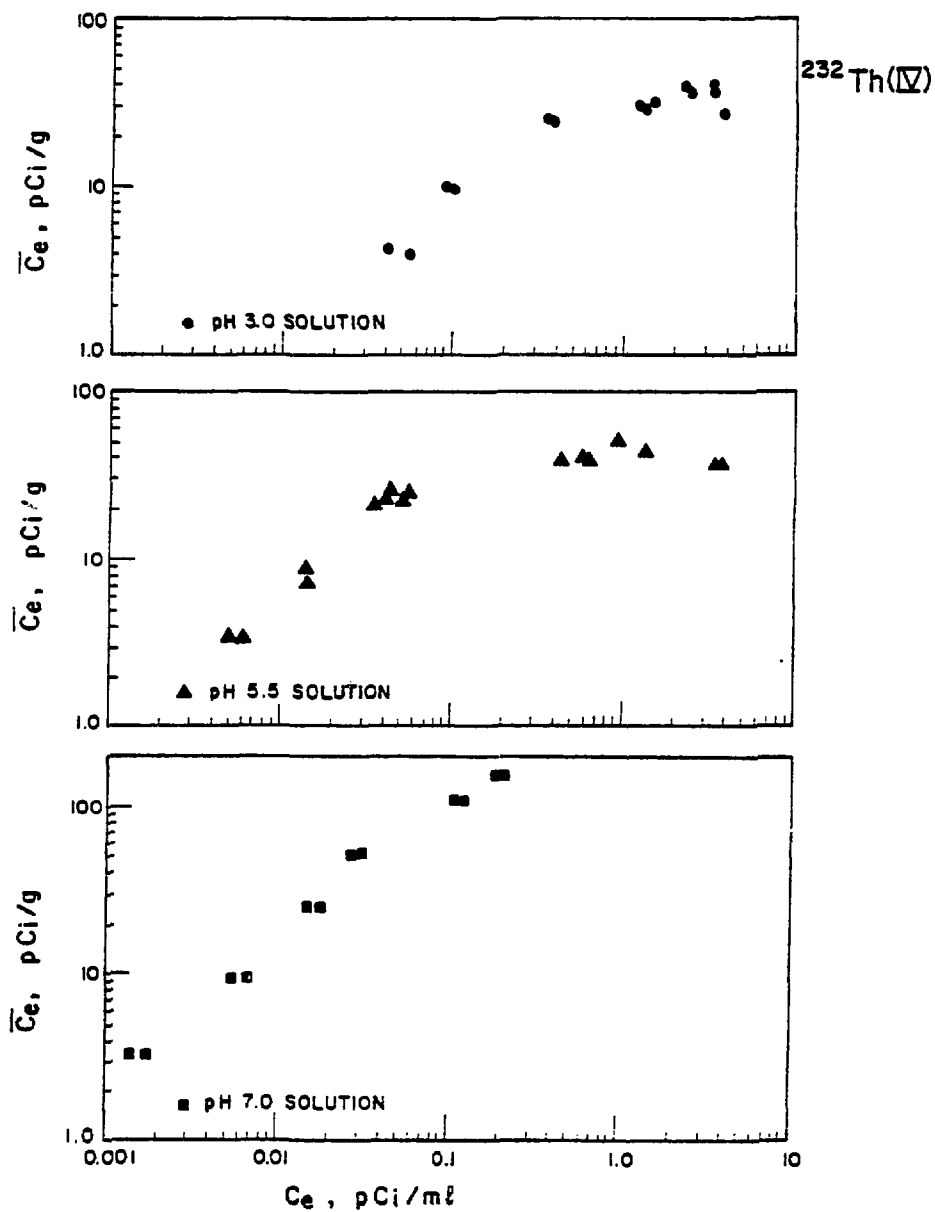


Figure 7.4 Sorption isotherms of $^{232}\text{Th}(\text{IV})$. Three equilibrating solutions were used: (1) pH 3.0 Ca-SO_4 ; (2) pH 5.5 Ca-SO_4 and (3) pH 7.0 $\text{Ca-HCO}_3\text{-SO}_4$.

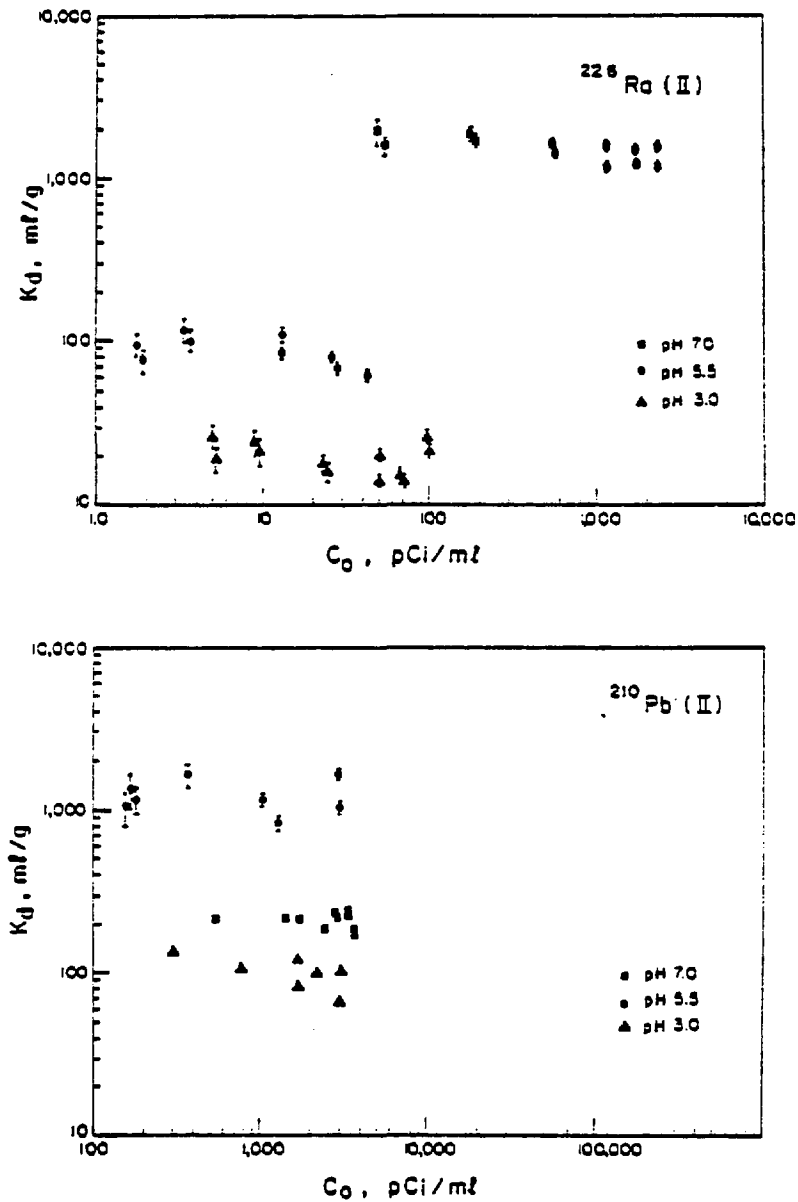


Figure 7.5 Distribution functions of $^{226}\text{Ra (II)}$ and $^{210}\text{Pb (II)}$. Error bars are incorporated for each K_d value.

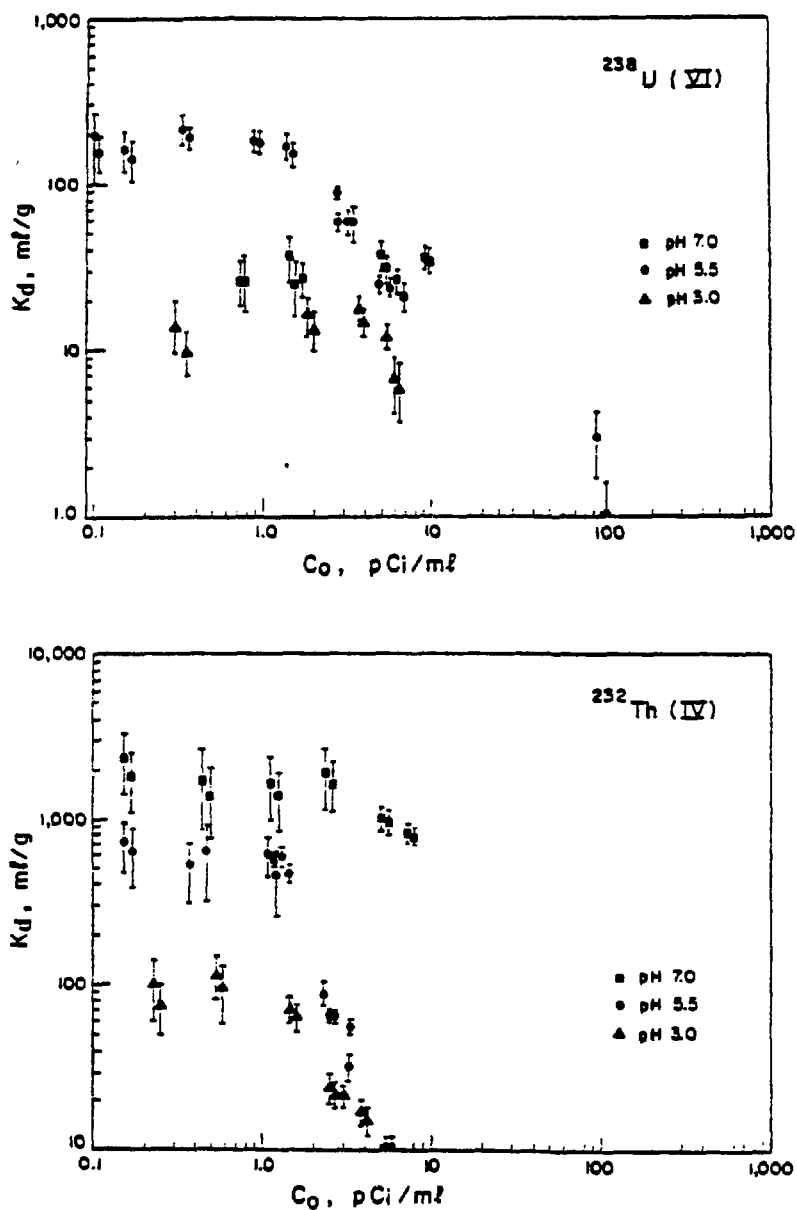


Figure 7.6 Distribution functions of ^{238}U (VI) and ^{232}Th (IV). Error bars are incorporated for each K_d value.

the curve, represents the decrease in the sorbed activity with respect to the solution activity. This is reflected by the decrease in the K_d values with increase in the solution activities in the distribution functions in Figure 7.6. The $^{238}\text{U(VI)}$ activities corresponding to the break-points in the adsorption of uranium (VI) on the Greyhawk sand at pH's 3.5 and 5.5 in Figure 7.6 are 5.5 and 1.5 pCi/ml, respectively. The decrease in the slopes of the distribution functions past each break-point in Figure 7.6 is more pronounced at pH 5.5 than that at pH 3.5. Explanations for these shapes in the $^{238}\text{U(VI)}$ distribution functions are given later in this Chapter. Examples of similar shapes in the distribution functions of $^{238}\text{U(VI)}$ with increasing solution activity are given by Masuda and Yamamoto (1971) and Rancon (1973).

The average K_d values of $^{238}\text{U(VI)}$ in the horizontal regions of the distribution functions in Figure 7.6 at pH's 3.5, 5.5 and 7.0 are 15, 173 and 30 ml/g, respectively. The maximum adsorption of uranium (VI) appears from Figure 7.6 to be in the pH 5.5 range. Rancon (1973) found a similar distribution of K_d values with respect to pH for the adsorption of U(VI) on argillaceous soil. Similarly, the work done by Dementyev and Syromyatnikov (1968) on the adsorption of uranium (VI) on geological materials indicated maximum adsorption in the pH range between 5 and 6.

The shapes of the adsorption isotherms and the distribution functions of $^{232}\text{Th(IV)}$ in Figures 7.4 and 7.6 are similar to those for ^{238}U . The ^{232}Th activities at the break-points in the distribution functions in Figure 7.6 at pH's 3.5, 5.5 and 7.0 correspond to 1.5, 1.3 and 2.6 pCi/ml, respectively. In comparison to these $^{232}\text{Th(IV)}$ K_d results, Rancon (1973) also found similar shapes in his distribution functions for the adsorption of ^{232}Th on argillaceous soil. The shapes of the distribution functions for $^{232}\text{Th(IV)}$ and for $^{238}\text{U(VI)}$ in this investigation have indicated that the K_d for each of these radionuclides is dependent on the initial solution activity in the higher activity range.

The average K_d values of $^{232}\text{Th(IV)}$ in the horizontal regions of the

distribution functions in Figure 7.6 at pH's 3.5, 5.5 and 7.0 are 86, 570 and 1748 ml/g, respectively. Rancon (1973) found a similar relationship in the increase of K_d values with increase in pH for Th(IV) in illite and argillaceous soil.

The results of the batch K_d values for $^{238}\text{U(IV)}$ and $^{238}\text{U(VI)}$ at pH's 3.0, 4.0, 5.0, 5.5, 6.0, 7.0 and 8.0 are given in Table 7.3. The K_d values for $^{238}\text{U(VI)}$ and $^{238}\text{U(IV)}$ at pH's below 5.0 and above 7.0 are low. At solution pH's between 5.0 and 7.0, the K_d values for both species are at a maximum. The K_d values for $^{238}\text{U(VI)}$ and $^{238}\text{U(IV)}$ are similar below pH 4.0. Above pH 4.0, the K_d values for U(IV) are greater than the K_d values for U(VI) by a factor of approximately two. Good agreement is found in the replication of the U(IV) and U(VI) K_d values as given in Table 7.3. The $^{238}\text{U(VI)}$ K_d values at pH's 3.0, 5.5 and 7.0 in Table 7.3 are similar to those values derived from earlier experiments as shown in Figure 7.6.

The effects of the solution to soil ratio on the magnitude of the $^{226}\text{Ra(II)}$ and $^{238}\text{U(VI)}$ batch K_d values are given in Table 7.4. The equilibration of 38.4 pCi/ml ^{226}Ra in a 10:1 solution to soil ratio corresponds to a K_d value of 59 ± 8 ml/g. This value is similar to the 61 ± 3 ml/g value that is derived from the equilibration of 41.5 pCi/l ^{226}Ra in a 20:1 solution to soil ratio. No apparent differences are found between the magnitude of the K_d values from the equilibration of ^{226}Ra in 10:1 and 20:1 solution to soil ratios and that from the equilibration of ^{226}Ra in a 5:1 solution to soil ratio. In contrast, the K_d values for $^{238}\text{U(VI)}$ decrease slightly with decrease in the solution to soil ratios from 20:1 to 5:1.

The results of the field K_d values for ^{238}U , ^{232}Th and ^{226}Ra are given in Table 7.5. These field K_d values are compared in Table 7.5 to the corresponding batch K_d values. Also, the ^{226}Ra K_d values from the batch and field techniques are compared in Table 7.5 to a column K_d value for ^{226}Ra (Clarke, 1982). At solution pH5 in Table 7.5, the field K_d value for

TABLE 7.3COMPARISON OF K_d VALUES FOR $^{238}\text{U(IV)}$ AND $^{238}\text{U(VI)}$ AS A FUNCTION OF pH

pH	$K_d^{238}\text{U(IV)}$, ml/g	$K_d^{238}\text{U(VI)}$, ml/g
3	7 ± 2 , 7 ± 2	8 ± 1 , 9 ± 2
4	12 ± 2 , 13 ± 2	17 ± 2 , 20 ± 3
5	214 ± 20 , 256 ± 39	137 ± 24 , 149 ± 26
5.5	352 ± 44 , 384 ± 61	162 ± 28 , 173 ± 42
6	335 ± 53 , 355 ± 36	168 ± 40 , 194 ± 43
7	91 ± 10 , 119 ± 16	39 ± 4 , 49 ± 6
8	17 ± 3 , 19 ± 3	6 ± 1 , 8 ± 2

TABLE 7.4

EFFECT OF LIQUID : SOLID RATIO ON $^{226}\text{Ra}(\text{II})$ AND $^{238}\text{U}(\text{VI})$ BATCH K_d VALUES

LIQUID : SOLID RATIO	$^{226}\text{Ra}(\text{II})$		$^{238}\text{U}(\text{VI})$	
	Co , pCi/ml	K_d , ml/g	Co , pCi/ml	K_d , ml/g
5:1	76.8	73 ± 6	5.36	16 ± 2
10:1	38.4	59 ± 8	2.68	36 ± 3
20:1	41.5	61 ± 3	5.55	24 ± 3 , 25 ± 3
20:1	-	-	2.81	58 ± 5 , 88 ± 7

TABLE 7.5

COMPARISON AMONGST THE FIELD, BATCH AND COLUMN K_d VALUES FOR ^{230}U , ^{232}Th and ^{226}Ra

Type of K_d Determination	pH	K_d ^{230}U , ml/g	K_d ^{232}Th , ml/g	K_d ^{226}Ra , ml/g
Field (Sample GR4-IV)	5.0	173	5,555 - 16,111	648 - 1128
Batch	5.0	235 - U(IV) 143 - U(VI)	-	-
	5.5	168 - U(IV) 168 - U(VI)	570	88
	7.0	105 - U(IV) 44 - U(VI)	1748	1526
Column	7.0	-	-	98 - 347

^{238}U (173 ml/g) is similar to that of the average batch K_d value for $^{238}\text{U(VI)}$ (143 ml/g) and close to that of the average batch K_d value for $^{238}\text{U(IV)}$ (235 ml/g). However, the field K_d values for ^{232}Th and ^{226}Ra at pH5 are both an order of magnitude greater than their respective batch K_d values at pH5. At pH 7.0, the ^{226}Ra batch K_d value is approximately an order of magnitude greater than the column K_d values (Clarke, 1982).

7.4 Interpretations

The slopes of the $^{226}\text{Ra(II)}$, $^{210}\text{Pb(II)}$, $^{238}\text{U(VI)}$ and $^{232}\text{Th(IV)}$ adsorption isotherms in Figures 7.1-7.4 are equal to unity at low solution activities for these radionuclides. Whereas the slopes of the $^{226}\text{Ra(II)}$ and $^{210}\text{Pb(II)}$ adsorption isotherms are maintained at unity at higher activities, the slopes of the $^{238}\text{U(VI)}$ and $^{232}\text{Th(IV)}$ adsorption isotherms decrease from unity at higher activities. The experimental data from the adsorption isotherms are matched with the Freundlich isotherm using the equation:

$$S = KC^a \quad (7.2)$$

As defined before, S is the solute activity on the soil, C is the solute activity in solution and the constant, a , represents the slope of a log-log plot of S versus C . When the slope of the adsorption isotherm is unity, then $a = 1$, the S/C ratio is constant and equilibrium conditions exist between the adsorption and desorption reactions for that radionuclide. For the activity range of radionuclides present in the Greyhawk groundwater (i.e. between 0.0001 to 0.2 pCi/ml), the adsorption isotherms for $^{226}\text{Ra(II)}$, $^{210}\text{Pb(II)}$, $^{238}\text{U(VI)}$ and $^{232}\text{Th(IV)}$ are found to be linear. This is reflected by the constant K_d values in the horizontal regions of the distribution functions for $^{226}\text{Ra(II)}$, $^{210}\text{Pb(II)}$, $^{238}\text{U(VI)}$ and $^{232}\text{Th(IV)}$ in Figures 7.5 and 7.6. These constant K_d values are used as input parameters in the transport models.

The curved shapes of the uranium and thorium distribution functions at pH's 3.5 and 5.5 can be explained by the background effect and by the law of mass action. The background effect is discussed first. If the leaching of the sand has released some activities of radionuclides in solution and if these background activities are larger than that added at the break-points in the distribution function curves for ^{238}U and ^{232}Th prior to equilibration, it would be reasonable to suggest that the corresponding K_d values for those radionuclides are influenced by the background activities. The amounts of background ^{238}U and ^{232}Th activities in the soil extracts from the batch reactors were determined by neutron activation analysis at the University of Toronto. The results of the background ^{238}U and ^{232}Th activities in different soil extracts are given in Tables 7.6 and 7.7. The ^{238}U activities in the pH 3.5 extracts are approximately a factor of two greater than that in pH 5.5 extracts. The differences in the ^{238}U activities in soil extracts between the different liquid to soil ratios are not significant. The ^{232}Th activities in all of the soil extracts are below the detection limit (1.1×10^{-3} pCi).

The effect of the background ^{238}U activities from the soil extracts on the shapes of the distribution functions is evaluated first. The added amounts of ^{238}U to the batch reactors corresponding to the break-point activities in the distribution function curves in Figure 7.6 are compared in Table 7.6 with the total background ^{238}U activities that have been released in solution. For all cases in Table 7.6, the added amounts of ^{238}U at the break-points in the ^{238}U distribution function curves are larger than that which are released naturally from the soil. Similar to the comparisons in Table 7.6 with ^{238}U , the added amounts of artificial ^{232}Th at the break-points in the ^{232}Th distribution function curves are seen in Table 7.7 to be larger than that which is released naturally from the soil. Therefore, it seems unlikely that the release of background activities of either uranium or thorium upon equilibrium in the batch reactors effect the magnitude of K_d .

The second possible explanation for the shapes of the uranium and thorium distribution functions is attributed to the law of mass action. Wahlberg and Fishman (1962) and Wahlberg et al. (1965) have successfully related the law of

TABLE 7.6

EFFECT OF BACKGROUND ^{238}U ACTIVITIES ON THE $^{238}\text{U(VI)}$ BATCH K_d VALUES

Equilibrating Conditions		Co $^{238}\text{U(VI)}$, pCi/ml	Kd $^{238}\text{U(VI)}$, ml/g	Background ^{238}U in soil extract , pCi/ml	Total Background of ^{238}U , pCi	Amount of $^{238}\text{U(VI)}$ Added , pCi
Liquid:Solid	pH					
1:1	3.0	3.78	18	8.0×10^{-3}	0.14	75.6
20:1	3.0	3.78	18	7.6×10^{-3}	0.14	75.6
1:1	5.5	1.51	168	4.1×10^{-3}	0.69	30.2
20:1	5.5	1.51	168	5.3×10^{-3}	0.89	30.2

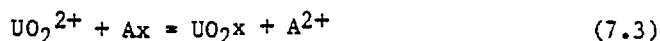
TABLE 7.7

EFFECT OF BACKGROUND $^{232}\text{Th(IV)}$ ACTIVITIES ON THE $^{232}\text{Th(IV)}$ BATCH K_d VALUES

Equilibrating Conditions		Co $^{232}\text{Th(IV)}$, pCi/ml	Kd $^{232}\text{Th(IV)}$, ml/g	Background $^{232}\text{Th(IV)}$ in soil extract , pCi/ml	Total Background $^{232}\text{Th(IV)}$, pCi	Amount of $^{232}\text{Th(IV)}$ Added , pCi
Liquid:Solid	pH					
1:1	3.0	1.59	70	$< 1.1 \times 10^{-3}$	<0.08	31.8
20:1	3.0	1.59	70	$< 1.1 \times 10^{-3}$	<0.08	31.8
1:1	5.5	1.68	600	$< 1.1 \times 10^{-3}$	<0.66	21.6
20:1	5.5	1.68	600	$< 1.1 \times 10^{-3}$	<0.66	21.6

mass action to explain for the shapes of cesium and strontium distribution functions. The shapes of the distribution functions for Cs and Sr obtained by these investigators are similar to those for $^{238}\text{U(VI)}$ and $^{232}\text{Th(IV)}$. Although the relationship found by Wahlberg and others was based on simple exchanger materials and solutions containing a single competing cation, it cannot be applied quantitatively to complex exchange materials and to solutions containing several competing cations. However, a semi-quantitative approach is used here to determine if any relationship exists between the K_d values that are derived by the application of the law of mass action and the shapes of the uranium and thorium distribution functions.

First, the effect of mass action on the $^{238}\text{U(VI)}$ activities is investigated below. Considering the divalent exchange reaction,



the uranyl ion, UO_2^{2+} , displaces a cation, A, from an exchanger, x. The selectivity coefficient for the above reaction is

$$K_{\text{UO}_2-\text{A}} = \frac{[\text{UO}_2\text{x}][\text{A}^{2+}]}{[\text{UO}_2^{2+}][\text{Ax}]} \quad (7.4)$$

Equation 7.4 simplifies to

$$K_{\text{UO}_2-\text{A}} = K_{d_{\text{U(VI)}}} \cdot \frac{[\text{A}^{2+}]}{[\text{Ax}]} \quad (7.5)$$

and can be rearranged to give

$$K_{d_{\text{U(VI)}}} = K_{\text{UO}_2-\text{A}} \cdot \frac{[\text{Ax}]}{[\text{A}^{2+}]} \quad (7.6)$$

The summation of the concentrations of $[Ax]$ and $[UO_2x]$ is equal to the cation exchange capacity of the soil (C.E.C.) and the summation of the concentrations of $[UO_2^{2+}]$ and $[A^{2+}]$ is equal to the total concentration of cations in solution. When trace amounts of $[UO_2^{2+}]$ are present in the batch reactors, $[Ax]$ is approximately equal to C.E.C., $[A^{2+}]$ is equal to the total concentration of cations in solution and equation (7.6) is rewritten as:

$$K_{d_{U(VI)}} = K_{UO_2-A} \cdot \frac{C.E.C.}{[A^{2+}]} \quad (7.7)$$

Thus at trace concentration of $[UO_2^{2+}]$, the K_d value for uranium (VI) is constant, as reflected by the horizontal region in the distribution functions in Figure 7.6. However, as larger quantities of UO_2^{2+} ions in solution begin to compete with other cations for the same exchange sites, then equation 7.7 does not further apply. Instead, as the concentrations of UO_2^{2+} increase in solution, the K_d values for uranium (VI) decrease. Therefore, at high radionuclide concentrations, the K_d values decrease according to the law of mass action.

Comparisons amongst the concentrations of major cations and UO_2^{2+} in the three equilibrating solutions are given in Table 7.8. For the sake of simplicity, the formation of complexes are not assumed in these calculations. The 0.025 to 2.52 meq/l solution concentration range of UO_2^{2+} in Table 7.8 is chosen to correspond to the initial ^{238}U activities between 1.0 and 100 pCi/ml in the area of the negative slopes of the $^{238}U(VI)$ distribution functions in Figure 7.6. The maximum UO_2^{2+} concentration at 2.52 meq/l is found to approach the total concentrations of cations in the pH 5.5 equilibrating solution rather than in the pH 3.0 or pH 7.0 solutions. This is reflected by the more pronounced slope for the distribution function curve at pH 5.5. Therefore, the above rational on mass action principles explains for the shapes of the $^{238}U(VI)$ distribution function curves.

TABLE 7.8

CONCENTRATION COMPARISONS BETWEEN MAJOR CATIONS
AND UO_2^{2+} and Th^{4+} IN THE EQUILIBRATING SOLUTIONS

Constituent	pH 3.0 Solution , meq/l	pH 5.5 Solution , meq/l	pH 7.0 Solution , meq/l
Ca^{2+}	7.78	2.69	10.03
Mg^{2+}	6.75	0.61	0.73
Na^+	0.31	0.15	0.20
K^+	0.14	0.04	0.12
Mn^{2+}	0.06	0.002	0.001
Al^{3+}	1.78	0.06	0.006
Fe^{3+}	0.03	0.008	0.003
Pb^{2+}	9.7×10^{-6}	9.7×10^{-6}	9.7×10^{-6}
Σ cations	16.85	3.56	11.09

Number of meq/l UO_2^{2+} = 2.52 meq/l if $^{238}\text{U(VI)}$ activity = 100 pCi/ml
 = 0.025 meq/l if $^{238}\text{U(VI)}$ activity = 1 pCi/ml

Number of meq/l Th^{4+} = 1.6 meq/l if $^{232}\text{Th(IV)}$ activity = 10 pCi/ml
 = 0.16 meq/l if $^{232}\text{Th(IV)}$ activity = 1 pCi/ml

The concentrations of major cations and $^{232}\text{Th(IV)}$ in the equilibrating solutions are compared in Table 7.8. Neglecting the formation of complexes, the 0.16 to 1.6 meq/l concentration range of Th^{4+} ions in Table 7.8 was chosen to correspond to the one to ten pCi/ml area of the negative slopes of the $^{232}\text{Th(IV)}$ distribution function curves in Figure 7.6. Similar to the $^{238}\text{U(VI)}$ case, the highest Th^{4+} concentration corresponds more closely to the total cation concentrations at pH 5.5 rather than at pH's 3.0 and 7.0. This is reflected by the distinctive shape in the distribution function curve of $^{232}\text{Th(IV)}$ at pH 5.5 in Figure 7.6.

7.5 Summary

At initial solution activities less than 1.5 pCi/ml, the slopes of the $^{226}\text{Ra(II)}$, $^{210}\text{Pb(II)}$, $^{238}\text{U(VI)}$ and $^{232}\text{Th(IV)}$ adsorption isotherms were equal to unity. This was reflected by the constant K_d values in the horizontal regions in each of the distribution function curves. Therefore, at activities below 1.5 pCi/ml, the K_d values for the radionuclides of interest are independent of the initial solution activities. These K_d values of radionuclides within the 0-1.5 pCi/ml concentration range are used as input parameters in the transport models. The activities of radionuclides in groundwater at the field site are much less than 1.5 pCi/ml.

At initial solution activities greater than 1.5 pCi/ml, the $^{226}\text{Ra(II)}$ and $^{210}\text{Pb(II)}$ adsorption isotherms maintained constant slopes at unity, whereas the slopes of the $^{238}\text{U(VI)}$ and $^{232}\text{Th(IV)}$ adsorption isotherms had decreased. Therefore, at high $^{238}\text{U(VI)}$ and $^{232}\text{Th(IV)}$ activities, the respective K_d values are a function of the initial solution activities.

The K_d values for all of the radionuclides, at low and at high activities, were dependent on the solution pH. The magnitude of the K_d values for $^{226}\text{Ra(II)}$ and $^{232}\text{Th(IV)}$ were directly proportional to the solution pH. The magnitude of the K_d values for $^{238}\text{U(VI)}$, $^{238}\text{U(IV)}$ and $^{210}\text{Pb(II)}$ were also directly proportional to solution pH for pH values between 3.0 to 5.5. Above pH 5.5, the K_d values of $^{238}\text{U(VI)}$, $^{238}\text{U(IV)}$ and $^{210}\text{Pb(II)}$ were

inversely proportional to pH. No conclusions were drawn for the change in the $^{238}\text{U(VI)}$, $^{238}\text{U(IV)}$ and $^{210}\text{Pb(II)}$ K_d values with increase in solution pH because of the variance in the chemical compositions amongst solution pH's 3.0, 5.5 and 7.0. Several investigators have also found that the maximum adsorption of uranium on soils occurs in the pH 5.0 to 6.0 range.

The slopes of the distribution functions of $^{238}\text{U(VI)}$ and $^{232}\text{Th(IV)}$ decreased with increased solution activities of the corresponding radionuclides. The negative slopes of the distribution function curves were not the result of background effects from the leaching of the sand. Instead, it was suggested that the negative slopes were caused from the increased competition of the radionuclide concentrations with respect to the concentrations of other solution cations for the available exchange sites. Therefore, at increased concentrations of uranium and thorium in separate batch reactors, the resulting K_d values decrease according to the law of mass action.

CHAPTER 8

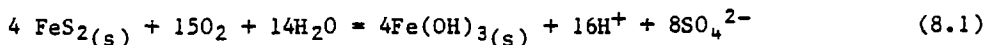
MODELLING OF CONTAMINANT BEHAVIOUR IN THE SAND AQUIFER

In this chapter, an attempt has been made to explain the spread of waste-rock-derived contamination in groundwater at the Greyhawk site since 1957 based on geochemical and mathematical modelling. Geochemical modelling entails the sequence of geochemical events responsible for the subsurface contamination at the site during the past 25 years, starting from the leaching of radionuclides from the waste rock and leading to the transport of the waste-rock-derived radionuclide species in the sand aquifer below. Contaminant migration models are provided to simulate the extent of contamination of the waste-rock-derived radionuclides in groundwater for the past 25 years. The simulated values are compared to the 1982 frontal positions of radionuclide contamination downgradient from the waste rock in the sand aquifer. The purpose of the comparisons between the simulated values and the actual values is to assess the applicability of the models and the use of laboratory-determined parameters.

8.1 Waste Rock Weathering

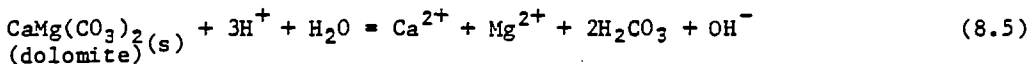
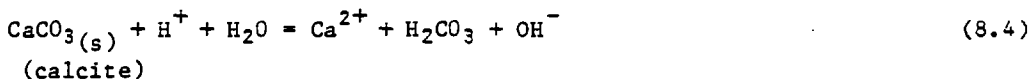
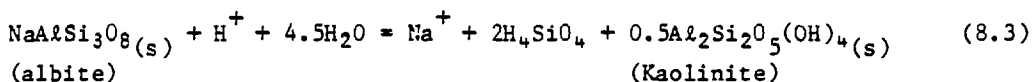
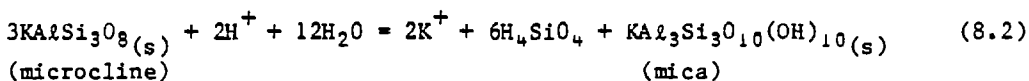
Mineral weathering-mass balance calculations are presented in order to develop a hypothesis for the origin of the contaminants in the zone D groundwater. Minerals that appear to be likely sources of contaminants are listed and their main weathering reactions are postulated. Appropriate concentrations of dissolved products that are produced by the weathering processes are specified from the mineral reactions and the combined results are compared to the observed concentrations in the groundwater in zone D. For the weathering calculations, the following minerals are assumed to be the main source of major ions in the leachate that form within the gabbroic and pegmatitic waste rock mass, namely: pyrite ($\text{FeS}_{2(s)}$), microcline

($\text{KAlSi}_3\text{O}_8(\text{s})$), albite ($\text{NaAlSi}_3\text{O}_8(\text{s})$), dolomite ($\text{CaMg}(\text{CO}_3)_2(\text{s})$) and calcite ($\text{CaCO}_3(\text{s})$). The mineralogical evidence supporting this choice of representative waste rock composition is presented in Chapter 6. The weathering reactions that might occur for these minerals are as follows: (1) the irreversible reaction of oxygen with pyrite, as



(pyrite)

and (2) the buffering of the released hydrogen ions by the feldspar and carbonate minerals, as



The concentrations of the products in the leachate that are produced by reactions 8.1 to 8.5 inclusively are calculated. This leachate composition is affected by the availability of oxygen within the waste rock mass.

A cell approach is used to determine the amount of oxygen present within the pore spaces of the waste-rock mass. Assuming a porosity at 30%, the amounts of oxygen present at 10, 20, 30, 50, 70 and 100 percent water saturation in the voids of the waste rock mass are calculated to be 80, 40, 20, 9, 4 and 0.3 mmole/l, respectively. The effects on the composition of the leachates resulting from the presence of 4, 20 and 40 mmole/l of oxygen within the waste

rock mass that contains the following systems, (1) rainwater-pyrite and (2) rainwater-pyrite-microcline-albite-calcite-dolomite, have been computed by the computer programme, PHREEQE, as previously described in Chapter 6. The calculated results are given in Table 8.1. The leachates influenced by the rainwater-pyrite system increase in concentrations of SO_4 , Fe and H ions with increase in oxygen content. For the rainwater-pyrite-microcline-albite-calcite-dolomite system, the computed concentrations of Ca, Mg, Na, Al, Fe, HCO_3 , SO_4 and SiO_2 in the resulting leachates increase with increase in the oxygen content. In addition to these ion-speciation computations for each of the resulting leachates, mineral saturation indices were computed by PHREEQE. The mineral weathering products that were computed to be saturated in the pyrite-microcline-albite-calcite-dolomite leachate were goethite ($\text{FeO}(\text{OH})_{(\text{s})}$), hematite ($\text{Fe}_2\text{O}_3(\text{s})$), magnetite ($\text{Fe}_3\text{O}_4(\text{s})$), gibbsite ($\text{Al}_2\text{O}_3 \cdot 3\text{H}_2\text{O}_{(\text{s})}$), quartz ($\text{SiO}_2(\text{s})$) and the following clay minerals: kaolinite ($\text{Al}_2\text{Si}_2\text{O}_5(\text{OH})_4(\text{s})$), illite ($\text{K}_{.6}\text{Mg}_{.3}\text{Al}_{2.3}\text{Si}_{3.5}\text{O}_{10}(\text{OH})_2(\text{s})$) and Ca-montmorillonite ($\text{Ca}_{.17}\text{Al}_{2.33}\text{Si}_{3.67}\text{O}_{10}(\text{OH})_2(\text{s})$).

The chemical compositions of the leachates that have been computed from mineral weathering reactions using PHREEQE are compared in Table 8.1 with the chemical compositions of the two major types of zone D groundwater. The composition of the NE zone D type of groundwater, as reflected by the pH 7 calcium-sulphate-bicarbonate water, is similar to the leachate composition resulting from the rainwater-pyrite-microcline-albite-calcite-dolomite interaction at oxygen concentrations ranging from 4 to 20 mmole/l. The composition of the pH 3.0-4.0 calcium-magnesium-sulphate zone D groundwater in the NW is between the two computed leachate compositions for the rainwater-pyrite and rainwater-pyrite-microcline-albite-calcite-dolomite interactions at 4 and 20 mmole/l of oxygen.

From the above comparisons between the observed concentrations in the zone D groundwater and the calculated concentrations in leachates that are affected by waste rock weathering, an explanation is given for the occurrence of the low pH sulphate groundwater that is found only below the waste rock at the NW sector

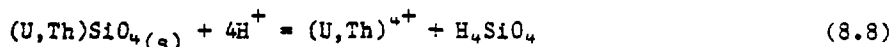
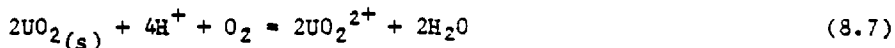
TABLE 8.1

COMPARISONS BETWEEN THE CHEMICAL COMPOSITIONS OF THE ZONE D GROUNDWATER AND WATER
COMPUTED FROM MINERAL WEATHERING REACTIONS

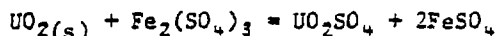
Description	Added O ₂ in computations ,mmole/l	Ca ,mg/l	Mg ,mg/l	Na ,mg/l	K ,mg/l	HCO ₃ ,mg/l	SO ₄ ,mg/l	Cl ,mg/l	SiO ₂ ,mg/l	Al ,mg/l	Fe ,mg/l	pH
A. Zone D Groundwater:												
(1) N.W. Type												
sample L (1981)		112	59.2	6.5	7.9	<5	627	1.23	53.0	5.6	67.0	3.6
sample GR4 (1981)		72.2	31.4	7.0	3.1	<5	348	0.99	25.9	<5	0.05	4.7
sample GR4 (1979)		156	82.0	7.0	5.4	<5	820	3.0	-	16.0	0.5	4.5
(2) N.E. Type												
sample H16-2 (1982)		101	4.7	2.8	2.6	277	108	-	-	-	0.07	7.3
sample H2-2 (1979)		201	8.9	4.7	4.8	201	337	1.0	-	-	-	6.5
B. Water Influenced by:												
(1) Rainwater/pyrite												
	4	0.53	0.15	0.35	0.14	<1	220	0.1	0.6	-	63.8	2.63
	20	0.53	0.15	0.35	0.14	<1	1097	0.1	0.6	-	320	1.94
	40	0.53	0.15	0.35	0.14	<1	2196	0.1	0.6	-	638	1.64
(2) Rainwater/pyrite/ feldspars/carbonates												
	4	43.6	27.7	2.2	0.002	130	220	0.1	14.1	2.0	63.8	7.93
	20	192	117	3.2	0.003	462	1097	0.1	22.0	3.2	320	6.97
	40	351	210	3.7	0.004	702	2196	0.1	25.8	3.8	638	6.65

of the field site. It is reasonable to suggest that the carbonate content within the gabbro in the small pegmatite-gabbroic waste rock pile in the NW became depleted earlier by the reaction with products from pyrite oxidation, and thereafter, resulting in a progressive decrease in the pH of the underlying groundwater. The waste rock piles to the NE, on the other hand, are larger and consist of separate piles of predominantly pegmatite and predominantly gabbroic waste rock. Pyrite is not present within the pegmatitic waste rock. Because of the larger excess of the carbonate content (4.2%) than sulphur (1.2%) in gabbroic rock and because of the larger masses of the waste rock piles in the NE, the pH of the groundwater underlying the NE waste rock piles is expected to be neutral.

The amounts of radionuclides that are dissolved from uraninite ($\text{UO}_2(\text{s})$) and uranothorite ($(\text{U,Th})\text{SiO}_4(\text{s})$) minerals in pegmatitic waste rock are largely affected by the pH of the leachate. The solubility of these radioactive minerals in pegmatite was found in Chapter 6 to increase with increase in the hydrogen ion activity. At the site, the significant source of hydrogen ion concentrations is from the oxidation of pyrite and the infiltration of rock by rainwater. The resulting acidic leachate contacts the radioactive minerals and may cause the release of radionuclides into solution by the following postulated reactions,



Oxidation of the insoluble tetravalent uranium in $\text{UO}_2(\text{s})$ at the field site can proceed more rapidly in the presence of bacteria, such as iron-oxidizing thiobacilli (Lungren and Silver, 1980; Ritcey and Silver, 1982) and/or by ferric sulphate formed through the indirect action of bacteria on pyrite (Lungren and Silver, 1980):

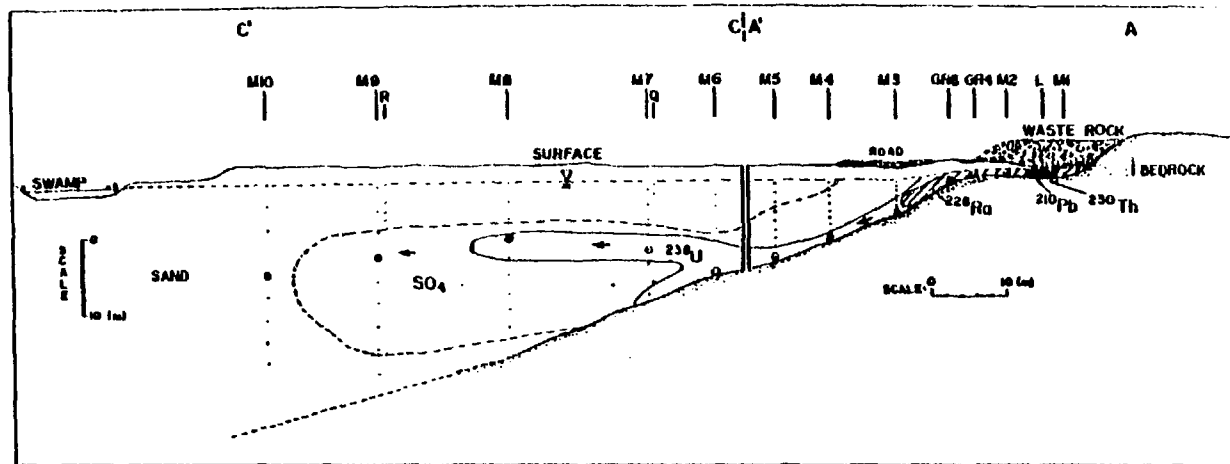










The release of $^{238}\text{U}(\text{IV})$, $^{238}\text{U}(\text{VI})$, $^{234}\text{U}(\text{IV})$ and $^{234}\text{U}(\text{VI})$ species in solution from $\text{UO}_2(\text{s})$ in equations 8.6 and 8.7 is accompanied by the simultaneous release of $^{226}\text{Ra}(\text{II})$, $^{210}\text{Pb}(\text{II})$ and $^{230}\text{Th}(\text{IV})$ and other members of the uranium-238 decay series. The radioactive species released in solution from $(\text{U,Th})\text{SiO}_4(\text{s})$ in equation 8.8 are members of both the uranium-238 and thorium-232 decay series.

8.2 Transport Processes of the Waste-Rock-Derived Radionuclides

The spatial-activity distributions of radionuclides in groundwater, shown in Chapter 5, indicated high activities below the waste rock and a wide range in the travel distances by the waste-rock-derived radioactive contaminants in the sand aquifer. This wide range results from differences in the physical, geochemical, biochemical and radioactive decay processes for each radionuclide of interest. The effects of each of these processes are discussed following a brief summary on the distributions of the concentrations and activities of the chemical and radioactive contaminants in groundwater along the two flow systems, namely the northwest and the northeast groundwater flow regimes.

The migration trends of the radioactive contaminants from the waste rock piles in groundwater along the northwest flow regime are considered first. The proposed flow line, L-M10 in Figure 8.1, has been chosen to be representative of these trends in the northwest flow regime because of the alignment with the general groundwater flow direction and also with the waste-rock-influenced zone, as depicted by the shapes of the SO_4 and radionuclide plumes in Figure 8.1. This flow line extends approximately 100 meters laterally downflow from the waste rock. The activities and concentrations of the dissolved radionuclides and chemical species along the L-M10 flow line are graphically shown in Figure 8.2. The radionuclide and chemical composition of groundwater in Figure 8.2 show decline in most of the dissolved constituents away from the waste rock. The dissolved constituents, which decrease in values along L-M10, are ^{238}U , ^{226}Ra , ^{210}Pb , ^{230}Th , Ca, Mg, Na, K and SO_4 . Values that increase in



-  Waste rock deposited on terrain from 1966 to 1959
-  Section of waste rock excavated in September 1979
-  Water table, June 7, 1982
-  Piezometer tip
-  Multi-level sampling point
-  General groundwater flow direction
-  L-M10 Flowline
-  M16-M19 Flowline

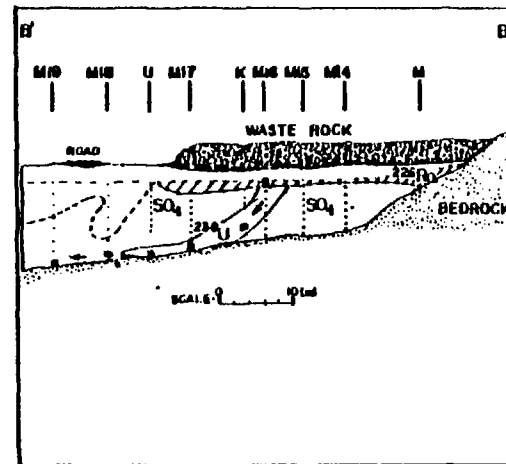


Figure 8.1 Zones of the maximum extent of SO₄, ²³⁸U, ²²⁶Ra, ²¹⁰Pb and ²³⁰Th contamination from the waste rock in the sand aquifer. Superimposed are the locations of the NW proposed flow line, L-M10, and the NE proposed flow line, M16-M19.

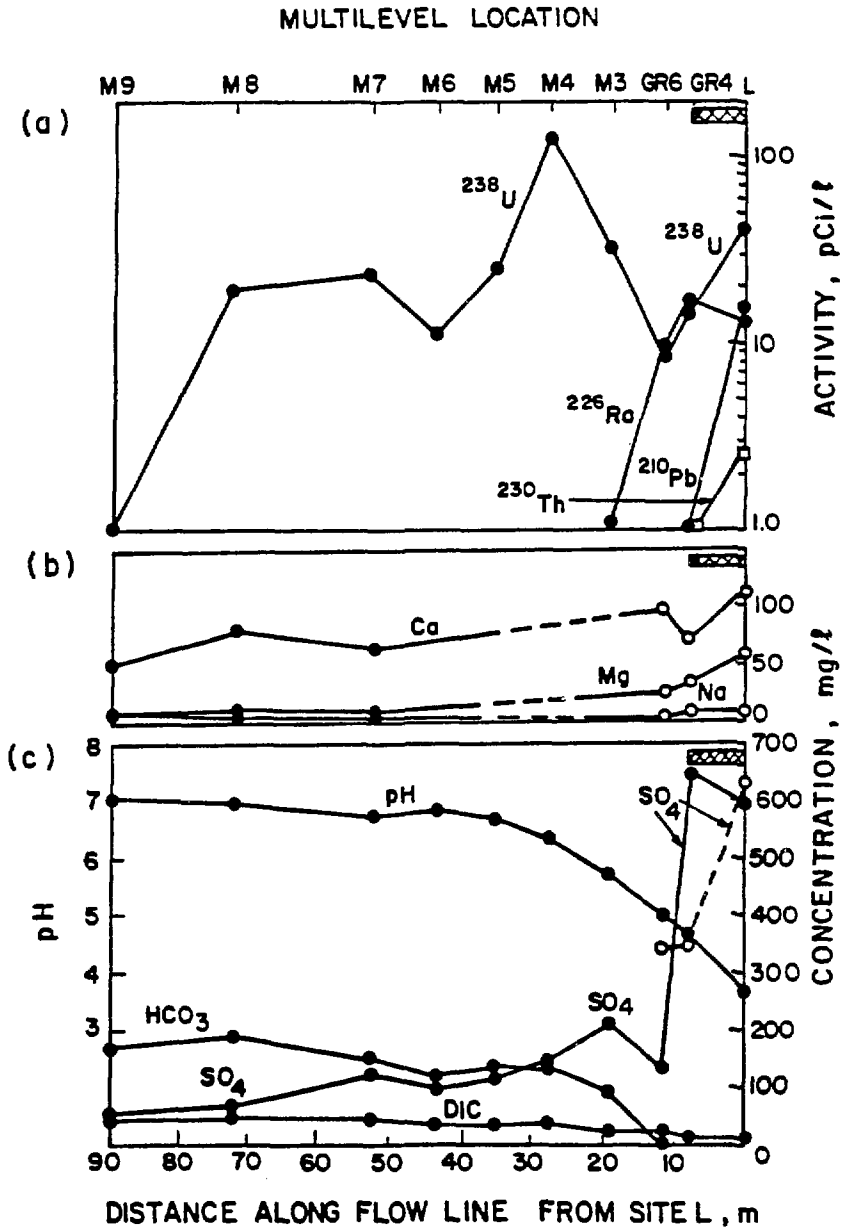


Figure 8.2 Activities and concentrations of dissolved radionuclides and chemical species along the proposed NW flow line, L → M10. (a) Radionuclides (b) major cations, (c) major anions and pH. Data points: □ 1979; ○ 1981; ● 1982. ▨ Location of waste rock.

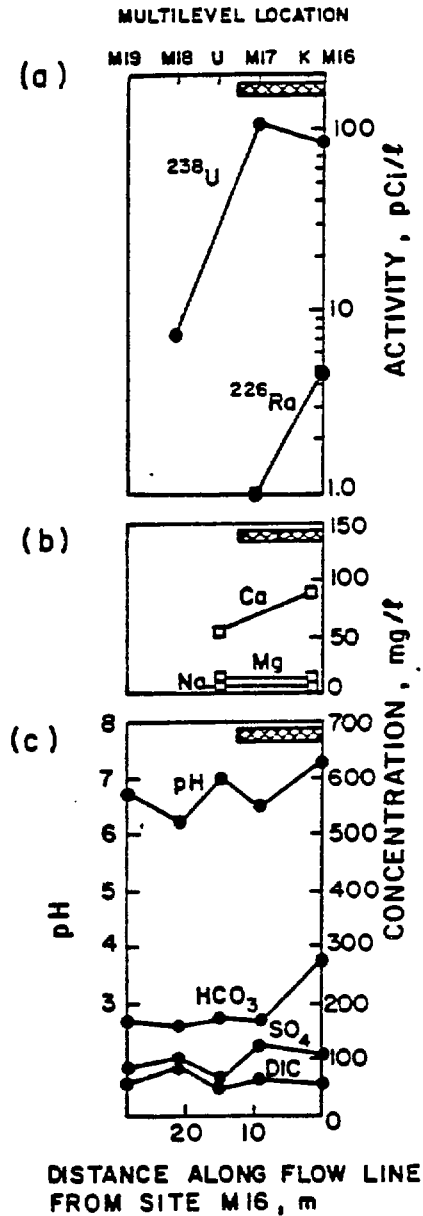


Figure 8.3 Activities and concentrations of dissolved radionuclides and chemical species along the proposed NE flow line, M16 + M19. (a) Radionuclides, (b) major cations, (c) major anions and pH. Data points: ○ 1979; ● 1982. ▨ Location of waste rock.

groundwater along L-M10 are noticed for pH, DIC and HCO_3^- .

The migration trends of the contaminants in the northeastern flow regime can be considered along a flow line extending from sites M16 to M19. The location of the M16-M19 flow line is given in the cross sectional diagram in Figure 8.1. Sample sites along the M16-M19 flow line have been chosen based on the groundwater-flow direction as shown in Chapter 4 and the hydrochemical patterns as shown in Chapter 5. The hydrochemical and radiological trends in groundwater along M16-M19 are shown in Figure 8.3. Values of ^{238}U , ^{226}Ra , Ca and HCO_3^- decrease along this 28 meter flow line, whereas the pH and the concentrations of Mg, Na, K, SO_4 and DIC do not change significantly along the same flow line. The activities of ^{210}Pb , ^{230}Th and ^{232}Th in groundwater along M16-M19 are below their respective detection limits (refer to Chapter 5).

The effect of dispersion, which causes mixing, is first considered for the interpretation of the decreasing concentrations and activities of contaminants downflow from the waste rock. Dispersion, both vertical and longitudinal types, causes reduction in solute concentrations. As groundwater migrates downflow from the waste rock, recharge from rain and snowmelt enters the sand aquifer and mixes with the contaminated groundwater along the top of the plume. This process is defined as vertical dispersion and is most effective in those parts of the sand aquifer with high groundwater flow velocities. The groundwater flow velocities are the highest in the vicinity of the waste rock, where velocities exceed 70 m/yr in the northwest flow regime and 10 m/yr in the northeast flow regime.

More significant than vertical dispersion in the reduction of the concentrations of the contaminants in the sand aquifer is longitudinal dispersion. Sudicky et al. (1980) have provided a tracer test in a sand aquifer on the estimation of the three principal values of the dispersion coefficient. The results from their field test indicated that the ratios of longitudinal to horizontal transverse dispersivity were less than five. In comparison, the vertical dispersion of the tracer slug in their field investigation was very weak. It is reasonable to suggest that similar conditions also exists at the Greyhawk site. Because longitudinal dispersion is considered to be more

significant at Greyhawk in comparison to the other two types of dispersion, a one-dimensional, mathematical approach that incorporates the longitudinal dispersion coefficient is used below to describe the decline in solute concentration downgradient from the waste rock.

To relate the decreasing concentration trends of a solute species downflow from the waste rock by longitudinal dispersion, the 1982 measured sulphate concentration profile along the L-M10 flow line is compared to a computed concentration profile for the migration of a non-reactive solute species after 25 years. The latter profile is computed from the Ogata-Banks (1961) analytical solution for the one-dimensional advection-dispersion equation for the migration of a non-reactive species. A similarity in a comparison between the measured and computed concentration profiles would indicate that the subsurface migration of the sulphate species is solely influenced by longitudinal dispersion and not by geochemical retardation processes. Sulphate, because of its conservative nature in oxidizing porous medium, has been chosen to represent the migration of a non-reactive chemical species in the sand aquifer. PHREEQE calculations provide evidence that chemical reduction of sulphate does not occur along the L-M10 flow line. Although chloride is also considered as a non-reactive species in sandy aquifer systems, the concentration of chloride in the Greyhawk groundwater is very low and, as such, chloride profiles have not been compared with the computed profiles from the analytical solution.

The input parameters in the Ogata-Banks analytical solution are as follows: three groundwater velocities at 70 m/yr, 9.0 m/yr and 1.6 m/yr for three corresponding zones along the L-M10 flowline at 0-19.2 m, 19.2-72.8 m, and 72.8 - 101.3 m.; a range of longitudinal dispersivities from 1 to 100 meters; and a travel time at 25 years. The results are shown in Figure 8.4. The computed concentration profiles in groundwater after 25 years are compared in Figure 8.4 to the decreasing concentration profile of sulphate in groundwater along L-M10. It can be seen that there is no agreement between the computed and measured profiles in the vicinity of the waste rock. However, the comparison does suggest that the concentration of sulphate in groundwater at the source has increased in recent years.

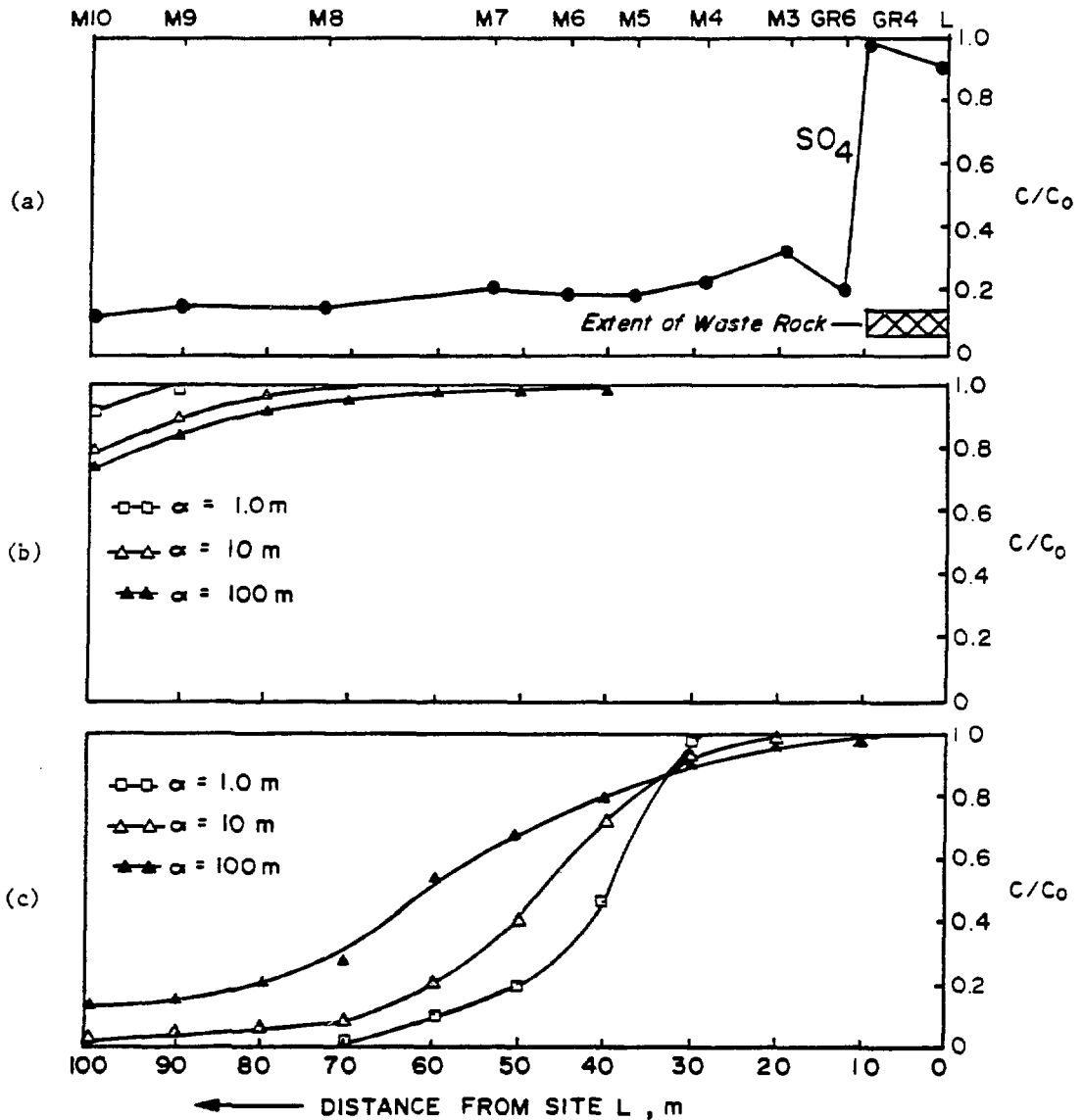


Figure 8.4 Comparison between the measured sulphate concentration profile (a) in groundwater along the L-M10 flowline in 1982 and the computed profiles: (b) the Ogata-Banks solution, assuming a constant source concentration for the past 25 years and (c) the modified version of the Ogata-Banks solution, assuming an increased source concentration for the past 5 years. The computed profiles in (b) and (c) represent 25 years of migration of a non-reactive solute species in groundwater.

A special version of the Ogata-Banks solution (King, 1983) that accounts for a change in the source concentration has been used for the Greyhawk problem. It is assumed that the sulphate concentration emanating from the source has sharply increased for the past 5 years. The computer program by King (1983) has been modified to account for the changes in the groundwater velocities downgradient from the waste rock along the L-M10 flowline. The computed results are plotted in Figure 8.4 as concentration profiles for the range in the longitudinal dispersivities used from 1.0 to 100 meters. These computed concentration profiles are compared in Figure 8.4 with the measured sulphate concentration profile along the L-M10 flowline. The comparison indicates similarities near the source for a longitudinal dispersivity of 1.0 m and near site M10 for a longitudinal dispersivity of 100 m. These results are similar to the field tracer injection experiment by Sudicky et al (1980), in that the longitudinal dispersivity in the sand aquifer increases downgradient from the source.

The physical and geochemical processes affecting the attenuation of the activities of radionuclide species downgradient from the waste rock in groundwater are distinguished based on a comparative technique. That is, molar ratios of sulphate to each of the radionuclide species along the L-M10 flowline are calculated in order to identify the processes responsible for the relative changes in the concentrations for that particular species. Increase in molar ratios downflow from the waste rock indicates reduction in solute concentration by chemical means. Decrease in molar ratios suggests the addition of that species to the groundwater flow path. Because the spread of radionuclide contamination in groundwater was largely seen for uranium and radium, molar ratios of $\text{SO}_4/^{238}\text{U}$ and $\text{SO}_4/^{226}\text{Ra}$ have been calculated along the L-M10 flow line. The results are shown in Figure 8.5. The fluctuations of the $\text{SO}_4/^{238}\text{U}$ ratio from sites L to GR6 are directly related to the attenuation of the

SO_4 and ^{238}U species originating from the waste rock. The decreases in the $\text{SO}_4/^{238}\text{U}$ ratio from sites GR6 to M4 can either be the addition of ^{238}U from the waste rock piles, or possibly, from the leaching of the bedrock surface. The constant ratios between sites M5 to M8 are consistent with the expectation that dispersion is the only major process in this area. The abrupt increase in the $\text{SO}_4/^{238}\text{U}$ ratio at 75-80 meters downflow from site L marks the extent of the ^{238}U migration from the waste rock. Similarly, the abrupt increase in the $\text{SO}_4/^{226}\text{Ra}$ ratio in Figure 8.5 at 20 meters downflow from site L indicates the extent of the ^{226}Ra front. The effects of dispersion in the determination of the shapes of the ^{226}Ra front, or even the shapes of the contaminant fronts for ^{210}Pb and ^{230}Th , are expected to be negligible.

Next, geochemical processes are considered to explain for the trend in the decreasing concentrations and activities of the contaminant species downflow from the waste rock areas in Figures 8.2 and 8.3. These processes include acid-base reactions, dissolution-precipitation reactions, oxidation-reduction reactions, adsorption-desorption reactions, and complexation. First, acid-base reactions are used below to explain for the low pH groundwater containing the high activities of radionuclides below the waste rock at site L and the trend in the increasing pH values in groundwater along the L-M10 flow line.

Earlier in this chapter it had been explained that the source of hydrogen ions and radionuclides in groundwater below the pegmatite-gabbroic waste rock in the NW sector was derived from the oxidation and dissolution of pyrite and the radioactive minerals for the past 25 years. Similar to the geochemical conditions of acid production at the Greyhawk site, pyrite-containing uranium mill tailings in the Elliot Lake area (Blair et al, 1980 and Morin et al, 1982) have also been oxidized for the past two decades. However, the severity of the impact of waste rock leaching in the production of hydrogen ions and radionuclide species in the groundwater zone at the Greyhawk site is

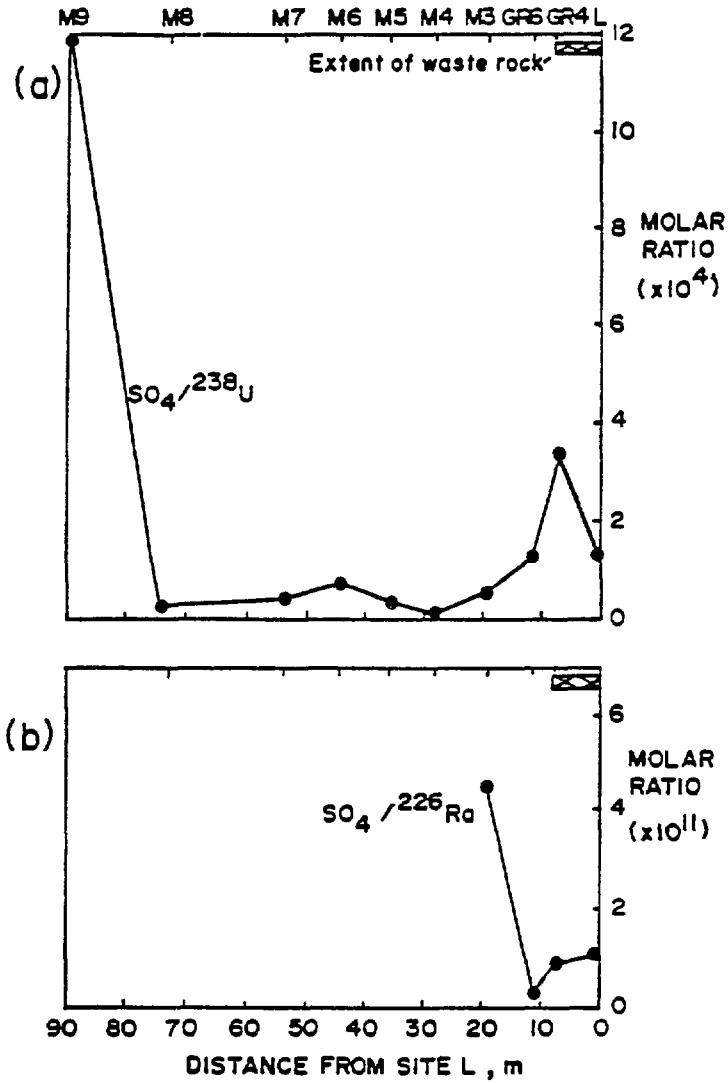


Figure 8.5 Molar ratios of (a) $\text{SO}_4/^{238}\text{U}$ and (b) $\text{SO}_4/^{226}\text{Ra}$ in groundwater samples along the NW flow-line, L to M10, in 1982.

considerably less than that from the weathering of the Elliot Lake tailings. The low pyritic content (approximately 1%) in the gabbro and the particle size of the waste rock may be the causes of the slow rate of oxidation at the Greyhawk site. The Elliot Lake tailings, on the other hand, are sand and silt sized particles and contain 7% by weight pyrite. For both sites, an acidic leachate, containing high activities of radionuclides, has been produced and has been supplied to an underlying sand aquifer. The low pH contaminated groundwater at both sites becomes completely neutralized at approximately 20 meters downgradient from its source; thereby immobilizing most of the radionuclides.

The neutralization of the hydrogen ions by the Greyhawk soil is caused for the most part by the dissolution of calcite, as interpreted from the acid neutralization column experiments in Chapter 6. Calcite dissolution is also considered to be the cause of hydrogen ion neutralization in an area of tailings seepage in the Elliot Lake district (Morin et al, 1982). Assuming the groundwater at site L as the point source of hydrogen ions to the sand aquifer and assuming that the hydrogen ions are neutralized by the calcite in the sand along the NW flow line, L-M10, as



a groundwater pH profile at site L during the past 25 year weathering history has been constructed from the equation:

$$t = d_H^+ \cdot \left(\frac{\text{g-eq/l CaCO}_3(s)}{\text{g-eq/l H}^+} \right) / v_w \quad (8.10)$$

Equation 8.10 is a modification of equation 6.3. The parameters of equation 8.10 are: t = time, d_H^+ = distance of acid front downflow from site L in 1982 with respect to the g-eq/l H^+ value (refer to groundwater pH profiles as shown in Figure 5.15), v_w = groundwater velocity (i.e. 70 m/yr from sites L to M3), g-eq/l CaCO_3 = number of gram-equivalents of calcite in a unit cell and g-eq/l H^+ = number of gram equivalents of hydrogen ions in a unit cell.

The g-eq/l CaCO_3 parameter in equation 8.10 has been determined from cell calculations following a mass-balance approach. At a porosity of 36%, the

volume of saturated sand within a cell containing one liter of water is calculated to be 1778 ml. Because the density of the sand is 2.72 g/cm^3 (Clarke, 1982), the weight of the sand in the cell is calculated to be 4836 grams. From the carbonate analyses of the Greyhawk sand in Veska (1983), a value of 0.016% by weight as CaCO_3 has been chosen to represent the average value in the sand aquifer. Under these conditions, the g-eq/l value of CaCO_3 in a unit cell of the sand aquifer is 0.016 g-eq/l.

From known values of d_{H^+} , V_w and g-eq/l CaCO_3 , values of t have been calculated from equation 8.10 at various g-eq/l values of H^+ ions. From these calculations, a pH versus time plot as shown in Figure 8.6 has been constructed to graphically display the variation in groundwater pH at site L during the past 25 years. Values of t have only been calculated in the pH range from pH 3.4 to pH 4.2. At pH values greater than 4.5, the values of t are calculated to be greater than 25 years. As a result, the pH 4.2 value (i.e. at $t = 17.5$ years ago) was joined to an estimated pH 7.0 value (i.e. at $t = 25$ years ago) in Figure 8.6. The rationale for the selection of the pH 7.0 value at the initial time when waste rock weathering started, was based on the calculated leachate composition from the rainwater-pyrite-feldspar-carbonate interaction as shown in Table 7.1. The abrupt decrease in pH from 7.0 to 4.2 at site L indicates that there must have been an excessive increase in the hydrogen ion concentration in groundwater from pyrite oxidation during the latter period of waste rock weathering. This observation is in agreement with the assumption made earlier to explain for the sulphate trend along L-M10, in that the sulphate concentrations emanating from the source, as a result of pyrite oxidation, have sharply increased in the past 5 years. Because of the large change in the groundwater pH at site L for the past 25 years and because the leachability of radionuclides from waste rock increase with decrease in solution pH, the activities of the leached radionuclides from the waste rock to the underlying water table cannot be considered to have been constant since 1957.

In addition to acid-base reactions, other geochemical processes, such as dissolution-precipitation reactions, oxidation-reduction reactions, adsorption-desorption reactions and complexation can also influence the migration of the

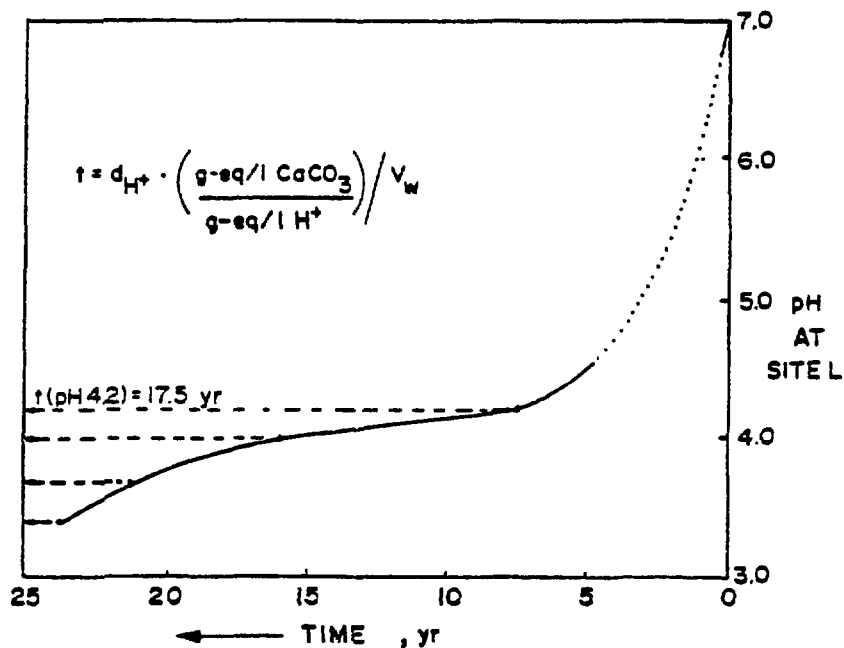


Figure 8.6 pH variation in groundwater at site L with time. The pH vs time curve was plotted based on the calculations from the modified one-dimensional retardation equation as given in the insert. The total carbonates in the field sand was estimated at 0.016% as $\text{CaCO}_3(s)$.

radionuclide species in the contamination zone. To assess the importance of all of these processes simultaneously, the chemical and radiochemical data on groundwater from sites L, GR4, GR6, M3, M5, M7, M8 and M9 along the L-M10 flow line and from sites M16, M17 and M18 along the M16-M19 flowline have been evaluated using the ion speciation and geochemical equilibrium program, PHREEQE. PHREEQE calculates the concentrations of each of the major, minor, trace and radionuclide ions, ion pairs and complexes in the groundwater samples. The complexes and ion pairs that have been considered are those which have been expected to form from the predominant anions in the Greyhawk groundwater, namely: OH^- , SO_4^{2-} , HCO_3^- and CO_3^{2-} . The radionuclide ions, ion pairs and complexes that have been considered include U^{4+} , UOH^{3+} , $\text{U}(\text{OH})_2^{2+}$, $\text{U}(\text{OH})_3^+$, $\text{U}(\text{OH})_4^0$, USO_4^{2+} , $\text{U}(\text{SO}_4)_2^0$, UO_2^+ , UO_2^{2+} , UO_2OH^+ , $\text{UO}_2(\text{OH})_2^{2+}$, $\text{UO}_2(\text{OH})_3^+$, $\text{UO}_2\text{SO}_4^0(\text{aq})$, $\text{UO}_2(\text{SO}_4)_2^{2-}$, $\text{UO}_2\text{CO}_3^0(\text{aq})$, $\text{UO}_2(\text{CO}_3)_2^{2-}$, $\text{UO}_2(\text{CO}_3)_3^{4-}$, Th^{4+} , $\text{Th}(\text{OH})^{3+}$, $\text{Th}(\text{OH})_2^{2+}$, $\text{Th}(\text{OH})_3^+$, $\text{Th}(\text{OH})_4^0(\text{aq})$, ThSO_4^{2+} , $\text{Th}(\text{SO}_4)_2^0(\text{aq})$, Ra^{2+} , RaOH^+ , $\text{RaSO}_4^0(\text{aq})$, Pb^{2+} , PbOH^+ , $\text{Pb}(\text{OH})_2^0(\text{aq})$, $\text{Pb}(\text{OH})_3^-$, $\text{Pb}(\text{OH})_4^{2-}$, $\text{Pb}_2\text{OH}^{3+}$, $\text{Pb}_3(\text{OH})_4^{2+}$, $\text{PbSO}_4^0(\text{aq})$, $\text{Pb}(\text{SO}_4)_2^{2-}$, PbHCO_3^+ , $\text{PbCO}_3^0(\text{aq})$ and $\text{Pb}(\text{CO}_3)_2^{2-}$. (The equilibrium constants for the formation of these complexes and ion pairs are given in Veska (1983)). The above list includes the major redox species of uranium in groundwater in the (IV), (V) and (VI) oxidation states. PHREEQE also calculates the degree of disequilibrium that exists between the ionic species in groundwater and various radiogenic and non-radiogenic compounds and minerals. The list of the radiogenic compounds and minerals in the computer program includes uraninite ($\text{UO}_2(\text{s})$), $\text{UO}_3(\text{s})$, $\text{UO}_2(\text{OH})_2(\text{s})$, $\text{U}_3\text{O}_8(\text{s})$, $\text{U}_4\text{O}_9(\text{s})$, coffinite ($\text{USiO}_4(\text{s})$), uranophane ($\text{Ca}(\text{UO}_2)_2(\text{SiO}_3\text{OH})_2(\text{s})$), thorianite ($\text{ThO}_2(\text{s})$), $\text{RaSO}_4(\text{s})$, $\text{RaCO}_3(\text{s})$, $\text{Ra}(\text{OH})_2(\text{s})$, $\text{Pb}(\text{OH})_2(\text{s})$, $\text{PbSO}_4(\text{s})$, $\text{Pb}_3(\text{OH})_2(\text{CO}_3)_2(\text{s})$ and $\text{PbCO}_3(\text{s})$. (The dissolution reactions for each of these radiogenic compounds and minerals and respective equilibrium constants are given in Veska (1983)).

The calculated concentrations of the U(VI), U(IV), Th(IV), Ra(II) and

Pb(II) species in groundwater along the L-M10 flow line are graphically shown in Figure 8.7 as percentage distribution diagrams. Similar distributions of Th(IV), Ra(II) and Pb(II) species in groundwater downflow from site GR6 have been made based on their lower limits of detection. Thermodynamically, the percentage of the U(VI) species was found to be more predominant in groundwater than either of the U(IV) or U(V) species. The speciation of radionuclides in groundwater in the vicinity of the waste rock, as shown in Figure 8.7, has indicated significant complexation of U(VI), U(IV), Th(IV) and Pb(II) species with sulphate ions to form UO_2SO_4^0 , $\text{U}(\text{SO}_4)_2^0$, $\text{Th}(\text{SO}_4)_2^0$ and PbSO_4^0 . The ion pair, RaSO_4^0 is also significant in groundwater in the vicinity of the waste rock. Downflow from site L along the L-M10 flowline, the predominant radionuclide species are $\text{UO}_2(\text{CO}_3)_2^{2-}$, $\text{U}(\text{OH})_5^-$, $\text{Th}(\text{OH})_4^0$, Ra^{2+} and PbCO_3^0 . The formation of the negatively-charged U(VI) and U(IV) species suggests that the migration of uranium in the sand aquifer is not largely limited to the adsorption properties of the sand.

The speciation of U(VI) and U(IV) in groundwater along the M16-M19 flow line is now discussed. The percentage distribution of the U(VI) species from sites M16 to M18 changed from 55% to 75% as the $\text{UO}_2(\text{CO}_3)_2^{2-}$ complex, from 43% to 15% as the $\text{UO}_2(\text{CO}_3)_3^{4-}$ complex and from 2% to 10% as the UO_2CO_3^0 complex. As for the U(IV) species, $\text{U}(\text{OH})_5^-$ was dominant along the M16-M19 flow line.

The results of the saturation indices from the computer output for groundwater samples along the L-M10 flowline are shown in Figure 8.8. (Because the concentrations of Pb and ^{226}Ra are found to be below detection at sites M7, M8 and M9, saturation indices of the Pb and ^{226}Ra compounds at these sites have been calculated based on the lower limits of detection). The low pH groundwater at site L in Figure 8.8 is undersaturated with respect to gypsum, calcite, dolomite, gibbsite, $\text{Fe}(\text{OH})_3(\text{am})$, siderite, $\text{ThO}_2(\text{s})$, $\text{PbCO}_3(\text{s})$, $\text{PbSO}_4(\text{s})$, $\text{RaCO}_3(\text{s})$, $\text{RaSO}_4(\text{s})$, $\text{USiO}_4(\text{s})$, $\text{UO}_2(\text{s})$ and other radiogenic minerals and compounds. As the groundwater pH increases downflow from site L towards site M10, gibbsite, $\text{Fe}(\text{OH})_3(\text{am})$, and $\text{ThO}_2(\text{s})$ tend to be super-saturated.

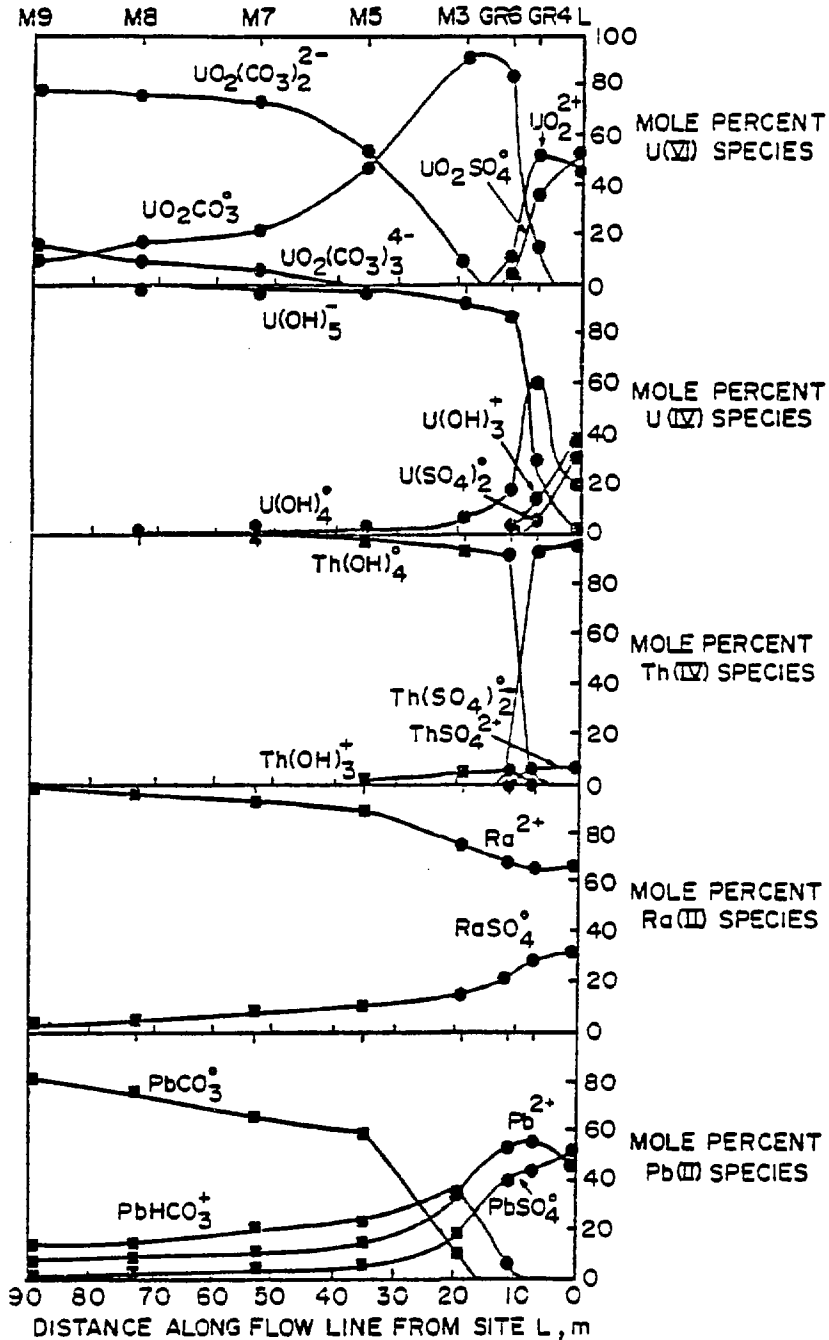


Figure 8.7 Mole percent distribution of dissolved U(VI), U(IV), Th(IV), Ra(II) and Pb(II) species along the proposed NW flow line, L-M10. Symbols: ● Computations from analytical data; ■ Computations from the lower limit of detection.

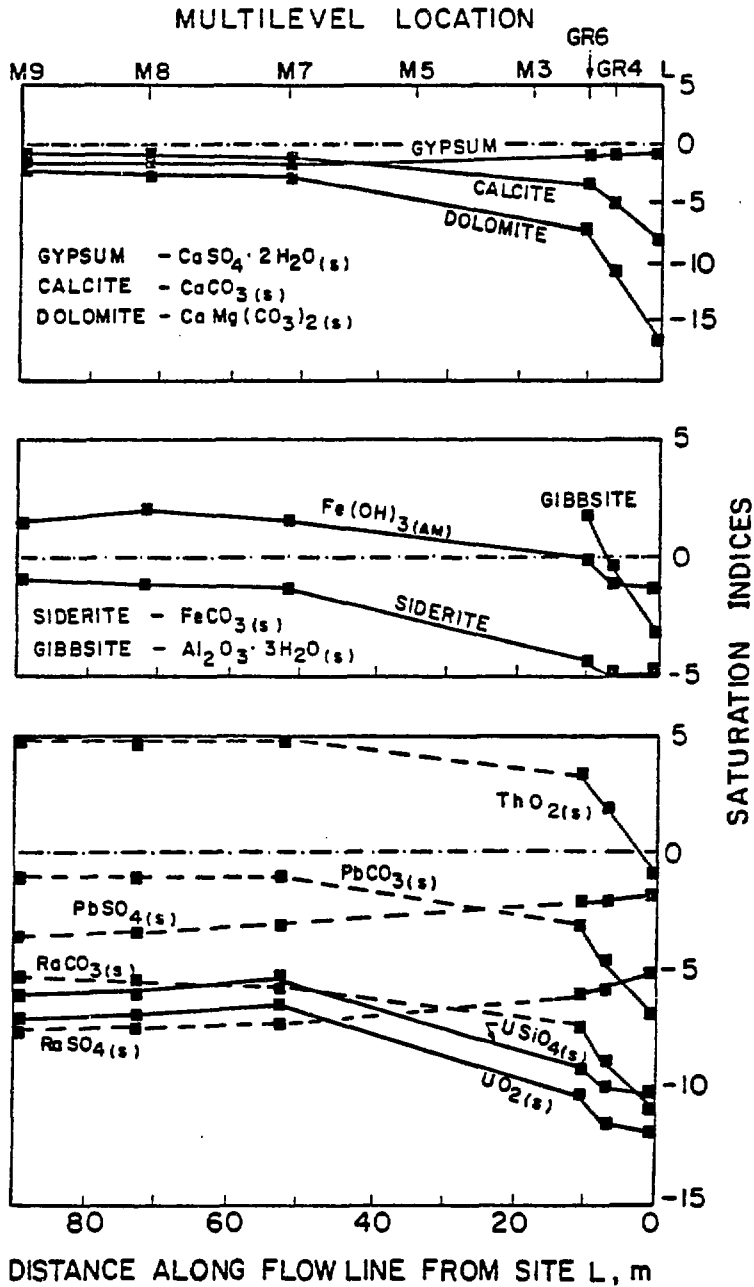


Figure 8.8 Saturation indices of minerals along the NW flow line from sites L to M10 (■—■ computed from analytical data; ■---■ computed from the lower limit of detection).

TABLE 8.2

SATURATION INDICES OF SOME MINERALS IN GROUNDWATER SAMPLES ALONG THE NE
FLOW LINE, M16-M19

MINERAL	SATURATION INDICES	
	SAMPLE M16-3.06	SAMPLE U-11.8
Gypsum	-1.1	-1.48
Calcite	+0.3	-0.72
Dolomite	-1.1	-1.94
Siderite	-3.8	-
Fe(OH) ₃ (AM)	+3.05	-
RaSO ₄ (s)	-6.4	-
RaCO ₃ (s)	-3.8	-
PbCO ₃ (s)	-0.9	-
PbSO ₄ (s)	-3.7	-
UO ₂ (s)	-14.6	-3.28
USiO ₄ (s)	-13.5	-2.09

Similarly, all minerals and compounds with the exception of calcite and $\text{Fe}(\text{OH})_3(\text{am})$ are undersaturated along the M16-M19 flow line, as shown in Table 8.2. Calcite saturation exists only in groundwater below the waste rock at site M16 and not at other sampling points located along the M16-M19 flow line. Calcite saturation below the water table at site M16 can possibly explain the low activities of ^{226}Ra and ^{210}Pb in groundwater at that site. That is, if calcite precipitation does occur in the NE groundwater below the waste rock, then it is reasonable to suggest that Ra^{2+} , Pb^{2+} and other divalent cations can coprecipitate with calcite.

The supersaturation of $\text{Fe}(\text{OH})_3(\text{am})$ and gibbsite downflow from the waste rock in both flow regimes indicates a possibility for the adsorption of radionuclides. Radionuclides and trace constituents are generally scavenged on the surfaces of iron and aluminum oxides (Feldman, 1975; Stumm and Morgan, 1970). Physical adsorption of radiocations on iron and aluminum oxides generally increase with increase in pH (Ames and Rai, 1978; Tokarev and Scherbakov, 1956). This generalization can explain the decreasing activities of radionuclides that are found in groundwater along the L-M10 flow line, along which, the groundwater pH increases from 3.7 to 7.0. In addition, the presence of molecular species of radionuclides in groundwater along the L-M10 and M16-M19 flow lines, such as $\text{Th}(\text{OH})_4^0$, RaSO_4^0 and PbSO_4^0 , can be weakly retained on colloidal-sized materials (Feldman, 1975) by physical adsorption. This process can either increase or decrease the mobility of radionuclides, depending on the size of the colloids. Adsorption of ^{226}Ra on the surfaces of colloids (Yagoda, 1946; Schubert and Conn, 1949) is suggested to be strong because of its carrier-free state in the Greyhawk groundwater.

Cation exchange can also retain radiocations on sand particles. In this process, the adsorption of one cation and the desorption of the same number of equivalents of another occur according to a mass-action approach. For example, an uranyl ion can exchange with two potassium ions and the exchange of these two ions can lead to the temporary uptake of the uranyl ions. However, it is expected that cation exchange reactions are more important for the migration of the radium, thorium and lead species in the sand aquifer because of the absence of negatively-charged complexes for these species in Figure 8.7.

A natural process that can cause variations in the activities of radionuclides in the Greyhawk groundwater with time is radioactive decay. The half-lives of ^{238}U , ^{234}U , ^{232}Th and ^{230}Th are greater than 10^4 years and thus any changes in the activities of these radionuclides in the young groundwater at the site cannot be due to radioactive decay. As for ^{226}Ra , the decay of the ^{226}Ra atoms (half life = 1600 years) that are leached from the waste rock to the underlying groundwater for a period of 25 years, decreases the ^{226}Ra activity in groundwater by only one percent. However, the decay of the released ^{226}Ra atoms in groundwater for 25 years can produce daughter products such as ^{210}Pb . For a closed system, such as groundwater that is well below the water table, the amount of ^{210}Pb activity in groundwater that can be produced from the decay of the released ^{226}Ra atoms for a 25 year ingrowth period is equivalent to 55 % of the ^{226}Ra activity in groundwater. Radioactive decay is an important process of the attenuation of the ^{210}Pb contamination in groundwater. For example, the ^{210}Pb (half life = 22 years) atoms in groundwater that have been leached from the waste rock 25 years ago, have decayed to 55% of its original activity.

Lastly, biochemical processes can also affect the relative amounts of radionuclides in groundwater in the contaminant zone. From the pyrite leaching experiments described in Chapter 6, it was found that the presence of the bacterium, Thiobacillus ferrooxidans, increased the rate of pyrite oxidation. A possible presence of this bacterium in the field, especially in the waste rock pile centered at site L, could explain for the corresponding high activities of radionuclides and low pH in groundwater at that site. Another biochemical process is microbial cell synthesis. For example, N, C, S, P and trace elements are required for the growth of organisms. It may be possible that some of the radionuclides can be incorporated in the structure of such organisms and thus can be retarded.

8.3 Geochemical Models on Radionuclide Migration

Geochemical models, based on the findings in sections 8.1 and 8.2, are proposed to explain in a qualitative manner, the origin and transport of the waste-rock-derived radionuclides in each of the two major flow regimes. First, a geochemical model is proposed to explain for the migration of the waste-rock-

derived radionuclides in groundwater along the NW flow line, L-M10. The activity distributions of radionuclides in groundwater along this flow line in Figure 8.2 represent the combined effects of pegmatitic and gabbroic waste rock leaching and subsurface migration since 1957. A schematic diagram of the geochemical model for the NW flowline in Figure 8.9, categorizes the sequence of events responsible for the observed activity distributions of radionuclides in groundwater, as: (1) the infiltration of the waste rock by rainwater and snow; (2) the weathering of pyrite, carbonates, silicates, uraninite and uranothorite in the waste rock mass; and (3) the migration of the waste-rock-derived contaminants in the sand aquifer. In the second stage of events in Figure 8.9, the production of hydrogen and sulphate ions from pyrite oxidation increases the solubility of $\text{UO}_2(\text{s})$ and $(\text{U,Th})\text{SiO}_4(\text{s})$. This has resulted in the release of high activities of radionuclides in a low pH leachate. The acidic, radioactive leachate enters the sand aquifer below the waste rock in the form of ions, ion pairs and complexes, such as UO_2SO_4^0 , UO_2^{2+} , $\text{U}(\text{OH})_3^+$, $\text{U}(\text{SO}_4)_2^0$, $\text{Th}(\text{SO}_4)_2^0$, Ra^{2+} , RaSO_4^0 , Pb^{2+} and PbSO_4^0 . The subsurface migration of these species in the sand aquifer is largely affected by geochemical processes. Hydrodynamic dispersion decreases the activity levels of all of the radionuclide species, downflow from the waste rock. The transport of uranium in groundwater is primarily promoted by complexation, as the UO_2SO_4^0 and $\text{U}(\text{SO}_4)_2^0$ complexes in the low pH groundwater below the waste rock and as the anionic $\text{UO}_2(\text{CO}_3)_2^{2-}$ and $\text{U}(\text{OH})_5^-$ complexes in the neutral pH groundwater downflow from the waste rock. The retardation mechanisms for uranium include adsorption on iron and aluminum oxides and cation exchange. The transport of the thorium, radium and lead species in the low pH sulphate groundwater below the waste rock is by the formation of complexes and ion pairs, which include $\text{Th}(\text{SO}_4)_2^0$, RaSO_4^0 and PbSO_4^0 . As the hydrogen ion and sulphate ion concentrations in groundwater decrease downflow from the waste rock, these complexes and ion pairs become unstable. Downflow from the waste rock, the Ra^{2+} , Pb^{2+} and PbHCO_3^+ species tend to form and are vulnerable to adsorption on the surfaces of the

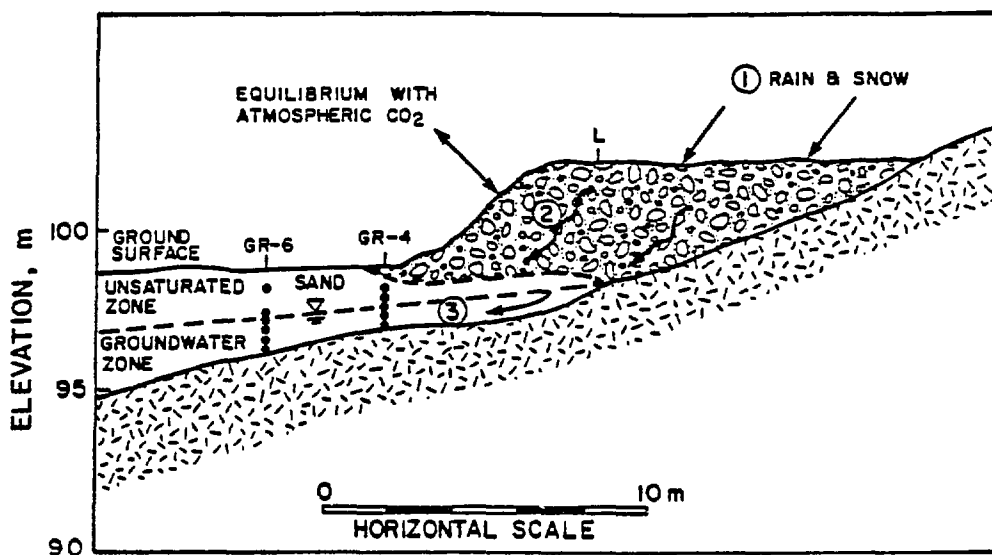


Figure 8.9 Schematic cross sectional diagram illustrating the sequence of geochemical events on the production and migration of waste-rock-derived leachate in the sand aquifer. The sequence of events are summarized below:

- (1) RAIN AND SNOWMELT - Rainwater, a dilute mixed electrolyte, low in total dissolved solids, is in equilibrium with the CO_2 of the earth's atmosphere at a value of $10^{-3.5}$ atm and has a pH of 4.5-5.7 in non-urban inland areas.
- (2) WEATHERING OF THE PEGMATITE AND GABROIC WASTE ROCK

The weathering process of waste rock occurs above the water table under oxidizing conditions and high CO_2 partial pressures ranging from 10^{-3} to 10^{-1} atm. The carbonic acid produced from the reaction of CO_2 and rainwater aids in the dissolution of carbonate and silicate minerals within the waste rock. Oxygen and oxidizing agents within the waste rock mass aid in the oxidation of such minerals as pyrite (FeS_2) within the gabbro and uraninite (UO_2) within the pegmatite. The resulting leachate produces a supply of dissolved radioactive and non-radioactive ions to the water table below.

- (3) MIGRATION OF CONTAMINANTS IN GROUNDWATER IN THE SAND AQUIFER

The transport of the radionuclides and the chemical constituents within the waste-rock-derived leachate by flowing groundwater is affected by physical and geochemical processes.

iron and aluminum oxides and to cation exchange reactions with other ions in the aquifer. Thorium ions, on the other hand, strongly hydrolyze to $\text{Th}(\text{OH})_4^0$ and precipitate as the insoluble, $\text{ThO}_2(\text{s})$, downflow from the waste rock.

Although complexation explains for the enhanced migration of uranium species in the sand aquifer, it does not explain why higher activities of the ^{238}U species are found in groundwater at site M4 (i.e. 121 pCi/l) and at neighbouring sites in the middle of the L-M10 flowline rather than at site L (i.e. 39 pCi/l) below the waste rock pile. Following are three possible explanations for this observation. The first explanation pertains to the variable dissolution rate of uraninite within the waste rock pile with time. During the initial period of the 25 year weathering history, there may have been an increase in the oxidation and dissolution of uraninite which may have produced leachate with 121 pCi/l of ^{238}U . After this initial period, the ^{238}U activities released to the groundwater zone were less than 121 pCi/l.

The second possible explanation of the high ^{238}U activity at site M4 is concerned with the infiltration of water having H_2SO_4 through the waste rock pile and into the underlying bedrock fractures and fissures. Along this course of travel, the acidic groundwater can dissolve the $\text{UO}_2(\text{s})$ and $(\text{U,Th})\text{SiO}_4(\text{s})$ minerals, and thus, increased activities of ^{238}U , ^{234}U , ^{226}Ra , ^{210}Pb , ^{230}Th and ^{232}Th can be present in solution. In addition, the acidic groundwater may react with the carbonate and silicate minerals, to form a neutral-pH bicarbonate water and mobile UO_2CO_3^0 , $\text{UO}_2(\text{CO}_3)_2^{2-}$ and $\text{U}(\text{OH})_5^-$ complexes. The contaminated groundwater may then migrate towards the bedrock/sand interface at site M4 and emanate in the sand aquifer via bedrock springs.

The last possible explanation of the high ^{238}U activity at site M4 is based on the dissolution of an exposed uranium ore vein at the bedrock surface at high partial pressures of CO_2 over geological time. The ore vein may have been exposed at the bedrock/sand interface in the area between sites M3 and M5. In such a case, the lateral extent of the ^{238}U plume that would have

formed over geological time is expected to be much further than that which is observed in 1982.

Of the three possible explanations, the first appears to be the most likely to explain for the higher ^{238}U activities at site M4.

The geochemical model for the migration of waste-rock-derived radionuclides in groundwater along the M16-M19 flowline during the last 25 years differs from that proposed along the L-M10 flow line. The distribution of radionuclides in groundwater along M16-M19 in Figure 8.3 represents the combined effects of pegmatite waste rock leaching and subsurface migration since 1957. Of particular note in Figure 8.3, are the high ^{238}U activities in the neutral pH groundwater below the waste rock. Based on the rock leaching experiments in Chapter 6, these high ^{238}U activities can only have been derived from the dissolution of pegmatitic waste rock at low pH.

The geochemical model proposed for the migration of the radionuclide species along the M16-M19 flow line is described as follows. Pyrite-containing gabbro in small pockets within the pegmatitic waste rock pile have been oxidized to produce hydrogen and sulphate ions. The acidic leachate contacts the $\text{UO}_2(\text{s})$ and $(\text{U,Th})\text{SiO}_4(\text{s})$ minerals within the pegmatite and subsequently produces high activities of the UO_2SO_4^0 , UO_2^{2+} , $\text{U}(\text{SO}_4)_2^0$, $\text{U}(\text{OH})_3^+$, $\text{Th}(\text{SO}_4)_2^0$, RaSO_4^0 , Ra^{2+} , PbSO_4^0 and Pb^{2+} species. Because of the lower proportion of gabbro to that of pegmatite in the predominantly pegmatite waste rock pile, the acidic leachate has been neutralized through the dissolution of the silicate and carbonate minerals. The resulting neutral pH, bicarbonate leachate, containing UO_2CO_3^0 , $\text{UO}_2(\text{CO}_3)_2^{2-}$, $\text{U}(\text{OH})_5^-$, $\text{Th}(\text{OH})_4^0$, Ra^{2+} , Pb^{2+} and PbHCO_3^+ , has migrated downwards through the waste rock pile toward the water table. The thorium, radium and lead species are immobilized by the sand and waste rock properties. The uranium species, on the other hand, are stable as the anionic carbonate complexes and migrates in the bicarbonate groundwater downflow from waste rock. The above model is considered to be reasonable because of the coexistence of high ^{238}U activities and high sulphate and

bicarbonate concentrations in groundwater below the waste rock along the M16-M19 flowline.

8.4 Application of Transport Models

Two major groundwater flow paths have been identified in Chapter 4. Along the NE flow path, the groundwater chemistry is predominantly a calcium-bicarbonate water that is relatively pH constant and the groundwater velocity is constant within the zone of contamination from the waste rock. The K_d values for radionuclides are not expected to significantly change along this flow path and thus, the advection-retardation model is applied. Along the NW flow regime, the groundwater chemistry evolves from a pH 3.4-3.7 calcium-magnesium-sulphate water beneath the waste rock to a calcium-bicarbonate water at a pH 7.0 downflow from the waste rock and the groundwater velocity significantly decreases downgradient from the waste rock. In this situation the K_d for a radionuclide is not considered to be constant along the flow path in the sand aquifer. A cell model, that can account for the variation in K_d for the radionuclides along the latter flow path, is followed for the simulation of the migration patterns for the radionuclides.

For the application of the K_d concept in either of the two transport models, the radioactive species must have undergone relatively fast mass transfer processes in the porous medium and must be described by linear adsorption isotherms at all solution-phase activities found at the field site. Generally, most fast, mass transfer processes are explained by adsorption-desorption reactions. From the previous section on transport processes in this chapter, the retardation of the U(VI), U(IV), Ra(II) and Pb(II) species in the sand aquifer was shown to be solely affected by adsorption-desorption reactions. The retardation of Th(IV), on the other hand, was considered to be affected by both, precipitation-dissolution reactions and adsorption-desorption reactions. However, because all of the adsorption isotherms from the batch K_d experiments for $^{232}\text{Th(IV)}$, $^{238}\text{U(VI)}$,

$^{226}\text{Ra(II)}$ and $^{210}\text{Pb(II)}$ have been found to be linear within the activity ranges for these radionuclides in the Greyhawk groundwater, then the K_d concept is applicable in both of the transport models for all of the mentioned radioactive species.

The 1982 frontal positions of the waste-rock-derived radionuclides in the sand aquifer are first calculated by the advection-retardation model. Although this model is only theoretically applicable for the evaluation of the trends along the NE flow regime, this model is also used to evaluate the trends along the NW flow regime as a first approximation. The equation for the one-dimensional advection-retardation model (equation 2.11) is,

$$\bar{V}_R = \frac{\bar{V}_0}{1 + \frac{\rho}{n} \cdot K_d}$$

where the parameters are those previously defined. Although groundwater flow is three dimensional in nature, in this model it is assumed that it is only one-dimensional. The other assumptions in the application of the advection-retardation model are that: (1) the effects due to dispersion are negligible and therefore plug flow advance of the radionuclide species is represented, (2) the groundwater chemistry along the flow path is spatially and temporally non-variable and (3) the K_d concept is applicable.

By rearranging equation 2.11, the frontal positions (d_R) of each radionuclide in the sand aquifer after 25 years are:

$$d_R = \frac{\bar{V}_0 \cdot 25}{1 + \frac{\rho}{n} \cdot K_d}, \text{ (meters)} \quad (8.11)$$

Although the porosity, n , for the sand at Greyhawk is between 0.33 to 0.40, a representative porosity at 0.36 was used. The bulk mass density, ρ , was calculated to be 1.75 g/cm^3 from the values of porosity at 0.36 and the particle mass density of the sand at 2.72 g/cm^3 (Clarke, 1982). The values

for groundwater velocity, \bar{V}_0 , and K_d used in the model are those presented in Chapters 4 and 7, respectively.

The advection-retardation model is first used to calculate the present day frontal positions of the waste-rock-derived radionuclides along the NE flow line, M16-M19. The waste rock at site M16 is considered to be the source of radionuclide species to the underlying groundwater in the NE flow line. The selection of site M16 as the source area is supported by the patterns in the spatial activity distribution of ^{238}U in groundwater shown in Figure 5.22. For the most part along the M16-M19 flow line, the groundwater velocity is 10 m/yr and the groundwater pH is between 6.0 and 7.0. A single velocity value is used because the transport distance of the radioactive contaminants from the waste rock under consideration is short and within the 10 m/yr velocity zone shown in Figure 4.12. The selected K_d values from experimental data in Chapter 7 for U(VI), U(IV), Ra(II), Pb(II) and Th(IV) at pH's 6.0 and 7.0, are given in Table 8.3. Application of these batch K_d values and the 10 m/yr groundwater velocity in equations 2.11 and 8.11 yield calculated values of radionuclide velocities and distances of the 25 year frontal positions of the radioactive contaminants, respectively at pH 6.0 and also at pH 7.0. These calculated results are given in Table 8.3.

The results in Table 8.3 indicate that the calculated frontal positions for $^{210}\text{Pb(II)}$ and $^{230}\text{Th(IV)}$ are similar to the respective, observed frontal positions. The only similarity for $^{226}\text{Ra(II)}$ between the calculated 25 year frontal positions and the observed frontal positions is found when the K_d value at pH 6.0 is used in the calculations. The comparison between the observed and calculated frontal positions for radium and uranium become more significant in Table 8.3 when a groundwater velocity at 42 m/yr is used in the calculations. The velocity at 42 m/yr has been measured in the field by the borehole dilution technique at a position adjacent to site M16. As discussed in Chapter 4, the accuracy of this velocity is questionable. The absence of an injection of a true point source of radionuclides to the groundwater zone along the M16-M19 flow line, indicates that the comparisons in Table 8.3 have to be viewed in a semi-quantitative manner.

TABLE 8.3

COMPARISONS BETWEEN THE CALCULATED AND OBSERVED FRONTAL POSITIONS ALONG THE H16-H19 FLOW LINE

SPECIES	Kd @ pH7.0 μt/g	GROUNDWATER VELOCITY, \bar{V}_0 m/yr	RADIONUCLIDE VELOCITY, \bar{V} (@ $\bar{V}_0 = 10$ m/yr) m/yr	CALCULATED 25 YEAR FRONTAL POSITIONS		OBSERVED FRONTAL POSITIONS APPROXIMATED FROM SITE H16 m
				(@ $\bar{V}_0 = 10$ m/yr) m	(@ $\bar{V}_0 = 42$ m/yr) m	
^{238}U (VI)	44	10	0.047	1.2	5.0	10
^{238}U (IV)	105	10	0.020	0.5	2.1	10
^{226}Ra (II)	1526	10	0.001	0.03	0.13	1-3
^{210}Pb (II)	215	10	0.009	0.23	0.96	0
^{230}Th (IV)	1748	10	0.001	0.03	0.13	0
SPECIES	Kd @ pH6.0 μt/g	GROUNDWATER VELOCITY, \bar{V}_0 m/yr	RADIONUCLIDE VELOCITY \bar{V} (@ $\bar{V}_0 = 10$ m/yr) m/yr	CALCULATED 25 YEAR FRONTAL POSITIONS		OBSERVED FRONTAL POSITIONS APPROXIMATED FROM SITE H16 m
				(@ $\bar{V}_0 = 10$ m/yr) m	(@ $\bar{V}_0 = 42$ m/yr) m	
^{238}U (VI)	181	10	0.012	0.3	1.3	10
^{238}U (IV)	345	10	0.006	0.15	0.6	10
^{226}Ra (II)	88	10	0.024	0.6	2.5	1 - 3
^{210}Pb (II)	1239	10	0.002	0.04	0.17	0
^{230}Th (IV)	570	10	0.004	0.09	0.38	0

The 25 year frontal positions of the waste-rock-derived radionuclides in groundwater along the NW flow line, L-M10, are now calculated. These calculations can only be considered as first approximations because of the spatial and temporal variations in groundwater chemistry. Site L is considered as the point source for the release of radionuclide species from the weathering of waste rock to the underlying groundwater. The rationale for the selection of this site is that the low pH groundwater at site L was found to contain the highest activities of radionuclides in the NW flow regime during the 1979 to 1982 monitoring period. Additional support for this selection is that the ^{210}Pb activity distribution in groundwater (Chapter 5) has shown site L to be a very local source along cross section A-A'. Along the L-M10 flow line, the groundwater velocity from sites L to M3 is taken to be constant at 70 m/yr (refer to Chapter 4). The pH significantly changes from 3.7 at site L to greater than 5.0 at site M3, over a lateral distance of 20 meters. The batch K_d values for the U(VI), U(IV), Th(IV), Ra(II) and Pb(II) species at pH 3.5 (Chapter 7) are assumed to be applicable over the 25 year period within the initial 20 meter flowpath from site L.

Application of the above parameters in equations 2.11 and 8.11 provided calculated values of radionuclide velocities and 25 year frontal positions, respectively. The calculated results are given in Table 8.4. Within the 20 meter section of the flow path from sites L to M3, it can be seen that the calculated and the observed migration patterns for ^{226}Ra , ^{210}Pb and ^{230}Th show an excellent agreement. Suprisingly, similarities beyond the 20 meter limit are found between the calculated 25 year frontal positions and the observed frontal positions for $^{238}\text{U(VI)}$ and $^{238}\text{U(IV)}$. That is, the calculated frontal positions for both $^{238}\text{U(VI)}$ and for $^{238}\text{U(IV)}$ are similar to that of the initial, observed ^{238}U frontal position, where the ^{238}U activities decline sharply from 121 pCi/l to 26 pCi/l.

Next, the cell model is applied as the second transport model to evaluate the migration trends of the radioactive contaminants along the L-M10 flow line.

TABLE 8.4

COMPARISONS BETWEEN THE CALCULATED AND OBSERVED FRONTAL POSITIONS ALONG THE L-H10 FLOW LINE

SPECIES	K _d @ pH3.5 ,ml/g	GROUNDWATER VELOCITY, \bar{V}_0 ,m/yr	RADIONUCLIDE VELOCITY, \bar{V} ,m/yr	CALCULATED 25 YEAR FRONTAL POSITIONS ,m	OBSERVED FRONTAL POSITIONS APPROXIMATED FROM SITE L ,m
²³⁸ U (VI)	13	70	1.1	28	30 - 80
²³⁸ U (IV)	10	70	1.4	36	30 - 80
²²⁶ Ra(II)	20	70	0.7	18	20
²¹⁰ Pb(II)	102	70	0.14	4	3 - 5
²³⁰ Th(IV)	86	70	0.17	4	3 - 5

Basically, the cell model includes mass transport processes as well as chemical mass transfer processes in the simulation of the mobilities of radionuclide species along the L-M10 flow line. The cell model accounts for the changes in the K_d values of radionuclide species in the sand aquifer with respect to the evolution of the groundwater chemistry from 1957 to 1982. The changes in the groundwater velocities downflow from site L in the sand aquifer are also incorporated in this model.

The cell model operates on a simplistic, conceptualized viewpoint of solute transport. The L-M10 flow line is arbitrarily divided into 13 cells, situated primarily between the multilevel piezometer sites shown in Figure 8.10. The cells are arranged in a series, paralleling the groundwater flow direction. The boundaries of each cell paralleling the flow path are impermeable, whereas permeable boundaries exist perpendicular to the flow path.

Prior to the simulations of the mobilities of the reactive, radionuclide species in each cell with time, information was first needed on the mobility of a non-reactive species in each of the cells along the L-M10 flowline for the past 25 years. Assuming site L as the point source for the release of the waste-rock-derived radionuclides to the groundwater zone, the travel times for a non-reactive constituent that recharged the sand aquifer at site L since 1957 have been determined and are presented in Figure 8.10. It is noticed that, after 25 years of migration of a non-reactive species in groundwater downgradient from the waste rock piles, the calculated extent of travel for that species is 101.3 meters from site L or at the end of the twelfth cell. This distance is in accordance with the apparent maximum extent of sulphate contamination from the waste rock in the sand aquifer. Sulphate is considered to be a non-reactive species. Therefore, the end of the 12th cell in Figure 8.10 represents the maximum extent of contamination of the weathered products from the waste rock in the sand aquifer up to 1982. The end of the 13th cell in Figure 8.10 represents an estimation of the maximum extent of waste-rock-derived contamination in the sand aquifer up to 1988.

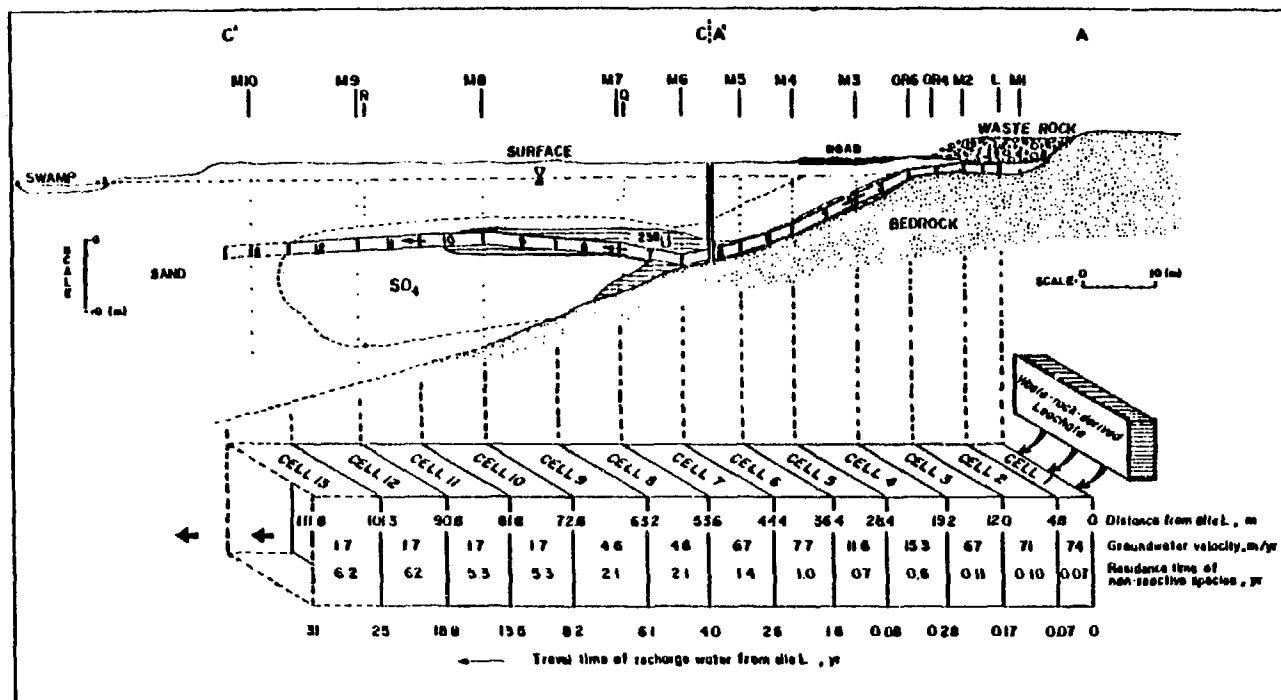


Figure 8.10

Schematic diagram of the cell model. Site L was assumed as the point source of radionuclide species to the sand aquifer. Given are the details of the cell dimensions, groundwater velocity and residence times in each cell. The end of the 12th cell, or 101.3 meters downflow from site L, represents the travel time of a non-reactive constituent that recharged the sand aquifer at site L, since 1957.

In the incorporation of the effects due to mass transport and chemical mass transfer processes in the simulations for the mobilities of radionuclides, a two step transport-react approach is used in the cell model. For example, a known activity of radioactive solute enters the first cell during the first iteration. At the end of the first iteration at 0.07 years, (i.e. the first time step in Figure 8.10), the radioactive solute reacts with the solid phase and a new activity for the equilibrated solute remaining in solution in the first cell is calculated by the equation,

$$\text{Solute activity remaining in solution within a cell} = \frac{\text{Total solute activity within that cell}}{1 + \frac{\rho}{n} \cdot K_d} \quad (8.12)$$

The above equation is based on the conservation of mass for a solute in the sand aquifer. At the start of the second iteration, the remaining solute activity in solution from the first cell enters into the second cell and at the same time, a new input of solute activity enters into the first cell. At the end of the second iteration at 0.17 years, the solute in both cells reacts with the solid phase and new activities are determined using equation 8.12 for each cell. This procedure is repeated for the remaining time steps as shown in Figure 8.10, for a total of 13.

The mass-balance equations involved in the first three time steps are given in Figure 8.11. In these equations, the initial and the equilibrated activities of the solute entering each cell at each time step are multiplied by coefficients. These coefficients are time factors. The time factors are relative to the residence times in the cells and are proportional to one another for each time step. Time factors are calculated by the equation,

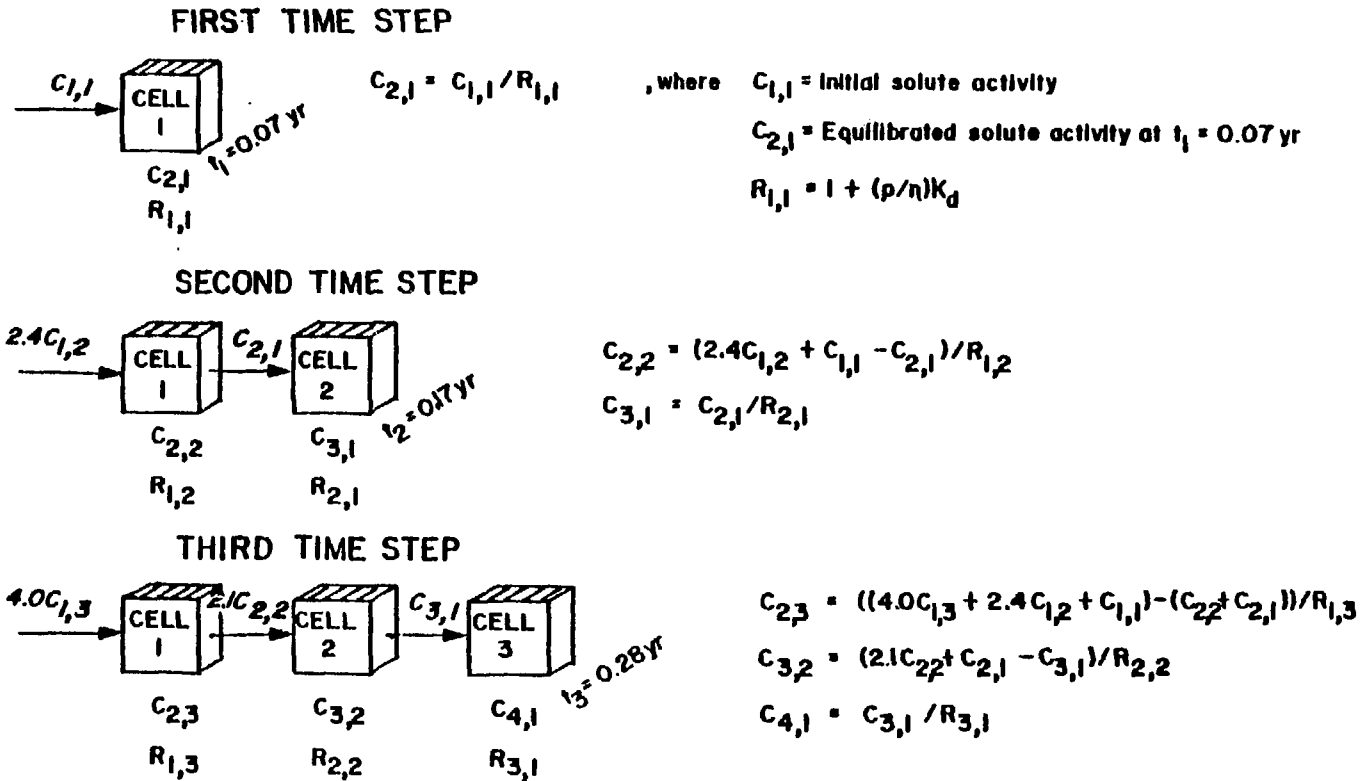


Figure 8.11

Mass balance equations. The equilibrated activities of a radioactive solute in each cell at each time step are calculated from these equations.

$$\text{Time Factor} = \frac{\text{Time step of cell } y(\text{yr}) - \text{Minimal travel time from site L to cell } x, y (\text{yr})}{\text{Residence time in cell } x, y (\text{yr})} \quad (8.13)$$

where $x = 1-13$, inclusively, and y is greater than and equal to x .

The product of the time factor and the activity of the solute represents the accumulated activity of that solute entering the cell as a function of time. The initial solute activities entering the first cell with each iteration in Figure 8.11 are not the same. A discussion on the selection of the appropriate parameters of the initial solute activities and K_d values for these mass balance equations is given later in this section.

For the cell model, the initial condition is,

$$C(x,0) = 0 ; \quad x > 0$$

and the boundary conditions are,

$$C(0,t) = C_o(t) ; \quad t > 0$$

$$C(L,t) = 0 ; \quad t > 0$$

,where

C_o = solute activity of leachate entering the groundwater zone below the waste rock at site L

C = solute activity in groundwater within a cell

$x = 0$ = Influent end of the L-M10 flowline

$x = L$ = Effluent end of the L-M10 flowline
, where L = length of flowline

t = time

Because dispersion has been considered earlier in this chapter to be negligible along the initial part of the L-MIO flowline, one-dimensional plugflow transport of the radioactive solutes has been only considered in the cell model. Another rationale for neglecting dispersion is because of the relatively high batch K_d values for the radionuclides of interest. An earlier testing of the cell model by Reynolds (1978) has indicated that dispersion does not effect the migration of a reactive solute species that has a high K_d (i.e. greater than 50 ml/g).

The computer program, as outlined in Veska (1983), has been used for simplifying the calculations of the equilibrated solute activities in each of the cells for each time step. The program includes all of the stated assumptions and conditions for the cell model. The equation that is used to calculate the equilibrated solute activities, $C(i,j1)$, for each cell in the computer program is as follows:

$$C(i,j1) = A(i-1,j1) \cdot C(i-1,j1) + \sum_{K=1}^{j2} (A(i-1,K) \cdot C(i-1,K) - C(i,K)) / R(i-1,j1) \quad (8.14)$$

,where

- i = (cell number - 1)
- j = iteration number
- N = total number of iterations
- $j1 = j + 1 - 1$
- $j2 = j1 - i$
- $K = 1, j2$
- A = time factor
- C = activity
- R = retardation factor (i.e. $R = 1 + \frac{\rho}{\eta} \cdot K_d$)

The initial solute activities that enter the first cell at each of the thirteen time steps, are different and increase with time. These values are derived from the leaching experiments in Chapter 6 and the procedure in

selecting these values is described below. From the groundwater pH at site L versus time plot in Figure 8.6, 12 pH values corresponding to the times of the first 12 time steps in the cell model are obtained. The pH value for the thirteenth time step or at 31 years, is assumed to be the same as that for the twelfth time step (i.e. at 25 years). The initial activities of ^{238}U , ^{226}Ra , ^{210}Pb and ^{230}Th that enter the first cell are derived from interpolations in Figure 8.12 using the 13 pH-derived values from Figure 8.6. Figure 8.12 gives activity versus pH curves for ^{238}U , ^{234}U , ^{226}Ra , ^{210}Pb and ^{230}Th in leachates from the pegmatite-gabbroic leaching experiments. The activity versus pH plots in Figure 8.12 include the results using both the batch and column leach techniques. The activities of radionuclides in the column leachates are used in the cell model because the values correspond more closely to those found in groundwater samples from the field site. The results of the pegmatite-gabbro leaching experiments are utilized because the waste rock pile at site L consists of a mixture of pegmatite and gabbro.

The procedure in the derivation of the input values of A and R for equation 8.14 is now described. Values of A for each cell at each time step are calculated from equation 8.13. For the calculation of the R values, another empirical technique using interpolations is used. A pH versus distance plot of the 1982 acid front along the L-M10 flow line is given in Figure 8.13. This present-day pH profile in groundwater represents the effects of acidic leachate migration from waste rock in the sand aquifer for the past 25 years. In the attempt to estimate the progression of the acid front downflow from site L since 1957, the time steps, corresponding to the 12 pH - derived values of groundwater at site L from Figure 8.6, are plotted on the y-axis in Figure 8.13. A family of lines is then drawn paralleling the 1982 pH profile in Figure 8.13 for all of the given time steps. The pH profile for the 13th time step is drawn in Figure 8.13 to represent an approximation of the 1988 acid front. From the middle of each cell in Figure 8.13, pH values are interpolated from the acid front curves at each time step. From these pH values, corresponding K_d values for Ra(II),

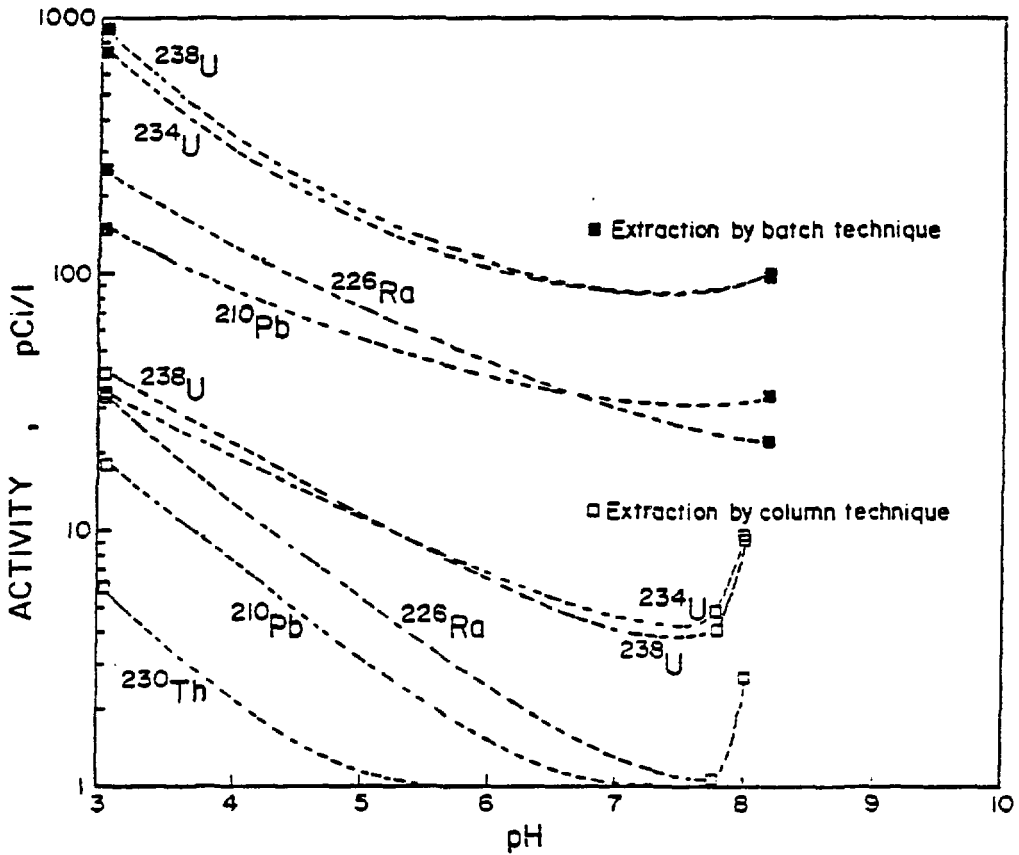


Figure 8.12 Activities of ^{238}U , ^{234}U , ^{226}Ra , ^{210}Pb and ^{230}Th in pegmatite/gabbro leachates as a function of pH. The top and bottom set of curves represent the average activities of radionuclides extracted in solution from the leaching of a pegmatite/gabbro mixture by the batch and column leach techniques, respectively.

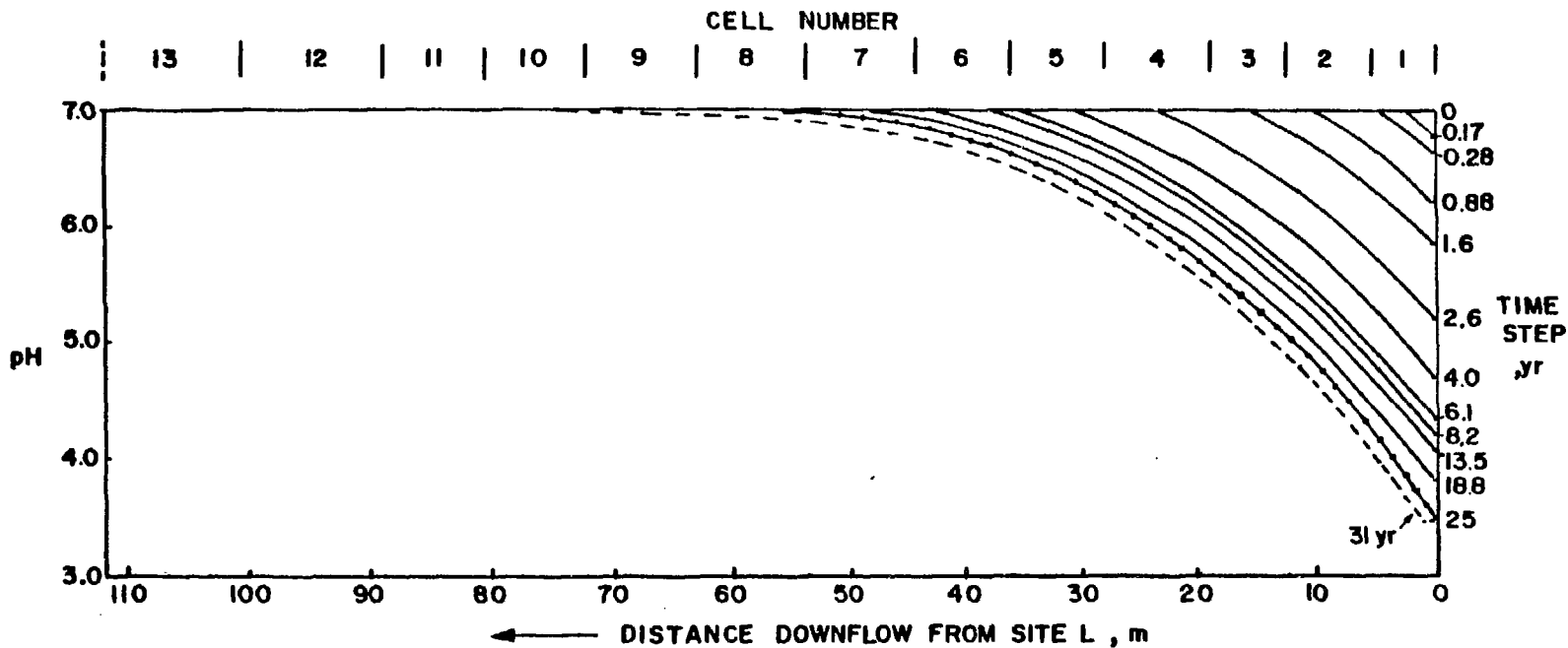


Figure 8.13 Progression of the acid front in groundwater downflow from site L in the sand aquifer as a function of time. —••••• 1982 observed acid front; — 1956-1982 estimated acid fronts for each time step; --- 1988 estimated acid front.

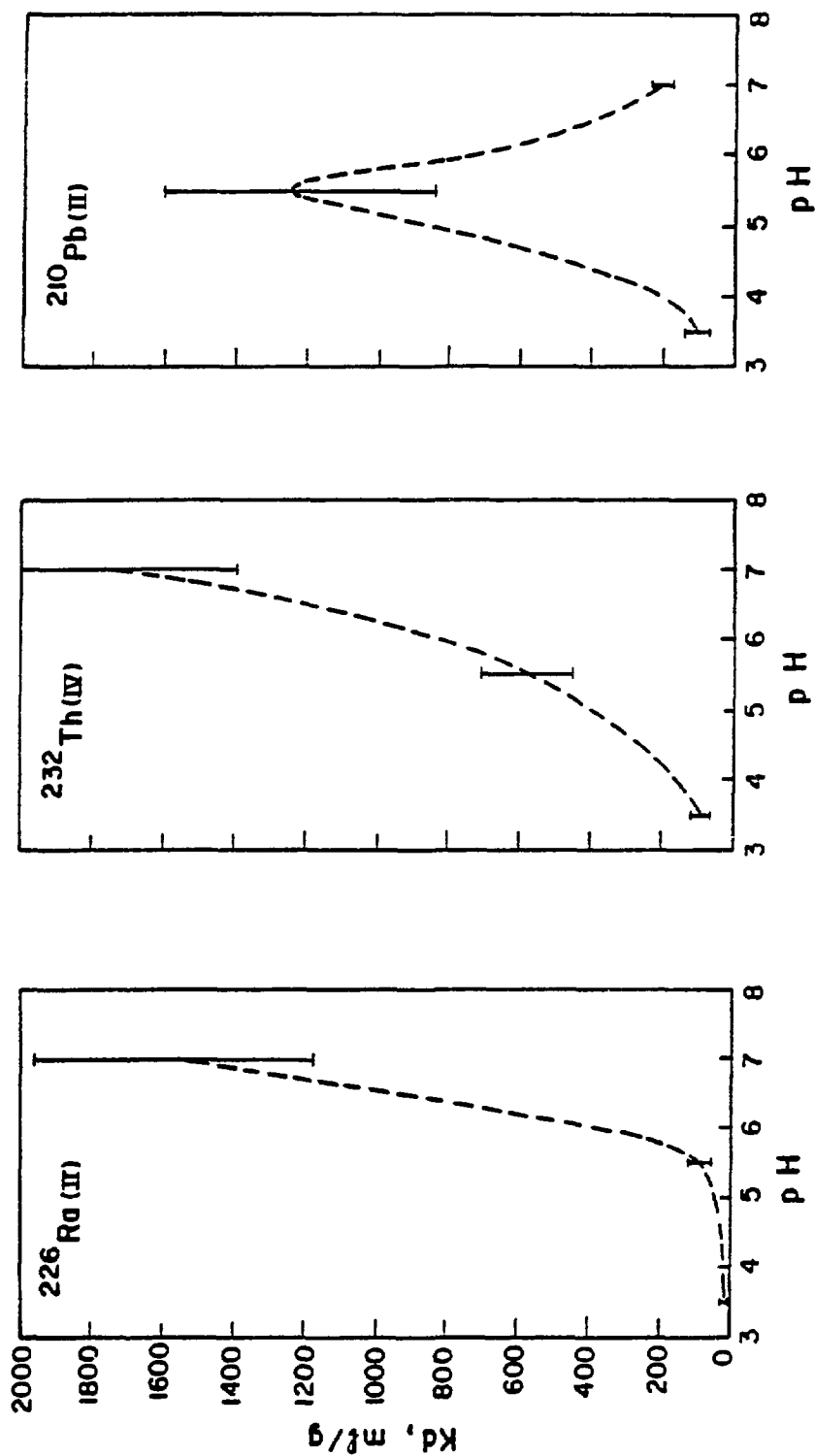


Figure 8.14 K_d values of $^{226}\text{Ra(II)}$, $^{232}\text{Th(IV)}$ and $^{210}\text{Pb(II)}$ versus pH. The vertical bars indicate the range of maximum and minimum K_d values. The chemical composition of the equilibrating solution was different for each batch K_d determination at different pH.

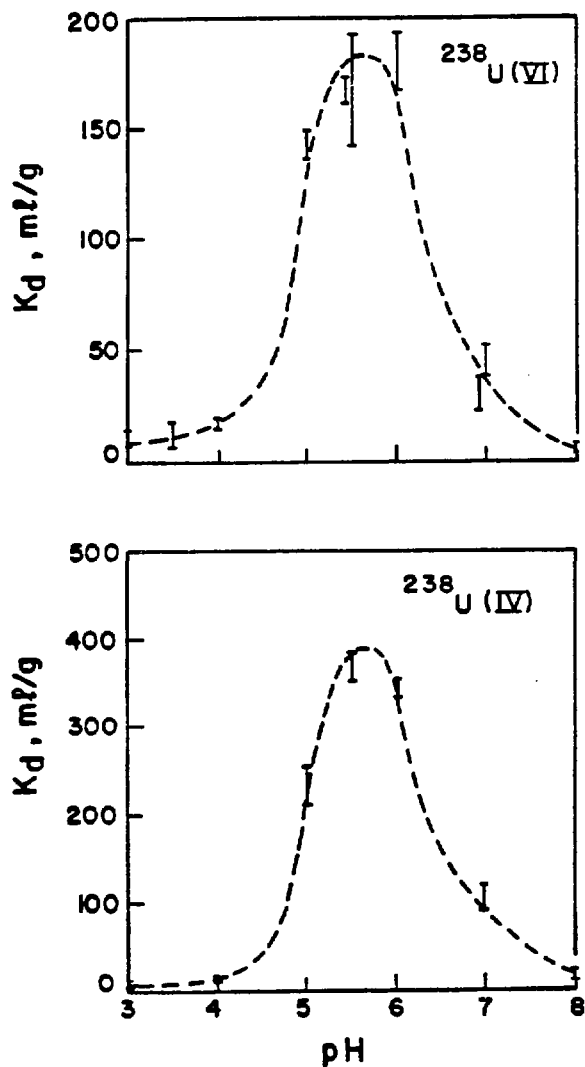


Figure 8.15 K_d values of U(VI) and U(IV) versus pH.

The vertical bars indicate maximum and minimum K_d values. The chemical composition of the equilibrating solution was different for each batch K_d determination at different pH.

Th(IV), Pb(II), U(VI) and U(IV) are interpolated from the respective K_d versus pH plots in Figures 8.14 and 8.15. These interpolated K_d values for each cell at each time step led to the calculation of the R values.

The results of the simulated activities of the ^{226}Ra , ^{210}Pb and ^{230}Th species along the L-M10 flow line are displayed as activity versus distance profiles in Figures 8.16, 8.17 and 8.18, respectively. Simulations for the activities of ^{226}Ra and ^{210}Pb have been made for a 25 year period. The ^{230}Th activity has been simulated for a 22 year period because ^{230}Th has only been analyzed in the 1979 groundwater samples. The longitudinal profiles of the simulated activities for ^{226}Ra , ^{210}Pb and ^{230}Th in groundwater along the zone of contamination in these figures are compared with those of the respective analytical activities in 1982 and 1979. Analytical activities, as referred to from hereon, represent the measured activities of radionuclide species in groundwater. For each of the three comparisons in Figures 8.16, 8.17 and 8.18, good agreement is observed.

The longitudinal profiles of the simulated activities of ^{230}Th , ^{210}Pb and ^{226}Ra in groundwater along the L-M10 flow line at 25 years and 31 years are displayed in Figure 8.19. The simulated activities in these cells at 25 years and 31 years along the L-M10 flow line represent the respective 1982 and 1988 spread of ^{230}Th , ^{210}Pb and ^{226}Ra contamination from the waste rock in the sand aquifer. Observation of Figure 8.19 shows that the continued spread of ^{230}Th , ^{210}Pb and ^{226}Ra contamination in the sand aquifer from 1982 to 1988 will not be appreciable and that these contaminants pose no immediate danger to nearby residents.

The results of the simulated ^{238}U activities in groundwater in each of the 13 cells at 25 years are plotted as an activity versus distance profile in Figure 8.20. Because the proportions of the tetra- and hexavalent states of uranium are unknown in the Greyhawk groundwater, longitudinal profiles for the simulated activities of $^{238}\text{U(VI)}$ and $^{238}\text{U(IV)}$, assuming 100% abundance of each redox species, are both displayed in Figure 8.20. The U(VI) species is shown to be more abundant than its counterpart downflow from site L. The longi-

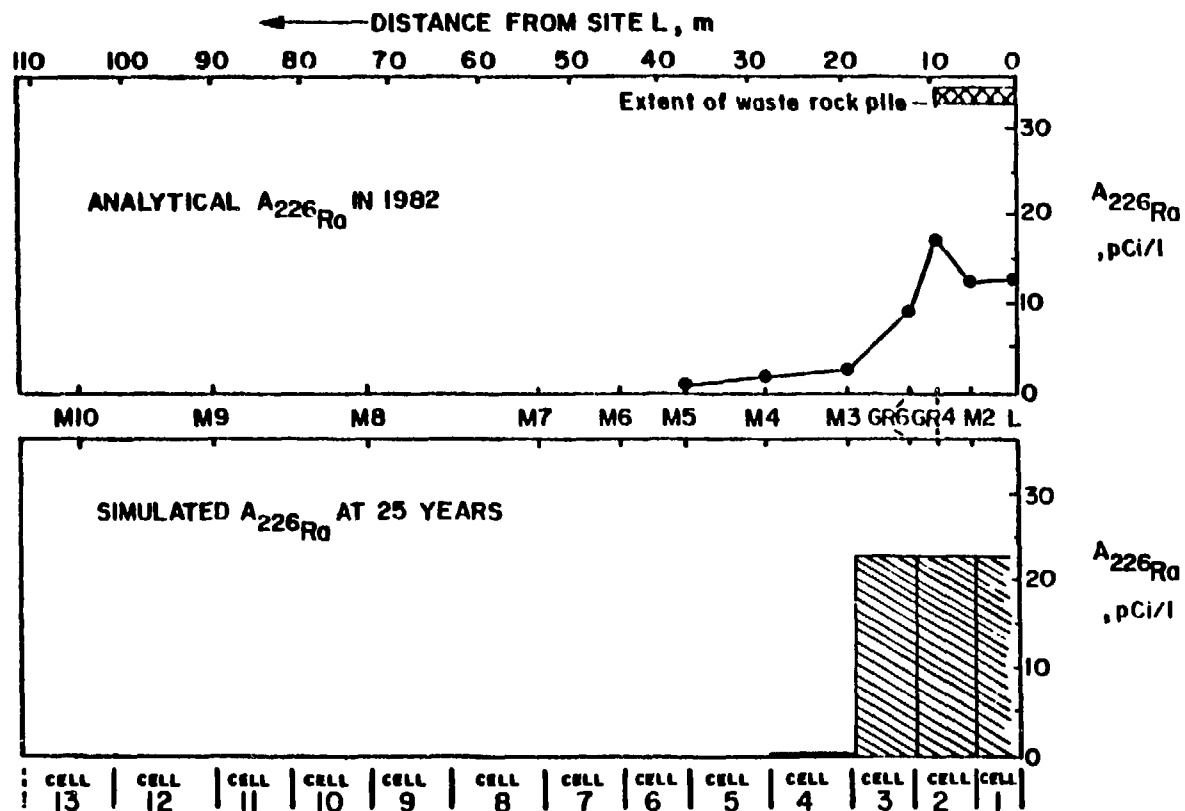


Figure 8.16

Longitudinal profiles of simulated and analytical activities of radium - 226 in groundwater along the L-M10 flow line. The simulated activity distribution at 25 years represents the calculated 1982 extent of radium-226 migration from site L since initial contamination of the aquifer in 1956-57.

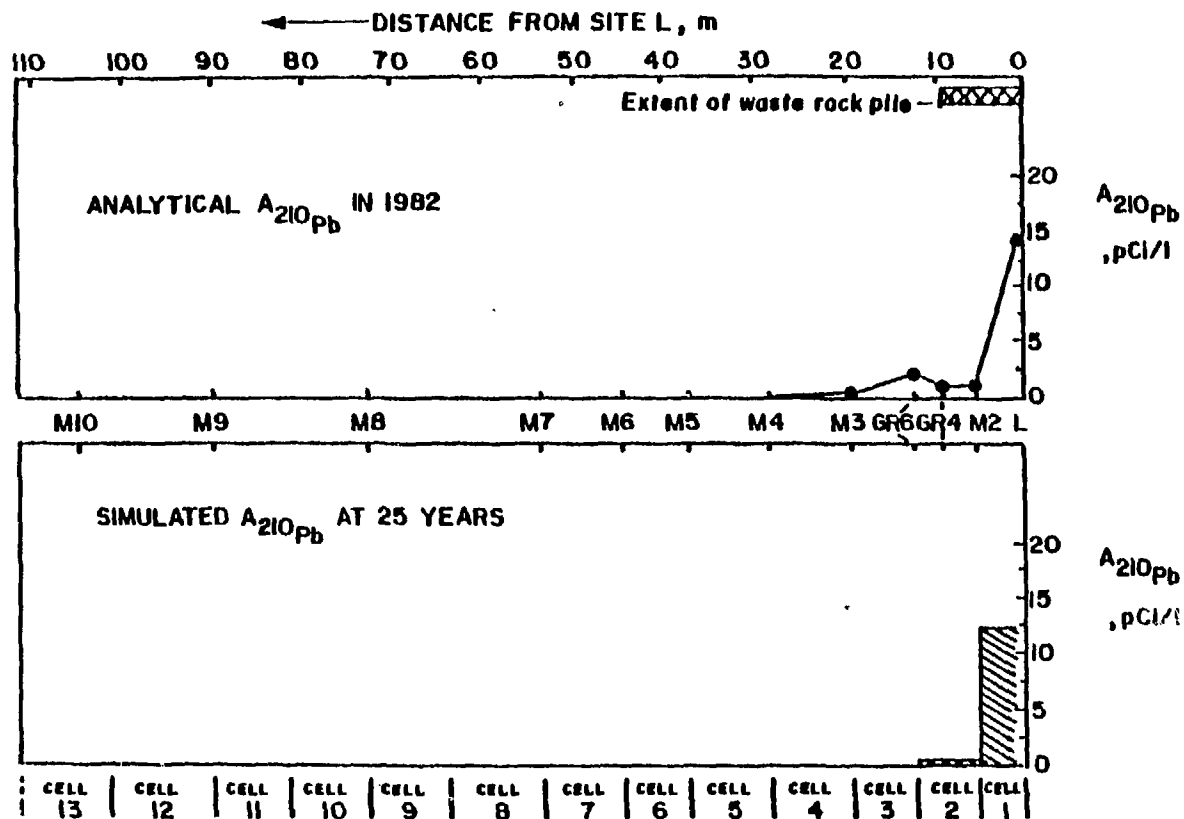


Figure 8.17

Longitudinal profiles of simulated and analytical activities of lead-210 in groundwater along the L-M10 flow line. The simulated activity distribution at 25 years represents the calculated 1982 extent of lead-210 migration from site L since initial contamination of the aquifer in 1956-57.

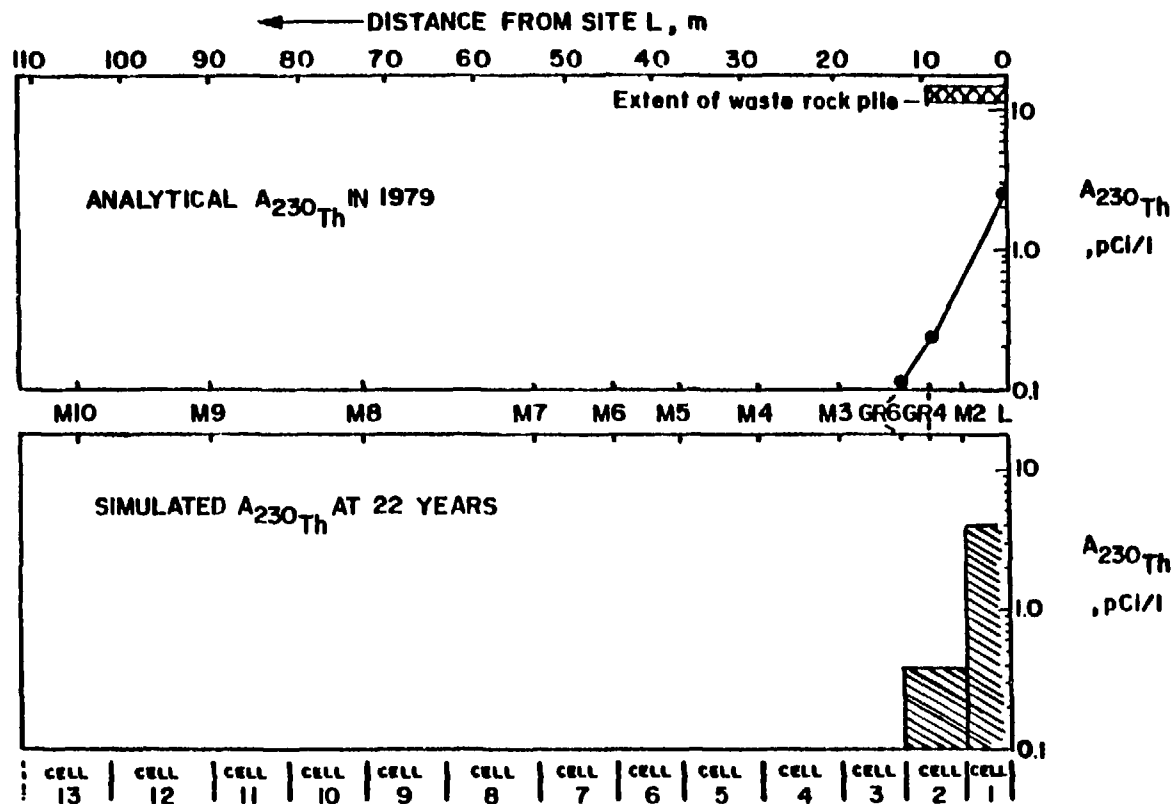


Figure 8.18

Longitudinal profiles of simulated and analytical activities of thorium-230 in groundwater along the L-M10 flow line. The simulated activity distribution at 22 years represents the calculated 1979 extent of thorium-230 migration from site L since initial contamination of the aquifer in 1956-57.

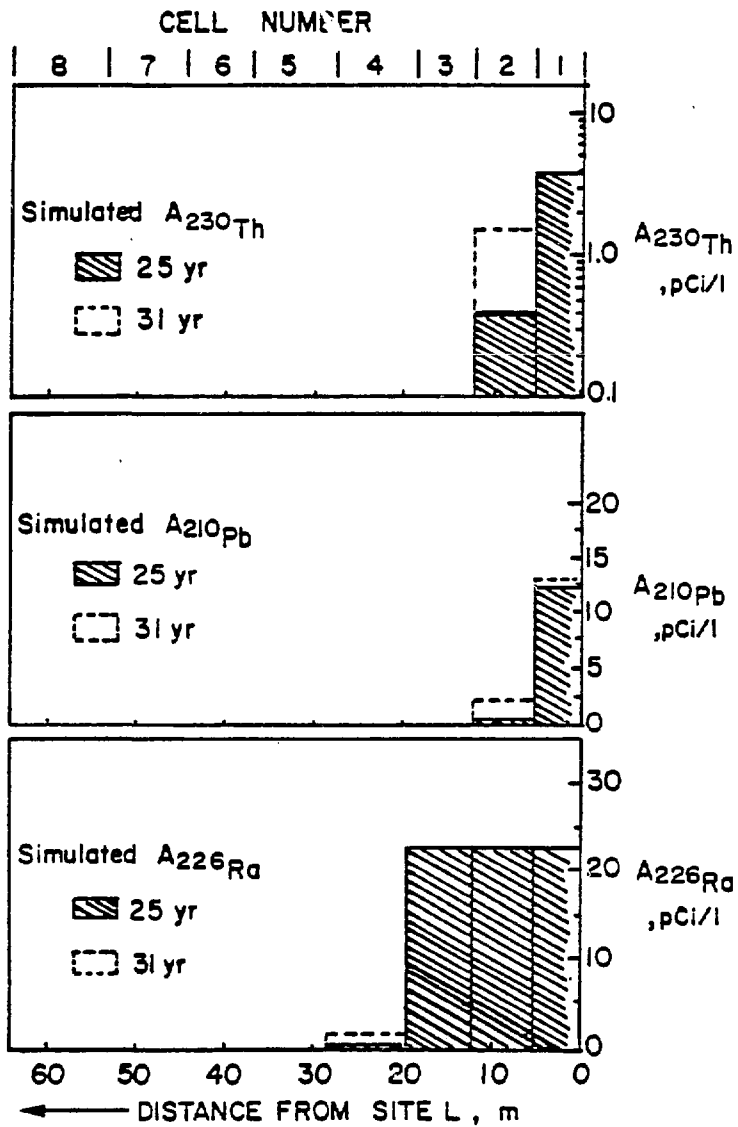


Figure 8.19 Comparison amongst the simulated longitudinal activity profiles of ^{230}Th , ^{210}Pb and ^{226}Ra at 25 years and 31 years along the L-M10 flowline.

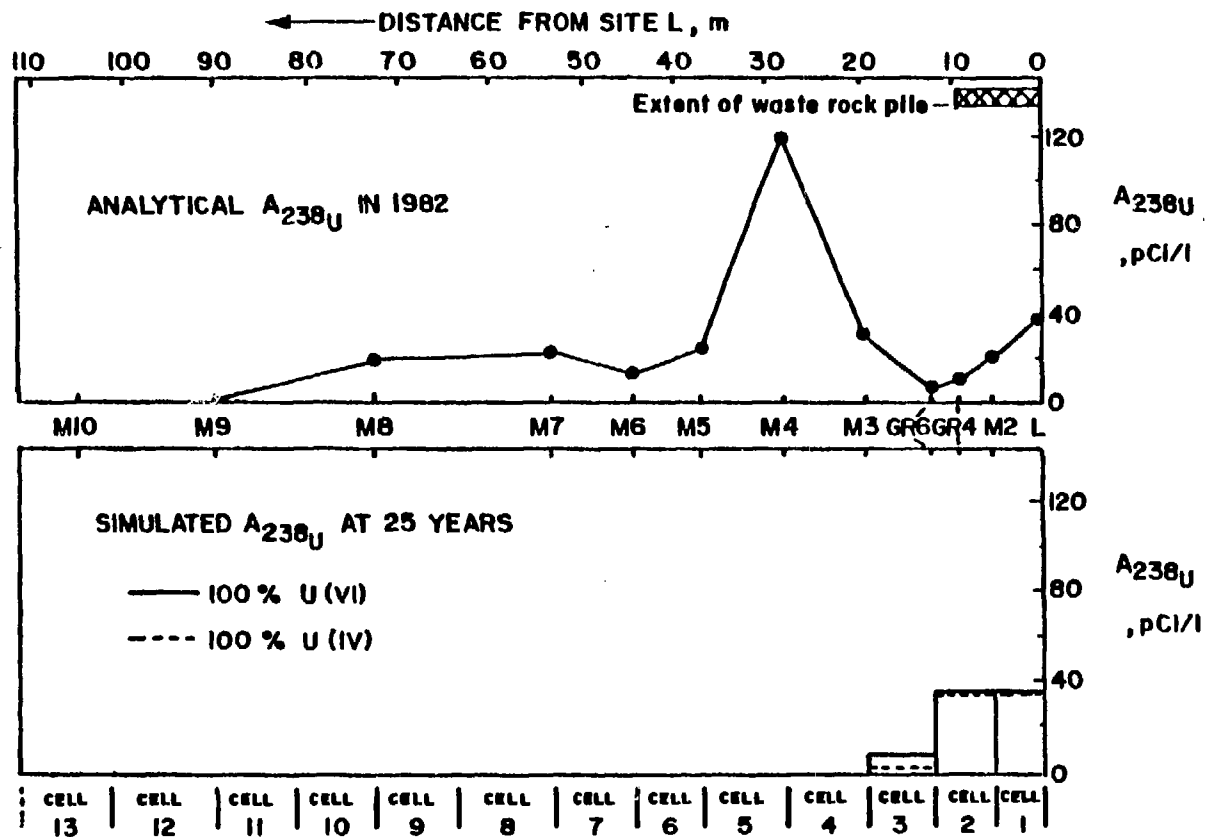


Figure 8.20

Longitudinal profiles of simulated and analytical activities of uranium-238 in groundwater along the L-M10 flow line. Simulations are made separately for uranium (VI) and uranium (IV) species. The simulated activity distributions at 25 years represents the calculated 1982 extent of uranium-238 migration from site L since initial contamination of the aquifer in 1956-57.

tudinal profiles of the simulated activities of the $^{238}\text{U(VI)}$ and $^{238}\text{U(IV)}$ species are compared in Figure 8.20 with that of the analytical ^{238}U activities in groundwater in 1982 along the L-M10 flow line. The comparisons between the analytical and simulated activities show that there is good agreement from sites L to M3, or approximately 20 meters downflow from site L. Further downflow, the agreement is poor.

To improve on the agreement between the simulated and analytical activities of ^{238}U in groundwater downflow from site M3, the K_d values of ^{238}U in the field are assumed to be a factor of ten less than that of the batch K_d values. The rationale for the order of magnitude decrease in K_d values is based on the previously-described difference between the calculated and observed frontal positions for ^{238}U in groundwater downflow from site M16 in Table 8.3. Simulations of the $^{238}\text{U(VI)}$ and $^{238}\text{U(IV)}$ activities at 25 years, using respective K_d values that are reduced by a factor of ten, have produced the longitudinal profiles in Figure 8.21. This decrease in the K_d values by an order of magnitude has extended the simulated $^{238}\text{U(VI)}$ contamination along the L-M10 flow line toward site M7, or approximately 55 meters downflow from site L. This re-calculated distance agrees with the initial frontal position of the analytical ^{238}U activities in groundwater shown in Figure 8.21.

The cell model has also been used to assess the explanation made earlier in section 8.3 on the presence of higher ^{238}U activities in groundwater at site M4, as shown in Figure 8.21. This had been done by simulating the activities of $^{238}\text{U(VI)}$ and $^{238}\text{U(IV)}$ species along the L-M10 flowline using the following assumptions, namely: (1) the ^{238}U activity input at site L is constant at 121 pCi/l for a 25 year period and (2) the K_d values for U(VI) and U(IV) are an order of magnitude less than those for the respective batch K_d values. The simulated values for $^{238}\text{U(VI)}$ and $^{238}\text{U(IV)}$ are plotted and are compared with the analytical ^{238}U values along the L-M10 flowline in Figure 8.22. The comparison between the simulated and the analytical ^{238}U values shows good agreement downflow from site M4 and poor agreement between sites M4 and L. It is reasonable to suggest from Figure 8.22 that the ^{238}U activity in groundwater at site L was 121 pCi/l or even higher from intensive

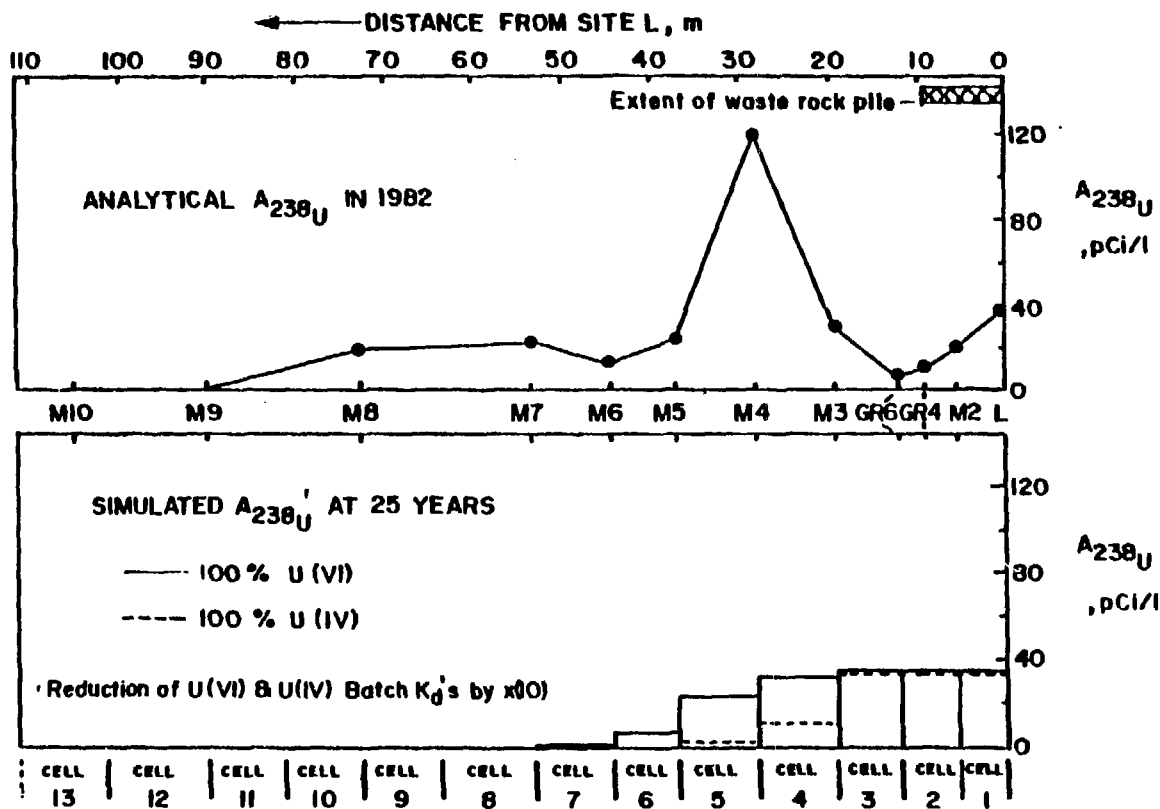


Figure 8.21 Longitudinal profiles of simulated and analytical activities of uranium - 238. Reduction in batch K_d values for uranium (VI) and uranium (IV) by an order of magnitude.

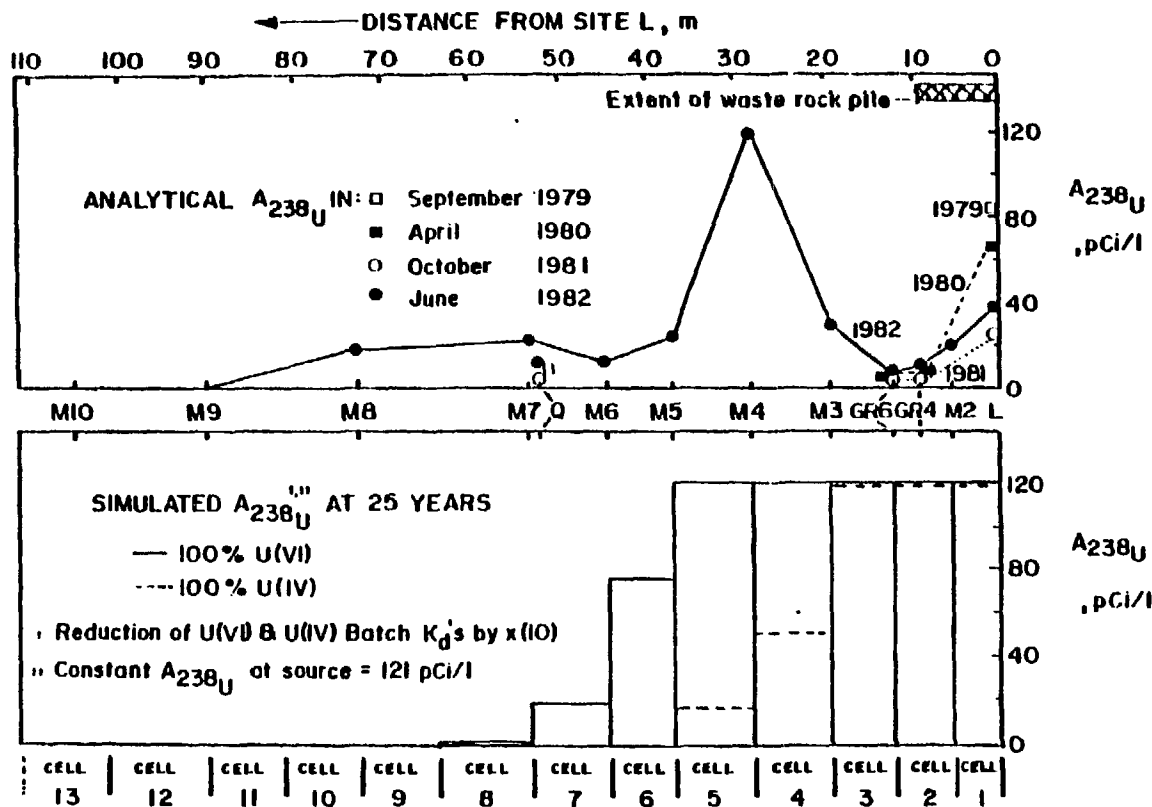


Figure 8.22 Analytical and simulated uranium - 238 longitudinal activity profiles downflow from site L. Top: Analytical activity of uranium - 238 with respect to time and distance. Bottom: Simulated activity of uranium - 238 at 25 years - Reduction in batch K_d values for U(VI) and U(IV) by an order of magnitude and an assumed constant input at site L at 121 pCi/l of uranium - 238.

uraninite oxidation and dissolution during the initial stages of waste rock weathering. Furthermore, it can be suggested that this contaminated groundwater from the initial period of waste rock weathering up to 1982 had migrated to site M4 and that the newly-formed groundwater below the waste rock had decreased below 121 pCi/l as a result of decreases in the rates of uraninite oxidation and dissolution. The latter can be noted in Figure 8.22 by the decrease in the observed ^{238}U activities in groundwater at site L from 1979 to 1982. It is also possible that this decrease in ^{238}U activities in groundwater since 1979 may have been caused by the removal of part of the waste rock pile in 1979 by a bulldozer. Such uncontrollable events affecting the release of radionuclides from the waste rock to the sand aquifer for the past 25 years have made accurate simulations of the ^{238}U migration patterns difficult.

The cell model was tested for its behaviour towards the number of cells employed in the simulations. For its evaluation, the activities of the mobile, $^{238}\text{U(VI)}$ and $^{226}\text{Ra(II)}$ species in groundwater along the L-M10 flow line are simulated for a 25 year period by varying the number of cells from 6 to 12 to 17. The distribution of the 6 cells is roughly equally spaced along the L-M10 flowline, whereas the distributions of the 12 and 17 cells are spaced in detail near the waste rock vicinity, where the changes in the activities of radionuclide species have been found to be the greatest. All of these distributions along L-M10 are displayed in Figure 8.23. The longitudinal profiles of the simulated activities for ^{238}U and ^{226}Ra in the 6, 12 and 17 cells at 25 years are given in Figure 8.23. The differences in the simulated ^{226}Ra activity distributions amongst the 6, 12, and 17 cells are negligible. The simulated $^{238}\text{U(VI)}$ activity distribution in the 6, 12 and 17 cells, on the other hand, shows a tendency in the longitudinal profiles to converge to a particular shape and distribution with increase in the number of cells.

In summary, the simulated frontal positions for the migration of ^{226}Ra , ^{210}Pb and ^{230}Th in the sand aquifer, using both the advection-retardation model and the cell model, are similar to the respective frontal positions that

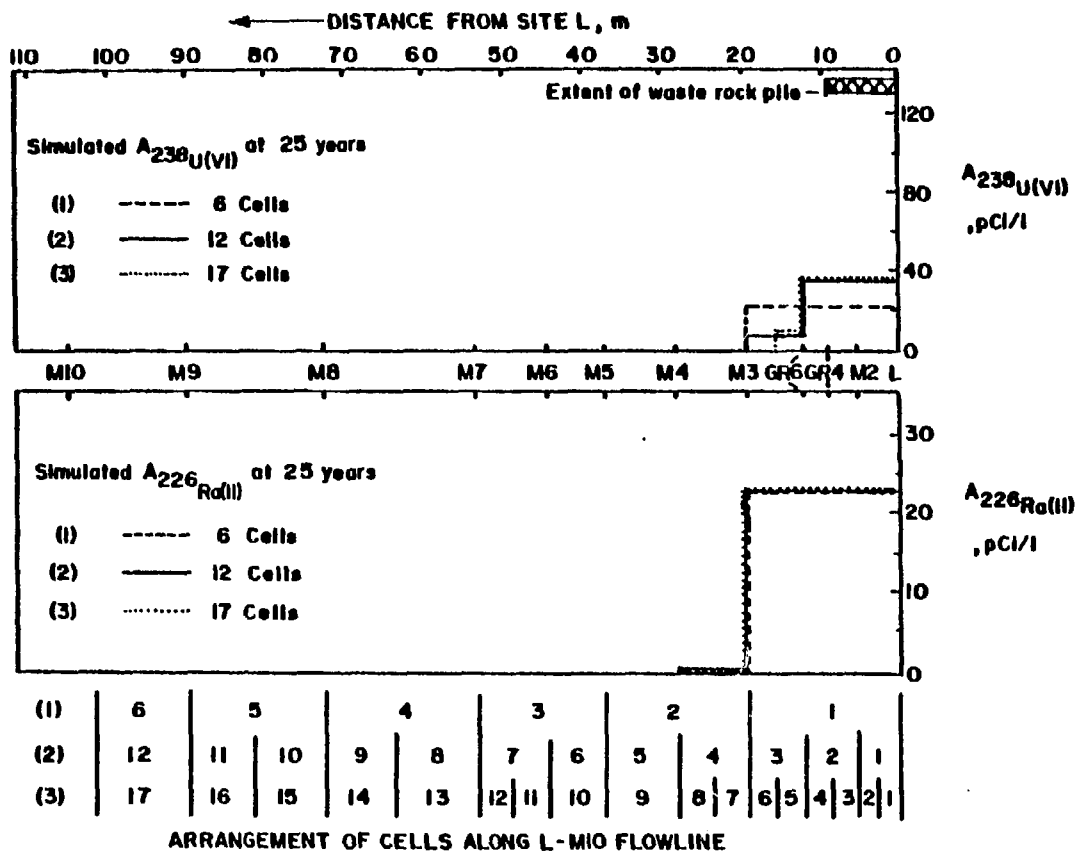


Figure 8.23 Effect of the number of cells on the simulation of $^{238}\text{U(VI)}$ and $^{226}\text{Ra(II)}$ activities in groundwater for a period of 25 years.

are observed in the field. A similar condition for uranium is not found in this investigation. Agreement between the simulated and observed frontal positions for ^{238}U is only found when the batch K_d values for U(VI) have been reduced by an order of magnitude.

A possible explanation for the agreement and discrepancy between the simulated and observed fronts for radionuclides is that equilibrium conditions along the L-M10 flowline do not exist. If this is true, then the determined batch K_d values for the radionuclides, which are representative of equilibrium conditions, need to be applied in the transport models with caution for the evaluation of the Greyhawk field problem. The groundwater velocities along the initial part of the L-M10 flowline (Figure 8.10) are very fast, i.e. averaging 70 m/yr or 0.2 m/day. As a result, some of the radioactive contaminant species that are released from the waste rock into this dynamic flow system, may not be equilibrated within the porous medium. This can be the case for the U(VI) and the U(IV) species, that possess low batch K_d values, ranging from 6 to 194 ml/g and 7 to 384 ml/g, respectively (Figure 8.15). As for the Ra(II), Pb(II) and Th(IV) species in groundwater, this explanation is not relevant because these species are characterized by high batch K_d values (Figure 8.14). For example, the increase in groundwater pH downflow from the acid front zone in the NW flow regime immobilizes the ^{226}Ra , ^{230}Th and ^{210}Pb contaminants because their batch K_d value are greater than 1000 ml/g. Based upon this explanation of a dynamic system at the Greyhawk site, the use of the two transport models for the evaluation of the migration patterns of the waste-rock-derived radioactive contaminants is only applicable for radium, lead and thorium, and to uranium in a limited manner. Further work on the determination of 'dynamic' K_d for uranium at different velocities in a column can be helpful in testing the applicability of the models.

The simulations made by the transport models do not include the effects due to several factors at the field site. These include: (1) heterogeneity of the sand aquifer as noticed in the NW sector (Chapter 4); (2) variable groundwater flow velocities during each year (Chapter 4); (3) variable weathering rates of

waste rock (Chapters 5 and 6); and (4) the absence of an ideal point source. Furthermore, the determination of batch K_d by the experimental procedure followed has its limitations when it is applied as a parameter in the transport models. For example, the equilibration of a radioisotope between solution and solid phases using a mechanical shaker, as described in Chapter 7, can result in the breakdown of the sand particles to smaller grain sizes, which would possess larger surface areas for increased adsorption of radionuclides. The 20:1 liquid to solid ratio used in the batch K_d experiments, instead of the 1:5 ratio that is normally found in sandy aquifers, does not give the K_d values applicable for evaluating the migration patterns of the waste-rock-derived radionuclides. Indeed, a decrease by a factor of two in the U(VI) K_d values with decrease in the liquid to solid ratio from 20:1 to 5:1 was observed as detailed in Chapter 7.

Of the six radionuclides investigated, only the activities of ^{226}Ra in groundwater were found to exceed the ICRP drinking water limit. An assessment of the impact of ^{226}Ra contamination in the sand aquifer became warranted. The short-term impact of ^{226}Ra contamination from waste rock in the sand aquifer has already been assessed by the cell model. The cell model had been used to predict the spread of ^{226}Ra contamination, as well as the ^{210}Pb and ^{230}Th contamination, in the sand aquifer up to 1988. The results of the 1988 predictions suggest that there are no appreciable changes in the 1982 migration patterns for these three radionuclide species.

To assess the long-term impact of ^{226}Ra contamination in the sand aquifer, it became necessary to calculate the future extent of the acid front extending from the waste rock. The reason for this calculation, is that the migration patterns for ^{226}Ra are dependent on the acid front movement in the sand aquifer (Chapter 5 and 8). The continual progression of the 1982 acid front from site L for 100 years is calculated using equation 8.10, a modified form of the one-dimensional retardation equation. The maximum lateral extent of the 2082 acid front from site L is calculated at 40 meters, i.e. in close proximity to site M5. Therefore, the maximum extent of ^{226}Ra contamination in

the sand aquifer in the year 2082 is approximated at 40 meters downgradient from the waste rock.

Most probably, the actual extent of ^{226}Ra contamination after 100 years will be less than the calculated value at 40 meters. It was noted earlier that there was a gradual decrease in the activities of radionuclides and in the hydrogen ion concentration in groundwater at site L from 1979 to 1982. This is reflected in part by the neutralization of the released hydrogen ions from pyrite oxidation by the carbonates in the gabbro, which are more abundant than that for pyrite, also within the same rock type. Assuming a hypothetical case where all of the pyrite in the 6088 tons of gabbro mass centered at site L is completely dissolved over a geological time span, the total amount of hydrogen ions that would be released into solution from pyrite oxidation is 2.2×10^6 moles. Furthermore, assuming that this acidic leachate is confined within the waste rock mass, the total amount carbonates within the gabbro (e.g. calcite content = 2.33×10^6 moles) would be able to completely neutralize the acidic leachate.

However, some of the acidic leachate does escape neutralization with the carbonates in the waste rock and infiltrates to the water table below. Assuming that a neutral pH leachate would eventually result at site L after the year 2082, the progression of the acid front in the sand aquifer would eventually stop, yet the ^{226}Ra front would become displaced further downflow from its original position. For example, in the year 2082, the ^{226}Ra front in the sand aquifer is predicted from the advection-retardation model to become displaced by only one meter downflow from the 2082 frontal position for ^{226}Ra . Further predictions using the same model, indicate that the ^{226}Ra front in the sand aquifer at 250,000 years from 1982, will be displaced at 126 meters downflow from site L, at a position below the swamp. If the activity of ^{226}Ra in groundwater is constant at 20 pCi/l at all of the frontal positions for ^{226}Ra in the sand aquifer up to 2082, then the activities of ^{226}Ra in groundwater would decrease to 13.5 pCi/l and 10^{-46} pCi/l for the respective fronts of ^{226}Ra at 1000 years from 1982 and at 250,000 years from 1982. Therefore, the ^{226}Ra contaminated groundwater will never leave the field site with activities of ^{226}Ra greater than the Canadian target drinking water limit (2.7 pCi/l), and thus, it can be concluded that the uranium-mine waste rock dump site at Greyhawk probably does not require long-term surveillance.

In conclusion, the findings from this investigation on the subsurface migration of radioactive contaminants from the uranium-bearing waste rock at the Greyhawk site were found to be representative of a relatively-simple case. These findings, however, cannot be used to draw similarities at other waste-rock sites. The reasons being are because of the possible variations in the geological, hydrological and climatic settings that can exist amongst each site. For example, contaminated water from the waste source at Greyhawk has been emanating into the sand aquifer with very low concentrations of major ions and radionuclides for the past two decades. In comparison to other sites, higher concentrations of these waste-rock-derived species may be released to groundwater depending on the weathering rates, the uranium ore and sulphide mineral composition in the rock and other factors. At Greyhawk, the waste-rock-derived contaminants have been migrating downgradient from the source in the oxidized zone of the sand aquifer. In comparison to other sites, the contaminants may have migrated in a reduced zone, in a geological medium other than sand, in an aquifer with faster or slower groundwater velocities and/or in an aquifer containing groundwater from different sources. Regardless of these possible differences that can exist amongst various waste-rock-dump sites, the methodology used for the Greyhawk problem can be used at other sites for simulating the subsurface migration of radionuclides from waste rock.

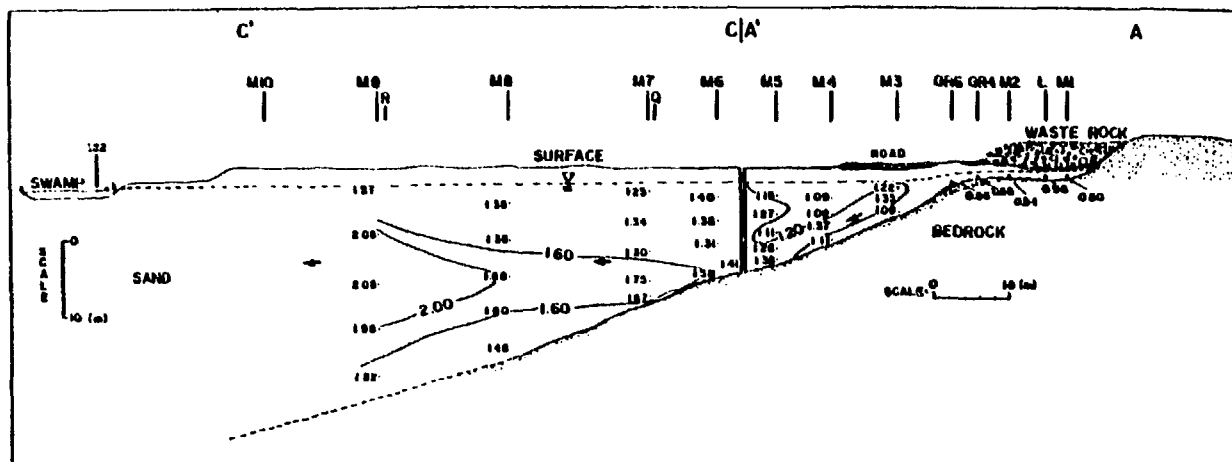
CHAPTER 9

DISEQUILIBRIA IN THE URANIUM - 238 SERIES IN GROUNDWATER







The activity ratios of $^{234}\text{U}/^{238}\text{U}$, $^{226}\text{Ra}/^{238}\text{U}$ and $^{210}\text{Pb}/^{238}\text{U}$ in the Greyhawk groundwater and in the rock leachates from the lab experiments have been measured. The purpose was to determine if disequilibrium between ^{238}U and each of its daughters, ^{234}U , ^{226}Ra and ^{210}Pb , exists in these solutions. If disequilibrium of the radionuclides of the uranium - 238 series occurs in groundwater, then the spatial trends of the activity ratios can serve to indicate the direction of contaminant migration of the waste-rock-derived radionuclides in the sand aquifer. Kaufman et al. (1969), Titayeva and Veksler (1977) and Cowart and Osmond (1974) have found that the distribution of the $^{234}\text{U}/^{238}\text{U}$ activity ratios in groundwater serves as a useful indicator of the uranium migration patterns within an aquifer. Isotopic disequilibrium between ^{234}U and ^{238}U in the Greyhawk groundwater is of particular interest in this investigation because the two uranium isotopes in nature are expected to behave the same chemically.

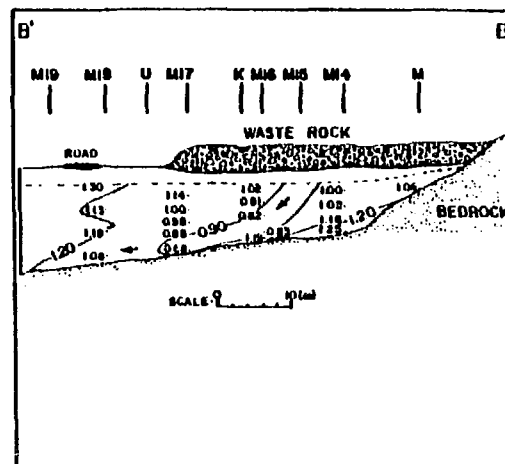
9.1 Spatial Distributions of $^{234}\text{U}/^{238}\text{U}$, $^{226}\text{Ra}/^{238}\text{U}$ and $^{210}\text{Pb}/^{238}\text{U}$ in Groundwater

To determine the state of disequilibrium between ^{238}U , and each of its daughters, ^{234}U , ^{226}Ra and ^{210}Pb in the contaminated groundwater zone, the activity ratios of $^{234}\text{U}/^{238}\text{U}$, $^{226}\text{Ra}/^{238}\text{U}$ and $^{210}\text{Pb}/^{238}\text{U}$ in the 1982 groundwater samples have been determined from the radio-analytical data as given in Veska (1983). The distribution of the $^{234}\text{U}/^{238}\text{U}$ activity ratios in groundwater is shown along cross sections A-A'-C-C' and B-B' in Figure 9.1. The spatial distribution of the $^{234}\text{U}/^{238}\text{U}$ activity ratios indicates values ranging from 0.80 to approximately 1.00 below the waste rock piles. Downflow



$^{234}\text{U}/^{238}\text{U}$ ACTIVITY RATIO

-  Waste rock deposited on terrain from 1966 to 1959
-  Section of waste rock excavated in September 1979
-  Water table, June 7, 1982
-  Piezometer tip
-  Multilevel sampling point
-  General groundwater flow direction



from the waste rock, the activity ratios of $^{234}\text{U}/^{238}\text{U}$ in groundwater progressively increase with distance, to values as high as 2.05 at site M9, i.e. approximately 90-100 meters downflow from the waste rock. Between sites M7 to M9 in Figure 9.1, a zone of high $^{234}\text{U}/^{238}\text{U}$ activity ratios in young groundwater (i.e. younger than 30 years) is found in the middle of the sand aquifer, coinciding with the shape of the previously-described plume of decreasing ^{238}U activities downgradient from the waste rock as shown in Figure 5.31 and with the general direction of groundwater flow. In comparison, the older groundwater in the deepest parts of the sand aquifer, where the age is greater than 30 years, is found to have lower activity ratios (Figure 9.1). The comparison of the distributions of the $^{234}\text{U}/^{238}\text{U}$ A.R.'s and that of the ^{238}U activities in groundwater confirms the findings from previous investigators, in that, the distribution of the $^{234}\text{U}/^{238}\text{U}$ A.R.'s in groundwater can serve as a useful indicator of uranium migration patterns within an aquifer.

The ^{238}U activities decrease with increase in the $^{234}\text{U}/^{238}\text{U}$ activity ratios in groundwater downgradient from the waste rock. A comparison of the $^{234}\text{U}/^{238}\text{U}$ activity ratios and the total uranium concentrations found in groundwater in the aquifer system at the site and those values found in groundwater from other aquifer systems is given in Table 9.1. For all of the field studies in Table 9.1, it can be seen that a low $^{234}\text{U}/^{238}\text{U}$ activity ratio is accompanied by a high uranium concentration in the area of groundwater recharge and that the $^{234}\text{U}/^{238}\text{U}$ A.R.'s gradually increase and the uranium concentrations decrease in groundwater along the flow path away from the recharge area. The $^{234}\text{U}/^{238}\text{U}$ A.R. distribution in the Greyhawk groundwater is unique because of the intensive sampling network in a local sand aquifer and the detailed spacing between the multilevel piezometers at approximately 5-15 meters apart over a short lateral distance of approximately 100 meters. In comparison, the other aquifer systems are regional and the lateral spacings of the sampling stations in these aquifers are approximately between tens of

TABLE 9.1EXAMPLES OF ^{234}U FRACTIONATION IN GROUNDWATER FROM VARIOUS AQUIFERS

Location and Reference	Description of Aquifer	$^{234}\text{U} / ^{238}\text{U}$ A.R.		Uranium Concentration ug/l	
		Recharge Zone	Downflow from Recharge Zone	Recharge Zone	Downflow from Recharge Zone
Central Texas (Kronfeld and Adams, 1974)	Trinity Sandstone Aquifer: ~160 km long	0.92 ± 0.10	11.52 ± 1.13	15.46 ± 0.50	0.046 ± 0.005
Southern Texas (Cowart and Osmond, 1974)	Carrizo Sandstone Aquifer: ~90 km long; ~400 m deep; sand contains quartz, lignite, pyrite and uranium-bearing zircons	0.52 ± 0.01	9.02 ± 1.03	1.49 ± 0.03	0.003 ± 0.001
Greyhawk Site, Bancroft, Ontario	Sand aquifer (~100 m long)	0.98 ± 0.05	2.05 ± 0.19	117.33 ± 4.35	1.23 ± 0.09

kilometers over long lateral distances of 90 km and 160 km. The number of groundwater samples analyzed for $^{234}\text{U}/^{238}\text{U}$ A.R.'s and total uranium from the Greyhawk, Central Texas and Southern Texas field sites were 68, 45 and 29, respectively.

The activity ratios of $^{226}\text{Ra}/^{238}\text{U}$, $^{210}\text{Pb}/^{238}\text{U}$ and $^{230}\text{Th}/^{238}\text{U}$ in groundwater at Greyhawk have not been measured for all of the sample points along the A-A'-C-C' and B-B' cross sections. The activities of ^{226}Ra , ^{210}Pb and ^{230}Th in groundwater have been found to be generally low (Chapter 5), with the exception of the high activities of ^{226}Ra and ^{210}Pb in the low pH zone in the vicinity of site L. From the ^{238}U , ^{226}Ra and ^{210}Pb activities in groundwater samples located along the L-M10 flow line (Chapter 8), the activity ratios of $^{226}\text{Ra}/^{238}\text{U}$ and $^{210}\text{Pb}/^{238}\text{U}$ have been determined and are plotted in Figure 9.2 as longitudinal profiles. Figure 9.2 also shows the degree of disequilibrium that exists between ^{238}U and each of its daughters by the deviations of the $^{234}\text{U}/^{238}\text{U}$, $^{226}\text{Ra}/^{238}\text{U}$ and $^{210}\text{Pb}/^{238}\text{U}$ activity ratios from 1.00. The $^{226}\text{Ra}/^{238}\text{U}$ A.R. and the $^{210}\text{Pb}/^{238}\text{U}$ A.R. in groundwater at site L are 0.32 and 0.37, respectively. Downflow from site L to site GR6, the $^{226}\text{Ra}/^{238}\text{U}$ A.R.'s increase to about 1.06 to 1.93 and the $^{210}\text{Pb}/^{238}\text{U}$ A.R.'s decrease between 0.07 to 0.29. Further downflow from site GR6, the activity ratios for both $^{226}\text{Ra}/^{238}\text{U}$ and $^{210}\text{Pb}/^{238}\text{U}$ decrease to about 0.01. The distances of these sites that correspond to the eventual decrease in the $^{226}\text{Ra}/^{238}\text{U}$ and $^{210}\text{Pb}/^{238}\text{U}$ activity ratios in Figure 9.2, are found to agree with the distances of the analytical ^{226}Ra and ^{210}Pb fronts in the sand aquifer.

The decreases in the activity ratios of $^{226}\text{Ra}/^{238}\text{U}$ and $^{210}\text{Pb}/^{238}\text{U}$ downflow from the waste rock in Figure 9.2 result from various geochemical processes that effect the migration of radium, lead and uranium species in groundwater (refer to Chapter 8). Downflow from site L, the pH and the bicarbonate concentrations in groundwater increase and thus, the mobility of the uranium species, in comparison to that of the ^{226}Ra and ^{210}Pb species,

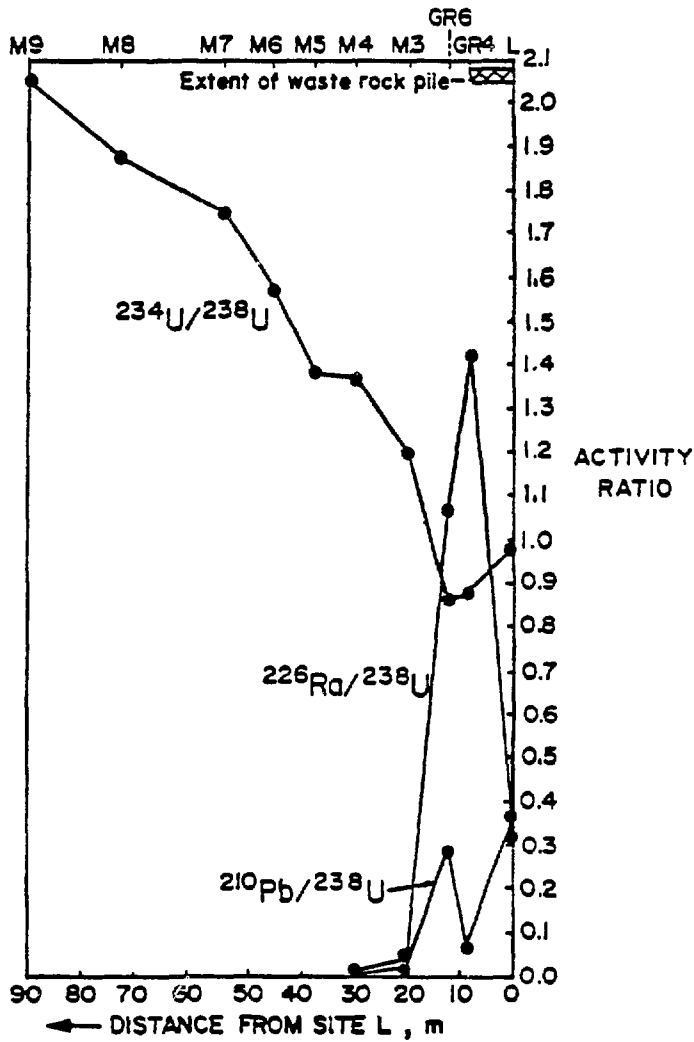


Figure 9.2 Longitudinal profiles of the analytical activity ratios for $^{234}\text{U}/^{238}\text{U}$, $^{226}\text{Ra}/^{238}\text{U}$ and $^{210}\text{Pb}/^{238}\text{U}$ in groundwater in 1982 along the L-M10 flowline.

increases due to the formation of the uranyl-carbonate complexes, $\text{UO}_2\text{CO}_3^\circ$ and $\text{UO}_2(\text{CO}_3)_2^{2-}$. The ^{226}Ra and ^{210}Pb species in the same bicarbonate groundwater downflow from site L are present as cations and cationic complexes, such as Ra^{2+} , Pb^{2+} and PbHCO_3^+ , that are vulnerable to adsorption by the sand particles. This is reflected by the higher K_d values at neutral pH for ^{226}Ra and ^{210}Pb than those values for ^{238}U (Chapters 7 and 8). Although the ^{226}Ra and ^{210}Pb fractionations from ^{238}U in groundwater along the L-M10 flow line have been explained by geochemical processes, the fractionation of ^{234}U cannot be explained in a similar manner. Explanations for the observed ^{234}U fractionation in groundwater in the sand aquifer are given later in this chapter.

9.2 Fractionation of ^{234}U , ^{226}Ra and ^{210}Pb in Leachates from Waste Rock Leaching Experiments

Activity ratios of $^{234}\text{U}/^{238}\text{U}$, $^{226}\text{Ra}/^{238}\text{U}$ and $^{210}\text{Pb}/^{238}\text{U}$ in leachates from the pegmatite and pegmatite-gabbro leaching experiments using the batch technique (Chapter 6) have been calculated. The activity ratios from these experiments, as summarized in Table 9.2, represent the leachate compositions after 40 days of rock/solution equilibration. Table 9.2 compares activity ratios between: (1) leachates from the leaching of unweathered and weathered pegmatitic grains; (2) leachates from the leaching of fresh grains and those that have been used from the previous extractions; (3) leachates from the leaching of pegmatite with various types of equilibrating solutions (i.e. deionized water and pH3 H_2SO_4); and (4) leachates from the leaching of pegmatite-gabbro mixtures at 50:50 and at 100:0.

Higher activity ratios of $^{234}\text{U}/^{238}\text{U}$, $^{226}\text{Ra}/^{238}\text{U}$ and $^{210}\text{Pb}/^{238}\text{U}$ in the leachates are found in Table 9.2 from the leaching of pegmatite with water as 1.32, 0.99 and 0.53, respectively than those from the leaching of

TABLE 9.2

COMPARISON OF ACTIVITY RATIOS OF $^{234}\text{U}/^{238}\text{U}$, $^{226}\text{Ra}/^{238}\text{U}$ AND $^{210}\text{Pb}/^{238}\text{U}$ IN
WASTE ROCK LEACHATES AFTER 40 DAYS OF EQUILIBRATION

FRESH OR USED GRAINS	ROCK TYPE	TYPE OF GRAIN SURFACE	TYPE OF EQUILIBRATING SOLUTION	$^{234}\text{U}/^{238}\text{U}$ A.R.	$^{226}\text{Ra}/^{238}\text{U}$ A.R.	$^{210}\text{Pb}/^{238}\text{U}$ A.R.
FRESH	PEGMATITE & GABBRO	UNWEATHERED	WATER	1.02±0.08	0.21±0.07	0.31±0.05
FRESH	PEGMATITE	UNWEATHERED	WATER	1.43±0.14	1.29±0.24	0.54±0.16
USED	PEGMATITE	UNWEATHERED	WATER	1.32±0.16	0.99±0.15	0.53±0.09
FRESH	PEGMATITE	WEATHERED	WATER	0.92±0.08	0.61±0.12	0.87±0.10
USED	PEGMATITE	WEATHERED	WATER	1.16±0.06	0.74±0.08	0.74±0.06
FRESH	PEGMATITE & GABBRO	UNWEATHERED	pH3 H ₂ SO ₄	0.85±0.03	0.29±0.02	0.17±0.01
FRESH	PEGMATITE	UNWEATHERED	pH3 H ₂ SO ₄	0.94±0.07	0.53±0.03	0.53±0.03
USED	PEGMATITE	UNWEATHERED	pH3 H ₂ SO ₄	0.86±0.05	0.27±0.02	0.23±0.01
FRESH	PEGMATITE	WEATHERED	pH3 H ₂ SO ₄	0.78±0.03	0.35±0.01	0.42±0.01
USED	PEGMATITE	WEATHERED	pH3 H ₂ SO ₄	0.80±0.03	0.38±0.02	0.25±0.01

pegmatite with pH3 H_2SO_4 , at 0.86, 0.27 and 0.23, respectively. The latter leachate composition is found to be similar to that of the pH 3.4-3.7 sulphate groundwater at site L in Figure 9.2.

Leachates from the 're-extracted' grains in Table 9.2 show lower activity ratios of $^{234}\text{U}/^{238}\text{U}$, $^{226}\text{Ra}/^{238}\text{U}$ and $^{210}\text{Pb}/^{238}\text{U}$ than those corresponding values from the leaching of fresh grains. This can be explained on the basis of the removal of the loosely-held ^{234}U , ^{226}Ra and ^{210}Pb atoms from the surfaces of the rock grains in the first extraction. A similar decreasing trend in the $^{234}\text{U}/^{238}\text{U}$ A.R.'s with increase in the fractional extraction of uranium ore has been observed by Umemoto (1973). Umemoto found the activity ratios to decrease from 1.357 to values as low as 0.886. The higher $^{234}\text{U}/^{238}\text{U}$ A.R. in the first extraction was explained by Umemoto as due to the easily extractable recoiled ^{234}U atoms in the crystal lattices.

The activity ratios of $^{234}\text{U}/^{238}\text{U}$ and $^{226}\text{Ra}/^{238}\text{U}$ in leachates from the leaching of unweathered grain surfaces are shown to be higher than those values in leachates from the leaching of weathered grain surfaces (Table 9.2).

The discussion of the results has been centered so far on the activity ratio compositions in pegmatite leachates only. The results of the leaching of the pegmatite-gabbro mixture (50:50) show lower activity ratios of $^{234}\text{U}/^{238}\text{U}$, $^{226}\text{Ra}/^{238}\text{U}$ and $^{210}\text{Pb}/^{238}\text{U}$ in the leachates than those values that have been attained in the pegmatite leachates for each type of equilibrating solutions used (Table 9.2).

9.3 Evaluation of the ^{234}U Fractionation in Groundwater

Several hypothesis have been put forward to explain the observed ^{234}U fractionation in groundwater from its parent, ^{238}U . These hypotheses are listed as follows:

- 1) Physical ejection of recoil ^{234}Th from the decay of ^{238}U atoms in uranium minerals that have precipitated within the reduced zone of the sand aquifer over geological time.

- 2) Mixing with older groundwater at depth that contains an excess of ^{234}U atoms and originates from the bedrock via bedrock springs.
- 3) Preferential leaching of ^{234}U atoms from waste rock under surficial weathering conditions.
- 4) Preferential leaching of ^{234}U atoms from waste rock and preferential migration of the released ^{234}U atoms in the sand aquifer.

Each of these hypotheses is discussed below.

The first hypothesis is similar to that which is proposed by Kronfeld (1974) and Cowart and Osmond (1974) for old groundwater in deep confined aquifers. These investigators found that, in regional aquifers, the change in the uranium isotopic activity ratio generally occurs across an oxidation-reduction barrier zone which has accumulated ^{234}U and ^{238}U atoms over geological times (e.g. over a million years). Kronfeld (1974) suggested that the excess ^{234}U atoms in such deep groundwater resulted from the decay of ^{234}Th atoms, as produced from the entrapped ^{238}U atoms in the reduced zone. This hypothesis cannot be applied to the distribution of the $^{234}\text{U}/^{238}\text{U}$ A.R.'s in the sand aquifer at Greyhawk because of the young age of the groundwater.

The second hypothesis involves the mixing of two types of groundwater, namely: (1) young recharge water with an activity ratio of $^{234}\text{U}/^{238}\text{U}$ near unity and (2) older groundwater that has migrated along the bedrock fractures, has interacted with the uranium ore minerals and has discharged into the sand aquifer via bedrock springs with a $^{234}\text{U}/^{238}\text{U}$ activity ratio greater than 2.0. The hypothesis, however, is not applicable to the present study either. The reasons being: (1) that the highest $^{234}\text{U}/^{238}\text{U}$ A.R.'s in groundwater occur in the middle of the sand aquifer and not near the bedrock surface and (2) tritium indicates that the deep groundwater with the moderately-high $^{234}\text{U}/^{238}\text{U}$ A.R.'s near the bedrock surface at sites M5, M6 and M7 is of recent origin (Chapter 4).

From the evaluation of the results of the leaching experiments in Table 9.2, the third hypothesis only partially explains the ^{234}U fractionation in groundwater. For example, the maximum $^{234}\text{U}/^{238}\text{U}$ A.R. that is found in the leachates from the rock leaching experiments is 1.43 ± 0.14 .

The fourth hypothesis that is described below, concerns the preferential leaching of the ^{234}U atoms from the waste rock and the preferential migration of the released ^{234}U atoms in groundwater. Prior to 1957, the composition of the mined ore from the bedrock contained uranium in different oxidation states, namely 33% ^{234}U (VI) (decay-generated), 67% ^{234}U (IV) and 100% ^{238}U (IV) atoms (Kolodny and Kaplan, 1970; Chalov and Merkulova, 1969). As mining operations began in 1957, waste rock deficient in uranium ore was dumped on the sand deposit. As weathering released trace amounts of uranium from the waste rock during the period of 1957 to 1982, a percentage of the ^{238}U (IV) and ^{234}U (IV) atoms was oxidized to the hexavalent state through the action of oxygen, bacteria and ferric sulphate (Lungren and Silver, 1980; Ritcey and Silver, 1982). During this time, the ^{234}U and ^{238}U atoms, in different proportions of the tetra- and hexavalent oxidation states, were leached from the waste rock. The ^{234}U atoms were preferentially leached earlier than the ^{238}U atoms from the waste rock during the initial period of weathering with rainwater. This resulted in a $^{234}\text{U}/^{238}\text{U}$ A.R. = 1.43 in the waste-rock-derived leachate (refer to Chapter 6). When pyrite oxidation later became intensive in the weathering history of the waste rock mass, the amounts of extractable ^{234}U atoms in the resulting low pH leachate became slightly less than that of the extractable ^{238}U atoms with $^{234}\text{U}/^{238}\text{U}$ A.R.'s = 0.86 - 0.94 (refer to Chapter 6). Since 1957, the ^{234}U contaminant species released in groundwater below the waste rock has preferentially migrated faster in the sand aquifer than that of the released ^{238}U contaminant species. The reasons are because of a larger percentage of the released ^{234}U atoms has been in the more mobile hexavalent state than that of the released ^{238}U atoms and because of the lower K_d values for the U(VI) species than those for the U(IV) species in the porous medium. Furthermore, the simulated ^{238}U activities in groundwater along the L-M10 flow line following the cell model application in Chapter 8 had also indicated a higher mobility for the U(VI) species rather than that for the U(IV) species.

The additional assumptions that must be considered for the fourth hypothesis are: (1) the presence of a closed system in the sand aquifer, where the only source of uranium in groundwater is derived from the leaching of the waste rock piles adjacent to the uranium mine under surficial conditions and

(2) isotopic exchange between the tetra- and hexavalent oxidation states of the ^{234}U and ^{238}U species is very slow in groundwater.

The fourth hypothesis is examined in the framework of the cell model. The cell model is used to test this hypothesis by simulating the 1982 distribution of $^{234}\text{U}/^{238}\text{U}$ A.R.'s in the sand aquifer along the L-M10 flowline at various percentages of ^{234}U and ^{238}U in the tetra- and hexavalent states. An agreement between the simulated and analytical $^{234}\text{U}/^{238}\text{U}$ A.R. distributions in groundwater would provide information on the 1982 composition of the ^{238}U and ^{234}U species in the (IV) and (VI) oxidation states at site L for the testing of this thesis. Site L had previously been selected in Chapter 8 as the point source of contamination from the waste rock. All of the above assumptions made in the fourth hypothesis are included in this application of the cell model.

Computations of the $^{234}\text{U}(\text{VI})$, $^{234}\text{U}(\text{IV})$, $^{238}\text{U}(\text{VI})$ and $^{238}\text{U}(\text{IV})$ species in groundwater at 25 years in each of the 13 cells along the L-M10 flow line (Figure 8.10) are made by varying the percentages (0 to 100%) of the tetravalent uranium atoms at site L that have been oxidized to U(VI) since 1957. The starting percentages of the original $^{234}\text{U}(\text{IV})$ and $^{238}\text{U}(\text{IV})$ atoms in the rock at site L prior to oxidation are 67% and 100% respectively. Simulated activity ratios of $^{234}\text{U}/^{238}\text{U}$ in groundwater downflow from site L are derived from the computed activities of the $^{234}\text{U}(\text{VI})$, $^{234}\text{U}(\text{IV})$, $^{238}\text{U}(\text{VI})$ and $^{238}\text{U}(\text{IV})$ species using the cell model. The simulated $^{234}\text{U}/^{238}\text{U}$ A.R.'s at 25 years are compared to the analytical $^{234}\text{U}/^{238}\text{U}$ A.R.'s in groundwater in Figure 9.3 as longitudinal profiles along the L-M10 flowline. Longitudinal profiles for the simulated A.R.'s and the analytical A.R.'s in groundwater in Figure 9.3 are similar if it is assumed that 30% of the original tetravalent ^{234}U and ^{238}U atoms prior to 1957 have been oxidized to U(VI) during the weathering process. From these results, the distribution of the uranium species in groundwater at site L is 53% as $^{234}\text{U}(\text{VI})$, 47% as $^{234}\text{U}(\text{IV})$, 30% as $^{238}\text{U}(\text{VI})$ and 70% as $^{238}\text{U}(\text{IV})$. Therefore, because a larger amount of the ^{234}U atoms is in the hexavalent state in the contaminated groundwater than that of the ^{238}U atoms and because of the lower K_d values

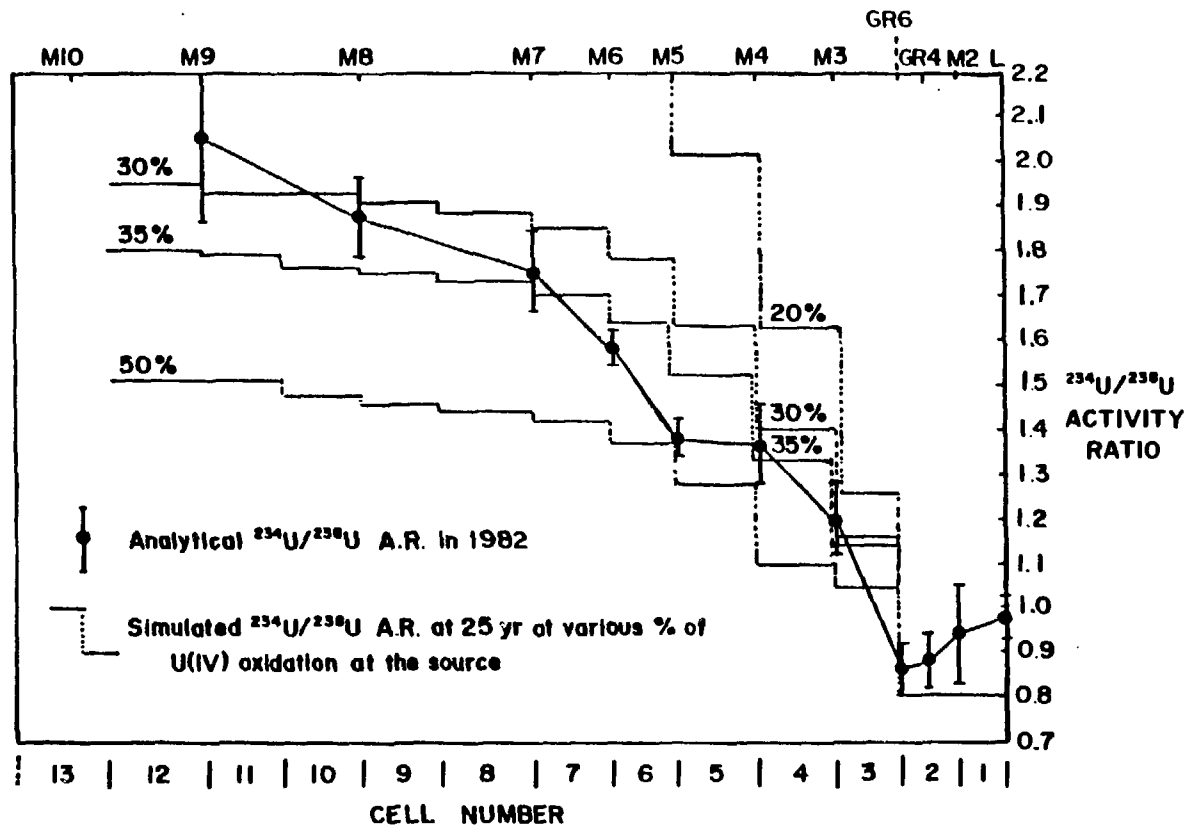


Figure 9.3 Longitudinal profiles of simulated and analytical activity ratios (A.R.) of $^{234}\text{U}/^{238}\text{U}$ in groundwater along the L-M10 flowline. Error bars are incorporated for each analytical $^{234}\text{U}/^{238}\text{U}$ A.R. value. For the simulations, the following assumptions were made: (1) 33% original ^{234}U atoms in waste rock prior to weathering were in the U(VI) state (Kolodny and Kaplan, 1970); (2) the ^{234}U (IV) and ^{238}U (IV) atoms in waste rock were partially oxidized from 1957 to 1982 and (3) the point source of ^{234}U (IV), ^{234}U (VI), ^{238}U (IV) and ^{238}U (VI) contamination from waste rock in groundwater is located at site L.

for U(VI) species than U(IV) species in the porous medium, the preferential leaching of the ^{234}U atoms from the waste rock and the preferential migration of the released ^{234}U atoms in groundwater explain for the progressive increase in the $^{234}\text{U}/^{238}\text{U}$ A.R.'s in the sand aquifer downflow from the waste rock.

In conclusion, the cell model has been proven successful in the explanation of the ^{234}U fractionation in groundwater downflow from the waste rock. Uranium-234 fractionation is found to have been caused by differences in the distribution of the oxidation states of the ^{234}U and ^{238}U atoms in the contaminated groundwater. The successful application of batch K_d values of the U(VI) and U(IV) species in the cell model for the evaluation of ^{234}U fractionation indicates another example where laboratory-determined parameters are suitable for simulating the mobilities of radionuclides in groundwater.

The activity ratios of $^{234}\text{U}/^{238}\text{U}$ in the sand aquifer have also been considered to be good parameters for investigating contaminant migration at the site. The trends from the distribution of the $^{234}\text{U}/^{238}\text{U}$ A.R.'s in groundwater were useful in the confirmation of the uranium migration patterns in the sand aquifer. The direction of increasing $^{234}\text{U}/^{238}\text{U}$ A.R.'s in the young groundwater downgradient from the waste rock was found to coincide with the general direction of groundwater flow.

CHAPTER 10

SUMMARY AND CONCLUSIONS

- (1) A method for the sequential elemental separation of ^{238}U , ^{234}U , ^{232}Th , ^{230}Th , ^{226}Ra and ^{210}Pb in a single sample of water, soil or rock and the subsequent determination of the activity for each of the mentioned radionuclides was developed. For the determination of ^{238}U , ^{234}U , ^{232}Th , ^{230}Th , ^{226}Ra and ^{210}Pb in groundwater by this method, the relative error is less than 10% for activities greater than 20 pCi/l and the coefficient of variation at the 95% confidence level is less than 20% for activities greater than 2 pCi/l. The detection limits for the analyses of these radionuclides are 0.1 pCi for ^{238}U , ^{234}U , ^{232}Th and ^{230}Th and 0.5 pCi for ^{226}Ra and ^{210}Pb . In conclusion, this particular method provides good precision, accuracy and sensitivity for the determination of the radionuclides of interest in environmental samples.
- (2) A field site was chosen for this study at the abandoned Greyhawk uranium-mine site near Bancroft, Ontario, where accumulated piles of waste rock with low-grade uranium ore ($<0.01\%$ U_3O_8) were left on a bedrock outcrop and a sand aquifer from the 1956 to 1959 mining period. During this mining period at Greyhawk, the high-grade uranium ore was removed to a nearby-processing facility. The waste rock and the high-grade uranium ore were mined from a large intrusive batholith of Precambrian age, i.e. between 0.9 to 1.2 billion years. The waste rock contains two rock types, namely: (1) pegmatite, which contains silicate minerals and uranium and thorium minerals and (2) gabbro, which contains negligible amounts of uranium and thorium minerals and largely silicate, carbonate and pyrite minerals. The sand aquifer at the field site, with a surficial area of approximately 2.0 hectares, is believed to be glacial fluvial in origin. The depth to bedrock surface in the sand aquifer increases rapidly with distance from the bedrock outcrop, i.e. in excess of 21m at a distance of 60m from the outcrop. Recharge water enters the sand aquifer from the area of the waste rock and bedrock outcrop and moves laterally in the sand aquifer to a nearby swamp about 125m away.

- (3) Good agreement between groundwater velocity values determined by three independent methods in the sand aquifer was found. The groundwater velocity is about 70 m/yr below the waste rock along the NW flow regime and about 10 m/yr below the waste rock along the NE flow regime. The velocity decreases to less than 2 m/yr towards the swamp in the south. The arithmetic and geometric means of the hydraulic conductivity of the sand, as estimated from these three methods, are 1.6×10^{-3} cm/s.
- (4) The four year hydrogeological and radiological investigations (1978 to 1982) identified the present-day spread of chemical and radionuclide contaminants derived from the waste rock in groundwater in the sand aquifer. Contaminant plumes of sulphate, bicarbonate, DIC, ^{226}Ra , ^{210}Pb , ^{238}U and ^{234}U extending from the waste rock piles in the sand aquifer were delineated. The shapes of the waste-rock-derived contaminant plumes follow the general direction of groundwater flow in the sand aquifer. The maximum extent of groundwater contamination, based on elevated concentrations of sulphate, bicarbonate and DIC, was found to extend approximately 100 to 125 meters laterally downflow from the piles of waste rock. The lateral extent of contamination of ^{238}U in groundwater was about 80 meters downflow from the waste rock, whereas the lateral extent of contamination of ^{226}Ra , ^{210}Pb , ^{230}Th and ^{232}Th in groundwater was less than 20 meters. The calculated ^{238}U , ^{226}Ra , ^{210}Pb and ^{230}Th velocities in the aquifer, based on the observed frontal positions and an estimated 25-year migration period, are 3.2 m/yr, 0.8 m/yr, 0.12 m/yr, and 0.04 m/yr, respectively. These results are site specific. To our knowledge, there are no other cases of radionuclide migration from waste rock reported in the literature to which these results can be compared.
- (5) The release of radionuclides from the waste rock was investigated from the pegmatite leaching experiments. The factors that were found to affect the release of radionuclides are: (1) weathered and unweathered rock surfaces; (2) number of repeated extractions from the same rock grains; (3) active surface area of rock grains; (4) solid-liquid ratio; (5) pH of the extractant; and (6) sulphate ion concentration in the extractant. Of these six factors, the pH of the extractant is considered to be the most

important factor because of the related solubility-controlled effects. The unknown but probably complex interactions of these factors on the groundwater composition below the waste rock for the past 25 years caused simulations of the 1982 frontal positions of the waste-rock-derived radionuclide species in the sand aquifer to have considerable uncertainty.

- (6) A geochemical model was developed to represent the effects of a sequence of stages responsible for the observed activity distributions of radionuclides in groundwater, namely: (1) the infiltration of the waste rock by rainwater and snowmelt, (2) the weathering of pyrite, carbonates, silicates, uraninite and uranothorite in the waste rock mass; and (3) the migration of the waste-rock-derived contaminants in the sand aquifer. In the second stage, the production of hydrogen and sulphate ions from pyrite oxidation increases the solubility of uraninite and uranothorite. This results in the release of high activities of radionuclides in the low-pH leachate. In the third stage, the acidic, radioactive leachate enters the sand aquifer below the waste rock. The leachate contains ions, ion pairs and complexes, such as UO_2SO_4^0 , UO_2^{2+} , $\text{U}(\text{OH})_3^+$, $\text{U}(\text{SO}_4)_2^0$, $\text{Th}(\text{SO}_4)_2^0$, Ra^{2+} , RaSO_4^0 , Pb^{2+} and PbSO_4^0 . The subsurface migration of these species in the sand aquifer is strongly influenced by geochemical processes, such as complexation reactions, adsorption-desorption reactions, precipitation reactions and acid-base reactions. As the groundwater pH increases downgradient from the waste rock, the uranium species form anionic complexes, $\text{UO}_2(\text{CO}_3)_2^{2-}$ and $\text{U}(\text{OH})_5^-$, that are stable and mobile in the aquifer, whereas the radium, lead and thorium species are largely retarded by the sand properties. The major retardation process for uranium, radium and lead in the aquifer is by adsorption. Thorium is retarded in the aquifer by both adsorption and precipitation processes.

- (7) Laboratory-determined parameters from the waste rock leaching experiments and radionuclide partitioning experiments were incorporated in two contaminant transport models to provide simulations of the movement of the waste-rock-derived radionuclides in groundwater along the NW and NE flow regimes for the past 25 years. The two models used are the simple advection-retardation model and a one-dimensional cell model. The

advection-retardation model was used for simulations along the NE flow regime where the groundwater chemistry and velocity have little variability. The results indicated that the simulated frontal positions for ^{226}Ra , ^{210}Pb and ^{230}Th are similar to the 1982 frontal positions observed in the field. The simulated frontal positions for $^{238}\text{U}(\text{IV})$ and $^{238}\text{U}(\text{VI})$ were both found to be approximately a factor of ten less than the ^{238}U front observed in the field in 1982.

The cell model was used for the simulations in the NW sector of the field site where the groundwater chemistry and velocity are non-uniform along the flow regime. The simulated ^{226}Ra , ^{210}Pb and ^{230}Th activity distributions in groundwater downflow from the waste rock for a 25-year period provided good agreement with the field activity distributions in 1982. For the case of ^{238}U , good agreement between the simulated and analytical activity distributions was found at approximately 20 meters downflow from the source. Further downflow, the agreement for the ^{238}U case was poor. The $^{238}\text{U}(\text{VI})$ species in groundwater was found from the simulations using the cell model to migrate ahead of the $^{238}\text{U}(\text{IV})$ species.

With the possible exception of $^{238}\text{U}(\text{IV})$ and $^{238}\text{U}(\text{VI})$, the laboratory-determined values were found to provide reasonable results in the two contaminant transport models for the simulations of the $^{226}\text{Ra}(\text{II})$, $^{210}\text{Pb}(\text{II})$ and $^{230}\text{Th}(\text{IV})$ mobilities in the sand aquifer.

- (8) Radium-226 is the only radioactive contaminant species in the sand aquifer that had been found from this investigation to exceed the drinking water standards. A prediction using the cell model on the extent of ^{226}Ra contamination in the sand aquifer up to the year 1988 indicated that no appreciable changes in the 1982 migration patterns for ^{226}Ra will occur because ^{226}Ra is so readily adsorbed in the sand. The long-term impact of ^{226}Ra contamination in the sand aquifer was assessed by predictions using the advection-retardation model for the maximum extent of travel at 100, 1000 and 250,000 years from 1982. The respective travel distances for ^{226}Ra from the waste rock at these times were calculated at 40 meters, 41 meters and 126 meters. In these calculations, it was assumed that the acid front in the aquifer will be neutralized by the year

2082. The ^{226}Ra activity in groundwater corresponding to the latter frontal position, which reaches the swamp after 250,000 years, has been calculated to decay to less than one pCi/l. Therefore, according to the evaluations made using the transport models, long-term surveillance of the uranium-mine waste rock dump site at Greyhawk will probably not be necessary as long as the waste rock and aquifer are not significantly altered by man's activities.

- (9) The 1982 spatial distributions of the $^{234}\text{U}/^{238}\text{U}$, $^{226}\text{Ra}/^{238}\text{U}$ and $^{210}\text{Pb}/^{238}\text{U}$ activity ratios in groundwater indicated disequilibrium conditions between ^{238}U and each of its daughters downgradient from the waste rock. The trends from the distribution of the $^{234}\text{U}/^{238}\text{U}$ activity ratios in groundwater were useful in the confirmation of the uranium migration patterns in the sand aquifer. This suggests that the activity ratios of $^{234}\text{U}/^{238}\text{U}$ may be used to assist in the identification of migration patterns of contaminants emanating from other waste rock dump sites.

To our knowledge, all other field cases concerning large changes in the $^{234}\text{U}/^{238}\text{U}$ activity ratios in the literature pertain to large regional aquifers where sampling points are kilometers apart. Our investigation establishes that it is possible for moderately-large changes in the $^{234}\text{U}/^{238}\text{U}$ activity ratios to occur over short distances in a shallow aquifer.

The fractionations of ^{226}Ra and ^{210}Pb from ^{238}U in groundwater downflow from the waste rock were explained by geochemical processes. The ^{234}U fractionation from ^{238}U in groundwater was attributed to the presumed existence of ^{234}U and ^{238}U in differing amounts in two oxidation states, namely, (IV) and (VI). This hypothesis was supported by the results of the cell model. The model provided a good representation of the field data for the case where the 1982 percentage distribution of the uranium redox species in groundwater at the source contained 53% as ^{234}U (VI), 47% as ^{234}U (IV), 30% as ^{238}U (VI) and 70% as ^{238}U (IV). Because of the larger amount of the ^{234}U atoms in the hexavalent state in groundwater and because of the lower K_d values for the U(VI) species in the porous medium, it was concluded that the preferential leaching of the

^{234}U atoms from the waste rock and the preferential migration of the released ^{234}U atoms in groundwater, resulted in the observed uranium isotopic ratio distribution in the sand aquifer.

The application of batch K_d values of U(VI) and U(IV) in the cell model for the evaluation of the ^{234}U fractionation in the sand aquifer is another indication of the applicability of laboratory-determined parameters for simulating the mobilities of radionuclides in sand aquifers.

- 10) The findings of this investigation are site-specific. Studies have not been made to determine the applicability of the results to other uranium waste-rock dump sites. The hydrogeological conditions at the Greyhawk site are relatively devoid of complexities in comparison to the conditions at many uranium mine sites.

The Greyhawk findings, however, lead to some expectations regarding the importance of various factors on radionuclide release and migration in groundwater at other waste-rock sites. For example, it is reasonable to expect that the evolution of the pH of water infiltrating through waste rock at other sites is an important factor influencing the levels to which the radionuclide concentrations rise in the leachate and the mobilities of radionuclides in groundwater. The prediction of radionuclide mobility is therefore intimately related to measurements or predictions of leachate and groundwater pH. With the exception of uranium, the findings of this study are encouraging with regard to the usefulness of laboratory-determined parameters and geochemical equilibrium models for indicating at pH levels between 5-7 strong retardation of radionuclides in shallow aerobic sand aquifers, and at much lower pH levels much less retardation. The methods used for determining the groundwater velocity in the sand aquifer at the Greyhawk site are those applicable to other waste-rock sites in sand aquifers, although in a more complex aquifer system more disagreement between velocity results would be expected.

REFERENCES

- Adams, J.A.S., Osmond, J.K. and Rogers, J.J.W. 1959. The geochemistry of thorium and uranium. In: *Physics and Chemistry of the Earth* (eds. Ahrens, L.H., Press, F., Rankama, K. and Runcorn, S.K.) pp. 298-348. Pergamon Press.
- Adams, J.A.S. and Richardson, K.A. 1960. Thorium, uranium and zirconium concentrations in bauxite. *Econ. Geol.* 55, p. 1653.
- Adams, J.A.S. and Weaver, C.E. 1958. Thorium-to-uranium ratios as indicators of sedimentary processes. An example of geochemical facies. *Bull. Amer. Assoc. Petrol. Geol.* 42, p. 387.
- Ahrland, S., Liljenzén, J.O. and Rydberg, J. 1973. Solution chemistry of the actinides. In: *Comprehensive Inorganic Chemistry*, Vol. 5. Actinides pp. 465-635. Pergamon Press.
- Allard, B. 1982. Solubilities of actinides in neutral or basic solutions. In: *Actinides in Perspective* (ed. Edelstein, N.M.) pp. 553-580, Pergamon Press.
- Ames, L.L. and Rai, D. 1978. Processes influencing radionuclide mobility and retention. In: *Radionuclide Interactions with Soil and Rock Media*. U.S. Environmental Protection Agency Vol 1, pp. 1-242.
- Andreyev, P.F. and Chumachenko, A.P. 1964. Reduction of uranium by natural organic substances. *Geochem. Intl.* 1, 3-7.
- Asikainen, M. 1981. State of disequilibrium between ^{238}U , ^{234}U , ^{226}Ra and ^{222}Rn in groundwater from bedrock. *Geochim. Cosmochim. Acta.* 45, 201-206.
- Baes, C.F., Jr. and Mesmer, R.E. 1976. *The Hydrolysis of Cations*. Wiley-Interscience.
- Baetsle, L.H. 1967. Computational methods for the prediction of underground movement of radionuclides. *Journal of Nuclear Safety.* 8, 576-588.
- 1969. Migration of radionuclides in porous media. In: *Health Physics* (ed. Duhamel, A.M.F.) Vol. 2. pt. 1. pp. 707-730. Pergamon Press.
- Ball, J.W., Jenne, E.A. and Nordstrom, D.K. 1978. WATEQ2 - A computerized chemical model for trace and major element speciation and mineral equilibria of natural waters. In: *Chemical Modelling in Aqueous Systems*: American Chemical Society Symposium Series 93. (ed. Jenne, E.A.) pp. 815-835.
- 1979. Additional and revised thermochemical data and computer code for WATEQ2. U.S. Geol. Surv. Water Res. Invest. 78-116. 109 pp.

- Banks, R.B. 1974. A mixing cell model for longitudinal dispersion in open channels. *Water Resour. Res.* 10, 357-358.
- Baturin, G.N. and Kochenov, A.V. 1969. Migration of uranium in rivers and the time of its presence in waters of the world ocean, of seas and lakes. *Geokhimiya* 6, 715-723.
- Bell, K.G., Goodman, C. and Whitehead, W.L. 1940. Radioactivity of sedimentary rocks and associated petroleum. *Bull. Am. Assoc. Petroleum Geol.* 24, 1529.
- Bernat, M. and Goldberg, E.D. 1969. Thorium isotopes in marine environment. *Earth Planet Sci. Lett.* 5, 308-312.
- Billings, G.K. 1962. A geochemical investigation of the Valley Spring Gneiss and Packsaddle Schist, Llano Uplift, Texas. *Texas Jour. Sci.* 9, p. 328.
- Blair, R.D., Cherry, J.A., Lim, T.P. and Vivyurka, A.J. 1980. Groundwater monitoring and contaminant occurrence at an abandoned tailings area, Elliot Lake, Ontario. In: *Proceedings of the First International Conference on Uranium Mine Waste Disposal*, Vancouver: Society of Mining Engineers of the American Institute of Mining Engineers. pp. 411-444.
- Brown, R.M. 1961. Hydrology of tritium in the Ottawa Valley. *Geochim. Cosmochim. Acta* 21, 199-216.
- Carberry, J.J. and Bretton, R.H. 1958. Axial dispersion of mass in flow through fixed beds. *Soc. Pet. Eng. Jour.* 4, 367-375.
- Chalov, P.I. and Merkulova, K.I. 1969. Possibility of controlled separation of ^{234}U and ^{238}U by external oxidation of uranium in minerals. *Geochem. Intl.* 6, 159-162.
- Chamberlain, J.A. 1964. Hydrogeochemistry of uranium in the Bancroft-Haliburton region, Ontario *Geol. Surv. Can. Bull.* 1030F 19 pp.
- Cherdyntsev, V.V., Chalov, P.I. and Khaidarov, G.Z. 1955. Transactions of the 3rd Session of the Committee for Determination of Absolute Ages of Geological Formations. *Izv. Akad. Nauk. SSSR.*
- Cherdyntsev, V.V. 1971. Uranium-234. *Israel Program for Scientific Translations.*
- Cherry, J.A., Blackport, R.A., Dubrovsky, N., Gillham, R.W., Lim, T.P., Murray, D., Reardon, E.J. and Smyth, D.J.A. 1980. Subsurface hydrology and geochemical evolution of inactive pyrite tailings in the Elliot Lake Uranium District, Canada. In: *Proceedings of the Third Symposium on Uranium Tailings Management*, Colorado State University.
- Clark, S.P. Jr., Peterman, Z.E. and Heier, K.S. 1966. Abundances of uranium, thorium and potassium. In: *Handbook of Physical Constants*: Geol. Soc. Am. Mem. 97.

- Clarke, W.S. 1980. Private communication, Re: slug tests at Greyhawk in summer 1980.
- _____. 1980. Radium transport through a granular geologic porous medium
Unpublished M.Sc. report. University of Waterloo.
- Cleary, R.W. 1978. Analytical models for groundwater pollution and hydrology:
Princeton University, Water Resources Program Report No. 78-WR-15.
- Cowart, J.B. and Osmond, J.K. 1974. ^{234}U and ^{238}U in the Carrizo Sandstone
Aquifer of South Texas. In: Isotope Techniques in Groundwater Hydrology,
Vol. 2. Intl. Atomic Energy Agency, Vienna, pp. 16-60.
- _____. 1977. Uranium isotopes in groundwater; their use in prospecting for
sandstone-type uranium deposits. Jour. of Geochem. Expl. 8, 365-379.
- Cowart, J.B., Kaufman, M.I. and Osmond, J.K. 1978. Uranium variations in ground-
water of the Floridan Aquifer and Boulder zone of South Florida. Jour. of
Hydrol. 36, 161-172.
- Dance, J.T. and Reardon, E.J. 1980. Cation migration in the dispersion test.
In: Hydrogeological Studies of a Sandy Aquifer at an Abandoned Landfill.
Dept. of Supply and Services. Contract No. OSU78-00195, 39 pp.
- Davis, G.L. 1947. Radium content of ultramafic igneous rocks. Am. Jour. of Sc.
245, 677.
- Dement'yev, V.S. and Syromyatnikov, N.G. 1965. Mode of occurrence of thorium
isotopes in groundwater. Geokhimiya 2, 211-218.
- Dement'yev, V.S. and Syromyatnikov, N.G. 1968. Conditions of formation of a
sorption barrier to the migration of uranium in an oxidizing environment.
Geochem. Intl, 5, 394-400.
- Dooley, J.R. Jr., Granger, H.C. and Rosholt, J.N. 1966. Uranium-234
fractionation in the sandstone-type uranium deposit of the Ambrosia Lake
District, New Mexico. Econ. Geol. 61, 1362-1382.
- Drozдовskaya, A.A. and Melnik, Y.P. 1968. New experimental and calculated data
on the migration of thorium under supergene conditions. Geokhimiya 4,
151-167.
- Duram, W.H., Hem, J.D. and Heidel, S.G. 1971. Reconnaissance of selected minor
elements in surface waters of U.S. USGS Circ. 643.
- Evans, R.D. and Goodman, C. 1941. Radioactivity of rocks. Bull. Geol. Soc. Am.
52, 459.
- Fairbridge, R.W. 1972. Encyclopedia of Geochemistry and Environmental Sciences:
Encyclopedia of Earth Sciences Series. Vol. IVA. Van Nostrand Reinhold.
1321 pp.

- Feldman, I. 1975. The colloidal nature of radionuclides in seawater In: Environmental Toxicity of Aquatic Radionuclides (eds. Miller, M.W. and Stannard, J.N.) Ann Arbor Science Publishers. pp. 183-190.
- Fix, P.G. 1956. Hydrochemical exploration for uranium. U.S. Geol. Survey Prof. Paper 300, 667-671.
- Fleischer, R.L. 1980. Isotopic disequilibrium of uranium: alpha-recoil damage and preferential solution effects. Science 207, 979-981.
- Fleischer, R.L. and Raabe, O.G. 1978. Recoiling alpha-emitting nuclei: mechanisms for uranium-series disequilibrium. Geochim. Cosmochim. Acta 42, 973-978.
- Freeze, R. and Cherry, J.A. 1979. Groundwater. Prentice Hall Inc. 604 pp.
- Fuger, J. and Oetting, F.L. 1976. The chemical thermodynamics of actinide elements and compounds. In: The Actinide Aqueous Ions Vol. II. Intl. Atomic Energy Agency, Vienna, pp. 16-60.
- Fung, P.C. Bird, G.W., Sanipelli, G.C. and Lopata, V.J. 1980. Aspects of feldspar dissolution. Nucl. Tech. 51, p. 188.
- Garrels, R.M. and Christ, C.L. 1959. Behaviour of uranium minerals during oxidation. In: Geochemistry and Mineralogy of the Colorado Plateau Uranium Ores (eds. Garrels, R.M. and Larsen, E.S.). Geol. Surv. Prof. Paper 320. pp 81-89.
- Gera, F. 1975. Geochemical behaviour of long-lived radioactive wastes. Oak Ridge National Laboratory. Contract No. W-7405-eng.-26. 77 pp.
- Gibson, W.M. 1961. The radiochemistry of lead. National Research Council. Washington, D.C. 158 pp.
- Gillham, R.W., Cherry, J.A. and Sharma, H.D. 1978. Survey to locate potential field sites for the study of radium migration in groundwater. WRI Report, University of Waterloo, Waterloo, Ontario.
- Gillham, R.W., Cherry, J.A., Sharma, H.D. and Veska, E. 1979. An evaluation of the Greyhawk mine area for conducting detailed investigations of the migration of radium-226 and associated contaminants in unconsolidated geological materials. WRI 704-02-02. University of Waterloo.
- Gillham, R.W., Sharma, H.D., Reddy, M.R., Cooper, E.L. and Cherry, J.A. 1981. Barium and radium migration in unconsolidated Canadian geological materials. Atomic Energy Control Board.
- Gillham, R.W. and Cherry, J.A. 1982. Contaminant transport by groundwater in non-indurated deposits. In: Recent Trends in Hydrogeology (ed. Narisimhan, T.N.) Geol. Soc. Amer. Spec. Publ.
- Goleva, G.A., Polyakov, V.A. and Nechayeva, T.P. 1970. Distribution and migration of lead in groundwaters. Geochem. Intl. 7, 256-268.

- Golubev, V.S. and Garibyants, A.A. 1971. Heterogeneous processes of geochemical migration: Consultants Bureau (trans. from Russian).
- Grandstaff, D.E. 1974. Kinetics of uraninite oxidation: Implications for the Precambrian atmosphere, Unpubl. Ph.D. dissertation, Princeton University, 153 pp.
- _____. 1976. A kinetic study of the dissolution of uraninite. *Econ. Geol.* 71(8), 1493-1506.
- Grenthe, I. and Ferri, D. 1981. Actinide species in groundwater systems. In: *Proc. OECD/NEA Workshop on Near-field Phenomena in Geological Repositories for Radioactive Waste*, Seattle (in press).
- Grisak, G.E., Merritt, W.F. and Williams, D.W. 1977. A fluoride borehole dilution apparatus for groundwater velocity measurements. *Can. Geotech. Jour.* 14(4), 554-561.
- Grisak, G.E. and Jackson, R.E. 1978. An appraisal of the hydrogeological processes involved in shallow subsurface radioactive waste management in Canadian terrain. *Inland Waters Directorate. Fisheries and Environment Canada. Scientific Series No. 84.*
- Grove, D. and Wood, W. 1979. Prediction and field verification of subsurface water quality changes during artificial recharge, Lubbock, Texas. *Groundwater* 17(3), 250-257.
- Hancock, R.G.V. 1981. Personal communication, Chief operator at Slowpoke Reactor, University of Toronto.
- Hansen, J.O. and Huntington, G.L. 1969. Thorium movements in morainal soils of the High Sierra, California. *Soil Science.* 108, 257-265.
- Harriss, R.C. and Adams, J.A.S. 1966. Geochemical and mineralogical studies on the weathering of granitic rocks. *Amer. Jour. of Science* 264, 146-173.
- Havlik, B., Grafova, J. and Nycova, B. 1968a. Radium-226 liberation from uranium ore processing mill waste solids and uranium rocks into surface streams - I. *Health Physics.* 14, 417-422.
- Havlik, B., Nycova, B. and Grafova, J. 1968b. Radium-226 liberation from uranium ore processing mill waste solids and uranium rocks into surface streams - II. *Health Physics.* 14, 423-430.
- Health and Welfare Canada, 1978. *Guidelines for Canadian Drinking Water Quality.* Canadian Government Publishing Centre. 79 pp.
- Heier, K.S. and Carter, J.L. 1964. Uranium, thorium and potassium contents in basic rocks and their bearing on the nature of the upper mantle. In: *The Natural Radiation Environment* (eds. Adams, J.A.S. and Lowder, W.M.), p.75
- Heier, K.S. and Rogers, J.J.W. 1963. Radiometric determination of thorium, uranium and potassium in basalts and in two magmatic differentiation series. *Geochem. Cosmochim. Acta.* 27, p. 137.

- Hem, J.D. and Duram, W.H. 1973. Solubility and occurrence of lead in surface water. *Jour. Amer. Water Works Assoc.* 65, 562-568.
- Hewitt, D.F. 1957. Cardiff and Faraday Townships, Ont. Dept. Mines, Map 1957-1.
 _____ 1959. Geology of Cardiff and Faraday Townships. Ont. Dept. Mines, 66th, Ann. Rept. 3.
 _____ 1978. Rocks and minerals of Ontario. Ont. Dept. Mines. Geol. Cir. 13.
- Higgins, G.H. 1959. Evaluation of the groundwater contamination hazard from underground nuclear explosions. *Jour. Geophy. Res.* 64, 1509-1519.
- Horvath, E. 1965. Laboratory examination of certain factors affecting the aqueous leaching of the uranium content of rocks. Part 1. *Atomki Kozlemenyek* 7, 85-94.
- Hussain, N. and Krishnaswami, S. 1980. U-238 series radioactive disequilibrium in groundwaters: implications to the origin of excess U-234 and fate of reactive pollutants. *Geochim. Cosmochim. Acta.* 44. 1287-1291.
- Hvorslev, M.J. 1951. Time lag and soil permeability in groundwater observations. U.S. Army Corps Engrs. Water Ways Exp. Sta. Bull. 36, Vicksburg, Miss.
- Hyde, E.K. 1960. The radiochemistry of thorium. National Research Council. Washington, D.C. 70 pp.
- Irean, M. and Read, R.H. 1981. Low-level activity of radium-226 in water measured with a 3 x 3 inch NaI(Tl) crystal. *Nucl. Instruments and Methods* 179, 389-392.
- Katz, J.J. and Seaborg, G.T. 1957. The Chemistry of the Actinide Elements. John Wiley & Sons Co. Inc. 508 pp.
- Kaufman, M.I. Rydell, H.S. and Osmond, J.K. 1969. $^{234}\text{U}/^{238}\text{U}$ disequilibrium as an aid to hydrologic study of the Floridan Aquifer. *Jour. of Hydrol.* 9, 374-386.
- Kigoshi, K. 1971. Alpha recoil Th-234: Dissolution into water and the $^{234}\text{U}/^{238}\text{U}$ disequilibrium in nature. *Science.* 173, 47-48.
- King, K.S. 1983. Carbon isotope geochemistry of a landfill leachate. M.Sc. thesis. University of Waterloo.
- Kobayaski, Y. and Mandsley, D.V. 1974. Biological Applications of Liquid Scintillation Counting. Academic Press. 196 pp.
- Koczy, F.F. 1956. Geochemistry of the radioactive elements in the ocean. *Deep-Sea Res.* 3, 93-103.
 _____ 1963. The natural radioactive series in organic material. In: Radioecology, Proc. of 1st Nat'l. Symp. Colorado (eds. Schultz, V. and Klement, A.W. Jr.), Reinhold pp. 611-613.

- Kolodny, Y. and Kaplan, I.R. 1970. Uranium isotopes in seafloor phosphorites. *Geochim. Cosmochim. Acta.* 34, 3-24.
- Korkisch, J. 1969. *Modern Methods for the Separation of Rarer Metal Ions.* Pergamon Press.
- Kronfeld, J. and Adams, J.A.S. 1974. Hydrologic investigations of the groundwaters of Central Texas using $^{234}\text{U}/^{238}\text{U}$ disequilibrium. *Jour. of Hydrol.* 22, 77-88.
- Lang, A.H., Griffith, J.W. and Steacy, H.R. 1962. Canadian deposits of uranium and thorium. *Geol. Surv. Can. Econ. Geol. Series No.* 16.
- Langmuir, D. 1978. Uranium solution-mineral equilibria at low temperatures with applications to sedimentary ore deposits. *Geochim. Cosmochim. Acta.* 42, 547-569.
- Langmuir, D. and Herman, J.S. 1980. The mobility of thorium in natural waters at low temperatures. *Geochim. Cosmochim. Acta.* 44, 1753-1766.
- Lemire, R.J. and Tremaine, P.R. 1980. Uranium and plutonium equilibria in aqueous solutions to 200°C. *Jour. Chem. & Engng. Data.* 25, 361-370.
- Levinson, A.A. and Coetzee, G.L. 1978. Implications of disequilibrium in exploration for uranium ores in the surficial environment using radiometric techniques. *Minerals Sci. Engng.* 10(1), 19-27.
- Lundgren, D.G. and Silver, M. 1980. Ore leaching by bacteria. *Ann. Rev. Microbiol.* 34, 263-283.
- Manskaya, S.M., Drozdora, G.V. and Yemel'yanova, M.P. 1956. Fixation of uranium by humic acids and melanoidins. *Geokhimiya*, 4.
- Masuda, K. and Tamamoto, T. 1971. Studies on environmental contamination by uranium 2. Adsorption of uranium on soil and its desorption. *Jour. Rad. Res.* 12(3), 94-99.
- Megumi, K. 1976. Concentrations of uranium series nuclides in soil particles in relation to their sizes. *Jour. Rad. Res.* 17(1) 21-22.
- Moffett, D. and Tellier, M. 1978. Radiological investigations of an abandoned uranium tailings area. *Jour. Environ. Qual.* 7, 310-314.
- Morin, K.A., Cherry, J.A., Lim, T.P. and Vivyurka, A.J. 1982. Contaminant migration in a sand aquifer near an inactive uranium talings impoundment, Elliot Lake, Ontario. *Can. Geotech. Jour.* 19(1).
- Morse, R.H. 1971. Comparison of geochemical prospecting methods using radium with those using radon and uranium. *Geochem. Expl. CIM Spec.* 11, 215-230.
- Moses, A.J. 1963. *Analytical Chemistry of the Actinide Elements.* MacMillan Co. 137 pp.
- Murray, E.G. and Adams, J.A.S. 1958. Amount and distribution of thorium, uranium and potassium in sandstones. *Geochim. Cosmochim. Acta.* 13, p. 260.

- Nathwani, J.S. and Phillips, C.R. 1979. Rate controlling processes in the release of radium-226 from uranium mill tailings. *Water, Air and Soil Pollution*, 11, I and II, 301-317.
- Nishiwaki, Y., Honda, Y., Kimura, Y., Morishima, H., Koga, T., Miyaguchi, Y. and Kawai, H. 1972. Behaviour and distribution of radioactive substances in coastal and estuarial waters. In: *Radioactive Contamination of the Marine Environment*. Intl. Atomic Energy Agency, Vienna, pp. 177-193.
- NRC 1977, *Drinking Water and Health*, National Research Council, Washington, D.C.
- Ogata, A. and Banks, R.B. 1961. A solution of the differential equation of longitudinal dispersion in porous media. *U.S. Geol. Surv. Prof. Paper* 411-A.
- Ontario Water Resources 1965. Radiological water pollution in the Elliot Lake and Bancroft areas. *Ont. Water Res.* 48 pp.
- Osmond, J.K., Rydell, H.S. and Kaufman, M.I. 1968. Uranium disequilibrium in groundwater. An isotopic dilution approach in hydrologic investigations. *Science*. 162, 997-999.
- Osmond, J.K. and Cowart, J.B. 1976. The theory and uses of natural uranium-isotopic variations in hydrology. *Atomic Ener. Rev.* 14(4), 621-679.
- Palei, P.N. 1970. *Analytical Chemistry of Uranium*. Humphrey Science Publ. 421 pp.
- Paquette, J. and Lemire, R.J. 1981. A description of the chemistry of aqueous solutions of uranium and plutonium to 200°C using potential-pH diagrams. *Nucl. Sci. & Engng.* 79, 26-48.
- Parker, V.B., Wagman, D.D. and Evans, W.H. 1971. Selected values of chemical thermodynamic properties. U.S. Dept. of Commerce. NBS Tech. Note 270-6.
- Parkhurst, D.L., Thorstenson, D.C. and Plummer, L.N. 1980. PHREEQE - A computer program for geochemical calculations. *U.S. Geol. Surv. Water Res. Invest.* 80-96.
- Percival, D.R. and Martin, D.B. 1974. Sequential determination of radium-226, radium-228, actinium-227 and thorium isotopes in environmental and process waste samples. *Anal. Chem.* 46(12), 1742-1749.
- Pickens, J.F. and Lennox, W. 1976. Numerical simulation of waste movement in steady groundwater flow systems. *Water Res. Research.* 12, 171-180.
- Pfizer, R. 1956. The distribution of thorium and uranium in sedimentary rocks and the oxygen content of the Precambrian atmosphere. Thesis. Rice Institute.
- Pon, K. 1980. Unpublished Chemistry 492 Project, University of Waterloo.
- Puphal, K.W. and Olsen, D.R. 1971. Electrodeposition of alpha-emitting nuclides from a mixed oxalate-chloride electrolyte. *Anal. Chem.* 44(2), 284-289.

- Rancon, D. 1973. The behaviour in underground environments of uranium and thorium discharges by the nuclear industry. In: Environmental Behaviour of Radionuclides Released in the Nuclear Industry. Intl. Atomic Energy Agency, Vienna. pp. 333-346.
- Rand, M.C., Greenberg, A.E., Taras, M.J. and Franson, M.A. 1975. Standard Methods. 14th ed. Amer. Public Health assoc. 1193 pp.
- Reardon, E.J. 1981. K_d 's - Can they be used to describe reversible ion sorption reactions in contaminant migration. Groundwater 19(3), 279-286.
- Reynolds, W.D. 1978. Column studies of strontium and cesium transport through a granular geologic porous medium. M.Sc. thesis, University of Waterloo.
- Ritcey, G.M. and Silver, M. 1982. Lysimeter investigations on uranium tailings at CANNET. Can. Min. Metall. Bull. 75(846), 134-143.
- Rodden, C.J. 1950. Analytical Chemistry of the Manhattan Project. McGraw-Hill Co.
- Rogers, J.J.W. and Adams, J.A.S. 1974. Thorium solubilities in water. In: Handbook of Geochemistry (ed. Wedepohl, K.H.) Springer Verlag.
- Rosholt, J.N. 1958. Radioactive disequilibrium studies as an aid in understanding the natural migration of uranium and its decay products. Proc. 2nd U.N. Intl. Conf. on Peaceful Uses of Atomic Energy, Geneva Vol. 2.
- Rosholt, J.N., Butler, A.P., Garner, E.L. and Shields, W.R. 1965. Isotopic fractionation of uranium in Sandstone, Powder River Basin, Wyoming and Slick Rock District, Colorado, Econ. Geol. 60, 199-213.
- Rosholt, J.N., Doe, B.R. and Tatsumoto, M. 1966. Evolution of the isotopic composition of uranium and thorium in soil profiles. Geol. Soc. Am. Bull. 77, 987-1004.
- Schubert, J. and Conn, E.E. 1949. Radiocolloidal behaviour of some fission products. Nucleonics 4(6), 2-11.
- Schubert, A.J., Russell, E.R. and Myers, L.S. 1950. Dissociation constants of radium inorganic acid complexes measured by ion exchange. Jour. Biol. Chem. 185, 387-398.
- Senftle, F.E. and Keevil, N.B. 1947. Thorium-uranium ratios in the theory of genesis of lead ores. Trans. Am. Geophys. Union. 28, 732.
- Serne, R.J. 1974. Experimental data published In: Radionuclide Interactions with Soil and Rock Media. (ed. Ames, L.L. and Rai, D. (1978). U.S. Environmental Protection Agency. Vol. 1, p. 144.
- Sheppard, M.I. 1980. The environmental behaviour of radium. Whiteshell Nucl. Res. Establ. Atomic Energy of Canada Ltd. No. 6796.

- Sill, C.W. 1969. Separation and radiochemical determination of uranium and the transuranium elements using barium sulphate. *Health Physics* 17, 89-107.
- _____. 1977. Determination of thorium and uranium isotopes in ores and mill tailings by alpha spectrometry. *Anal. Chem.* 49(4), 618-621.
- Sill, C.W. and Willis, C.P. 1965. Radiochemical determination of lead-210 in mill products and biological materials. 37(13) 1661-1671.
- Simpson, E.S. 1973. Finite state mixing-cell models. Presentation at Annual Meeting of American Geophysical Union: Hydrology Section.
- Smales, A.A. and Wager, L.R. 1960. *Methods in Geochemistry*. Interscience Publ. Inc. 464 pp.
- Smith, J.M. 1970. *Chemical Engineering Kinetics*. McGraw-Hill Book Co.
- Smithson, G.L. Dalton, J.L. and Mason, G.L. 1979. Radiochemical procedures for determination of selected members of the uranium and thorium series. *Canmet Report* 78-22. p. 47.
- Starik, I.F. and Polevaya, N.I. 1958. The Leachability of ThX and RdTh from Minerals (Eng. trans., U.S. A.E.C. Report. A.E.C.-tr-4208) 108 pp.
- Stead, F.W. 1964. Distribution in groundwater of radionuclides from underground nuclear explosions. In: *Proc. Third Plowshare Sym. Engng. with Nuclear Explosives TID-7695*. pp. 127-138.
- Stumm, W. and Morgan, J.J. 1970. *Aquatic Chemistry*. Wiley-Interscience. 583 pp.
- Sudicky, E.A., Cherry, J.A. and Frind, E.O. 1980. Hydrogeological Studies of a sandy aquifer at an abandoned landfill: Part 4. A natural gradient tracer test In: Vol. 1. CFB Borden Landfill Study. WRI Report No. OSU78-00195, University of Waterloo.
- Szabo, B.J. 1982. Extreme fractionation of $^{234}\text{U}/^{238}\text{U}$ and $^{230}\text{Th}/^{234}\text{U}$ in spring waters, sediments and fossils at the Pomme de Terre Valley, Southwestern Missouri. *Geochim. Cosmochim. Acta.* 46, 1675-1679.
- Szalay, S. and Samsoni, Z. 1969. Investigation of the leaching of uranium from crushed magmatic rock. *Geochem. Intl.* 6, 613-623.
- Thompson, P. 1973. Procedures for extraction and isotopic analysis of uranium and thorium from speleotherm. Tech. Memo. 73-9. Dept. of Geology. McMaster University, Hamilton, Ontario.
- Thurber, D.L. 1962. Anomalous $^{234}\text{U}/^{238}\text{U}$ in nature. *Jour. Geophy. Res.* 62(II), 4518-4520.
- Titayeva, N.A. and Veksler, T.I. 1977. The state of radioactive equilibrium in the uranium and thorium series as an indicator of migration of radioactive elements and active interaction between phases under natural conditions *Geochem. Intl.* 14(4), 99-107.
- Tokarev, A.N. and Scherbakov, A.V. 1956. *Radiohydrogeology Engl. Trans. U.S. A.E.C. Rept. ACE-tr-4100* (1960) 346 pp.

- Tomlinson, M. 1982. Chemistry for underground retention of wastes from nuclear energy. *Chemistry in Canada* 34(1), 19-22.
- Umemoto, S. 1973. Variation of $^{234}\text{U}/^{238}\text{U}$ during the fractional extraction of minerals. In: *Proceedings of Symposium of Hydrogeochemistry and Biogeochemistry Vol. 1*. pp. 273-283.
- Van Beek, C.G.E.M. and Pal, R. 1978. The influence of cation exchange and gypsum solubility on the transport of sodium and calcium sulphate through soils. *Jour. of Hydrol.* 36, 133-142.
- Van Breemen, N. and Wielemaker, W.G. (I) 1974. Buffer intensities and equilibrium pH of minerals and soils: I. The contribution of minerals and aqueous carbonate to pH buffering. *Soil Sci. Soc. Amer. Proc.* 38, 55-60.
- _____. (II) 1974. Buffer intensities and equilibrium pH of minerals and soils: II. Theoretical and actual pH of minerals and soils. *Soil Sci. Soc. Amer. Proc.* 38, 61-66.
- Vandergraaf, T.T. 1981. Personal communication. Research in rock/water interactions at Whiteshell Nuclear Research Establishment. Atomic Energy of Canada Ltd.
- Vdovenko, V.M. and Dubasov, Y.U.V. 1975. *Analytical Chemistry of Radium*. John Wiley & Sons, 198 pp.
- Veselsky, J. 1974. An improved method for the determination of the ratio $^{234}\text{U}/^{238}\text{U}$ in natural water. *Radiochim. Acta.* 21, 151-154.
- Veska, E. 1983. Origin and subsurface migration of radionuclides from waste rock at an abandoned uranium mine near Bancroft, Ont. Unpublished Ph.D. thesis, University of Waterloo.
- Vinogradov, A.P. 1959. The geochemistry of rare and dispersed chemical elements in soils. Transl. from Russian Consultants Bureau. Inc. 209 pp.
- Wagman, D.D., Evans, W.H., Parker, V.B., Halow, I. Bailey, S.M. and Schumm, R.H. 1968. Selected values of chemical thermodynamic properties. *NBS Techn. Note* 270-3.
- Wahlberg, J.S. Baker, J.H, Vernon, R.W. and Dewar, R.S. 1965. Exchange adsorption of strontium on clay minerals. *U.S. Geol. Surv. Bull.* 1140-C.
- Wahlberg, J.S. and Fishman, M.J. 1962, Adsorption of cesium on clay minerals. *U.S. Geol. Surv. Bull.* 1140-A.
- Wedepohl, K.H. 1978. *Handbook of Geochemistry*. Springer-Verlag, Berlin.
- Welhan, J.A. 1974. Feasibility of the oxygen-18 mass balance method in the calculation of the water balance of a small lake. Unpubl. M.Sc. thesis. University of Waterloo.
- Woodford, A.D. 1965. *Historical Geology*. Freeman and Co. 512 pp.
- Yagoda, H. 1946. Radiocolloid aggregates in uranium minerals. *Amer. Min.* 31, 462-470.